

**Western Australian School of Mines
Department of Petroleum Engineering**

**Gas Hydrate Analysis and Modelling of Monoethylene Glycol
Regeneration and the Impact of Additives**

Khalid Alef

**This thesis is presented for the Degree of
Doctor of Philosophy
of
Curtin University**

January 2020

DECLARATION

To the best of my knowledge and belief this thesis contains no material previously published by any other person except where due acknowledgment has been made.

This thesis contains no material which has been accepted for the award of any other degree or diploma in any university.

Signature:

(Khalid Alef)

Date:

COPYRIGHT

I warrant that I have obtained, where necessary, permission from the copyright owners to use any third-party copyright material reproduced in the thesis, or to use any of my own published work in which the copyright is held by another party (e.g. publisher, co-author).

Signature:

(Khalid Alef)

Date:

DEDICATION

I would like to dedicate this thesis to my beloved parents whose love, example and selfless support have secured the foundation for the discipline and application necessary to achieve success.

In loving memory of my beloved grandparents (late) for their endless love, prayers and encouragement.

ACKNOWLEDGEMENT

All praise and thanks belong to God, Al-Mighty for everything including this work.

I am most grateful to my main supervisor, Dr. Ahmed Barifcani for his advanced technical guidance, endless support and encouragement. Beside my supervisor, my sincerest thanks go to the members of my thesis committee, Dr. Stefan Iglauer, Dr. Christopher Lagat, and Chairperson, Dr. Mofazzal Hossain, for their time, encouragement, and expertise throughout this project. I would also like to thank my colleagues, Dr. Khalifa Al Harooni and Dr. Callum Smith for their valuable assistance throughout my project. Special thanks also go to the technicians at the Department of Petroleum Engineering and Curtin Corrosion Engineering Industry Centre, especially Dr. Guanliang Zhou and Mr. Leigh Bermingham for their help in the research laboratory.

I would especially like to thank my family, mentors and friends. My wife who has been extremely supportive of me throughout this entire process and has made countless sacrifices to help me get to this point. My mentors and friends who have helped in pointing me to the right direction in key times of my development academically, professionally, and spiritually. Without such a team behind me, I doubt that I would be in this place today.

Last but not least, I would like to acknowledge the contribution of an Australian Government Research Training Program Scholarship in supporting this research.

ABSTRACT

Natural gas is increasingly becoming a favourable alternative resource to meet energy demands. However, natural gas production, processing, and transportation faces serious flow assurance challenges such as hydrate formation. Conventionally, monoethylene glycol (MEG) is injected to inhibit gas hydrate formation. Due to the large quantities of MEG required, it is re-used after a complex regeneration process. During this process, MEG may undergo a type of degradation that may ultimately decrease its hydrate inhibitory performance. In this project, significant experimental and computational effort has been applied to investigate MEG degradation, evaluate the MEG regeneration and reclamation process during water breakthrough, and the impact of several other chemicals on gas hydrate formation.

The impact of MEG degradation on hydrate formation was studied for the first time over multiple trials of experimentation equivalent to numerous MEG inventory turnovers. The novel and the only MEG laboratory-scale regeneration and reclamation research facility in Australia was utilised for the work. It was found that MEG degradation can occur even at lower exposure temperatures albeit in longer exposure times. The study gave insights and established a way to diagnose the operating pH at various stages of the MEG regeneration and reclamation process as well as how it can be modified to ensure expected objectives are met. An original contribution to knowledge from this study is the production of highly valuable hydrate phase equilibria data and metastable regions for systems of MEG covering a wide pressure range of 50 to 200 bar. Moreover, a novel empirical model for prediction was developed capturing the degradation of MEG over regeneration cycles. The impact of this research to the field and future knowledge is significant. Firstly, a blind spot has been exposed, whereby the lack of inhibition performance of degraded MEG would need to be considered in hydrate control philosophies. Secondly, a predictive tool is now immediately available to MEG operators to help determine the amount of degradation against regeneration cycle. When considering a typical 5 kT MEG inventory system, an additional average cost of approximately USD \$227,000 for MEG top-ups at each inventory turnover would be required to ensure expectations are met.

Additional empirical models were developed to allow for prediction of degraded and

non-degraded, regenerated and non-regenerated, and corrosion inhibitor presence or absence in MEG solutions. Such prediction capability will allow MEG end-users to effectively monitor MEG quality, and ensure the integrity of the hydrate control program that is applied in the field. In other respects, methods to prepare and degrade MEG samples have been developed and standardized.

Methyldiethanolamine (MDEA) has increasingly been used alongside MEG as a pH stabilizer. The impact of this chemical on gas hydrate formation has only recently been recognized, however it has never been modelled. In this study, the effect of MDEA in the presence and absence of MEG has been studied at a high-pressure range. The combined effect of MDEA (7.5 wt%) with MEG (20 wt%) showed an equivalent hydrate performance of 20.95 wt% MEG. New phase equilibria data, and empirical and thermodynamic models using the Cubic Plus Association (CPA) equation of state were produced as original contributions to knowledge. The impact of this research to the field and future knowledge is significant, since this will allow for accurate prediction of the effect of MDEA in a time where the effect of this chemical has not been considered in any available hydrate simulation software.

Moreover, a plethora of chemicals are also injected alongside MEG for various reasons such as corrosion inhibition, oxygen scavenging and scale inhibition. Selections of each type of chemical have been thoroughly tested using a high-pressure PVT cell to determine the hydrate phase boundaries. The effect of film forming corrosion inhibitor (FFCI) on gas hydrate formation in the presence of MEG or kinetic hydrate inhibitor (KHI) has been investigated and it was found to have an inhibitory performance. High levels of dissolved oxygen in the presence of MEG was found to promote gas hydrate formation.

PUBLICATIONS BY THE AUTHOR

This Ph.D. thesis by publication consists of eight (8) first-author peer-reviewed publications in high-impact journals, and two (2) refereed conference articles. Other publications or collaborations relevant to the thesis are also listed. The copyright permission statement for each publication are given in Appendix C. Signed statements of contribution by others are given in Appendix D.

1. **Alef, K.**, Smith, C., Iglauer, S., Gubner, R., Barifcani, A., 2018c. The Effect of Regenerated MEG on Hydrate Inhibition Performance Over Multiple Regeneration Cycles. *Fuel* 222, 638–647. doi: 10.1016/j.fuel.2018.02.190.
2. **Alef, K.**, Gubner, R., Iglauer, S., Barifcani, A., 2019a. Evaluation of MEG Reclamation and Natural Gas Hydrate Inhibition During Corrosion Control Switchover. *Journal of Petroleum Science and Engineering* 176, 1175–1186. doi: 10.1016/j.petrol.2018.08.052.
3. **Alef, K.**, Barifcani, A., 2018. The Effect of Salt-Laden Degraded MEG on Gas Hydrate Inhibition. Presented at the SPE Kingdom of Saudi Arabia Annual Technical Symposium and Exhibition, Society of Petroleum Engineers. doi: 10.2118/192447-MS.
4. **Alef, K.**, Iglauer, S., Gubner, R., Barifcani, A., 2018b. Hydrate Phase Equilibria for Methyldiethanolamine and Empirical Modeling for Prediction. *J. Chem. Eng. Data* 63, 3559–3565. doi: 10.1021/acs.jced.8b00440.
5. **Alef, K.**, Iglauer, S., Barifcani, A., 2019b. Thermodynamic Modeling of Hydrate Phase Equilibria in Methyldiethanolamine Solution in the Presence or Absence of Monoethylene Glycol. *J. Chem. Eng. Data* 64, 4148–4153. doi: 10.1021/acs.jced.9b00552.
6. **Alef, K.**, Barifcani, A., 2020. Effect of N-Methyl-Diethanolamine and Film Forming Corrosion Inhibitor on Gas Hydrate, and Empirical Modeling for Degradation. *Journal of Petroleum Science and Engineering* 184, 106522. doi: 10.1016/j.petrol.2019.106522.
7. **Alef, K.**, Iglauer, S., Barifcani, A., 2018a. Effect of Dissolved Oxygen, Sodium Bisulfite, and Oxygen Scavengers on Methane Hydrate Inhibition. *J. Chem. Eng. Data* 63, 1821–1826. doi: 10.1021/acs.jced.8b00150.
8. **Alef, K.**, Barifcani, A., 2019. Hydrate Phase Equilibria of Phosphonate Scale

Inhibitors, Amines, and Ethylene Glycol. *J. Chem. Eng. Data* 64, 3205–3210. doi: 10.1021/acs.jced.9b00366.

9. **Alef, K.**, Iglauer, S., Barifcani, A., 2017. An Innovative Approach to Assessing Gas Hydrate Inhibition and Corrosion Control Strategies, In One Curtin International Postgraduate Conference (OCPC), Miri, Sarawak, Malaysia: Curtin.
10. **Alef, K.**, Iglauer, S., Barifcani, A., 2019c. Degradation and Hydrate Phase Equilibria Measurement Methods of Monoethylene Glycol. *MethodsX* 6, 6–14. doi: 10.1016/j.mex.2018.12.004.

Other publications or collaborations indirectly connected to the thesis are:

11. Sadeq, D., **Alef, K.**, Iglauer, S., Lebedev, M., Barifcani, A., 2018. Compressional Wave Velocity of Hydrate-Bearing Bentheimer Sediments with Varying Pore Fillings. *International Journal of Hydrogen Energy* 43, 23193–23200. doi: 10.1016/j.ijhydene.2018.10.169.

TABLE OF CONTENTS

DECLARATION	I
COPYRIGHT	II
DEDICATION	III
ACKNOWLEDGEMENT	IV
ABSTRACT	V
PUBLICATIONS BY THE AUTHOR	VII
TABLE OF CONTENTS	IX
LIST OF FIGURES	XIV
LIST OF TABLES	XVIII
Chapter 1 Introduction	1
1.1 Background	1
1.2 Literature Review	3
1.2.1 Interest in Gas Hydrates	4
1.2.2 Hydrate Structure and Physical Properties	5
1.2.3 Hydrate Formation and Dissociation Mechanism	9
1.2.4 Hydrate Phase Equilibria Modelling	14
1.2.5 Hydrate Inhibition	18
1.2.6 Regeneration and Reclamation of MEG	21
1.2.7 Degradation of MEG	23
1.3 Significance and Research Gap	23
1.4 Thesis Objectives	27
1.5 Thesis Structure	28
Chapter 2 Effect of Regenerated MEG on Gas Hydrate, and Empirical Modelling for Prediction	31
2.1 Introduction	33
2.2 Methodology	34

2.2.1	Materials and Equipment	34
2.2.2	Process and Procedure.....	37
2.3	Results and Discussion	39
2.3.1	Observations.....	39
2.3.2	Initial Testing	42
2.3.3	Equilibrium Results – Cycling.....	43
2.3.4	Empirical Model.....	49
2.3.5	Application of Model to Experimental Data.....	51
2.4	Conclusions and Recommendations.....	52
Chapter 3	Evaluation of MEG Reclamation and Natural Gas Hydrate Inhibition during Corrosion Control Switchover.....	54
3.1	Introduction	55
3.2	Methodology	56
3.2.1	Materials and Equipment	58
3.2.2	Procedure.....	61
3.3	Results and Discussion	63
3.3.1	Switchover Operation.....	63
3.3.1.1	Effect of pH on MDEA removal.....	66
3.3.1.2	Effect of FFCI.....	68
3.3.1.3	Effect of pH on Acetic Acid Removal.....	70
3.3.1.4	Effect of pH on Divalent Salts Removal	71
3.3.2	Natural Gas Hydrate Inhibition.....	71
3.3.2.1	Preliminary Hydrate Testing.....	71
3.3.2.2	Reclaimed MEG Hydrate Equilibria.....	73
3.4	Conclusion.....	79
Chapter 4	Effect of Salt-Laden Degraded MEG on Gas Hydrate Inhibition.....	81
4.1	Introduction	82

4.2	Methodology	84
4.3	Results and Discussion	86
4.3.1	Salt-laden MEG.....	87
4.4	Conclusions	91
Chapter 5	Hydrate Phase Equilibria for Methyldiethanolamine and Empirical Modelling for Prediction	92
5.1	Introduction	93
5.2	Methodology	94
5.2.1	Materials and Apparatus	94
5.2.2	Method	96
5.3	Results	97
5.3.1	Pure MDEA Tests	98
5.3.2	MEG Tests	100
5.3.3	Empirical Modelling	103
5.4	Conclusion.....	109
Chapter 6	Thermodynamic Modelling of Hydrate Phase Equilibria of Methyldiethanolamine.....	110
6.1	Introduction	111
6.2	Methodology	113
6.2.1	Experimental Section	113
6.2.2	Thermodynamic Modelling.....	115
6.3	Results	120
6.3.1	Experimental Phase Equilibria.....	120
6.4	Conclusions	124
Chapter 7	Effect of Corrosion Inhibitors with Kinetic Hydrate Inhibitor on Gas Hydrate, and Empirical Modelling of MEG Degradation.....	125
7.1	Introduction	126
7.2	Methodology	128

7.2.1	Materials & Apparatus	128
7.2.2	Isochoric Method	129
7.2.3	Isothermal method.....	131
7.3	Results and Discussion	132
7.3.1	FFCI and FFCI + MEG mixtures.....	132
7.3.2	KHI Mixtures	135
7.3.3	Empirical Modelling	139
7.3.3.1	Model Validation	142
7.4	Conclusion.....	146
Chapter 8	Effect of Dissolved Oxygen, Sodium Bisulfite, and Oxygen Scavengers on Methane Hydrate Inhibition	148
8.1	Introduction	149
8.2	Experimental Methodology	150
8.2.1	Materials and Chemicals	150
8.2.2	Test Apparatus and Experimental Procedure.....	152
8.3	Results	153
8.3.1	Effect of Dissolved Oxygen.....	154
8.3.2	Effect of Sodium Bisulfite	155
8.3.3	Effect of Proprietary Oxygen Scavenger (OS-P).....	159
8.3.4	Effect of Nonsulfite-Based Oxygen Scavenger (IFEox2).....	160
8.4	Conclusions	161
Chapter 9	Hydrate Phase Equilibria of Phosphonate Scale Inhibitors, Amines, and Ethylene Glycol.....	163
9.1	Introduction	164
9.2	Methodology	165
9.2.1	Materials.....	165
9.2.2	Experimental Method.....	166
9.3	Results	168

9.3.1	Scale Inhibitors.....	169
9.3.2	Amines (MEA and DEA).....	172
9.4	Conclusions	174
Chapter 10	Utilization of MEG Pilot Plant and MEG Degradation Methods	175
10.1	An Innovative Approach to Assessing Gas Hydrate Inhibition and Corrosion Control Strategies.....	176
10.1.1	MEG Operation.....	177
10.1.2	Gas Hydrate Testing.....	182
10.1.2.1	Flow Assurance Software	182
10.1.2.2	Empirical Modelling.....	183
10.1.3	Use Cases	183
10.1.4	Conclusion	185
10.2	Degradation and Hydrate Phase Equilibria Measurements of Monoethylene Glycol.....	186
10.2.1	Method Details	186
10.2.2	Degradation of MEG.....	186
10.2.3	Hydrate Testing of Degraded MEG	191
10.2.4	Method Validation	193
10.2.5	Conclusion	195
Chapter 11	Summary and Conclusions.....	197
11.1	Further Research Potential.....	200
	BIBLIOGRAPHY	201
	APPENDICES	221
	APPENDIX A. Outline of Algorithm, and MDEA Data.....	221
	APPENDIX B. Computer Script to Process Test Data.....	223
	APPENDIX C. Copyright Permission Statements.....	224
	APPENDIX D. Statements of Contribution by Others	232

LIST OF FIGURES

Figure 1.1: Publications related to gas hydrates from 1972 to 2019 (data attained from Web of Science).	4
Figure 1.2: Cage shapes formed by water: a) 5^{12} (pentagonal dodecahedron), b) $5^{12}6^2$ (tetrakaidecahedron), c) $5^{12}6^4$ (hexakaidecahedron), d) $4^35^66^3$ (irregular dodecahedron) and, e) $5^{12}6^8$ (icosahedron) (after Sloan Jr and Koh, 2007).	5
Figure 1.3: Resulting hydrate structure types based on hydrate formers (guest) size and number of occupied water cavities (after Giavarini et al., 2011).	6
Figure 1.4: Hydrate structure and cavity types (where i , n_i and m_i denote face type, number of edges and number of faces respectively).	7
Figure 1.5: Cubic Structure I: (a) Packing of structure I hydrate, (b) Electron density map of tetrakaidecahedra cage (perpendicular to the plane of the hexagons) from the hydrate of acetylene (after Kirchner, 2004).	7
Figure 1.6: Cubic Structure II: (a) Packing of structure II hydrate, (b) Electron density map of hexakaidecahedral cage (within the plane of both symmetry axes) from the hydrate of propane (after Kirchner, 2004).	8
Figure 1.7: Hexagonal Structure sH: (a) Packing of structure sH hydrate, (b) Electron density map of icosahedral cage (top left is along the (1 2 1)-plane while others are perpendicular to the 6-fold axis as shown) from the hydrate of adamantane and methane (after Kirchner, 2004).	8
Figure 1.8: Summary of the labile clustering mechanism (after Sloan Jr and Koh, 2007).	10
Figure 1.9: Labile cluster growth enacted on a pressure and temperature trace (after Sloan Jr and Koh, 2007).	11
Figure 1.10: a) Formation of hydrate: consumption of gas vs time, b) Pressure and temperature trace for methane hydrate (after Sloan Jr and Koh, 2007).	12
Figure 1.11: The two means by which a hydrate solid can cause pipeline rupture: (a) high velocity and momentum impact at bend, and (b) momentum impact combined with gas compression pipe obstruction (after Sloan 2007).	21
Figure 1.12: MEG Regeneration pilot plant at the Curtin University – CCEIC.	25
Figure 1.13: MEG reclamation unit (rotary evaporator) at the MEG pilot plant.	26
Figure 1.14: PVT cell capable of hydrate testing at high-pressures.	26
Figure 1.15: Thesis structure illustrated.	30
Figure 2.1: Schematic of the PVT Sapphire cell where P and T denote pressure and temperature respectively.	36
Figure 2.2: Observations of foaming due to MDEA, and coloration in cycles 1, 5, and 9 as compared to pure MEG.	40
Figure 2.3: Observable stages of hydrate testing of cycled MEG.	41
Figure 2.4: Hydrate profile for methane and water mixture from this study compared to simulation software (average absolute deviation of 1.64%) and literature (1.80%).	42
Figure 2.5: Hydrate profile for methane and 20 wt% MEG solution.	43

Figure 2.6: Methane hydrate phase profiles for pure MEG (20 wt%) and cycles 1–9, dotted lines refer to exponential fitting curves.	44
Figure 2.7: Acetic Acid concentration (ppm) of cycles 1-9.	46
Figure 2.8: Dissolved oxygen levels (ppb) within the reclaimed MEG solution for each cycle.	48
Figure 2.9: Temperature of the liquid and vapor phases within the reclamation unit over 9 cycles (sensor accuracy of ± 0.03 °C).	48
Figure 2.10: MDEA concentration (mM) in samples of cycles 1-9.	49
Figure 2.11: P versus T -Hydrate Equilibrium Shift (ΔT_{0-9}).	50
Figure 3.1: Experimental setup (bench-scale MEG regeneration/reclamation pilot plant).	57
Figure 3.2: PVT sapphire cell used for gas hydrate testing.	57
Figure 3.3: Material balance for the MEG pilot plant operation (cycle time of ~ 10 h).	62
Figure 3.4: Target pH compared to actual pH in the lean glycol tank (LGT) and feed blender (FB). .	64
Figure 3.5: Actual and target MDEA and FFCI concentrations as a function of time.	65
Figure 3.6: Electrical conductivity (EC) of post-reboiler and reclaimed MEG solutions.	66
Figure 3.7: pH and MDEA concentration in post-reboiler and reclaimed MEG solutions as a function of time.	67
Figure 3.8: pH and FFCI concentration in post-reboiler and reclaimed MEG solutions as a function of time.	69
Figure 3.9: Physical and colour changes in salt slurry from the reclamation unit with and without FFCI.	69
Figure 3.10: pH and acetic acid concentration in post-reboiler and reclaimed MEG solutions as a function of time.	71
Figure 3.11: Methane hydrate phase boundary for 30 wt% MEG solution compared with Multiflash prediction and literature (Haghighi et al., 2009b; Robinson and Ng, 1986; Vajari, 2012).	73
Figure 3.12: Natural gas hydrate phase boundaries for reclaimed MEG samples A-C.	76
Figure 3.13: Hydrate metastable region for reclaimed MEG sample A.	77
Figure 3.14: Hydrate metastable region for reclaimed MEG sample B.	78
Figure 3.15: Hydrate metastable region for reclaimed MEG sample C.	79
Figure 4.1: Basic schematic of the experimental apparatus utilized in this study including the PVT cell.	86
Figure 4.2: Methane hydrate phase boundary of pure water compared to literature and software.	87
Figure 4.3: Hydrate phase boundaries for non-degraded and degraded MEG samples compared to HYSYS prediction.	88
Figure 4.4: Gradual formation of methane hydrate in solution.	89
Figure 4.5: Change in colour between non-degraded and degraded MEG samples.	91
Figure 5.1: Schematic of the high-pressure PVT sapphire cell used in this study which is capable of performing hydrate inhibition testing.	96
Figure 5.2: Methane hydrate phase boundaries for pure water and pure MEG (20 wt%) as compared to literature and software predictions.	98
Figure 5.3: Methane hydrate phase boundaries for pure MDEA (2.5–7.5 wt%) and their equivalent MEG	

concentrations using Multiflash.	100
Figure 5.4: Stages of hydrate testing in MEG–MDEA (2.5 and 7.5 wt%) mixtures.	101
Figure 5.5: Measured and simulated phase boundaries for combined 20 wt% MEG with MDEA (2.5 and 7.5 wt%).	103
Figure 5.6: Pressure versus $\Delta T_{7.5}$, hydrate equilibrium temperature shift for between water and pure MDEA at 7.5 wt%.	105
Figure 5.7: Comparison of predicted to experimental data for MDEA and MEG mixtures from this study.	107
Figure 5.8: Comparison of predicted to experimental data for MDEA solutions from literature.	107
Figure 6.1: Hydrate phase diagram showing hydrate-free regions of quaternary mixture of water–methane–MEG–MDEA.	112
Figure 6.2: Schematic of the experimental apparatus used in this study.	114
Figure 6.3: Methane hydrate equilibria for MDEA (3.5 wt%). The MDEA molecular structure is shown, where red = oxygen, blue = nitrogen, white = hydrogen, and grey = carbon.	121
Figure 6.4: Methane hydrate equilibria for MDEA (3.5 wt%) combined with MEG (25 wt%). The MDEA and MEG molecular structures are shown, where red = oxygen, blue = nitrogen, white = hydrogen, and grey = carbon.	122
Figure 6.5: Comparison of model calculation to MDEA hydrate phase equilibria data from Akhflash et al. 2017.	123
Figure 6.6: Comparison of model calculation to MDEA phase equilibria data from Alef et al. (2018).	124
Figure 7.1: The apparatus used for solution preparation, and hydrate testing using a high-pressure PVT cell in this study. P_l denotes cell pressure, while T_1 , T_2 , T_3 denote temperatures of vapor phase, liquid phase and air bath respectively.	129
Figure 7.2: Pressure-temperature curves for the cooling and heating stages of the isochoric method for 20 wt% MEG solution. Methane hydrate phase boundary simulated in Multiflash is plotted as a dashed curve.	130
Figure 7.3: Methane hydrate phase boundaries for aqueous FFCI (0.5, 3 and 4 wt%) and their equivalent MEG concentration using Multiflash.	134
Figure 7.4: Hydrate phase boundary for the combined mixture of 3 wt% FFCI with 20 wt% MEG compared with a 20 wt% MEG only solution.	135
Figure 7.5: Stages of hydrate testing of KHI in the presence of MDEA and FFCI.	136
Figure 7.6: Pressure drop curves against time for KHI with MDEA and FFCI in memory water.	137
Figure 7.7: Induction and growth times for KHI with/without MDEA and FFCI.	137
Figure 7.8: Hydrate equilibrium temperature shift for MEG and MDEA + MEG degraded solutions.	142
Figure 7.9: Comparison of calculations using model compared to experimental data for MDEA solutions exposed to 165 °C and 180 °C.	143
Figure 7.10: Comparison of calculations using model compared to experimental data for MDEA + MEG solutions exposed to 135, 165, 185 and 200 °C.	144

Figure 7.11: The algorithm to determine equilibrium temperature of aqueous MDEA, and MDEA + MEG solutions at varying concentrations.	146
Figure 8.1: Schematic of the test apparatus used for the preparation of MEG/oxygen scavenger solutions.	152
Figure 8.2: Methane hydrate phase boundary for 20 wt% MEG + 80 wt% water solution.....	154
Figure 8.3: Hydrate phase boundaries of 20 wt% MEG solution with low (<20 ppb) and high (>7500 ppb) oxygen content.	155
Figure 8.4: Hydrate phase boundaries for aqueous NaHSO ₃ solutions.	157
Figure 8.5: Hydrate phase boundaries for aqueous NaHSO ₃ + MEG solutions.	159
Figure 8.6: Hydrate phase boundary of proprietary oxygen scavenger, OS-P (0.025 wt%) in 20 wt% MEG solution.	160
Figure 8.7: Hydrate phase boundary of IFEox2 (0.01 wt%) in 20 wt% MEG solution.	161
Figure 8.8: Conversion of erythorbic acid to erythorbate salt by neutralization reaction by DEAE. .	161
Figure 9.1: High-pressure PVT cell used in this study for performing hydrate inhibition testing.	167
Figure 9.2: Hydrate phase boundary for pure MEG (5 wt%) compared to software predictions.	169
Figure 9.3: Hydrate phase boundaries for scale inhibitors (IDMP, NTMP, and DTPMP) at 35 ppm compared pure water.	171
Figure 9.4: Hydrate phase boundaries for scale inhibitors (IDMP, NTMP, and DTPMP) at 350 ppm compared pure water.	171
Figure 9.5: Hydrate phase boundaries of MEA, DEA, and MEG at 5 wt% as compared to pure water.	172
Figure 9.6: Hydrate phase boundaries for MEA and DEA at 5 wt% and their equivalent MEG concentrations using Multiflash.	173
Figure 10.1: Simulation of field formation water.....	178
Figure 10.2: Simulation of pipeline conditions to create contaminated MEG solution.....	179
Figure 10.3: Contaminated MEG going through pre-treatment to remove insoluble contaminants...	180
Figure 10.4: MEG from CMT arrives at the reboiler and distillation (RBD) where water is removed thus increasing MEG concentration.....	181
Figure 10.5: The MEG reclamation unit (MRU) removes soluble contaminants from the incoming MEG solution.....	182
Figure 10.6: Basic schematic of a high-pressure PVT cell apparatus capable of gas hydrate testing.	182
Figure 10.7: Example of interpolation of a gas hydrate profile shift, showing multiple concentrations.	183
Figure 10.8: Schematic for the suggested experimental set-up of the reclamation unit.	188
Figure 10.9: Schematic for the preparation of the test solution and autoclave set.	191
Figure 10.10: Schematic of experimental set-up for hydrate testing using PVT Cell.	192
Figure 10.11: Comparison of degraded MEG with fresh MEG, and literature comparison of methane-water hydrate.....	195
Figure A-1: Outline of the algorithm to predict equilibrium temperature of pure MDEA, and MEG-MDEA solutions at MDEA concentrations of 0 – 7.5 wt%.	222

LIST OF TABLES

Table 1.1: Thesis objectives and peer-reviewed publications corresponding to each chapter.	29
Table 2.1: Top-up cost due to MEG recovery losses and degradation.	32
Table 2.2: Pure MEG composition from chem-supply.	37
Table 2.3: Hydrate equilibrium temperature shift (ΔT_s) of cycles 1, 5 and 9 compared to pure MEG hydrate profile and the regression functions of the fitted data. ^{ab}	44
Table 2.4: Hydrate Equilibrium Temperature shift (ΔT_s) from Pure MEG hydrate profile (cycles 2, 3, 4, 6, 7, 8). ^a	45
Table 2.5: Constants for Eqns. (2.3) and (2.6).	51
Table 2.6: Model calculations versus raw data.	52
Table 3.1: Fluid compositions (brine/formation water, rich MEG, and lean MEG).	59
Table 3.2: The composition of natural gas used in this study.	60
Table 3.3: Target concentrations of FFCI and MDEA.	62
Table 3.4: Phase equilibrium data for 30 wt% MEG solution compared with Multiflash prediction and literature.	72
Table 3.5: Hydrate formation and dissociation (equilibria) data from this study. ^a	73
Table 3.6: Reclaimed MEG samples (A-C) compositions, regression functions, and metastable regions.	75
Table 4.1: Salt-laden MEG solution composition.	85
Table 4.2: Materials utilized in this study.	86
Table 4.3: Methane equilibria data of this study with relative temperature shifts.	88
Table 5.1: List of materials used in the experiments.	95
Table 5.2: Experimental matrix of hydrate inhibition tests conducted using the isochoric method.	97
Table 5.3: Equilibria data for pure water and pure MDEA samples measured in this study. ^a	99
Table 5.4: New methane hydrate phase equilibria data for 20 wt% MEG/water–MDEA mixture. ^a ..	103
Table 5.5: Constants used in Eqn. (5.6) for pure MDEA and MEG–MDEA mixtures.	106
Table 5.6: Statistical comparison of model and experimental data. ^a	108
Table 6.1: Materials and their properties used in this study. ^a	115
Table 6.2: Parameters for the associating compounds in this study to be used in the CPA EoS.	117
Table 6.3: Optimized values for interaction parameter k_{ij} for MEG and MDEA with non-associating compounds. ^a	117
Table 6.4: Coefficients for optimized interaction parameters for water–MEG, water–MDEA, and MEG–MDEA mixtures.	118
Table 6.5: AARE of model and experimental methane hydrate phase equilibria data for MDEA and MEG. ^a	121
Table 6.6: Comparison of published data with the proposed model.	123
Table 7.1: Experimental matrix for tests using the isochoric hydrate testing method.	131
Table 7.2: The experimental matrix of hydrate inhibition tests conducted using the isothermal method.	132

Table 7.3: Equilibria data for pure FFCI solutions and MEG mixture measured in this study. ^a	133
Table 7.4: Experimental data for KHI, MDEA and FFCI solutions under a sub-cooling of ~10 °C. ^{ab}	139
Table 7.5: Constants to be used in Eqn. (7.7) for aqueous MEG and MDEA + MEG mixtures.	142
Table 7.6: Calculations using model compared to experimental data for MEG and MDEA + MEG mixtures from literature.....	145
Table 8.1: Materials utilized in this study.	151
Table 8.2: Composition of the oxygen scavenger developed by Kundu and Seiersten (2017).	151
Table 8.3: Oxygen scavenger dosage in each test solution.	152
Table 8.4: Methane hydrate equilibria data for sodium bisulfite solutions. ^a	156
Table 9.1: List of chemicals utilized in this study.....	166
Table 9.2: Experimental test matrix and chemical structures.	167
Table 9.3: Equilibria data produced in this study for meg, scale inhibitors (IDMP, NTMP, and DTPMP), and amines (MEA and DEA). ^a	173
Table 10.1: Experimental data of degraded and non-degraded MEG solutions using reported methods.	194
Table A-1: Effect of MDEA (5 wt%) on MEG (20 wt% and 25 wt%).	221

Chapter 1 Introduction

1.1 Background

As the search for alternative energy resources continues and the scarcity of oil increases, natural gas has increasingly become a favourable alternative which is available abundantly in various parts of the world. Although natural gas is a non-renewable resource, it is however, a clean fuel which produces fewer pollutants and greenhouse gases compared to coal and oil (Jaramillo et al., 2007). The hundreds of projects around the world for the production, processing, and storage of natural gas are indicative of the widely spread distribution of this energy resource compared to coal (Stanek and Bialecki, 2014). It is estimated that there are approximately 200 trillion cubic meters of reserves, which at the current rate of production is sufficient to continue for 60 years (Holz et al., 2015). Natural gas is primarily utilized for heating and cooking in the domestic context (Brkić and Tanasković, 2008). Industrially, it is primarily used for generation of power (Shukla et al., 2009); however, many natural gas components serve as a feedstock to countless industrial processes including organic compounds, plastics, and petrochemicals (Ross et al., 1996). Recently, natural gas has been utilized for the running of transport vehicles such as freight trains, busses, trucks, and LNG cargo ships (Gazzard, 2008; Kamimura et al., 2006).

On the other hand, there exists numerous flow assurance challenges concerning natural gas production and transportation (Sloan Jr and Koh, 2007). At any of these stages, natural gas may come into contact with condensed, production/formation water to form ice-like structures known as gas hydrates at certain pressures and temperatures leading to pipeline blockages, pressure build-up, and dangerous projectiles that could rupture the pipeline (Sloan Jr and Koh, 2007). Especially, in the transportation of gas through subsea pipelines from wellhead to onshore processing usually provides the typical conditions of pressure and temperature for the formation of hydrates. Despite the high cost associated with such events, they may also result in catastrophic consequences that could cause fatalities and damage to the environment (Camargo et al., 2011; Englezos, 1993).

The work of Hammerschmidt (1934) was the start of the contemporary era of gas

hydrate research. He discovered that the blockage of gas lines at a temperature greater than the ice formation temperature were due to gas hydrates as opposed to normal ice formation (Hammerschmidt, 1934). The capability to predict hydrate formation conditions was another significant development in this field. Katz (1945) and their team of researchers collated the pressure-temperature data from gas hydrate experiments that resulted in the formation of hydrates from varying gases given enough water presence (Katz, 1945).

Gas hydrates are a crystal lattice network made up of common gas components such as methane to butane, acid gases, and nitrogen encaged by molecules of water (Koh, 2002; Sloan Jr and Koh, 2007). Most gas hydrates can be classified into three types of structures: 2 cubic and 1 hexagonal (Carroll, 2014; Kirchner et al., 2004; Ripmeester et al., 1987; Sloan Jr and Koh, 2007). The mechanism of gas hydrate formation is built based on the theories pertaining to water crystallization (Sloan Jr and Koh, 2007). The process commences with the nucleation phase which typically happens on the water-gas interface (Long and Sloan, 1996). Succeeding this phase, the growth of hydrate begins to occur which is a complicated process (thermodynamic) deeply reliant on conditions of mass and heat transfer. As for the dissociation of gas hydrates, it is endothermic and occurs around the hydrate solid (Sloan Jr and Koh, 2007). The process can be instigated by changing the surrounding pressure and temperature of the hydrate solid.

The control and prevention of gas hydrates may typically be achieved by chemical injection, thermal heating, depressurization, dehydration, and water removal (Son and Wallace, 2000). In terms of chemical injection, a hydrate inhibitor such as MEG as opposed to methanol is widely employed due to it being the safer, cleaner, and reusable (through MEG regeneration) alternative (Brustad et al., 2005). Where MEG is utilized as part of the hydrate control philosophy for a field, MEG begins its journey after the wellhead mixing with the produced hydrocarbon, ultimately dropping the thermodynamic hydrate phase equilibrium to lower temperatures (Son and Wallace 2000). At the onshore arrival facilities, the production fluid is separated and pre-treated. The aqueous phase comprising of water, MEG, and other chemicals (organic compounds and salts) are routed to the MEG Regeneration Unit (MRU) for the removal of salts, water, and contaminants via flash drums (reclamation), reboilers (re-

concentration), and distillation columns (Nazzari and Keogh, 2006). Variations of these processes are dependent on the needs of the project at hand and the minimum allowable salt limit in the production network (Psarrou et al., 2011; Teixeira et al., 2015). The resulting clean MEG is then sequentially re-injected after the wellhead to continue the cycle.

The use of MEG especially in the context of regeneration leads to the challenge of MEG degradation whether oxidative or thermal. Preliminary research suggests that MEG undergoes thermal degradation at certain temperatures generating organic acids, specifically formic and acetic acids (AlHarooni et al., 2015; Rossiter et al., 1985). However, a gap in the literature that is evident regarding experimentally evaluating the performance of MEG across the entire MEG loop as well as through multiple regeneration cycles. Moreover, the lack of modelling of this degradation effect for hydrate inhibitory performance of MEG.

1.2 Literature Review

Hydrates are often referred to as ‘clathrates’, which is a term that some say is derivative after the Greek term ‘khlatron’ with a connotation suggesting a barrier of some sort, or from the Latin word ‘clatratus’ meaning latticed or barred (AlHarooni et al., 2017). Nonetheless, it is indicative of the crystalline nature of hydrates whereby cavities are formed from surrounding host molecules that effectively encage guest molecules forming a crystalline inclusion compound (Chatti et al., 2005). The guest molecules may be classified in four categories: water-soluble acid gases, water-soluble ternary or quaternary alkylammonium salts, water-soluble polar compounds, and hydrophobic compounds (Jeffrey and McMullan, 2007). If the compound consists of water, they are called ‘clathrate hydrates’, and when the encaged guest molecule is gaseous, they are called ‘gas hydrate’. Within the context of gas hydrates, the encaged gaseous molecule is referred to as the ‘guest’, while the encaging water molecules (i.e., forming a caged cavity) are referred to as the ‘host’ (Chatti et al., 2005). Common gases/guests or also known as ‘hydrate formers’ are methane (C1), ethane (C2), propane (C3), n-butane (nC4), i-butane (iC4), hydrogen sulphide (H₂S), carbon dioxide (CO₂), and nitrogen (N₂). The encaging water molecules bond together via dispersion forces holding the cage structure in place although there are no chemical bonds between the host and guest molecules (Sloan Jr and Koh, 2007). Structures as such can store a significant

amount of gas resulting in upwards of 170 m³ of gas for every 1 m³ of hydrate that is formed (Sloan Jr and Koh, 2007).

1.2.1 Interest in Gas Hydrates

As of the early 19th century, interest in gas hydrate forming compounds was kick started with the chlorine hydrate finding made by Sir Humphrey (Davy, 1832). Since then various discoveries and developments in the chemical nature and properties of hydrates have been made. However, hydrate forming natural gas hydrocarbons was merely discovered towards the end of the century (Villard, 1888). Hydrates within nature, primarily in deep sea sediments and permafrost were discovered fairly recently (Makogon, 1965). These hydrates have been identified as a source of energy and thus, more research effort has been put into developing methods of extraction. On the other hand, with the rise in natural gas production, hydrates are found to be a hindrance to flow. While hydrate formation may serve beneficial in other areas like waste water and gas storage, they pose a serious flow assurance risk and thus, many studies have been conducted to understand hydrate kinetics, hydrate phase equilibria, and prevention techniques (Hammerschmidt, 1934; Sloan Jr and Koh, 2007). This heightened increase in research related to gas hydrates is demonstrated in Figure 1.1 (data attained from Web of Science for topic ‘Gas Hydrates’).

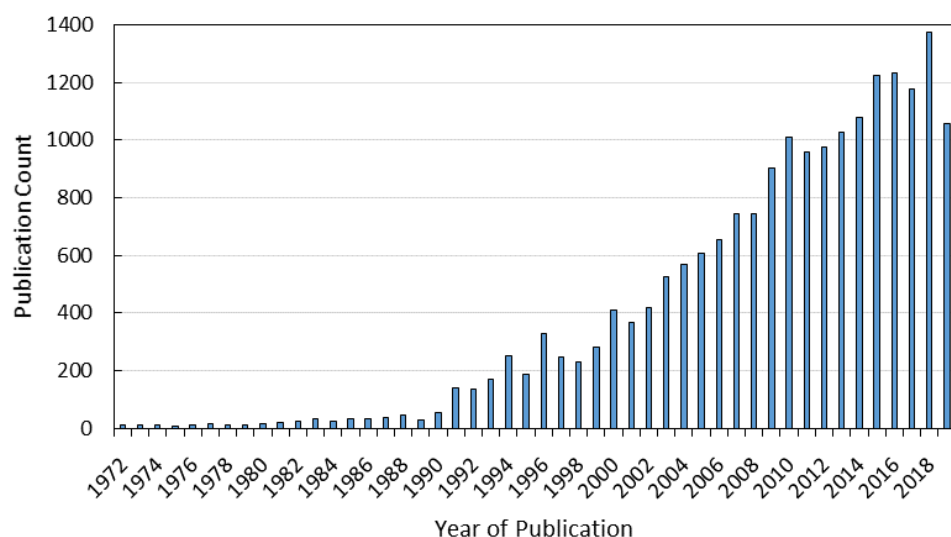


Figure 1.1: Publications related to gas hydrates from 1972 to 2019 (data attained from Web of Science).

1.2.2 Hydrate Structure and Physical Properties

Gas hydrates are essentially a lattice network formed by cages of water that encompass gas molecules like methane or ethane (Sloan Jr and Koh, 2007). The series of water cages are held together in place via the hydrogen bonding across molecules of water, whereby any one molecule either serves as an acceptor or donor of the bonds, subsequently a 3D network is formed (Kirchner et al., 2004). Water forms five different cage structures (polyhedra) as illustrated in Figure 1.2, where each cornice denotes a water molecule. The polyhedral nomenclature description as suggested by Jeffrey and McMullan (1967) is $n_i^{m_i}$, where i , n_i and m_i denote face type, quantity of edges, and quantity of faces respectively.

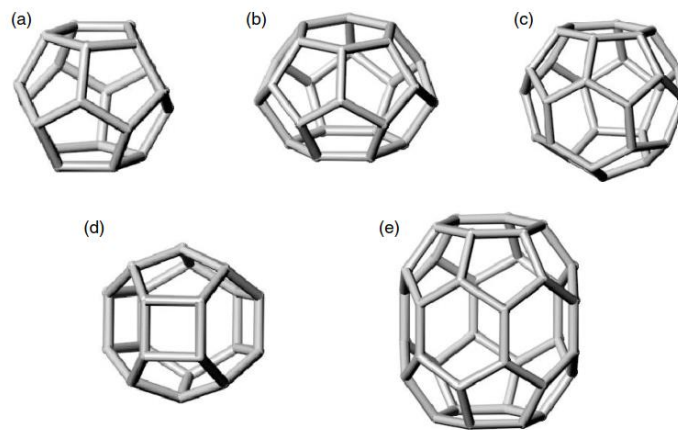


Figure 1.2: Cage shapes formed by water: a) 5^{12} (pentagonal dodecahedron), b) $5^{12}6^2$ (tetrakaidecahedron), c) $5^{12}6^4$ (hexakaidecahedron), d) $4^35^66^3$ (irregular dodecahedron) and, e) $5^{12}6^8$ (icosahedron) (after Sloan Jr and Koh, 2007).

While there is no chemical bonding amid the water and gaseous molecules, there are however, van der Waals forces (Kitaigorodsky, 1984). Such forces albeit weak, keep the hydrate structure intact. The cavities in gas hydrates are found to be expanded much more than that of ice which is in line with the finding of Rodger (1990), that the forces maintaining the structure are repulsive as opposed to attractive (Rodger, 1990).

Common gas hydrate structures are categorized into three different structures, sI (cubic), sII (cubic), and sH (hexagonal). The actual dimensions of the guest or 'trapped' molecules encapsulated within the water network lattice defines the hydrate structure. Figure 1.3 illustrates the varying gas hydrate structures resulting from numerous gas molecules (Giavarini and Hester, 2011). Methane and ethane guest

molecules amidst others that have a van der Waals diameter in the range of 4.2 to 6 Å will form hydrates of structure I. Hydrates of structure II are formed by guests such as propane and butane which have a diameter between 6 and 7 Å. While structure H hydrates are formed from bigger molecules such as pentane and neohexane which have a diameter in the range of 7 and 9 Å supplemented by smaller molecules (Ripmeester et al., 1987; Sloan Jr and Koh, 2007). Figure 1.4 illustrates how a basic water cage propagates into a gas hydrate structure. In this section gas hydrate structures and their properties are discussed.

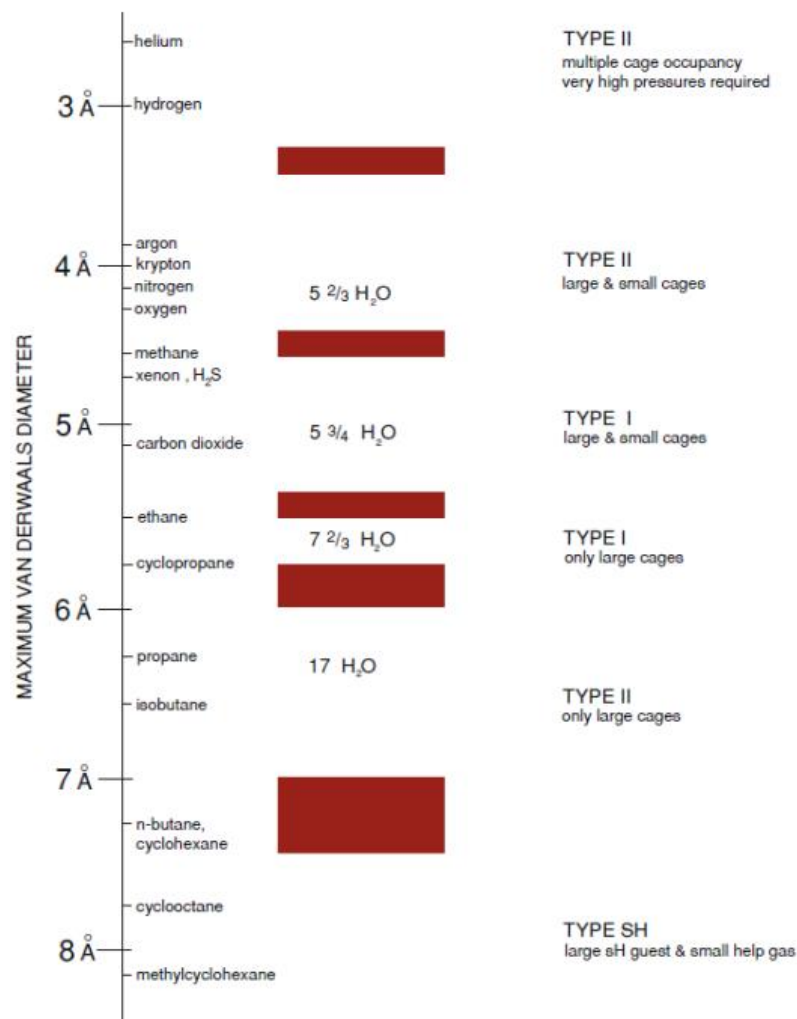


Figure 1.3: Resulting hydrate structure types based on hydrate formers (guest) size and number of occupied water cavities (after Giavarini et al., 2011).

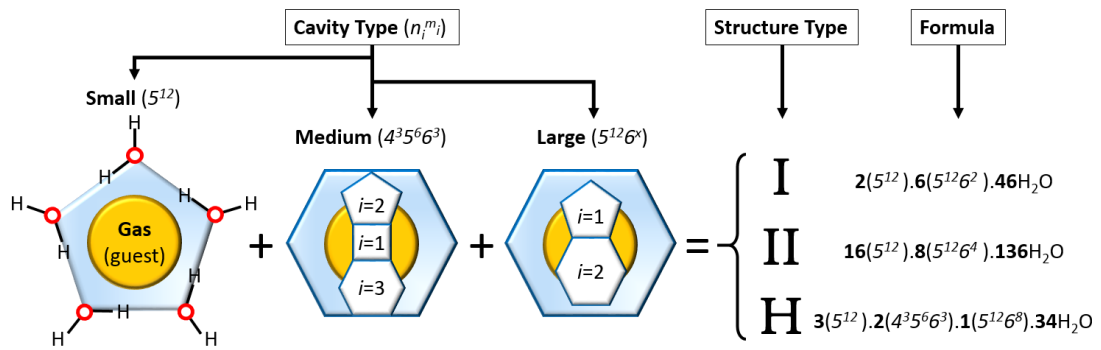


Figure 1.4: Hydrate structure and cavity types (where i , n_i and m_i denote face type, number of edges and number of faces respectively).

The sI hydrate structure comprises of two sizes or types of cavities. Figure 1.5(a) illustrates the typical sI hydrate, where the centrally located pentagonal dodecahedron (5^{12}) is encircled by 8 tetrakaidecahedra ($5^{12}6^2$). The packing within this structure is based on the linkage of vertices across the 5^{12} cavities, while there is no linkage of face planes amid the hedra. Moreover, the $5^{12}6^2$ cavities are arranged by the vertices in columns with the empty space in-between occupied by the 5^{12} cavities (Koh, 2002; Sloan Jr and Koh, 2007). Kirchner, 2004 developed a novel technique to support the first single-crystal diffraction studies of gas hydrates of the three structures. They showed the electron density maps to illustrate the occupancy of certain cages within the hydrate structures (Figure 1.5(b)).

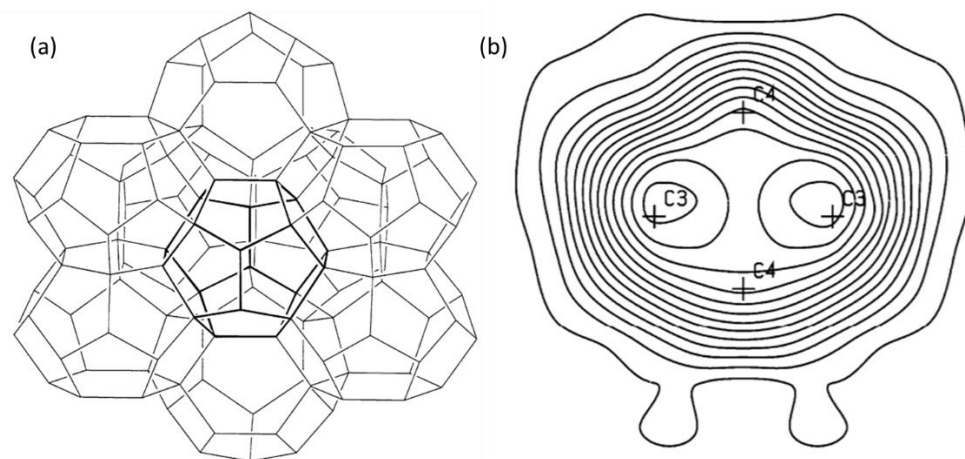


Figure 1.5: Cubic Structure I: (a) Packing of structure I hydrate, (b) Electron density map of tetrakaidecahedra cage (perpendicular to the plane of the hexagons) from the hydrate of acetylene (after Kirchner, 2004).

Similar to sI, the sII hydrate structure has two types of cavities. As depicted in Figure

1.6, a relatively small 5^{12} cavity is surrounded by a network of diamonds formed from hexakaidecahedra ($5^{12}6^4$) cavities of tetrahedral-symmetry. The packing within this structure is defined such that the 5^{12} cavities share faces in all dimensions while the space is occupied by bigger hexakaidecahedra types.

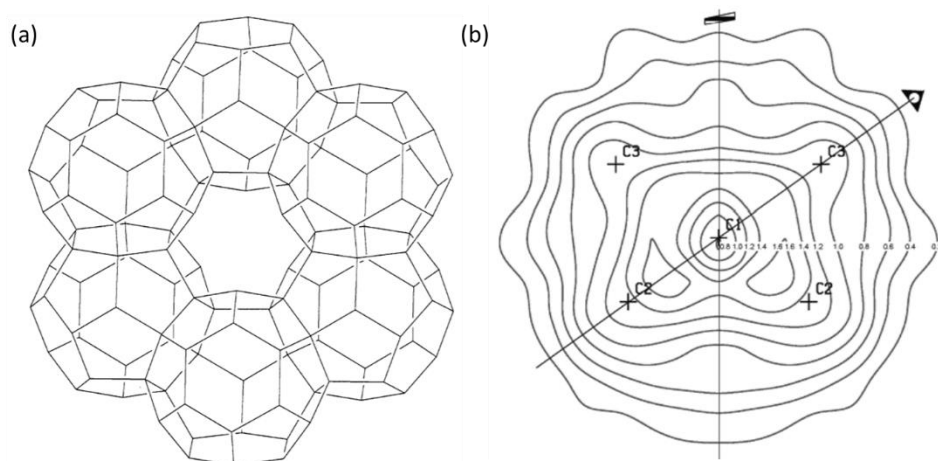


Figure 1.6: Cubic Structure II: (a) Packing of structure II hydrate, (b) Electron density map of hexakaidecahedral cage (within the plane of both symmetry axes) from the hydrate of propane (after Kirchner, 2004).

The sH hydrate structure is made up of three cavity types (Figure 1.7). It has a centrally located $5^{12}6^8$ (icosahedron) encircled by six $4^35^66^3$ (dodecahedra). The filling within this structure is via 2-dimensional sharing of faces, whereby smaller cavities (5^{12}) are filled in-between layers of larger cavities of the types $4^35^66^3$ and $5^{12}6^8$.

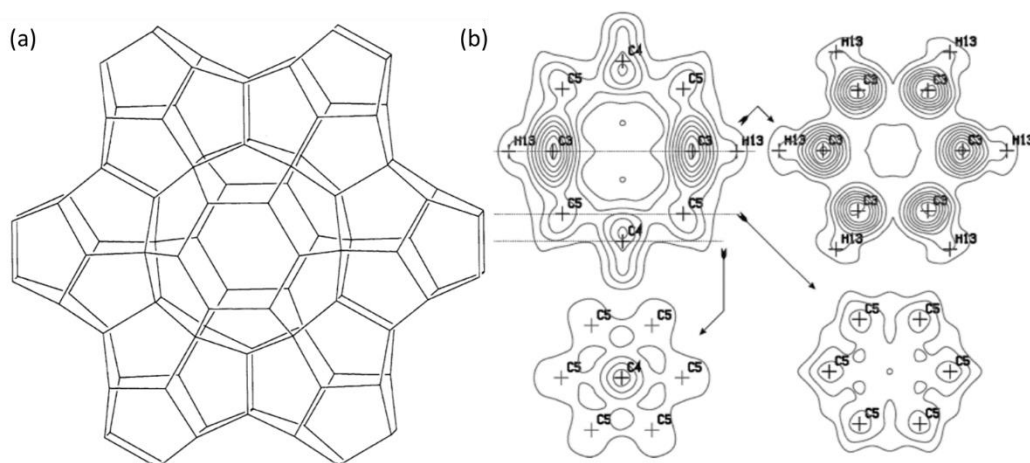


Figure 1.7: Hexagonal Structure sH: (a) Packing of structure sH hydrate, (b) Electron density map of icosahedral cage (top left is along the (1 2 1)-plane while others are

perpendicular to the 6-fold axis as shown) from the hydrate of adamantane and methane (after Kirchner, 2004).

1.2.3 Hydrate Formation and Dissociation Mechanism

The hydrate formation mechanism can be summarized by two major phases; the phase of nucleation followed by the growth phase. Nucleation phase is a stochastic process that can be compared to other growth scenarios involving crystalline growth like that of salt precipitation (Sloan Jr and Koh, 2007). A vital aspect of these scenarios is that of supersaturation, whereby the solvent comprises a larger quantity of dissolved solute than it can ordinarily hold at a certain temperature. The driving force for hydrate nucleation was identified by Christiansen and Sloan in 1995, to be the total molar variation in the Gibbs free-energy (Christiansen and Sloan, 1995). Nucleation has two types; heterogeneous nucleation (HEN) and homogeneous nucleation (HON), where the difference lies in the existence or absence of impurities (Sloan Jr and Koh, 2007). HEN takes place in the existence of an interface or foreign body (Kashchiev and Firoozabadi, 2002; Sloan Jr and Koh, 2007). HON is a rare type which involves a series of bimolecular collisions leading to sequential cluster formation. Only once the cluster attains a critical size then sustainable and monotonic growth will occur. Prior to this stage, the clusters within the metastable/bulk fluid shrink and grow (Sloan Jr and Koh, 2007). The higher prospect to occur in HEN as compared with HON is described as the reduction of energy and work required due to the solid surface so that nucleation can happen (Kashchiev and Firoozabadi, 2002).

Long and Sloan (1996) undertook experiments and found that nucleation of hydrates occurred at the interface of hydrocarbon and water (Long and Sloan, 1996). Other researchers established this phenomenon for hydrates of methane and carbon dioxide (Fujioka et al., 1994; Huo et al., 2001; Kimuro et al., 1993; Mori, 1998; Østergaard et al., 2001). Molecular Dynamic simulations has confirmed that nucleation sites are existing at areas of substantial concentration gradient (Moon et al., 2003). Moreover, the water-hydrocarbon interface where nucleation plus growth happen is specifically a vapor-liquid interface consisting of a thin layer on both sides of this interface, although occurrence at other combinations of phases is also possible (Kashchiev and Firoozabadi, 2002). Two leading reasons are given for why nucleation at the interface tends to occur is due to the reduction of the Gibbs free-energy association by the

interface, and the natural presence of higher molecule concentration of the host and guests at the interface (Sloan Jr and Koh, 2007).

There exist two theories to explain the mechanism for the nucleation of hydrates: labile clustering and local structuring. Labile clustering involves labile clusters and is considered as the earliest mechanism, where labile clusters are defined as units that are unstable and can undergo change. The theory suggests that labile clusters agglomerate on any side of the vapour-water interfaces resulting in nucleation (Koh, 2002; Sloan Jr and Koh, 2007). An overview of labile clustering mechanism is given in Figure 1.8 and Figure 1.9. A local structuring theory was developed at the onset of the discovery of the thermodynamic nature of labile clusters to disintegrate as opposed to agglomerate during hydrate experiments involving carbon dioxide (Radhakrishnan and Trout, 2002). The theory of local structuring begins with the ordering of guest and water molecules locally in contrast to discrete clusters (Sloan Jr and Koh, 2007).

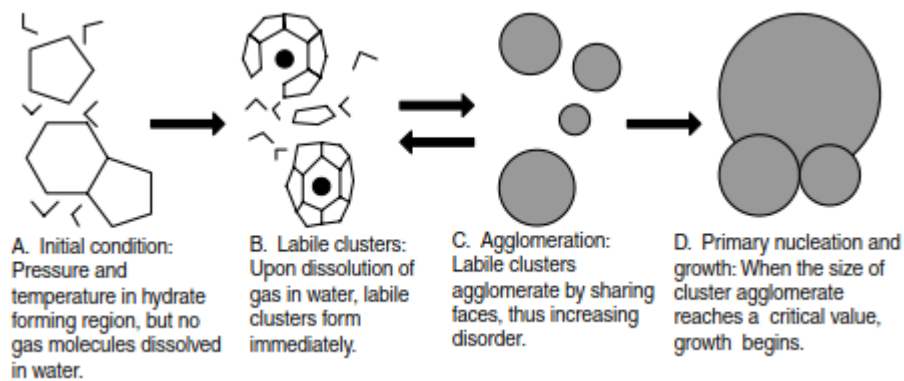


Figure 1.8: Summary of the labile clustering mechanism (after Sloan Jr and Koh, 2007).

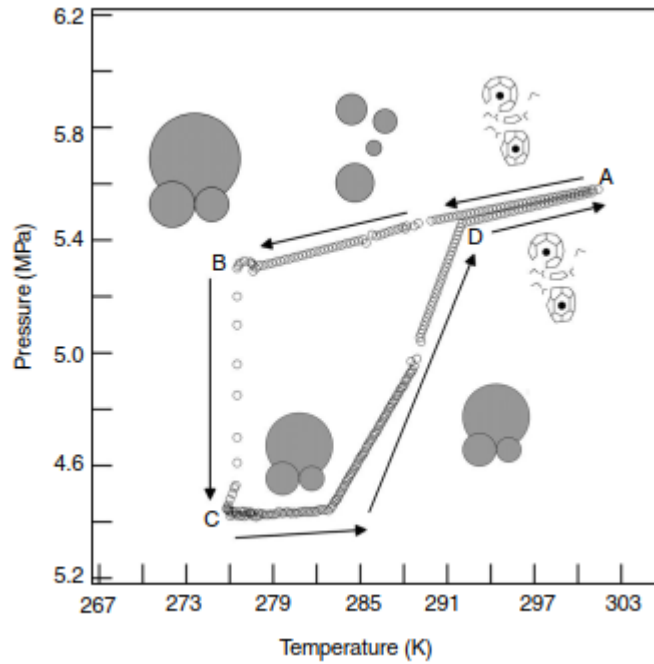


Figure 1.9: Labile cluster growth enacted on a pressure and temperature trace (after Sloan Jr and Koh, 2007).

Gas hydrates develop under specific circumstances; high pressure (typically 25 to 110 bar) and low temperature in the range of ~ 2 to 12 $^{\circ}\text{C}$ (Koh, 2002). Figure 1.10(a) and (b) demonstrate the key relationships of hydrate formation such as the pressure/temperature data and the gas consumption rate. The three stages pertinent to hydrate formation such as nucleation, growth and dissociation are shown in the pressure/temperature curve. Point A denotes the opening pressure and temperature which are within the hydrate-free region. While point B is within the hydrate-formation region. With the decrease in temperature to that of point B, gas hydrate formation will commence until the conditions of point C are attained which is where the critical size of hydrate exists. With the application of heat at point C, the dissociation of hydrate will commence, and in due course intersect the initial path of cooling (as denoted by points A to B). This juncture point is considered as the dissociation pressure and temperature or the hydrate equilibrium point. In terms of the gas consumption rate, it can be seen to initiate at a slow pace but quickly increase through the stage of growth, after which it begins to plateau out as the critical hydrate size is reached (Figure 1.10(a)).

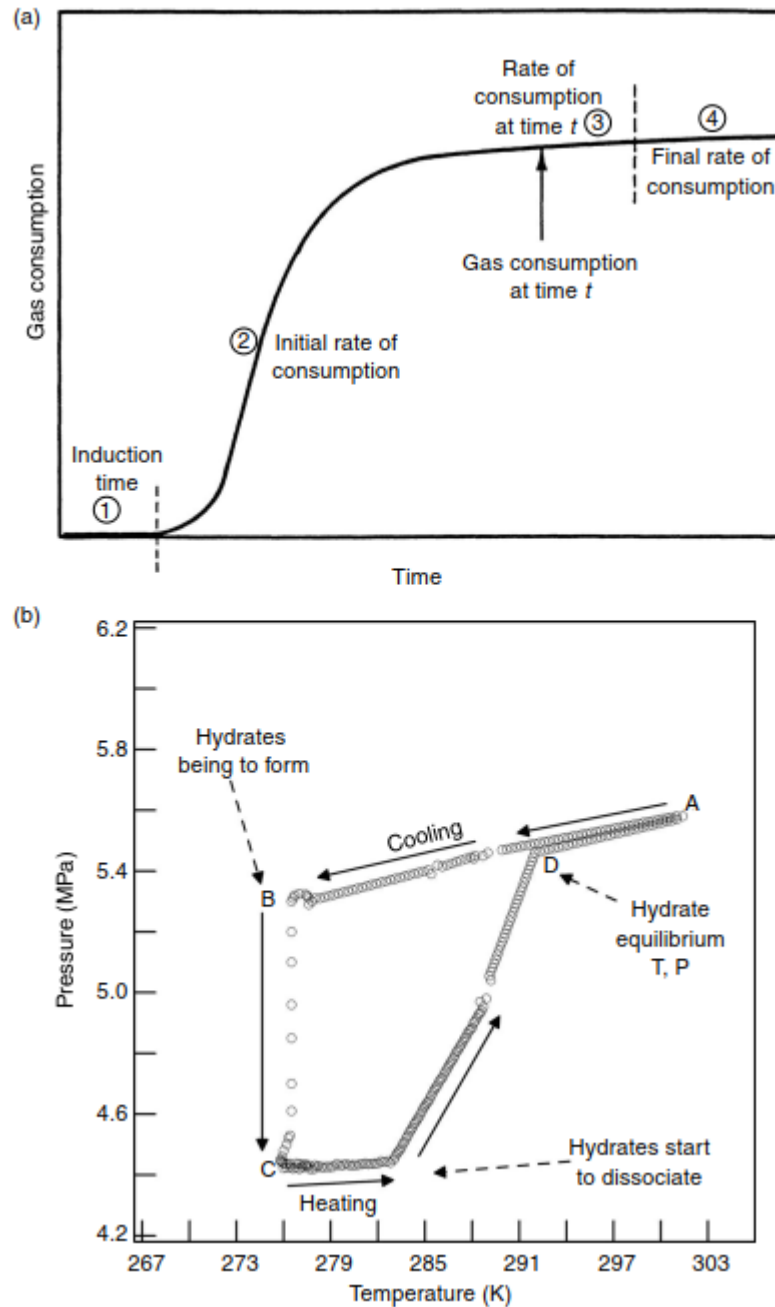


Figure 1.10: a) Formation of hydrate: consumption of gas vs time, b) Pressure and temperature trace for methane hydrate (after Sloan Jr and Koh, 2007).

The growth of hydrates can be likened to crystal growth which is affected by multiple factors. These factors include the transfer of molecular mass to the crystal, the transfer of heat from the exothermic reaction involving hydration from the growing crystal, and the kinetics of the hydrate crystal growth (Sloan Jr and Koh, 2007). Crystal growth correlations are grounded upon each of the above factors as the growth limiting factor (Malegaonkar et al., 1997; Skovborg and Rasmussen, 1994; Uchida et al., 1999). The

processes of crystal growth are four: single crystal, hydrate film, multiple crystal, and metastable phase growth. These processes are described below:

- Growth of a single crystal is convenient for the analysis of the hydrate crystalline structure utilizing neutron diffraction and X-ray methods (Udachin et al., 2001). This type of growth occurs mainly under lower driving forces and easier to attain for hydrates of ethylene oxide and tetrahydrofuran as compared to gas hydrates (Makogon et al., 1997).
- Hydrate film growing at the water-hydrocarbon boundary allows for studying growth models and mechanisms (Smelik and King, 2015; Taylor, 2007).
- Growth of multiple crystals facilitated by agitation is convenient for studying gas consumption during growth and determining hydrate kinetics (Bansal, 1994; Skovborg et al., 1993; Turner, 2005).
- Growth of metastable phases during hydrate growth provides valuable insights into the structural and thermodynamic changes in hydrates. The process can be achieved through employing Nuclear magnetic resonance (NMR) or X-ray diffraction and Raman spectroscopy (Sloan Jr and Koh, 2007).

The gas hydrate dissociation is an endothermic process such that energy is essential to separate the hydrogen bonding among water molecules, and the weak van der Waals forces across the water and gaseous molecules. This will begin to separate the crystal network lattice into smaller constituents (Sloan Jr and Koh, 2007). Some methods to dissociate hydrate plugs are thermal stimulation, de-pressurization, and treatment with a chemical inhibitor (Davies et al., 2006; Peters et al., 2000; Sloan Jr and Koh, 2007). An important aspect of gas hydrate prevention and control within process equipment and gas pipelines is thoroughly understanding equilibrium conditions and dissociation of gas hydrates (Li et al., 2006). In the case of thermal stimulation, the hydrate solid phase begins to break down producing tiny cavities allowing pockets of gas to be released while their corresponding host water molecules form a thin liquid film. This eventuates until the hydrate structure is completely transformed into the liquid phase (Smith et al., 2015).

1.2.4 Hydrate Phase Equilibria Modelling

Understanding the thermodynamics of gas hydrates will allow for prediction of hydrate formation conditions (Zelevinsky et al., 1999). Numerous methods and models incorporating equation of states and thermodynamics have been suggested in literature, but all have a degree of uncertainty, especially at high pressure ranges (Saeedi Dehaghani and Badizad, 2017). In the early 1950s, the water clathrate crystal structures and properties were determined (Barrer and Stuart, 1957), after which more rigorous predictions could be conceptualized for the equilibria of macroscopic properties based on the microscopic properties. It was recognized that hydrates have discrete cavities which enclose at least one guest particle. This allowed for statistical means to be used to depict the distribution of guest particles within the hydrate structure (Sloan Jr and Koh, 2007).

An initial statistical thermodynamic model was developed by Barrer and Stuart in 1957, to predict the properties of clathrate phases of water (Barrer and Stuart, 1957). In 1958, van der Waals and Platteeuw developed the initial well-based thermodynamic study to determine the hydrate equilibrium conditions. They used a partition function to illustrate the stability of the clathrate complex (Platteeuw and Waals, 1958).

A method with high accuracy was founded by van der Waals and Platteeuw in the year 1959. The van der Waals and Platteeuw (vdW-P) model derives the gas hydrate thermodynamic properties utilizing a simple statistics-based method, which assumes that a sphere-shaped cage formed by water molecules entrapping a gaseous molecule. The vdW-P model is comparable to the model of Langmuir for gas adsorption, where it is assumed that the encaged gas molecule's internal partition functions are equivalent to that of an ideal gas (Parrish and Prausnitz, 1972). The model predicts pressure and temperature by means of microscopic properties (i.e., intermolecular potentials). The affinity due to the occupation of a lattice cavity by a gas molecule is described by Langmuir constants (Lee and Holder, 2002). Langmuir constants are obtained by applying the cell theory of Lennard-Jones-Devonshire accounting for the interactions across the surrounding water molecules and the trapped gas molecule (Sloan Jr and Koh, 2007). vdW-P assumes that the hydrate cavities can only occupy a single gas (guest) compound whereby the trapped molecules are sufficiently small and will not distort the cavity structure, interactions between trapped molecules are negligible and

the cell potential is spherical symmetry (Van der Waals, 1959). The model acts as a reasonable compromise concerning accuracy and simplicity for the calculation of hydrate forming conditions. However, it has limitations in many practical applications due to its assumptions (Martin 2010).

McKoy and Sinanoglu (1963) further developed the vdW-P model, by using various intermolecular potentials, such as the Kihara potential instead of Lennard-Jones. They determined the pressure of hydrate dissociation for polyatomic gases and compared it to experimental data. The results based on Kihara potentials were more accurate than both the Lennard-Jones 12-6 and 28-7 potentials (McKoy and Sinanoğlu, 1963). The 28-7 potential gave the least satisfactory agreement with experimental data, and the 12-6 gave satisfactory results for molecules of monoatomic gases and CH₄ (Byk and Fomina, 1968). The Kihara core potential was deemed better at predicting the dissociation pressures of non-spherical, rodlike molecules (McKoy and Sinanoğlu, 1963), and thus the use of Kihara potentials have been predominate until now (Dehaghani and Karami, 2018). Child (1964) performed similar work to McKoy and Sinanoglu using the Kihara potential (Child, 1964; Sloan Jr and Koh, 2007). Nagata and Kobayashi (1966) also determined the Kihara potential to be superior to Lennard-Jones for predicting the dissociation pressures for methane and nitrogen hydrates, taking into consideration the shape and size of the encaged molecule, as well as assuming that trapped molecules rotate freely within the cavity (Nagata and Kobayashi, 1966).

Subsequently, Parrish and Prausnitz (1972) generalized vdW-P to create a systematic approach for the calculation of hydrate-gas equilibrium conditions within multi-component systems (Lee and Holder, 2002; Parrish and Prausnitz, 1972). The vdW-P theory was applied to all natural gases and mixed hydrates, including combinations of hydrate formers and non-hydrate formers, using the Kihara (spherical core) potential. Satisfactory agreement was found between predicted and experimental dissociation pressures (Parrish and Prausnitz, 1972). John and co-workers (1985) amended vdW-P by addressing deviation in Langmuir constants from ideal (smooth cell) values by developing a corresponding states prediction relationship (John et al., 1985). This paved the way for Kihara parameters to be attained through virial coefficient data (which describes guest-host interaction) rather than using the potential parameters

from experimental “fitting” parameters (Lee and Holder, 2002).

A further modification of the vdW-P model was given by Zele and co-workers (1999), who theorized that guest molecules may affect the host to host interactions in the crystal lattice, which opposes an assumption of vdW-P (Lee and Holder, 2002). They performed a series of molecular dynamic simulations to analyze the effect of guest size upon the lattice structure. They concluded that the stretching of the lattice owing to the existence of guest molecules may have a substantial effect upon the thermodynamic parameters of hydrate equilibrium. Consequently, they developed a thermodynamic model that considers the stretching of the lattice owing to the guest molecule size to improve the original assumptions in the vdW-P model. The model uses a reference chemical potential to determine the guest-dependent difference and is suitable for calculating hydrate equilibria for single and multi-component gases (Zele et al., 1999). In a different work, Lee and Holder (2002) developed a model from the work by Holder and John (1985) which also considers the distortion of the lattice by engaged guest molecules. A guest-dependant chemical potential difference was used with Kihara parameters from virial coefficient data to predict the equilibrium hydrate conditions for various hydrate-forming species (Lee and Holder, 2002).

Ballard and Sloan (2002) extended an existing hydrate fugacity model vdW-P, which used statistical thermodynamics (Van der Waals, 1959) alongside classical thermodynamics (Parrish and Prausnitz, 1972). Predictions made by the existing model were accurate at moderate temperatures and pressures, yet large deviations were found to exist at higher pressures ($P > 200$ bar). This implied that the definition of the standard hydrate state or empty lattice required work. Alterations were formulated to better describe the standard hydrate state and by establishing an activity coefficient from the exact volume of hydrate (Ballard and Sloan Jr, 2002).

More recently, modern correction methods of vdW-P attempt to rectify its inaccuracies at high pressures. *ab initio* quantum mechanical corrections are often implemented to determine potentials amongst molecules and atoms in hydrates (Sloan Jr and Koh, 2007). Cao et al. (2002), Klauda and Sandler (2003) and Anderson et al. (2005) did significant works on this topic (Anderson et al., 2005; Cao et al., 2002; Klauda and Sandler, 2003). A fugacity-based method was developed by Klauda and Sandler instead of using chemical potential to model hydrate phase behaviour (Klauda and

Sandler, 2003). Bandyopadhyay and Kluda improved the model based on fugacity in 2011 to use the Predictive Soave-Redlich-Kwong (PSRK) equation for defining those phases which are in equilibrium with hydrates (Bandyopadhyay and Kluda, 2011). Another modern method is the process of matching existing phase equilibria (macroscopic) and spectroscopic (microscopic) data to an improved vdW-P theory (Sloan Jr and Koh, 2007).

Of late, Hsieh et al. (2012) proposed a new pressure-temperature dependant Langmuir absorption constant, calculated by applying the square-well (SW) potential. A disadvantage of using the SW cell-potential over the more complicated cell potentials such as Lennard-Jones and Kihara is its inability to represent guest-water interaction in a wide range of conditions. Hsieh et al. (2012) compensated for this by using an empirical expression to consider the compression and distortion of the lattice in the free volume of the guest at increased pressures (Hsieh et al., 2012). Chin et al. (2013) stretched the work of Hsieh et al., by proposing a model which can be used for hydrates of natural or synthetic gas with numerous additives, including electrolytes and organic inhibitors (Chin et al., 2013).

Although there is a strong agreement of the reliability of vdW-P model, there is disagreement when it comes to choosing a model for determining the equilibrium state of the fluid phases. To take into account the equilibrium of coexisting fluid phases, several predictions have been developed to supplement the vdW-P model with proper EoS and / or activity coefficients. Youssef, et al. (2010) used vdW-P linked with the Cubic Plus Association (CPA) equation of state to calculate phase equilibria for systems void of an aqueous phase (Youssef et al., 2010). The Electrolyte Cubic Square-Well (eCSW) equation of state joined with vdW-P, was used by Haghtalab et al. (2012) to calculate the hydrate equilibrium conditions for numerous gases from methane to i-butane, nitrogen, and carbon dioxide. The eCSW equation of state comprises of two electrolyte terms and one non-electrolyte term, and is developed from the molar residual Helmholtz free energy (Haghtalab et al., 2012). In another study, Khosravani and Varaminian (2012) used Soave-Redlich-Kwong (SRK) and Valderrama variation of Patel-Teja (VPT) with CPA equation of state for modelling the liquid and vapour phases, in conjunction with vdW-P statistical method for the hydrate phase. They optimized the predictions of the Kihara potential and binary

interaction parameters by using two-phase equilibria data (V-L_w-H) (Karamoddin and Varaminian, 2013). Recently, El Meragawi, et al. (2016) used the Peng-Robinson (PR) equation of state with the Perturbed-Chain Statistical Associating Fluid Theory (PC-SAFT) along with vdW-P. Experimental data was utilized to optimize the parameters of the Kihara potential for increasing the degree of accurateness in calculating the hydrate equilibrium pressure. The outcome of this study was the decision that the PR model produced improved prediction performance (El Meragawi et al., 2016).

Following the development of hydrate formation thermodynamic models, computer simulation software were established for the calculation of hydrate phase equilibria. For example, Bishnoi et al. (1989) extended vdW-P model to flash programs (Bishnoi et al., 1989). These prediction software serve as powerful tools when investigating the hydrate phenomena. There are a number of commercial hydrate prediction programs available to date, such as CSMGEM, Multiflash, PVTsim and HYSYS (Ballard and Sloan, 2004; Khan et al., 2018). Accurate predictions of hydrate phase behaviour are essential to both the design and operation of natural gas processing facilities (Khan et al., 2018).

1.2.5 Hydrate Inhibition

Given the grave risks of hydrate formation within gas production and transportation, substantial research has been focused on the testing, development and application of innovative methods for gas hydrate inhibition (Cha et al., 2013; Heidaryan et al., 2010; Kelland, 2006). Adopting operating conditions such as low temperatures or high flowrates to avoid the hydrate formation region (as indicated in a typical pressure-temperature diagram) is often unfeasible, hence other hydrate prevention methods are required to be applied (Son and Wallace, 2000).

Typical hydrate control and prevention methods may include dehydration whereby water is removed from the production fluid, and injecting chemical hydrate inhibiting agents like monoethylene glycol (MEG) or methanol (Brustad et al., 2005; Son and Wallace, 2000). Since water is a key requirement for hydrate formation, eliminating it decreases hydrate formation risk. The dehydration method is highly popular and an economical approach in predominantly wet gas production fields due to the large quantity of inhibitor would otherwise be required. While for many fields where the

water production rate is variable, the injection of hydrate inhibitors seems more economical and practical. The two major classifications of hydrate inhibitors are known as thermodynamic hydrate inhibitors (THI) and low dosage hydrate inhibitors (LDHI).

There are two primary types of THI, which are glycols and alcohols. The central principle owing to their capability of hydrate inhibition is the change in the hydrate phase boundary or equilibrium conditions to an extent whereby process operating conditions can be made to become within a hydrate-free area (Grzelak and Stenhaug, 2016). Glycols and alcohols such as methanol and MEG comprise of hydroxyl groups that strive for hydrogen bonding between molecules of water. This in turn, limits the water-water bonding that can entrap gas molecules thus limiting the formation of hydrate structures (Kvamme et al., 2005). The performance of various THIs can be assessed through the capacity at which the chemical can decrease the hydrate equilibrium point (Kelland et al., 2000).

The idea of LDHIs was born out of the discovery that certain fish avoided freezing in sub-zero temperatures due to the secretion of a protein that stopped ice formation (Franks et al., 1987; Knott, 2001; Mehta et al., 2002). LDHIs are classified into two types: kinetic hydrate inhibitor (KHI) and anti-agglomerate (AA). KHIs are utilized in very small dosages (0.5 to 2 wt%) as opposed to THIs, and typically comprise of water soluble polymers (Kelland, 2006; Sloan Jr and Koh, 2007). They affect the time dependent processes of hydrate formation such as nucleation and growth (Grzelak and Stenhaug, 2016). AAs deter the advanced growth of hydrate nuclei by stopping the combining of hydrate structures. Although, they don't prevent the initial hydrate formation and growth, they can however, prevent hydrate structures from plugging a pipeline (Mehta et al., 2002).

There are several major methods to remediate gas hydrate plugs within pipelines (Sloan Jr and Koh, 2007). These methods include:

- i. Depressurization – this method can be considered as the most practical, common, and safest (Peters et al., 2000; Sloan Jr and Koh, 2007). The method works by reducing the pressure of the pipeline such that the hydrate phase equilibrium boundary is shifted thereby reducing the hydrate dissociation

temperature allowing for heat transfer radially and subsequent dissociation of the hydrate solid (Carson and Katz, 1942). Certain pipeline bathymetry can render this method useless due to the liquid head being greater than the hydrate plug dissociation pressure (Sloan Jr and Koh, 2007). A safe application of this method shall apply depressurization to both sides of the hydrate plug to reduce the risk of a dangerous projectile and pipeline rupture as illustrated in Figure 1.11 (Davies et al., 2006; Peters et al., 2000; Sloan Jr and Koh, 2007).

- ii. Thermal Stimulation – if depressurization method is inadequate for dissociating the hydrate plug, then direct heating to the pipeline can be applied (Davies et al., 2006). The method may be applied to avert hydrate formation from occurring in the first place by sustaining higher pipeline temperature than the formation temperature of gas hydrate (Loken et al., 1998; Urdahl et al., 2003). As the plug dissociates, trapped gas is released which increases the pressure, and thus, to avoid the risk of over-pressurization, gas should be vented appropriately (Davies et al., 2006; Koh et al., 2011).
- iii. Chemical Injection – injecting chemicals that produce heat from reaction or hydrate inhibitors (Freitas et al., 2002; Sloan Jr and Koh, 2007). Anti-agglomerates, for instance, work to stop the agglomeration of hydrate solids to form plugs while allowing fluid to flow (Koh et al., 2011).
- iv. Mechanical – if accessible, mechanically breaking up the hydrate plug by drilling or other means (Koh et al., 2011; Sloan Jr and Koh, 2007).

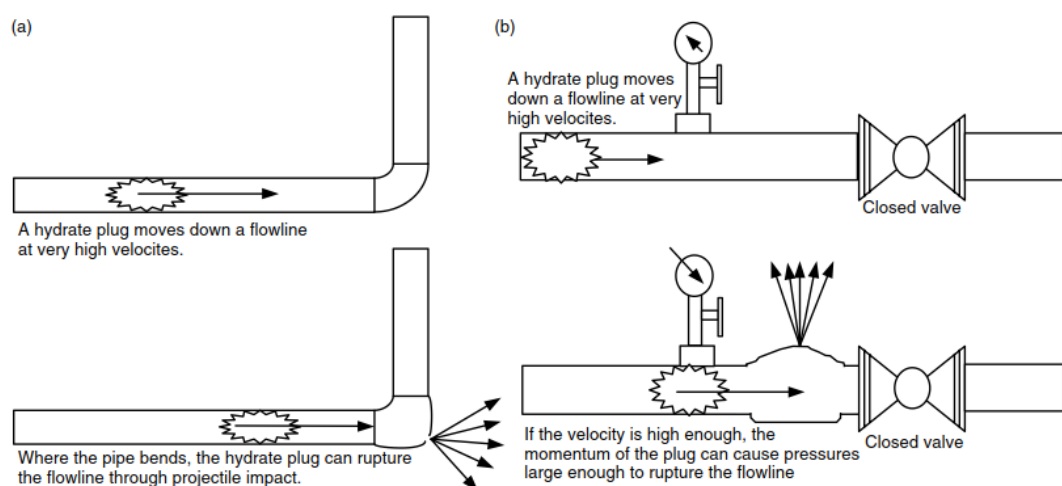


Figure 1.11: The two means by which a hydrate solid can cause pipeline rupture: (a) high velocity and momentum impact at bend, and (b) momentum impact combined with gas compression pipe obstruction (after Sloan 2007).

1.2.6 Regeneration and Reclamation of MEG

MEG is currently preferred in the industry as opposed to other inhibitors like methanol. This preference of MEG is expressed through the numerous projects using MEG worldwide including Gorgon and Wheatstone of Chevron, Australia; Britannia Satellites of ConocoPhillips, UK; Ormen Lange of Norsk Hydro, Norway; and South Pars of Total, Iran (Brustad et al., 2005). MEG is favoured over methanol due to the following reasons:

- Stability of MEG is due to its high boiling and flash points of 198 °C and 110 °C respectively, hence the loss to the vapour phase is minimal (Blackman and Gahan, 2014; Brustad et al., 2005).
- Methanol has high flammability (11 °C) and burns with an invisible flame making it difficult to detect its fire (Brustad et al., 2005). While MEG is non-flammable, and thus is preferred due to the additional safety in handling, storage, and transport (AlHarooni et al., 2015).
- MEG has a lower environmental impact than MeOH (Brustad et al., 2005; Chapoy and Tohidi, 2012).
- MEG solubility in final hydrocarbon products is much lower than Methanol and thus avoids hefty financial penalties (Nazzar and Keogh, 2006).
- Recyclability of MEG is achievable with high efficiency (Chapoy and Tohidi, 2012).

The recovery and subsequent re-use of MEG is essential to sustain an economical and environmentally friendly process since high MEG injection rates are needed for adequate hydrate control (Teixeira et al., 2015). The recovery of MEG for gas hydrate inhibition is a complex subject, and has recently been applied within the industry. Advances in the regeneration and reclamation of MEG were slow due to the wide use of methanol as an inhibitor for hydrate prevention (Son and Wallace, 2000). Throughout this time and till the 1990s, typical regeneration of MEG through re-concentration was most commonly applied (Nazzar and Keogh, 2006). Formation

water served as a major challenge owing to the damaging consequences on the regeneration units ranging from intense salt and scale deposition, and fouling of the reboiler (Nazzari and Keogh, 2006; Teixeira et al., 2015). Serious fouling due to suspended solids and build-up of precipitation from salts found in the injected chemicals and formation water, may all result in production down-time, failure of equipment, safety concerns, and other losses (Latta et al., 2013).

The variation in the boiling points of MEG and water serve a vital role in the separation of these components via distillation. MEG and water have a boiling point of 198 °C and 100 °C at atmospheric pressure respectively (Blackman and Gahan, 2014). Three common options exist for MEG recovery as outlined below (Brustad et al., 2005):

1. Re-concentration or Regeneration whereby water is removed from MEG laden with production water (rich-MEG) via a reboiler and distillation column. The process is conducted in atmospheric conditions, and the water is boiled off until a desired MEG concentration is achieved (typically 80-90 wt%). A limitation of this option is the lack of removal of non-volatile chemicals and high soluble salts such as those found in production fluids and pipeline corrosion by-products (Teixeira et al., 2015). Regeneration is suitable in cases where these chemicals are within the allowable tolerance. However, it cannot be applied in fields where formation water is being produced, due to the heightened risks of corrosion (Brustad et al., 2005).
2. Partial reclamation whereby a slip-stream of the regenerated MEG is routed to a reclamation unit to maintain the total contaminant and salt levels within the allowable tolerance. This option is cost effective but also advantageous since non-volatile components are not fully removed such as precious chemical additives like pH stabilizers or corrosion inhibitors which can be re-used in the MEG loop (Brustad et al., 2005; Teixeira et al., 2015).
3. Complete reclamation whereby the rich MEG stream is flashed in a vacuum separator removing non-volatile chemicals and high-soluble monovalent salts as waste. This option is generally applied where high production of formation water is expected. The resulting MEG-water mixture undergoes regeneration such that the MEG concentration is at the desirable limit (Brustad et al., 2005; Teixeira et al., 2015).

1.2.7 Degradation of MEG

Throughout the process of MEG recovery, the MEG may undergo numerous cycles of high-heat processes. Under these conditions, MEG may degrade and lose its ability to inhibit gas hydrates. There are three types of MEG degradation that have been identified in literature, as follows:

- Biodegradation of MEG may occur at certain river temperatures and the type of bacteria present (Dwyer and Tiedje, 1983; Evans and David, 1974).
- Oxidative degradation of MEG whereby MEG experiences high temperature in the presence of air/oxygen (Brown et al., 1986; Brustad et al., 2005; Clifton et al., 1985; Ezrin et al., 2000; Latta et al., 2016; Monticelli et al., 1988; Rossiter et al., 1985, 1983).
- Thermal degradation of MEG is the chemical decomposition of MEG into various organic acids when it is heated more than it can sustain (AlHarooni et al., 2017, 2015; AlHarooni et al., 2016; Jordan et al., 2005; Madera et al., 2003; McGinnis et al., 2000; Nazzer and Keogh, 2006; Psarrou et al., 2011; Ranjbar and Abasi, 2013; Rudenko et al., 1997; Teixeira et al., 2015; Yong and Obanijesu, 2015).

1.3 Significance and Research Gap

Despite MEG serving as a hydrate inhibitor in the face of a serious ongoing flow assurance challenge, there exists a large deficiency of empirical and theoretical data to cover the hydrate kinetics of MEG degradation samples. MEG degradation can drive operational costs as well as leave operators in a blind-zone where the perceived impact of MEG on gas hydrate formation is higher than the actual or real impact it will produce. Thus, to fill this research gap, in this study, thorough experimentation was conducted to develop the hydrate phase equilibria of these much-needed solutions (Chapter 2). Since MEG degradation is a new area, in this study, various innovative techniques and experimental apparatuses were developed such as the innovative MEG pilot plant situated in the Curtin Corrosion Engineering Industry Centre (Figure 1.12), MEG reclamation unit (Figure 1.13) and high pressure PVT cell (Figure 1.14) as employed in all Chapters, and published in Chapter 10. Moreover, novel empirical predictive models were developed to provide predictions of degraded and non-

degraded, regenerated and non-regenerated, corrosion inhibitor presence or absence in MEG solutions (Chapter 2 and Chapter 7).

Research effort in the field of MEG regeneration and reclamation has been focused mainly on the identification of by-products and overall system design (Brustad et al., 2005; Madera et al., 2003; Montazaud, 2011; Nazzari and Keogh, 2006; Teixeira et al., 2015). However, the reclamation system design needs more work especially when formation water breakthrough occurs in the life of the well. It may become highly risky to continue with the same corrosion control method, and thus, a switchover is required. It is at this time that numerous design considerations will fail to deliver due to the contrasting changes the system will experience such as the change in pH and/or the removal of specific chemicals. Thus, to fill this research gap, in this study, thorough field-like MEG regeneration and reclamation experimentation were conducted to mimic methods of corrosion control switchover (Chapter 3 and 4). The study gave insights and established a way to diagnose the operating pH at various stages of the process and how it can be modified to ensure expected objectives are met. The effect of chemical removal and preservation was investigated in the reclamation unit. The fouling tendency or viscosity of chemical accumulation in the reclamation unit was evaluated. Moreover, gas hydrate testing was conducted at key stages of the process to produce hydrate phase equilibria and metastable regions for understanding the kinetics of natural gas hydrates. An additional study was conducted at a higher thermal exposure of MEG with salt content to investigate the impact on hydrate formation.

MDEA is a key amine used in the gas processing industry as well as a pH stabilizer as part of a corrosion control method. This chemical has not been adequately considered in terms of its impact on the overall hydrate control program. The inhibitory effect of MDEA on gas hydrate formation was recently identified albeit at low pressures. Thus, in this work, the inhibitory effect was studied at higher pressures, producing valuable hydrate phase equilibria upon which a much-needed empirical model and algorithm for prediction was developed (Chapter 5). Moreover, additional research was conducted to develop a thermodynamic model to cater for MDEA which can be employed in hydrate prediction software (Chapter 6). These are a great contribution to the flow assurance research community and field operators since prediction tools, as such, are non-existent currently, nor are there any prediction software which considers

the inhibition effect of MDEA.

Similarly, numerous other chemical additives like film forming corrosion inhibitor, oxygen scavengers, scale inhibitors, and amines were investigated to understand their impact on formation of gas hydrate in the presence and absence of MEG (Chapters 7-9). Dissolved oxygen levels are cautiously kept to a minimum due to the posing corrosion risks, however there exists no research that delves into how it could impact the hydrate inhibitory performance of MEG or the potential MEG degradation it can cause (Brustad et al., 2005; Lehmann et al., 2016, 2014; Teixeira et al., 2015). In this study, the impact of dissolved oxygen on gas hydrate formation was studied (Chapter 8). Additionally, the impact of MDEA and FFCI was studied alongside a KHI using the isothermal method (Chapter 7), since the use of KHIs are steadily becoming popular in the industry due to the effectiveness of using low dosages albeit they are still expensive.

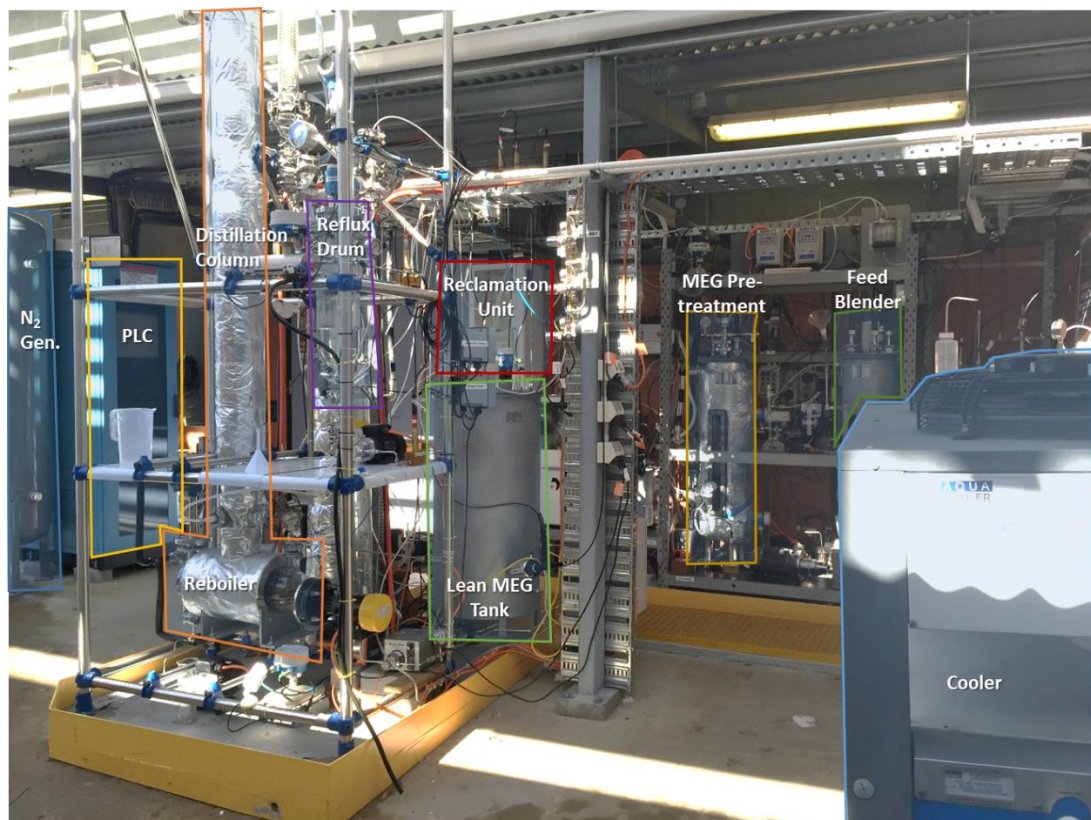


Figure 1.12: MEG Regeneration pilot plant at the Curtin University – CCEIC.



Figure 1.13: MEG reclamation unit (rotary evaporator) at the MEG pilot plant.



Figure 1.14: PVT cell capable of hydrate testing at high-pressures.

1.4 Thesis Objectives

The aim of this research study is to investigate MEG as a regenerated hydrate inhibitor as well as the effect of the numerous other chemical additives that are usually injected alongside MEG. These effects are then empirically and or thermodynamically modelled for the first time to be considered for predictive capability within hydrate control programs in the field. To achieve this purpose, comprehensive experimental studies integrating numerous fluid compositions, fluid preparation, regeneration, reclamation, and degradation are implemented. The project utilized advanced instrumentation comprising a MEG pilot plant for regeneration and reclamation experiments implementing corrosion control strategies, rotary reclamation system, high-pressure autoclave system, and a high-pressure PVT cell for numerous gas hydrate testing methods. The objectives of this research project are as follows:

- (a) Prepare different regenerated MEG samples via the MEG regeneration pilot plant, reclamation unit and autoclave system.
- (b) Investigate the effect of regenerated MEG and salt-laden MEG on natural gas and methane hydrate formation.
- (c) Investigate the effect of pH changes on the removal of MDEA, FFCI, acetic acid, and salts in the reclamation unit during corrosion control strategy switchover from pH stabilization to a film-forming corrosion inhibitor.
- (d) Report new natural gas and methane hydrate phase equilibria using isochoric and isobaric hydrate testing methods, hydrate formation profiles and meta-stability regions.
- (e) Develop novel empirical models and algorithm for prediction of hydrate phase equilibria of degraded and non-degraded, regenerated and non-regenerated, and corrosion inhibitor presence or absence of MEG solutions.
- (f) Develop standardized method to prepare, degrade, and test MEG for hydrate inhibition performance.
- (g) Investigate the effect of MDEA on gas hydrate formation, and in conjunction with MEG.
- (h) Develop novel empirical and thermodynamic model for prediction of hydrate phase equilibria of MDEA solutions with or without MEG.
- (i) Investigate the effect of FFCI and MDEA on gas hydrate formation, and in

conjunction with MEG, and KHI.

- (j) Investigate the effect of dissolved oxygen, and oxygen scavengers on gas hydrate formation with or without MEG, and produce new hydrate phase equilibria.
- (k) Investigate the effect of scale inhibitors on gas hydrate formation with or without MEG, and produce new hydrate phase equilibria.

1.5 Thesis Structure

The structure of the thesis is based upon the series of peer-reviewed publications that cover the objectives of the thesis, and address the identified research gaps as outlined in Table 1.1. This chapter (Chapter 1 Introduction) is followed by 9 chapters showcasing a summary and the peer-reviewed publication(s) corresponding to the relevant thesis objectives and the research gap as listed in Section 1.3. Figure 1.15 illustrates the structure of the thesis and how all the publications fit in, while depicting a typical gas production system where MEG regeneration is utilized. Chapters 2, 3 and 4 delve into MEG regeneration and the subsequent degradation effect. Chapters 5 and 6 delve into the effect of a common additive injected alongside MEG, MDEA on gas hydrate formation and its modelling for prediction. Chapter 7 delves into the effect of MDEA and a film forming corrosion inhibitor on gas hydrate formation, while also developing a series of MEG degradation empirical models. Chapter 8 delves into the effect of oxygen scavengers and dissolved oxygen on gas hydrate formation alongside MEG. Chapter 9 is similar to Chapter 8 but with a focus on scale inhibitors and amines. Chapter 10 delves into developing and showcasing the MEG pilot plant and MEG degradation experimental procedures.

Table 1.1: Thesis objectives and peer-reviewed publications corresponding to each chapter.

Chapter	Thesis Objective	Publication(s)
2	(a) (b) (e)	1 - (Alef et al., 2018c)
3 & 4	(a) (b) (c) (d)	2 - (Alef et al., 2019a) 3 - (Alef and Barifcani, 2018)
5 & 6	(g) (h)	4 - (Alef et al., 2018b) 5 - (Alef et al., 2019b)
7	(i) (e)	6 - (Alef and Barifcani, 2020)
8	(j)	7 - (Alef et al., 2018a)
9	(k)	8 - (Alef and Barifcani, 2019)
10	(a) (f)	9 - (Alef et al., 2017) 10 - (Alef et al., 2019c)

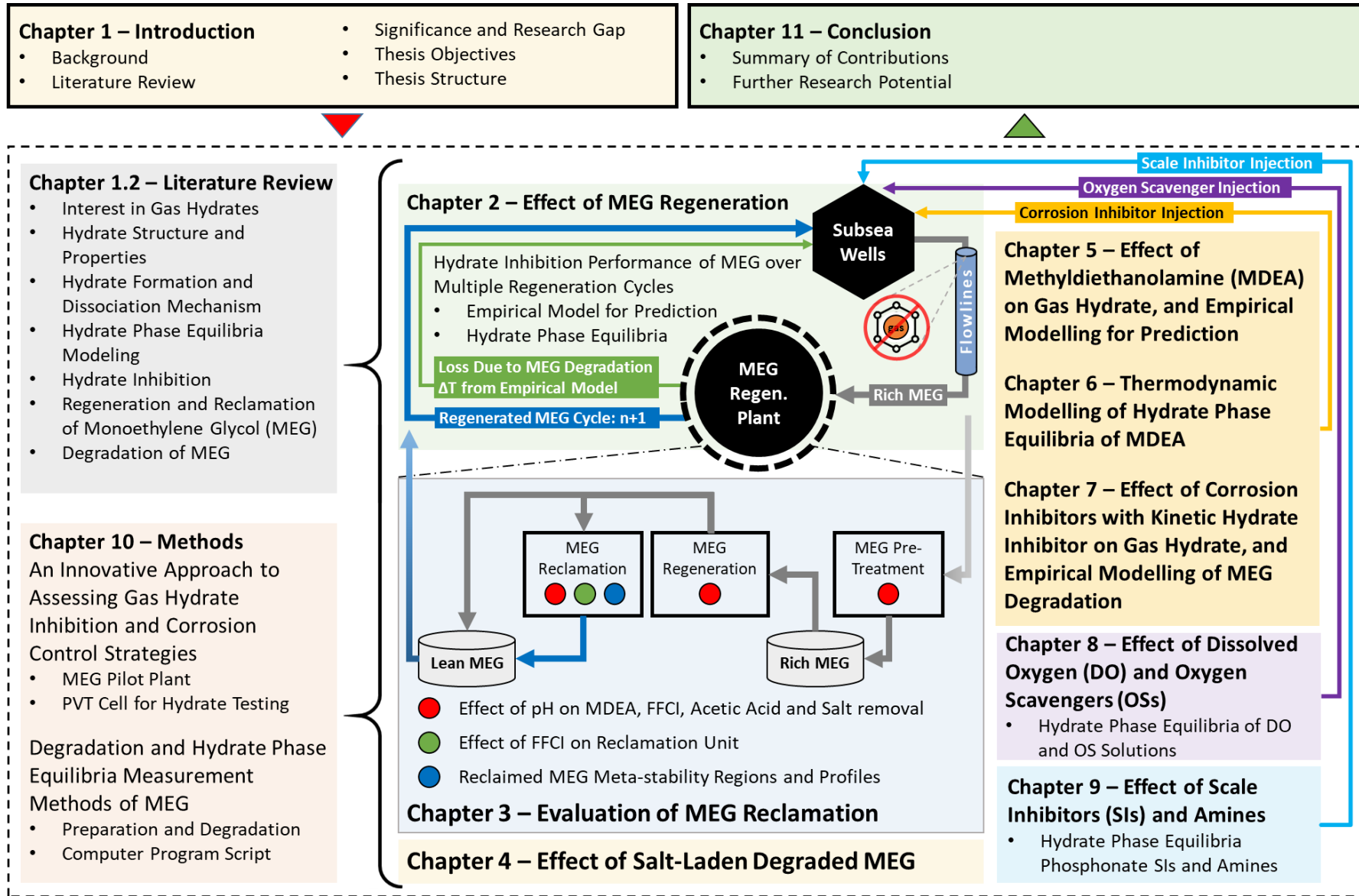


Figure 1.15: Thesis structure illustrated.

Chapter 2 Effect of Regenerated MEG on Gas Hydrate, and Empirical Modelling for Prediction

This chapter is comprised of the following publication:

- **Alef, K.**, Smith, C., Iglauer, S., Gubner, R., Barifcani, A., 2018c. The Effect of Regenerated MEG on Hydrate Inhibition Performance Over Multiple Regeneration Cycles. *Fuel* 222, 638–647. doi: 10.1016/j.fuel.2018.02.190

MEG is a favourable gas hydrate inhibitor mainly due to its recoverability through MEG regeneration facilities, and thus reducing costs. However, it is not clear how the hydrate inhibition performance of MEG is affected by multiple regeneration cycles. This chapter contributes a detailed study on the effect of MEG regeneration and reclamation on the hydrate inhibitory performance of MEG. This contribution satisfies the thesis objectives (a), (b), and (e) while fulfilling the research gaps outlined in Section 1.3.

An innovative field-like MEG pilot plant built at the Curtin Corrosion Engineering Industry Centre (CCEIC) was utilized to mimic the highly complex process. The cycled MEG samples were carefully analysed in the laboratory for their composition, and each sample was tested in a high-pressure sapphire cell for methane hydrate inhibition performance. The study found a directly proportional relationship between the number of cycles and the shift in hydrate equilibrium phase boundary. A maximum equilibrium shift of 2.21 °C was recorded for a 20 wt% MEG/deionized water sample that had experienced 9 MEG regeneration cycles as compared to pure MEG. The analysis suggests that the shift in hydrate equilibrium phase boundary was due to thermal degradation of MEG within the regeneration and reclamation units due to the presence of acetic acid. The study found that even though the operation was below MEG degradation temperature range, repeated heating of MEG may have caused its degradation. Additionally, the phase equilibria are empirically modelled as a function of the number of cycles to aid MEG end-users. Application of the model to experimental results provided accurate outcomes and had an average relative difference of 1.24% when determining hydrate equilibrium temperatures.

A predictive model as such can greatly support field operators to ensure that the

injected MEG will deliver the expected hydrate inhibitory performance of MEG, and that the MEG inventory is topped-up adequately and timely. Applying this to a typical project where the total MEG inventory is 5 kT and with a MEG recovery of 98% (Scott et al., 2016), it was found that an additional average cost of USD \$227,000 for MEG top-ups at each inventory turnover would be required to ensure the hydrate program employed on the field produces the expected results (Table 2.1). These figures are based on the cost of MEG at USD \$1000 per tonne (Kim et al., 2018). An average degradation proportion of MEG in the pressure range of 50 – 200 bar was calculated from the results to be ~4%.

Table 2.1: Top-up cost due to MEG recovery losses and degradation.

	Pure MEG	Cycles								
	0	1	2	3	4	5	6	7	8	9
MEG Recovered (kT)	-	4.9	5.09	5.19	5.29	5.39	5.5	5.6	5.71	5.82
MEG Loss (kT)	-	0.1	0	0	0	0	0	0	0	0
Degraded MEG (kT)	-	0.2	0.2	0.21	0.21	0.22	0.22	0.22	0.23	0.23
Total Top-up MEG (kT)	-	0.3	0.2	0.21	0.21	0.22	0.22	0.22	0.23	0.23
Total Inventory (kT)	5	5.2	5.3	5.4	5.5	5.61	5.72	5.83	5.94	6.06
Cost of Top-up (\$ Mil)	0	0.297	0.204	0.208	0.212	0.216	0.221	0.225	0.229	0.234

2.1 Introduction

An ongoing issue of concern in the field of flow assurance is the formation of gas hydrates in pipelines and process facilities. Gas hydrates can be the cause of serious damage to facilities, plugging in pipelines and even explosions near cornices (Chatti et al., 2005; Hammerschmidt, 1934; Sloan, 2005). Hydrates are classified as crystalline solids composed of host and guest molecules, or water and gas respectively. The water host forms a cage-like structure capturing gas molecules (such as carbon dioxide, methane, ethane and propane) within its cavities (Eslamimanesh et al., 2011; Sloan Jr and Koh, 2007). Hydrates, unlike ice, can form at a temperature higher than the ice formation temperature, and form when adequate water and gas molecules are present at high-pressure and low-temperature conditions which are typical sub-sea pipeline conditions (Zarinabadi and Samimi, 2011). Samimi (2012) has outlined various ways these conditions can be shifted to a hydrate-safe zone, either by depressurizing the pipeline, or through heating and thermal insulation, or to remove water through glycol dehydration (Samimi, 2012). Applying these techniques may not be suitable in all cases due to the lack of time, and economic constraints (McIntyre et al., 2004). However, the conventional strategy the industry has adopted is to utilize chemical additives known as hydrate inhibitors to achieve hydrate inhibition. Methanol (MeOH) and monoethylene glycol (MEG) are common hydrate inhibitors, however, MEG is looked upon as more favourable due to its chemical stability, high regeneration efficiency, lesser environmental effect, and low solubility in final gas products (AlHarooni et al., 2015).

An effective hydrate inhibition program requires a large quantity of MEG. This is troublesome if used-MEG is discarded into the environment, as well as costly to constantly replenish the MEG supply. The current best-practice is to recycle used-MEG and thus allowing the re-use of MEG. MEG recycling involves two critical processes, regeneration and reclamation. Regeneration, also known as re-concentration, utilizes distillation to re-concentrate MEG by removing the water present in the used-MEG/rich-MEG stream; the rich-MEG solution may be contaminated with chemical additives such as corrosion and scale inhibitors, drilling mud, and formation water. The deposition of these chemicals and precipitation build-up in process equipment can lead to equipment fouling, downtime in production,

concern in safety, and economic losses due to maintenance (Latta et al., 2013). The regenerated MEG is then pumped through to the reclamation unit, where the solution is thermally exposed under vacuum conditions to the vaporization temperature of MEG. This allows for the recovery of MEG and water whilst removing the contaminants as waste products (Latta et al., 2013).

Regeneration of MEG is a cost-effective strategy and has been the subject of numerous research with regards to design and process, but there is very little or no research into how the inhibition performance of MEG is affected by multiple regeneration/reclamation cycles. In this study, recycled MEG samples from an experiment simulating the switching between corrosion management strategies using a fully functional bench-scale MEG regeneration/reclamation plant was evaluated on their hydrate inhibition performance using a PVT sapphire cell (Figure 2.1). The recycled MEG samples from a total of 9 consecutive cycles, were tested in the PVT cell to determine whether the number of cycles have an impact on the hydrate inhibition performance. The results of this study give rise to a whole new aspect of MEG recycling, and allowing users to take the necessary steps to ensure minimal loss by adequately adjusting MEG injection rates.

Furthermore, one of the purposes of this communication is to present a model that accurately depicts this new information of experimental hydrate equilibria data. Presenting this research's experimental data in the form of a model is not only more convenient but ensures it is more accessible to industry and research personnel. A balance between simplicity and ease of use was the desired outcome for this model and it is based on mathematically interpolating (linearly) experimental pressure (P)-temperature (T) hydrate equilibria for a specified MEG cycle number, n . Exponential functions are chosen as the data-fitting equations since hydrate pressure-temperature equilibria correlate very well when described exponentially and the exponential data-fitting equation just has one term with only one occurrence of P and T (Smith et al., 2016, 2015).

2.2 Methodology

2.2.1 Materials and Equipment

As the MEG regeneration and reclamation process becomes increasingly complex, the

complexity increases in terms of experimentation in the laboratory. An innovative approach is the bench-scale MEG pilot plant housed in the Curtin Corrosion Engineering Industry Centre (CCEIC). The bench-scale pilot plant is designed and built for thorough experimentation and study of the behaviour of MEG in different field scenarios, in combination with production fluids, drilling mud and other chemical additives. The pilot plant has a real-time processing flow of up to 4 kg/h of lean-MEG. The plant comprises of four distinct yet related stages; a) preparation of brine, b) preparation of rich or contaminated MEG, c) re-concentration/regeneration unit, and d) reclamation unit. In this study, samples of reclaimed MEG from the reclamation unit were extracted to be evaluated on their hydrate inhibition performance.

A PVT sapphire cell (Figure 2.1) located in the Clean Gas Technologies Australia (CGTA) laboratory was used as the experimental apparatus for testing the samples for hydrate inhibition performance. The essential process of the cell was to provide steady heating and cooling in a controlled environment. The cell is made from strong sapphire material that is able to sustain increased pressures allowing it to operate at a maximum pressure of 500 bar. To ensure there was no contamination, a ventilation and purging line was connected to the sapphire cell which allowed for gas to be released to a safe atmospheric zone above the building. The total volume contained within the system inclusive of the cell (60 cm³) and tubing (26 cm³) is 86 cm³. Furthermore, the cell was insulated firmly from the outside surroundings by a tightly sealed accessible door with a window allowing for easy visual observations of the entire cell from the outside as well as through a camera system. The heating and cooling capability is within a temperature range of 60 °C to as low as -160 °C. A cooling system comprising of a compressor was utilized for cooling, whilst for heating an integrated electrical heater within the PVT cell was utilized, and an external chiller was used to supply chilled water to enhance compressor performance. The air bath chamber wherein the cell was securely fixed has a fan mounted on the roof for enhanced circulation of cool or heated air. Specific to this study, the cell was operated at a pressure and temperature range of 50–200 bar and 0–30 °C respectively.

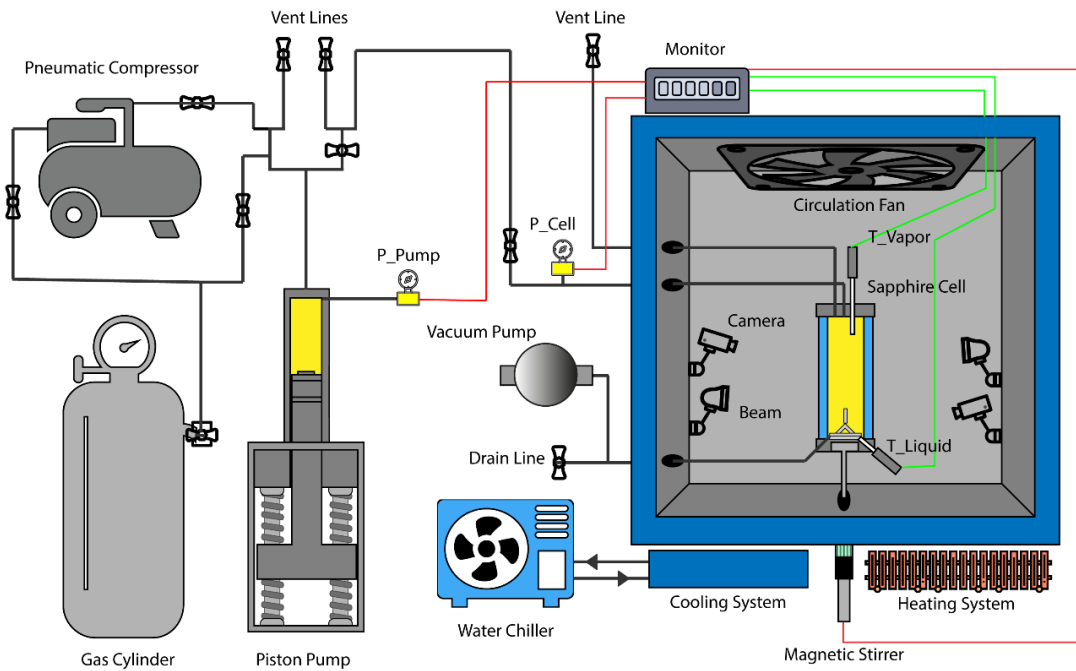


Figure 2.1: Schematic of the PVT Sapphire cell where P and T denote pressure and temperature respectively.

The cell was fitted with a magnetic stirrer to provide sufficient mixing between the gas and liquid. It also helps in the promotion of gas hydrate formation due to the disturbance it creates at the surface of the solution (Obanijesu et al., 2011; Sadeq et al., 2017). A lack of this disturbance leads to hydrate merely forming at the surface which prevents additional gas molecules from dissolving and hence severely delaying hydrate formation (Mori, 1998). The magnetic stirrer (diameter of 2 cm) was operated at ~ 500 rpm during each run of the experiment. The gas was pressurized via a piston pump controlled by ABB Mint Workbench software (build 5712). Pressure sensors (accuracy of ± 0.5 bar) linked to a proportional integral derivative (PID) controller which allows for pressure adjustment. The temperatures of the air bath chamber, vapor and liquid phases in the cell were monitored via multiple K-type thermocouples (accuracy of ± 0.03 °C). The Falcon application (version 4.30) was used to monitor and control temperature changes. Care was taken to ensure temperature changes were small (1 °C/h) in order to achieve steady state between the various phases within the cell. The heating and cooling system, piston pump and cameras were all controlled and maintained via the PVT computer system.

Pure monoethylene glycol (MEG) was sourced from Chem-Supply with a purity of

99.477 mol% (Table 2.2). Pure MDEA (purity ≥ 99 mol%) was sourced from Sigma-Aldrich, whilst FFCI is a proprietary film forming corrosion inhibitor (FFCI).

Table 2.2: Pure MEG composition from chem-supply.

Component	Mole %
Monoethylene glycol	99.477
Water	0.5
Diethylene glycol	0.02
Ash content	0.001
Acidity (as acetic acid)	0.001
Aldehyde (as formaldehyde)	0.0008
Chlorine	0.00001
Iron	0.000005

Analysis of the sample composition, ion concentrations and acids were determined using an ion chromatography and high-performance liquid chromatography (HPLC) system (Thermo Scientific Dionex U3000, accuracy of $\pm 0.1\%$). Electrical conductivity was measured using Mettler-Toledo InPro-7100 sensors (accuracy of $\pm 5\%$, operating temperatures of 0–135 °C). The concentration of MEG was determined with an ATAGO-PAL91S refractometer (accuracy of $\pm 0.4\%$) (Zaboon et al., 2017). The sensors used in this study were thoroughly washed with deionized water, and calibration was performed according to the manufacturer’s instructions.

2.2.2 Process and Procedure

Samples of recycled MEG were obtained from the bench-scale MEG pilot plant simulating a typical switching between corrosion management strategies in the occurrence of formation water. The simulated switchover was between pH stabilization (MDEA) to a film forming corrosion inhibitor (FFCI) (Latta et al., 2016). The experiment was conducted continuously over 9 cycles of inventory turnover with a total duration of 97 h. The regeneration process began after the rich-MEG solution had passed through the feed blender where initial solutions were mixed under turbulent conditions, and had undergone the pre-treatment stage where insoluble salts were removed from the MEG solution. In the regeneration unit, water was removed from

the MEG solution by packed distillation columns. The regeneration unit was operated at a temperature below the boiling point of MEG but slightly higher than the boiling point of water (<129 °C) to avoid thermal degradation of MEG. With the relatively low flow rates (1.2–1.5 kg/h), a vacuum rotary evaporator capable of flashing lean-MEG was utilized to simulate the reclamation process. The lean-MEG solution (80 wt% MEG/brine) from the reboiler was fed to the rotary evaporator by opening a relay valve which was monitored through a level sensor. Lean-MEG containing high dissolved salt concentration, as well as MDEA was flashed in the vacuum flask which was operated at 100 mbar. The reclamation unit was operated at vacuum conditions to avoid high temperatures that may cause MEG degradation. The flask was continuously heated with an oil bath operating at ~160 °C, which resulted in liquid and vapor temperatures of ~130 °C within the reclamation flask. Care was taken to ensure the MEG was not thermally degraded by ensuring that it was only exposed to the vaporization temperature of MEG. Furthermore, to maintain a uniform heat distribution, the flask was rotated at 30 rpm while being immersed in the oil bath. The flashed vapor was condensed in the overhead condenser and collected in the receiving flask which was controlled via a level sensor. When the level reached the desired value, the purified lean-MEG was sent to a storage tank. Samples from the receiving flask were taken at each inventory turnover representing an entire cycle.

The PVT cell was utilized for hydrate inhibition testing. The samples were diluted to 20 wt% MEG with deionized (DI) water. This was conducted to resemble actual field conditions as much as possible; typical concentrations of the lean-MEG to be injected are around 90 wt% MEG, however, the MEG solution gets diluted after injection due to the presence of formation water in the production pipelines hence decreasing the final concentration of the injected MEG solution to around 40 wt% MEG (Dugstad et al., 2003; Halvorsen et al., 2009; Kim et al., 2014). Methane with deionized water was tested to ascertain the accuracy of the PVT cell and consequent results. For cycles 1, 5 and 9, the full hydrate profile curve was determined by conducting 4 tests for each cycle at varying pressures (75, 100, 150, and 200 bar), whilst for the cycles in-between (2, 3, 4, 6, 7, and 8) a single test for each was conducted at an approximate pressure of 150 bar.

The isochoric method was employed for the measurement of equilibrium

(dissociation) points of the mixtures. This method is widely employed and well accepted (Luna-Ortiz et al., 2014; Sloan Jr and Koh, 2007; Tohidi et al., 2000; Zang and Liang, 2017). The process entailed that the liquid within the sapphire cell is steadily cooled to enable the formation of hydrate and then steadily heated to accurately detect the equilibrium (hydrate dissociation) point. It can be determined by finding the intersection of the cooling and heating curves of the process (Sloan Jr and Koh, 2007).

Important caution was taken to ensure temperature within the cell was controlled and monitored adequately enabling steady state to be reached at incremental changes. Thus, a rapid change in the temperature of the sapphire cell can result in missing the noticeable points of hydrate dissociation leading to inaccurate outcomes. The inside of the sapphire cell was thoroughly cleaned with acetone and rinsed with deionized water. Then the cell and surrounding apparatus was well vented and purged with nitrogen to ensure the entire apparatus was free from any contaminants that may affect the results. The cell was then connected to a vacuum pump to remove any remaining gases and liquids. The sample solution (8 mL) was then injected into the cell. It was then pressurized with methane gas from a connected gas supply cylinder until it reached the desired pressure. When the mixture reached thermal equilibrium, the cooling system was initiated. The cooling system was monitored and controlled using dedicated software (Falcon version 4.30). The temperature was steadily dropped at a rate of 3 °C per hour until the temperature of the vapor phase within the cell had reached a temperature 3 to 4° above the predicted hydrate formation temperature. At this stage the rate of cooling was drastically dropped to 1 °C per hour. The hydrate was allowed to grow until full blockage had occurred. The heating system was then initiated at a rate of 1 °C per hour. The dissociation or thermodynamic equilibrium point was determined accurately through the intersection of the cooling and heating curves of the process.

2.3 Results and Discussion

2.3.1 Observations

The pure MEG samples were observed to be colourless, whilst foaming was observed to occur for samples of the initial cycles (Figure 2.2). AlHarooni et al. (2016) also

observed foam formation and attributed it to MDEA reacting with contaminants present in the MEG solution. Foaming has negative consequences such as loss of solution, production downtime and increased costs due to the maintenance of equipment (Liu et al., 2015). Foam formation can occur due to contaminants such as formation water, feed-gas, oxygen ingress amongst other contaminants present in the solution (Al Dhafeeri, 2007; Kohl and Nielsen, 1997). As the number of cycles increased, the foam formation behaviour decreased, and this is evident due to the decrease in MDEA concentrations as shown in Figure 2.2 and further analysed in Figure 2.10.

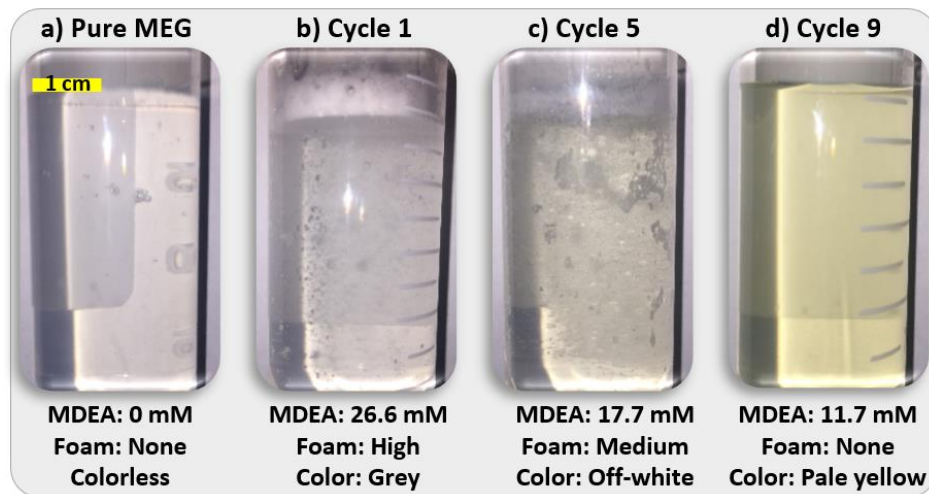


Figure 2.2: Observations of foaming due to MDEA, and coloration in cycles 1, 5, and 9 as compared to pure MEG.

The initial solution (Figure 2.3a), was colourless and no restriction to flow was observed as the magnetic stirrer operated at full speed (~ 500 rpm). As the mixture was steadily cooled for about 3 h, the first signs of hydrate formation appeared, formation of bubbles (Figure 2.3b). This was due to gas molecules beginning to dissolve in the water phase. There were no hydrate solids observed at this point. Soon thereafter, the bubbles increased and irregular hydrate solids began to accumulate on the upper surface (gas-liquid contact) whilst waves of bubbles circulated beneath (Figure 2.3c). This hydrate film was also observed by others (AlHarooni et al., 2017; Mori, 1998). The flow indicated by the speed of the magnetic stirrer remained unhindered (~ 500 rpm). However, as the mixture was cooled further, the bubbles decreased in size and subsided whilst stable layers of hydrate began to form radially on the inside walls of the cell. This transition was observed as the smaller hydrate solids agglomerated

into larger solids which started to affect the stirrer speed indicating that hydrate formation was now a real hindrance to the flow within the cell. The stirrer would abruptly stop intermittently with an average speed of (~ 400 rpm). The extent of this observation increased as the hydrate grew in size. The agglomeration of the hydrates continued until all visible liquid phase was consumed, resulting in full blockage of the cell at 4.5 h (Figure 2.3d). The magnetic stirrer was consuming energy but was not able to move the hydrate block asynchronous to plugging within pipelines thus stopping production. The heating system was then initiated to determine the dissociation point. A slow heating rate ($1\text{ }^{\circ}\text{C/h}$) was enabled to ensure the subtle dissociation rate was captured with high accuracy. Initial dissociation was first noticed as tiny cavities began to appear within the hydrate block (Figure 2.3e). As the number of cavities increased, a film of liquid began to accumulate at the bottom of the cell allowing the stirrer to slightly move with intermittent stops. With further heating, the hydrate block began to fragment into smaller pieces and more liquid filled the bottom of the cell, the stirrer was gaining speed and less stops indicating greater flow within the cell (Figure 2.3f). As the dissociation process continued, the separation of liquid and gas molecules from the hydrate phase became more evident and the liquid solution was observed to be quite cloudy with various strains of off-white colour (Figure 2.3g). The cell was heated until no hydrate solids were observed and the liquid was clear with a yellow colour (Figure 2.3h), the magnetic stirrer at this stage was rotating at full speed.

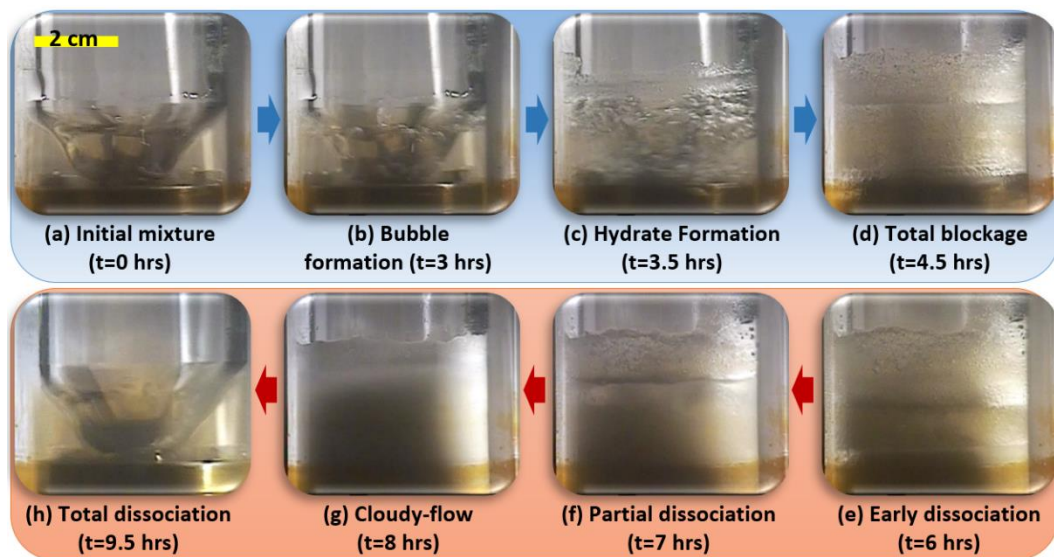


Figure 2.3: Observable stages of hydrate testing of cycled MEG.

2.3.2 Initial Testing

Methane hydrate testing was conducted on deionized water to establish the accuracy of our experimental apparatus and results. Methane (CH_4) and deionized water were chosen due to the widely available literature with results that can be used as a comparison. The full hydrate profile for CH_4 + deionized water was determined by conducting 5 tests at varying pressures (50, 75, 100, 150, and 200 bar) and were conducted three times for repeatability (average experimental error of 2.61%). The final results were compared to the literature (Jhaveri and Robinson, 1965; Marshall et al., 1964; McLeod and Campbell, 1961; Verma, 1974), as well as closely matching fluid packages in Aspen HYSYS (version 8.6), Multiflash (version 3.6), PVTsim (version 20) (Aspen HYSYS, 2007; Calsep PVTsim, 2011; Infochem Multiflash, 2007). Figure 2.4 shows that our results are highly consistent with literature and software results, only having an average absolute percent deviation (AAPD) of 1.64%.

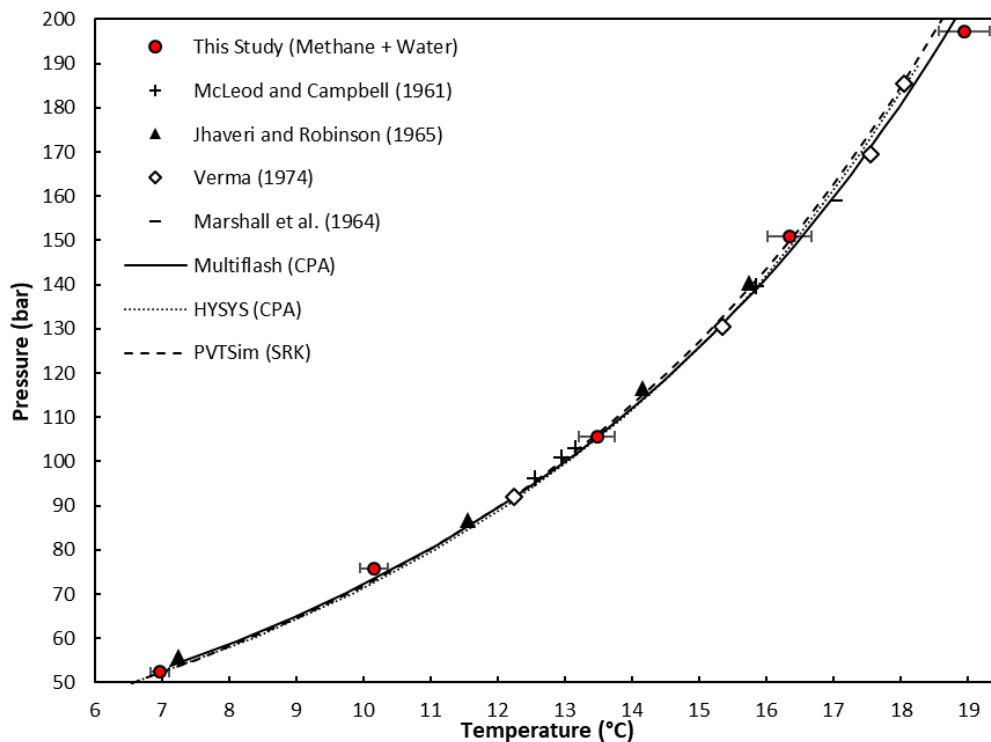


Figure 2.4: Hydrate profile for methane and water mixture from this study compared to simulation software (average absolute deviation of 1.64%) and literature (1.80%).

The methane hydrate of a 20 wt% pure MEG aqueous solution was profiled and compared to software prediction and literature data that was relatively close to the MEG concentration utilized in this study (Eichholz et al., 2004; Rock, 2002) – Figure

2.5. An AAPD of only 3.36% was found compared to software calculations, suggesting our results are highly accurate.

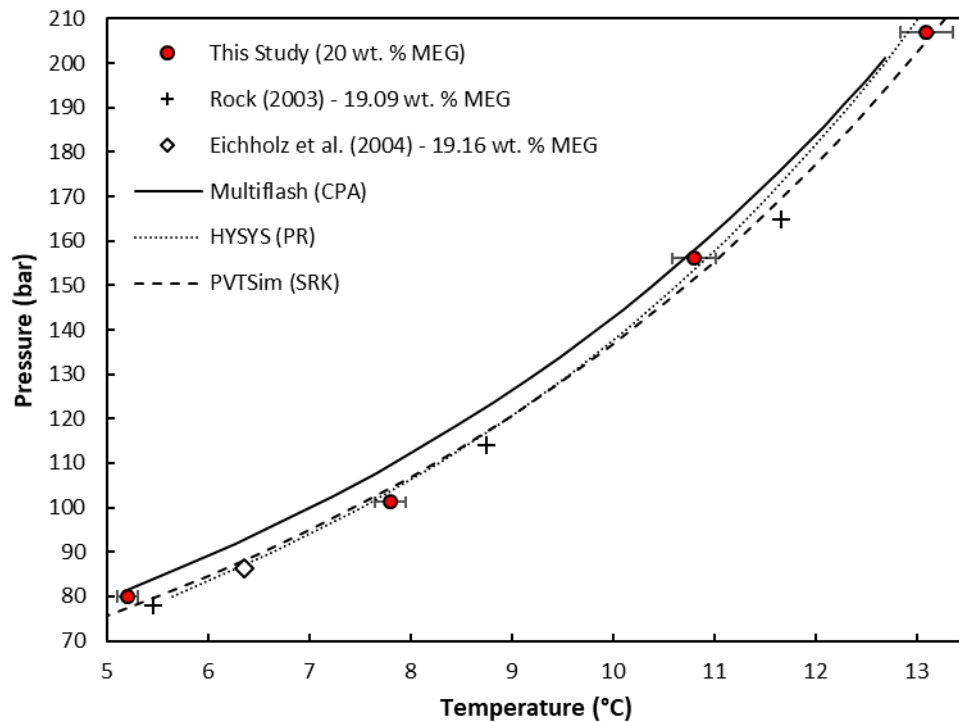


Figure 2.5: Hydrate profile for methane and 20 wt% MEG solution.

2.3.3 Equilibrium Results – Cycling

The effect of regenerated or cycled MEG on the methane hydrate phase profile was carefully measured using the sapphire cell at pressures between 75 and 200 bar. The measured equilibrium results for pure MEG and the 9 cycles of regenerated MEG are shown in Figure 2.6. Table 2.3 and Table 2.4 show the hydrate equilibrium temperature shift (ΔT_s) calculations for all the cycles relative to pure MEG. The hydrate phase profile for cycle 1 has an average shift of 0.37 °C for low pressures (50–100 bar) and -0.12 °C for high pressures (100–200 bar) compared to the hydrate profile of pure MEG solution (20 wt%). The middle cycle (5) and the final cycle (9) have shifted on average by 1 °C and 1.7 °C respectively for the pressure range of 50 to 200 bar (Table 2.3). The single testing points for cycles 2, 3, 4, 6, 7, and 8 at an approximate pressure of 150 ± 10 bar have shifted by 0.01, 0.38, 0.58, 1.08, 1.22, and 1.32 °C respectively (Figure 2.6 and Table 2.4).

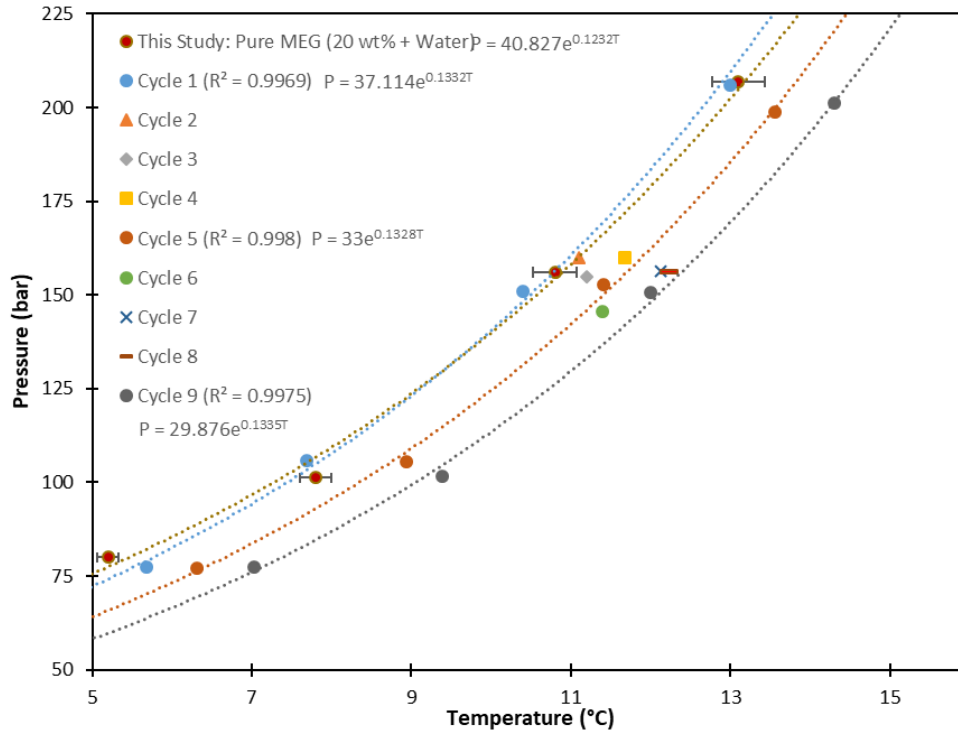


Figure 2.6: Methane hydrate phase profiles for pure MEG (20 wt%) and cycles 1–9, dotted lines refer to exponential fitting curves.

Table 2.3: Hydrate equilibrium temperature shift (ΔT_s) of cycles 1, 5 and 9 compared to pure MEG hydrate profile and the regression functions of the fitted data.^{ab}

Pressure (bar)	Pure MEG	Cycle 1		Cycle 5		Cycle 9	
	$P=$ $40.827e^{0.1232T}$	$P=$ $37.114e^{0.1332T}$	ΔT_s (°C)	$P=$ $33e^{0.1328T}$	ΔT_s (°C)	$P=$ $29.876e^{0.1335T}$	ΔT_s (°C)
	T_{exp} (°C)	T_{exp} (°C)		T_{exp} (°C)		T_{exp} (°C)	
50	1.65	2.24	0.59	3.13	1.48	3.86	2.21
75	4.94	5.28	0.34	6.18	1.24	6.9	1.96
100	7.27	7.44	0.17	8.35	1.07	9.05	1.78
125	9.09	9.12	0.03	10.03	0.94	10.72	1.64
150	10.57	10.48	-0.08	11.4	0.83	12.09	1.52
175	11.82	11.64	-0.18	12.56	0.74	13.24	1.43
200	12.9	12.64	-0.26	13.57	0.66	14.24	1.34

^a Standard error in pressure and temperature are ± 0.5 bar and ± 0.03 °C respectively.

^b P and T denotes pressure and temperature, respectively.

Table 2.4: Hydrate Equilibrium Temperature shift (ΔT_s) from Pure MEG hydrate profile (cycles 2, 3, 4, 6, 7, 8).^a

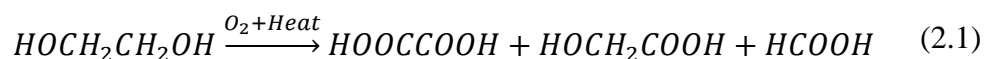
	Pressure (bar)	T_{exp} (°C)	$T_{Pure\ MEG}$ (°C)	ΔT_s (°C)
Cycle 2	160.05	11.10	11.09	0.01
Cycle 3	154.70	11.20	10.82	0.38
Cycle 4	159.95	11.67	11.09	0.58
Cycle 6	145.59	11.40	10.32	1.08
Cycle 7	156.47	12.13	10.91	1.22
Cycle 8	156.39	12.22	10.90	1.32

^a Standard error in pressure and temperature are ± 0.5 bar and ± 0.03 °C respectively.

The results reveal that there is a directly proportional relationship between the number of cycles and equilibrium temperature resulting in a rightward shift in the hydrate phase boundary (i.e. promotion of hydrate formation). Furthermore, the hydrate phase boundary for cycle 1 is slightly lower than the phase boundary for the pure MEG sample. This was due to the high initial concentration of MDEA present in the solution (Figure 2.10). MDEA has been found to have an enhanced hydrate inhibition effect thus confirming this finding (Akhfash et al., 2017; AlHarooni et al., 2017; AlHarooni et al., 2016). As the cycles increased, MDEA was steadily removed in the reclamation process due to the increased risk of corrosion in the presence of formation water (Lehmann et al., 2014). Hence, the added hydrate inhibition effect of MDEA is not very well pronounced for the later cycles.

A key limitation on the use of MEG as a hydrate inhibitor is its maximum exposure temperature. At temperatures above 135 °C MEG could suffer thermal decomposition, typically producing organic acids, particularly acetic and formic acids (AlHarooni et al., 2015). This is the main reason behind vacuum distillation for reclamation, as it reduces the required temperature for separation of MEG from the contaminants to below the degradation temperature. The area of degradation of MEG and the impact it has on hydrate inhibition has not been researched in great volume to date, however

dedicated research into the degradation of MEG began with the work of Rossiter et al. (1985) showing the degradation products of solutions of MEG include glycolic, oxalic and formic acids. The decomposition products are a result of thermal oxidation of MEG as shown in reaction Eqn. (2.1) (Rossiter et al., 1985).



Similar MEG degradation products were determined by others through ion chromatography and high performance liquid chromatography to be formic acid, acetic acid and glycolic acid (AlHarooni et al., 2015; AlHarooni et al., 2016; Madera et al., 2003). AlHarooni et al. (2016) concluded after a detailed study on analytical techniques for analysing various MEG samples that using high performance liquid chromatography was amongst the most effective analytical techniques, owing to high consistency across various samples and temperatures. The analysis revealed that acetic acid was present in all the samples (Figure 2.7). The acetic acid concentration increased with cycle number thus indicating an increasing amount of MEG degradation as cycles increased. The degradation of MEG into organic acids such as acetic acid decreased the quantity of effective MEG for hydrate inhibition. As a result, a rightward shift in the hydrate phase boundary occurred.

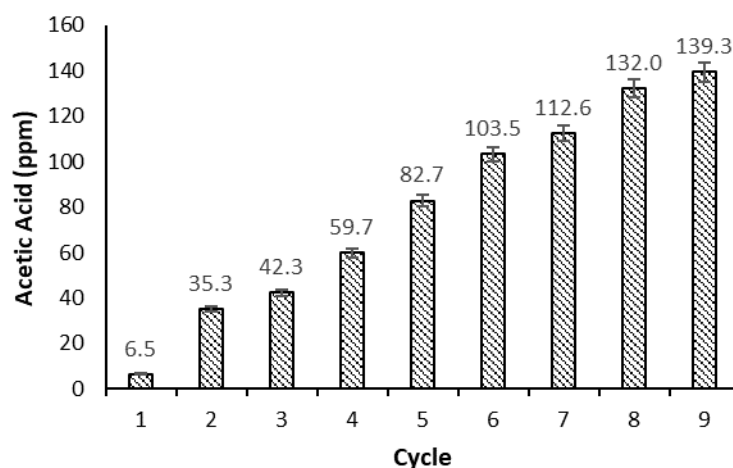


Figure 2.7: Acetic Acid concentration (ppm) of cycles 1-9.

Research by Psarrou et al. (2011) on the effects of MEG reclamation conditions on MEG degradation has shown that a macroscopic indicator of MEG degradation during regeneration and reclamation is the solution turning yellow (Psarrou et al., 2011).

Solution samples were analysed for its coloration as shown in Figure 2.2, where cycle 9 (Figure 2.2d) was observed to be pale yellow in colour, resembling the observation of Psarrou et al. (2011). Cycle 5 had an off-white colour as compared to the colourless pure MEG sample. This observation is in line with the findings of Psarrou et al. (2011), indicating that MEG suffered degradation and hence the drop in inhibition performance.

The degradation of MEG is a thermal oxidation process, therefore, it can be expected that the presence or absence of oxygen will affect the degradation of MEG. As investigated by Rossiter et al. (1985), elimination of oxygen from a MEG system can effectively reduce the degradation (Rossiter et al., 1985). This has been termed the 'deaeration effect'. In their studies, aerated and deaerated MEG solutions heated for 15 days at 100 °C, thermal oxidation resulted in MEG degradation. Furthermore, Rudenko et al. (1997) confirmed that at temperatures above 157 °C, thermal degradation without the oxidation component is possible (Rudenko et al., 1997). Dissolved oxygen levels were measured across the reclamation unit as shown in Figure 2.8. Dissolved oxygen levels are kept below 20 ppb ideally to prevent the risk of corrosion (Lehmann et al., 2014). The dissolved oxygen levels of the MEG solution for each cycle within the reclamation unit were relatively low (<38 ppb). Cycle 1 to 4 saw levels in the range of 29–38 ppb, whilst the remaining cycles saw levels below 25 ppb of dissolved oxygen (Figure 2.8). The reclamation unit utilized within this study was constantly purged with nitrogen to prevent oxygen contamination and hence an average level of 23 ppb dissolved oxygen was achieved. The analysis shows that very little (23 ppb) oxygen ingress occurred within the MEG pilot plant and it does not explain the rightward shift in the hydrate equilibrium temperatures as the cycles increase.

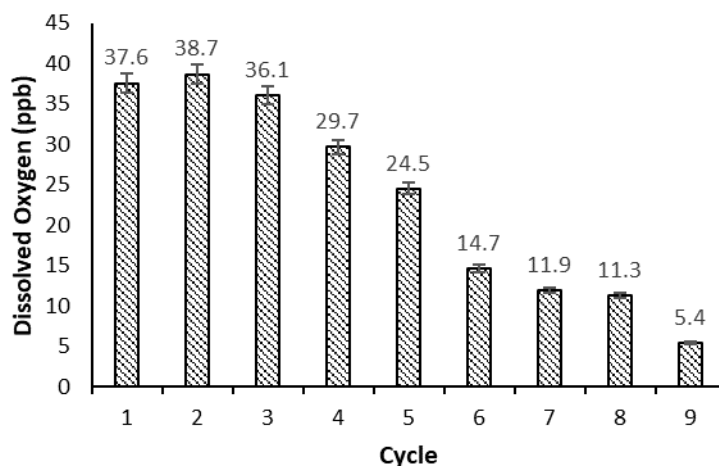


Figure 2.8: Dissolved oxygen levels (ppb) within the reclaimed MEG solution for each cycle.

The above strongly suggests that MEG degradation occurred although the reclamation unit was operated at a liquid and vapour temperature of $\leq 134\text{ }^{\circ}\text{C}$ and $\leq 126\text{ }^{\circ}\text{C}$ respectively (Figure 2.9). These findings suggest that whilst being below degradation temperature, repeated heating through recycling of MEG could affect its ability to inhibit hydrates.

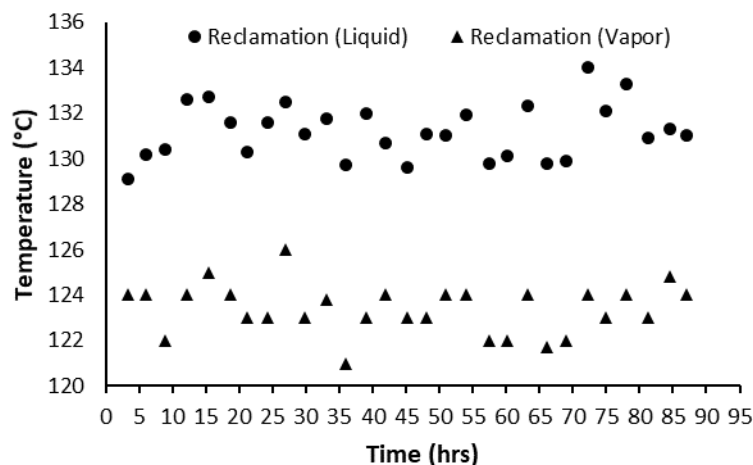


Figure 2.9: Temperature of the liquid and vapor phases within the reclamation unit over 9 cycles (sensor accuracy of $\pm 0.03\text{ }^{\circ}\text{C}$).

The presence of MDEA (Figure 2.10) results in enhanced hydrate inhibition performance with respect to cycle 1 – where MDEA is at its highest concentration, however as the cycles increase the added inhibition effect that MDEA brings was outpaced by other mechanisms that promote hydrate formation such as thermal

degradation, thus the hydrate phase boundaries were shifted to the right. Furthermore, FFCI was completely removed within reclamation as no trace of it was found after HPLC analysis was performed. However, AlHarooni et al. (2016) suggested that FFCI can act as a hydrate inhibitor (AlHarooni et al., 2016).

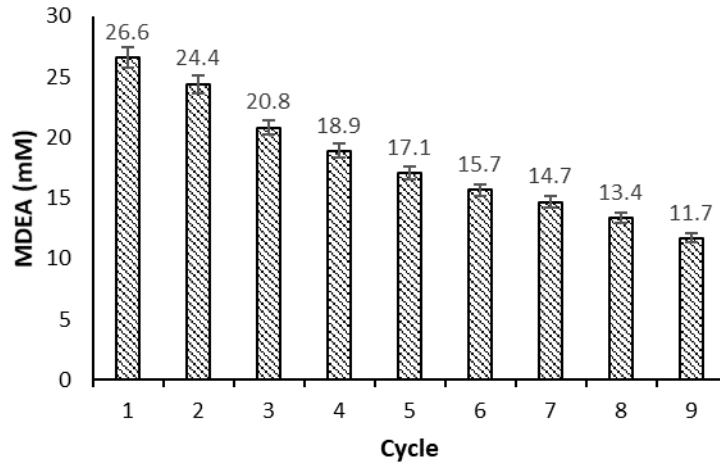


Figure 2.10: MDEA concentration (mM) in samples of cycles 1-9.

2.3.4 Empirical Model

With a clear trend between the cycling of MEG and the decreased hydrate inhibitory performance identified, providing a means of relating these variables is important. A simple but effective model was constructed by mathematically relating the experimental hydrate dissociation conditions (P , T) with the MEG cycle number. It is assumed that at a certain pressure, the relationship between the dissociation temperature and cycle number is linear. According to the data presented in Figure 2.6, the temperature increases by a relatively consistent interval with cycle number at a specified pressure, hence the applicability of a simple linear interpolating scheme. Using the experimental dissociation data for methane with pure MEG (cycle 0) and with $n=9$ cycles, an interpolation scheme capable of computing dissociation conditions after a number of cycles (n) is put forth.

Given the expectation that MEG sample's degree of methane hydrate inhibition decreases with higher n , this decrease will result in T being greater relative to the application of pure MEG ($n=0$). This is expressed by Eqn. (2.2):

$$T = T_0 + \Delta T_{0-n} \quad (2.2)$$

The first term in Eqn. (2.2) is representative of the dissociation temperature for pure MEG with $n = 0$ cycles, T_0 . The second term computes the temperature shift from cycle 0 to cycle n (ΔT_{0-n}). T_0 is simply evaluated using a best-fit exponential expression for the experimental hydrate equilibria data. The expression for all experimental data when correlated is given with P as the subject. The data-fitting equation can be rewritten in terms of T_0 according to Eqn. (2.3) (a and b are constants that best match the data set):

$$T_0 = a \ln\left(\frac{P}{b}\right) \quad (2.3)$$

Interpolation for this model centres around the ΔT_{0-n} term. The maximum deviation from T_0 corresponds to when $n = 9$ and this is designated as ΔT_{0-9} . Hence ΔT_{0-n} uses this known value (from experiment) to interpolate the actual ΔT , or deviation from T_0 , at a particular P and n , which therefore provides an overall T value. It is expected that ΔT_{0-9} (the difference between T_0 and T_9) will not be the same throughout the entirety of the experimented range of pressures, and will therefore be a function of pressure.

Derivation of ΔT_{0-n} involved the development of the experimental relationship between ΔT_{0-9} and P . As evident from the equilibria in Figure 2.6, the temperature interval between 0 and 9 cycles (ΔT_{0-9}) varies with pressure. To account for this, ΔT_{0-9} was calculated at several pressures and gave a strong exponential function ($R^2 = 1$). Figure 2.11 illustrates the strong correlation between these two parameters.

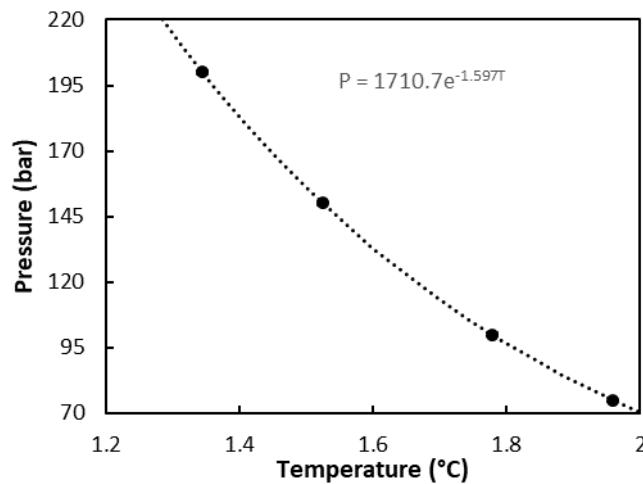


Figure 2.11: P versus T -Hydrate Equilibrium Shift (ΔT_{0-9}).

From Figure 2.11, the equation for ΔT_{0-9} is given as:

$$\Delta T_{0-9} = \left(\frac{1}{-1.597} \right) \ln \left(\frac{P}{1710.7} \right) \quad (2.4)$$

The ΔT_{0-9} term can be used to interpolate T for n cycles (ΔT_{0-n}) by multiplying Eqn. (2.4) with $n/9$:

$$\Delta T_{0-n} = - \left(\frac{n}{9 \times 1.597} \right) \ln \left(\frac{P}{1710.7} \right) \quad (2.5)$$

Substituting Eqns. (2.3), (2.5) into Eqn. (2.2) gives the overall expression (Eqn. (2.6)) for calculating T after n cycles (constants a , b , c and d listed in Table 2.5).

$$T = a \ln \left(\frac{P}{b} \right) + c \ln \left(\frac{P}{d} \right) n \quad (2.6)$$

Table 2.5: Constants for Eqns. (2.3) and (2.6).

a	b	c	d
8.117	40.827	-0.06957	1710.7

2.3.5 Application of Model to Experimental Data

To test whether the model matches the experimental data it is describing, data points in the proximity of 150 ± 10 bar were selected. The exact pressures and corresponding cycle number (n) were inserted into the model to calculate the resultant temperature, T_{calc} . Where required, raw data was calculated using their designated lines of best fit as opposed to individual points. Calculated values are compared to experimental values, T_{exp} , in Table 2.6 (unless noted, T_{exp} represents the actual data point).

Table 2.6: Model calculations versus raw data.

n	P (bar)	T_{calc} (°C)	T_{exp} (°C)	RD (%)
0	156.1	10.89	10.8 (10.89 ^a)	0.83
1	151	10.79	10.4	3.75
2	160.05	11.42	11.1	2.88
3	154.7	11.31	11.2	0.98
4	159.95	11.74	11.67	0.60
5	152.89	11.56	11.41	1.31
6	145.59	11.35	11.4	0.44
7	156.47	12.07	12.13	0.49
8	156.39	12.23	12.22	0.08
9	150.74	12.12	12 (12.12 ^a)	1.00

^a Calculated with line of best fit.

Any disagreement between T_{calc} and T_{exp} are represented by the relative difference as a percentage (RD%). Most calculations are within 0.1 - 0.2 °C of the corresponding experimental value and rarely differed by more than 2% with an average of 1.24%. It can be concluded that the developed model accurately represents the experimental data from which it was constructed.

2.4 Conclusions and Recommendations

This study evaluated the effect of multiple cycles of MEG inventory from a bench-scale MEG pilot plant simulating a switchover of corrosion strategies (pH stabilization with MDEA to FFCI). The samples from each cycle were analysed for their composition and tested using a PVT cell for hydrate inhibition performance. This study contributes new methane hydrate equilibria data of multiple cycles of regenerated MEG. The study found a rightward shift in the hydrate phase boundary for MEG suggesting a promotion in hydrate formation as the number of cycles of MEG regeneration increased. It found an average equilibrium temperature shift of 1.7 °C for cycle 9 as compared to pure MEG (20 wt% MEG/deionized water). The study strongly suggests that degradation of MEG can occur even if the reclamation unit is operated at temperatures below MEG's degradation temperature range. Degradation products,

primarily acetic acid were found in the analysis of MEG samples. Hence, it may be suggested that repeated heating through recycling of MEG could affect its ability to inhibit hydrates.

An empirical model based on the equilibria data of this study was developed to give insight to operators involved with MEG applications. The model has various modes of application. Specifically, it may be used to predict the decreasing effectiveness of MEG's hydrate inhibition performance over a specified number of regeneration cycles. Determining the equilibrium pressure and the temperature is indicative of the degree of degradation and increasing inefficiency of MEG with its continued cycling. With MEG's significant use in the oil and gas industry, the presented findings are beneficial as they can potentially aid MEG processing end-users to apply MEG more efficiently, particularly in relation to its hydrate inhibition capabilities.

Chapter 3 Evaluation of MEG Reclamation and Natural Gas Hydrate Inhibition during Corrosion Control Switchover

This chapter is comprised of the following publication:

- **Alef, K.**, Gubner, R., Iglauer, S., Barifcani, A., 2019a. Evaluation of MEG Reclamation and Natural Gas Hydrate Inhibition During Corrosion Control Switchover. *Journal of Petroleum Science and Engineering* 176, 1175–1186. doi: 10.1016/j.petrol.2018.08.052

This chapter contributes a detailed evaluation of the MEG regeneration and reclamation operation as applied in the context of corrosion control strategies. The switching of corrosion control strategies becomes of great importance as formation water production reaches critical levels. The study found that a fine balance of pH levels between the various processes must be achieved in order to successfully remove the amine while preserving the preferred corrosion inhibitor. The study recommends operating the pre-treatment unit at $\text{pH} > 8$ to precipitate out the divalent salts, and injecting acid before the regeneration unit, which allows for the volatile acetic acid to be removed via the reflux drum. It was found that FFCI and MDEA accumulation in the reclamation unit resulted in a highly viscous residue (1430.53 mPa-s) and a discoloration (from brown to very dark brown).

Furthermore, essential hydrate testing was conducted on the MEG samples and their metastable regions were determined. The new hydrate equilibria data revealed a hydrate promotion effect amongst the degraded MEG samples as opposed to pure non-degraded MEG. Moreover, MEG degradation products were identified to be acetic, formic, and glycolic acid. Observations reveal a colour change from colourless to slightly yellow depending on the extent of thermal degradation of the MEG samples. This contribution satisfies the thesis objectives (a), (b), (c), and (d) while fulfilling the research gaps outlined in Section 1.3.

3.1 Introduction

Corrosion, scale, and hydrate formation are some of the many challenges faced in the production of natural gas (Kan et al., 2002b; Nyborg, 2009; Sandengen, 2006). The challenges become even more complex when field formation water is produced. A corrosion control strategy may be adopted to lower the risk of corrosion and prevent corrosion damage to facility equipment and pipelines. Typical corrosion control strategies employ the pH stabilization method or utilize the injection of a corrosion inhibitor, such as a film-forming corrosion inhibitor (FFCI) (Latta et al., 2013). However, various factors must be considered when selecting a corrosion control method, including the environmental impact, corrosion, and scaling problems in the monoethylene glycol (MEG) regeneration process, and how corrosion products are consequently handled in the MEG closed loop (Halvorsen et al., 2006). Several field studies have illustrated the dynamic selection of corrosion control methods or a combination of various methods, including the concurrent use of scale inhibitors (Glenat et al., 2004; Hagerup and Olsen, 2003; Halvorsen et al., 2007; Halvorsen and Andersen, 2003; Latta et al., 2016; Olsen, 2006). In the pH stabilization method, a base such as methyl diethanolamine (MDEA) is added to the lean MEG injection stream to reduce the corrosion rate of gas condensate pipelines by artificially increasing the pH, thereby encouraging the formation of a protective scale on the inner walls of the production flowline (Dugstad and Seiersten, 2004; Halvorsen et al., 2007). However, pH stabilization increases the risk of scaling in the subsea architecture, particularly in the choke module and well jumpers, and it cannot be used once formation water breakthrough occurs, or initially when remnant completion fluids may pose a scale risk (Lehmann et al., 2014). This can negatively influence the MEG regeneration and reclamation process, as the formation water contains salts that, unless removed, may cause scaling and fouling within the equipment. In terms of corrosion control by corrosion inhibitors, four categories exist — cathodic, anodic, volatile, and mixed inhibitors. FFCIs are classified as mixed corrosion inhibitors and are commonly used. Essentially, FFCIs slow both the anodic and cathodic reactions, and they adsorb to the pipeline wall by forming a protective film that prevents corrosion (Lehmann et al., 2014). In this study, FFCI was employed as an alternative corrosion control method when pH stabilization was not feasible because of the increased risk of scale formation in the presence of formation water.

Gas hydrate formation in production and process pipelines is a serious problem, with dangerous consequences, such as pipeline blockage and damage to facilities (Chatti et al., 2005; Hammerschmidt, 1934; Sloan, 2005). The current industry practice is to inject chemical hydrate inhibitors, and MEG is commonly utilized. As increased costs are associated with the large volume of MEG required, MEG is recycled using MEG regeneration/reclamation facilities. Such facilities have two major processes: regeneration and reclamation. Regeneration uses distillation columns to remove water from the rich MEG stream; the rich MEG is contaminated with formation water and corrosion products, resulting in high total dissolved solids. Serious fouling caused by suspended solids and precipitation build-up due to salts from formation water or other injected chemicals in the plant can lead to production downtime, equipment failure, safety concerns, and other economic losses (Latta et al., 2013). Then, the regenerated MEG is taken through the reclamation unit, where it is heated above MEG's vaporization temperature under vacuum to recover MEG and water, while leaving behind non-volatile substances (e.g., salts and organic acids) as waste. The effect of continuous recycling of MEG on natural gas hydrates is not well known, especially when there are chances of MEG degradation during the regeneration and reclamation process. A loss in MEG quality may lead to lower performance of MEG as a hydrate inhibitor.

In this study, a MEG pilot plant housed at the Curtin Corrosion Engineering Industry Centre was used to simulate a switchover of corrosion control methods. The current strategy of pH stabilization with MDEA was switched to FFCI mode when field-wide formation water production became unmanageable through alternative means, such as production reallocation or scale inhibitor injection. The performance of the reclamation process was evaluated in terms of optimum operating pH for effective removal of salts, organic acids (such as acetic acid), and chemical additives, such as MDEA and FFCI. Further, the reclaimed MEG at the initial, middle, and final stages of the experiment was tested for natural gas hydrate inhibition, using a high-pressure PVT cell to evaluate hydrate inhibition performance and determine the possible loss in MEG quality.

3.2 Methodology

The experimental setup in this study essentially consisted of a reclamation unit as part

of a MEG pilot plant for MEG purification (illustrated in Figure 3.1) and a high-pressure PVT sapphire cell for hydrate testing (see Figure 3.2).

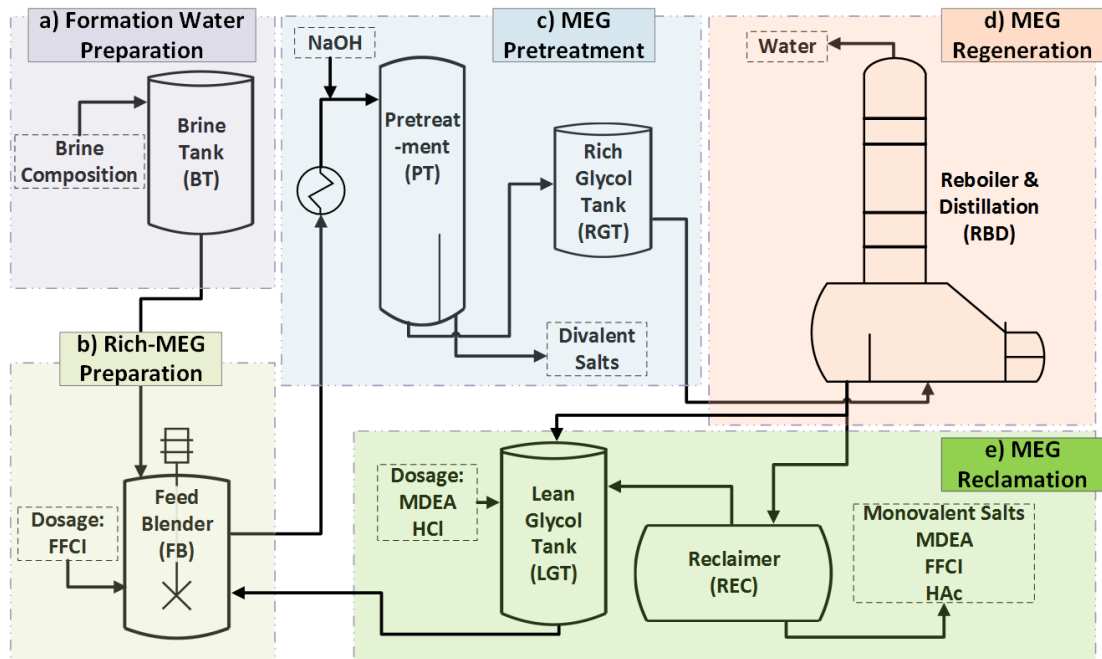


Figure 3.1: Experimental setup (bench-scale MEG regeneration/reclamation pilot plant).

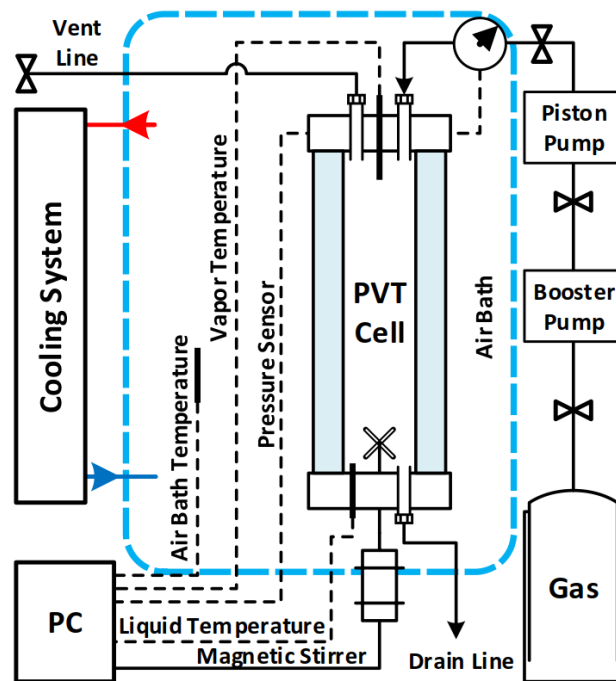


Figure 3.2: PVT sapphire cell used for gas hydrate testing.

3.2.1 Materials and Equipment

The pilot plant has been designed for studying the behaviour of MEG, production fluids, and other chemical additives under more realistic conditions compared with independent benchtop laboratory tests. The plant has a processing capacity of 1–4 kg/h of lean MEG. The plant has five stages: a) formation water preparation, b) rich MEG preparation, c) MEG pre-treatment (divalent salts removal), d) regeneration, and e) reclamation (see Figure 3.1). The plant consists of a brine tank, a lean glycol tank (LGT), a feed blender (FB), a pre-treatment unit, a rich glycol tank, a reboiler and distillation unit, and a reclamation unit. Formation water/brine was prepared based on field water composition (see Table 3.1) and stored in the brine tank. Similarly, lean MEG (see Table 3.1) based on the required field composition was prepared and stored in the LGT. The reclamation unit (rotary evaporator) used in this study was designed and supplied by Scitek Heidolph. It comprised the following components: a 20 L vacuum flask (flash separator), an oil bath, an overhead condenser, a collection flask to receive condensed MEG, a vacuum system, and a control box. The original setup did not allow for the measurement of the fluid temperature inside the rotary flask. Thus, a thermocouple was retrofitted into the slurry sump and connected to the programmable logical controller for slurry temperature measurements. The fill height of the vacuum flask was maintained by automatic additions of fresh lean MEG. A level sensor placed inside the rotary flask measured the liquid level, which was then used by the control system to automatically refill the flask with lean MEG based on the desired slipstream proportion (35% of output flow from the regeneration unit). The refill and drain times were configured accordingly. The input and output streams of the rotary evaporator were lined up with three probes to accurately measure the pH, electrical conductivity, and dissolved oxygen content. The rotary evaporator flask was modified to allow for purging with nitrogen to sustain a level of dissolved oxygen to below 20 parts per billion (ppb) owing to the corrosion risks involved. The temperature within the flask was carefully monitored in both liquid and vapour phases with K-type thermocouples ($\pm 0.75\%$ error) to avoid high temperatures that would have led to the degradation of the MEG. The data from all the instruments, including temperature, pressure, flowrate, pH, electrical conductivity, and dissolved oxygen measurements, were continuously recorded by the programmable logical controller system for subsequent analysis.

Table 3.1: Fluid compositions (brine/formation water, rich MEG, and lean MEG).

Component	Brine	Rich MEG	Lean MEG
MEG (wt.%)	0	57	80
Na (ppm)	4679	3767	3625
K (ppm)	106	85	77
Ca (ppm)	173	53	5
Mg (ppm)	13	7	5
Fe (ppm)	0.31	0.25	0.22
Sr (ppm)	15	8	5
Ba (ppm)	38	15	5
Li (ppm)	2.5	2	1.8
Cl (ppm)	7217	5812	5242
HCO ₃ (ppm)	828	667	601
SO ₄ (ppm)	6.2	5	4.5
Acetic acid (ppm)	500	403	363
Propanoic acid (ppm)	55	45	40
Butanoic acid (ppm)	4.6	3.7	3.4
Pentanoic acid (ppm)	2.3	1.9	1.7
Phenol (ppm)	32	26	23

A high-pressure PVT sapphire cell in the Clean Gas Technology Australia laboratory was used for natural gas hydrate inhibition testing. The cell was made from sapphire material and has a volume of 60 cc, with a pressure range of up to 50 MPa, and a temperature range of +60 to -160 °C.

MEG was supplied by Chem-Supply with a purity of 99.477 mol%. A high-temperature silicone heat transfer fluid, used in the oil bath of the reclamation unit known as Duratherm S, was supplied by Duratherm. MDEA, a clear liquid with a slightly yellow colour and an odour similar to ammonia, was supplied by Sigma-Aldrich with purity ≥ 99 mol%. A proprietary film forming corrosion inhibitor (FFCI) was utilized, having an amber colour with a moderate odour. The FFCI has a flash point of >62 °C, density of 1.025-1.095 (16 °C) and is completely soluble in water. Sodium hydroxide (≥ 97 mol%) and hydrochloric acid (32 wt%) supplied by Sigma-Aldrich were used to maintain the desired pH level and to ensure neutralization of MDEA during the switchover. Deionized water (electrical resistivity of 18.2 M Ω cm at 24.5 °C) and nitrogen (99.9959 mol%) were produced within the laboratory. Methane (ultra-high purity 99.995 mol%) and a synthetic natural gas mixture were sourced from BOC company for the hydrate inhibition testing (see Table 3.2).

Table 3.2: The composition of natural gas used in this study.

Component	Mole fraction
Methane	0.791
Ethane	0.070
Propane	0.040
n-Butane	0.020
iso-Butane	0.020
n-Pentane	0.017
iso-Pentane	0.017
Carbon dioxide	0.025

MEG concentration throughout the plant was measured using an ATAGO PAL-91S portable refractometer (accuracy of $\pm 0.4\%$). Accurate pH measurements are required to help lower the risk of scale formation and corrosion. Such pH measurements are complicated, as MEG and other additives have an effect on pH measurement and interference with the electrode's liquid junction potential can result in erroneous pH measurements (Bates, 1964; Kan et al., 2002a; Mussini et al., 1991). Thus, we adopted the method of Sandengen et al. (2007) for determining pH and installed Mettler-Toledo InPro 4800i pH sensors (accuracy of $< 0.1\%$ @ 25 °C) into the flow lines throughout the plant to obtain continuous measurements (Sandengen et al., 2007). The probes were thoroughly cleaned with deionized water and calibrated before and after experiments. Mettler-Toledo InPro 7100 sensors (accuracy of $\pm 5\%$ or better) were used throughout the facility to measure electrical conductivity, they have an operating temperature of 0-135 °C. The sensors were properly cleaned with deionized water and calibrated prior to use in experiments according to manufacturer's instructions. A HPLC system (Dionex U3000 with CAD detector, flow accuracy of $\pm 0.1\%$) was used for hourly measurement of residual FFCI concentrations to control the FFCI dosage rate. In addition, fluid compositions, MDEA concentration, and organic acids were analysed using an Ion Chromatography system (Dionex ICS-2100, flow accuracy of $< 0.1\%$), while alkalinity was monitored using a potentiometric titrator (HI902 accuracy of $\pm 0.5\%$ monovalent; $\pm 1\%$ divalent).

3.2.2 Procedure

The prepared fluids (brine, lean MEG, and FFCI) were transferred to the FB, where they were mixed, simulating the high shear stresses experienced in pressure reduction valves and turbulent pipeline flow. The resulting salt-laden rich MEG (56.9 wt% MEG in brine) was then routed to the pre-treatment unit, where divalent salts were removed. The resulting solution (contaminated with salts of monovalent cations) was stored in the rich glycol tank as feed for the regeneration unit. Then, this solution was pumped into the regeneration unit, where water was removed by distillation to form lean MEG at 80 wt% MEG. The output stream from the regeneration unit was divided into two streams; a slipstream went to the reclamation unit and the remainder went to the LGT. The proportion of output stream directed to the slipstream was dependent on the allowable limit of high soluble salts in the final lean MEG solution used in the operation. In this study, a slipstream of 35% of the output from the regeneration unit was directed toward the reclamation unit. The reclamation slipstream portion of lean MEG from the regeneration unit was routed to the rotary flask, controlled via a level sensor. The solution was flashed in the rotary flask, operating in vacuum conditions at ~ 10 kPa. Operating in vacuum conditions allows for the use of lower temperatures, which prevents the thermal oxidation of MEG (Latta et al., 2013). The rotary flask was heated to a temperature of ~ 130 °C by submerging it into an oil bath running at ~ 160 °C. Uniform distribution of heat was maintained by rotating the flask at a rate of 30 rpm. The MEG and water mixture vapour was cooled in the overhead condenser and collected in the collection flask. The condenser was cooled by a chiller operating at a temperature of 5.5 °C. The collected lean MEG, referred to as reclaimed MEG, was automatically transferred to the LGT. At the end of the experiment, the accumulated salt slurry was carefully removed from the rotary flask.

The switchover (MDEA to FFCI) was performed in a series of discrete steps, with MEG chemistry measured and stabilized after each step. Within each step, the dosage of each chemical was sequentially increased or decreased, based on regular sample analysis. Neutralization of MDEA was performed in four stages to reduce the risk of an excessive build-up of neutralized MDEA salts, which increases MEG solution viscosity, and to reduce the risk of hydrochloric acid (HCl) overdose, which may reduce the pH to levels at which corrosion rates are unacceptably high. Samples were

taken every 3 h and analysed, while samples to check for FFCI concentration in the FB and the LGT were taken on an hourly basis to prevent overdosing. The concentration of FFCI to be dosed into the LGT was determined using Eqn. (3.1), assuming that no chemical reactions or other losses occurred.

$$c(t) = \left(1 - e^{-\frac{t}{\tau}}\right) c_a + c_b \quad (3.1)$$

where t is time, τ is retention time, c_a is the feed (FFCI) concentration, and c_b is the concentration of FFCI already in the vessel.

Table 3.3: Target concentrations of FFCI and MDEA.

MDEA (mM) — LGT		FFCI (ppm) — FB	
Initial	End	Initial	End
100	0 (minimum)	0	1500

The material balance for the entire process is shown in Figure 3.3, with the target concentrations of FFCI and MDEA shown in Table 3.3. When the ramp-up of FFCI injection was completed and the rich MEG chemistry had stabilized, the cycle was ended. Each cycle represents a complete inventory turnover. The process was conducted for eight cycles and the entire experiment was performed twice to observe repeatability of the results and to improve facility operations.

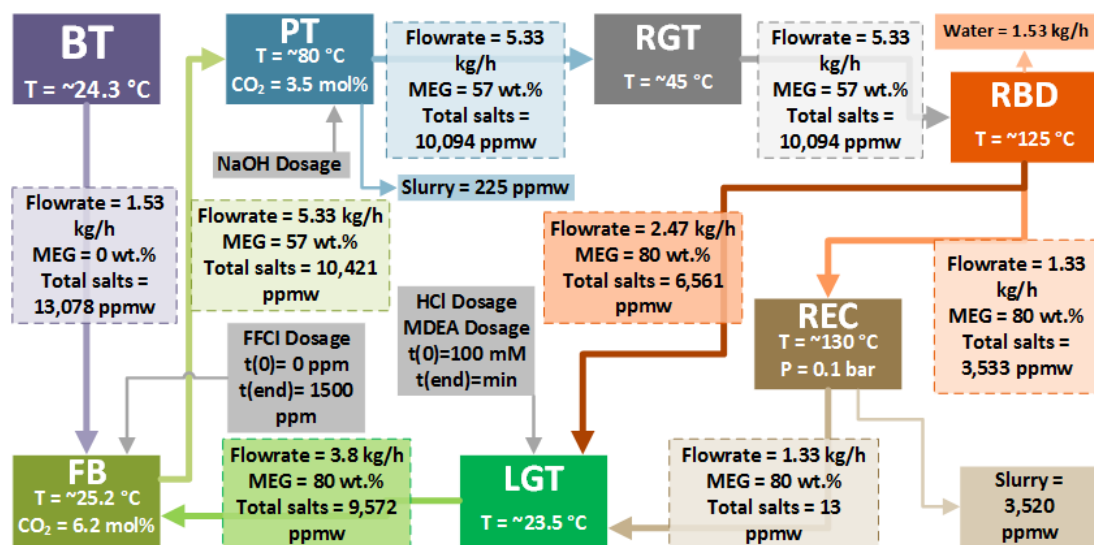


Figure 3.3: Material balance for the MEG pilot plant operation (cycle time of $\sim 10 \text{ h}$).

As for gas hydrate inhibition performance of the reclaimed MEG samples, the widely popular isochoric test method was employed for determining the hydrate dissociation (thermodynamic equilibrium) conditions, while hydrate formation points were visually observed over at least 5 runs. For all tests, a step-cooling and heating rate of 1 °C/h was adopted (Sloan Jr and Koh, 2007). Each test was conducted at least three times to test repeatability. Details of the procedure and test apparatus for hydrate testing have been explained in previous research studies (Alef et al., 2018a, 2018c; AlHarooni et al., 2017; Smith et al., 2016).

3.3 Results and Discussion

3.3.1 Switchover Operation

The objective of the switchover study was to determine if optimum operating conditions existed with the current plant configuration for the removal of both organic acids and MDEA, while also performing all the other necessary MEG plant processes, such as removal of unwanted salts. It was expected that pH would play a key role, as adjusting the pH level in the pre-treatment unit for the precipitation of divalent cations affects the required pH in the reclamation unit and, thus, the removal of organic acids and MDEA may have become problematic. The effect of pH on the MEG operation and, in particular, the reclamation unit was investigated by operating at different pH levels over the duration of the experiment. The initial pH target was set to 10 in the LGT and gradually stepped down by an amount of ~0.5 pH units each cycle via HCl neutralization. The experimentally measured pH values did not differ much (0.98% variance) from the target pH (see Figure 3.4), indicating that minimal overdosing of chemicals (sodium hydroxide (NaOH) and HCl) occurred. The lower pH level in the FB as compared to pH level within the LGT was the result of the initial makeup of rich MEG and the dissolved CO₂ gas.

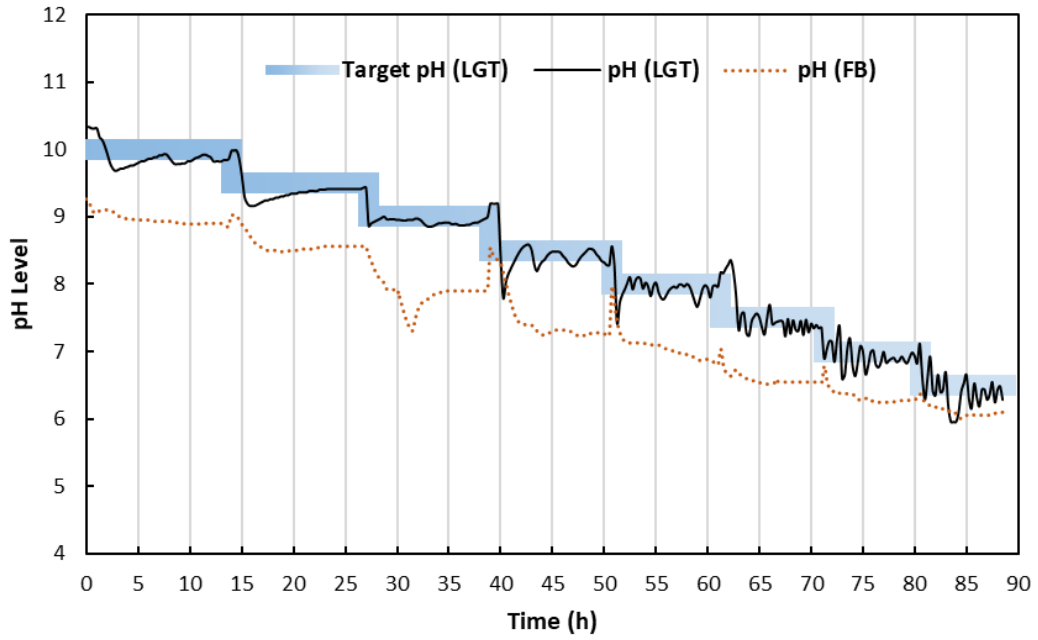


Figure 3.4: Target pH compared to actual pH in the lean glycol tank (LGT) and feed blender (FB).

Figure 3.5 shows FFCI and MDEA concentrations throughout the experiment within the FB and LGT, respectively. The target FFCI concentration within the FB was 1500 ppm, with a mean value of 1555 ppm, showing a standard deviation of 190 ppm. The target MDEA concentration within the lean MEG at the end of the experiment was optimistically set to zero, or as low as possible. However, the results show that the lowest concentration of MDEA achieved at the end of the experiment was 40–60 mM.

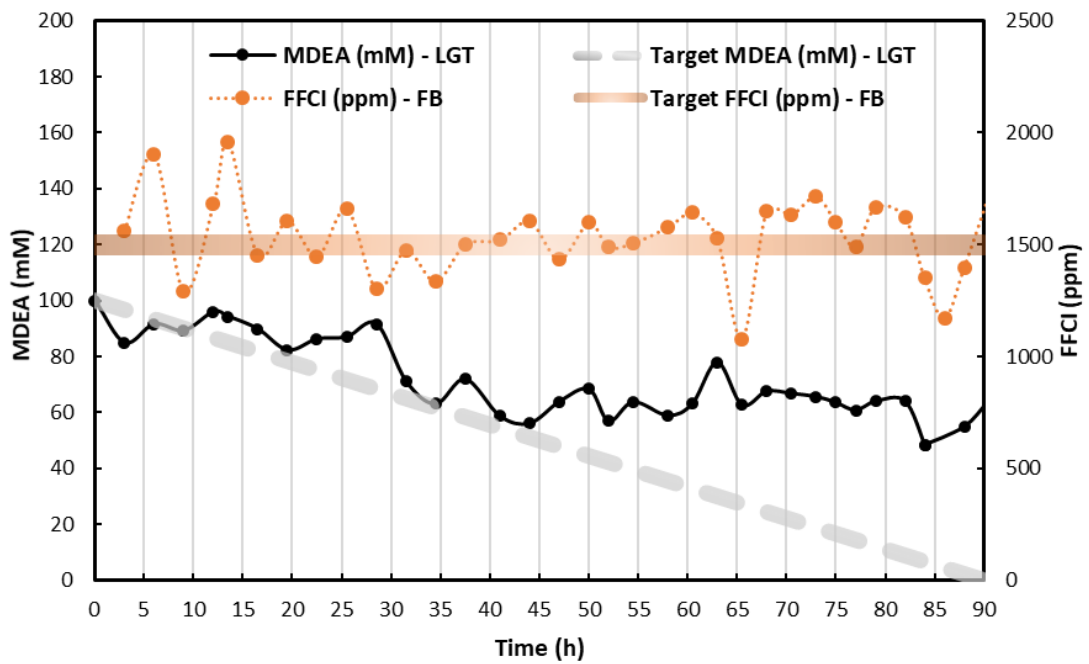


Figure 3.5: Actual and target MDEA and FFCI concentrations as a function of time.

The efficiency of the reclamation unit can be assessed with regard to the removal of salts and chemicals through electrical conductivity measurements. Figure 3.6 illustrates the electrical conductivity measurements of the MEG solution from the reboiler (feed to reclamation unit) and reclaimed MEG solution. As Figure 3.6 indicates, throughout the experiment, electrical conductivity was much lower in the reclaimed MEG solution compared with the feed to the reclamation unit. The difference ranges between $\sim 2200 \mu\text{S}/\text{cm}$, with a removal efficiency of 96%, confirming that the reclamation unit is highly efficient in removing the salts arriving in the feed solution. An increasing trend can be seen in the measured electrical conductivity of the MEG stream from the reboiler as well as a bump (80-200 $\mu\text{S}/\text{cm}$) between $t = 20-70 \text{ h}$ in the reclaimed solution. This increase can be attributed to the failure to remove MDEA as a result of unfavourable pH conditions and the lack of precipitation of divalent cations in the pre-treatment unit, which increased electrical conductivity in the MEG solution from the reboiler and reclamation units.

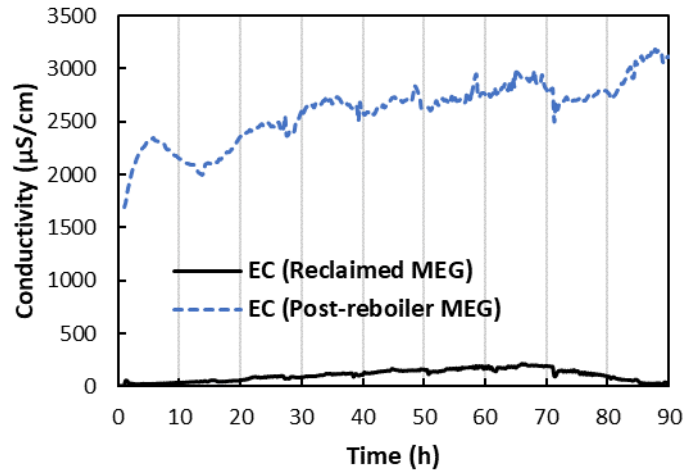
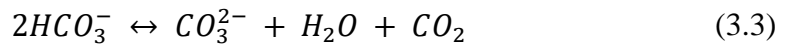


Figure 3.6: Electrical conductivity (EC) of post-reboiler and reclaimed MEG solutions.

3.3.1.1 Effect of pH on MDEA removal

The removal of MDEA is essential once formation water is produced. pH stabilizers elevate the pH of the system and, thus, increase scale formation and precipitation of divalent salts (Bikkina et al., 2012; Latta et al., 2013). Eqn. (3.2) to (3.5) show the breakdown of MDEA into its salt form, and the reaction of divalent ions, such as calcium ions (Ca^{2+}), with carbonate for precipitation of salts (Flaten et al., 2008; Latta et al., 2013).



The concentration of MDEA was measured in the feed stream to the reclamation unit (post-reboiler) and in the reclaimed MEG stream. MDEA concentrations together with the pH of reclamation stream have been plotted in Figure 3.7. The pH of the reclaimed solution at the beginning (0–20 h) was high (>10) in part because of the initial mixing of the chemical additives in each section of the plant, but mainly because of the initial high concentrations of MDEA (~ 100 mM). As Figure 3.7 shows, at this high pH range, MDEA concentration was accumulating in the reclaimed MEG solution, indicated by

the orange-shaded region. This signifies that none or very little MDEA was being removed in the reclamation unit. From $t = \sim 13.5$ to ~ 45 h, the MDEA concentration in the reclaimed MEG solution steadily decreased, while the pH dropped from ~ 10.5 to 9. Beyond the 45-h mark until $t = \sim 73$ h, the pH remained stable at ≤ 9 and MDEA continued to be removed from the reclamation stream (see the green-shaded region in Figure 3.7). At this lower pH range, the reclamation unit was able to convert MDEA to its salt form and, thus, it was precipitated out in the slurry. It was able to remove MDEA at an average rate of 14%. At this rate, it would take 425 h to completely remove MDEA from the MEG inventory, which is equivalent to 42.5 inventory turnovers. Beyond the $t = \sim 73$ h mark, the pH rose to about 9, and MDEA concentration within the reclaimed MEG stream began to increase (orange-shaded region). Clearly, a higher removal rate is required for a feasible operation. This could be achieved by further lowering the pH level within the reclamation unit.

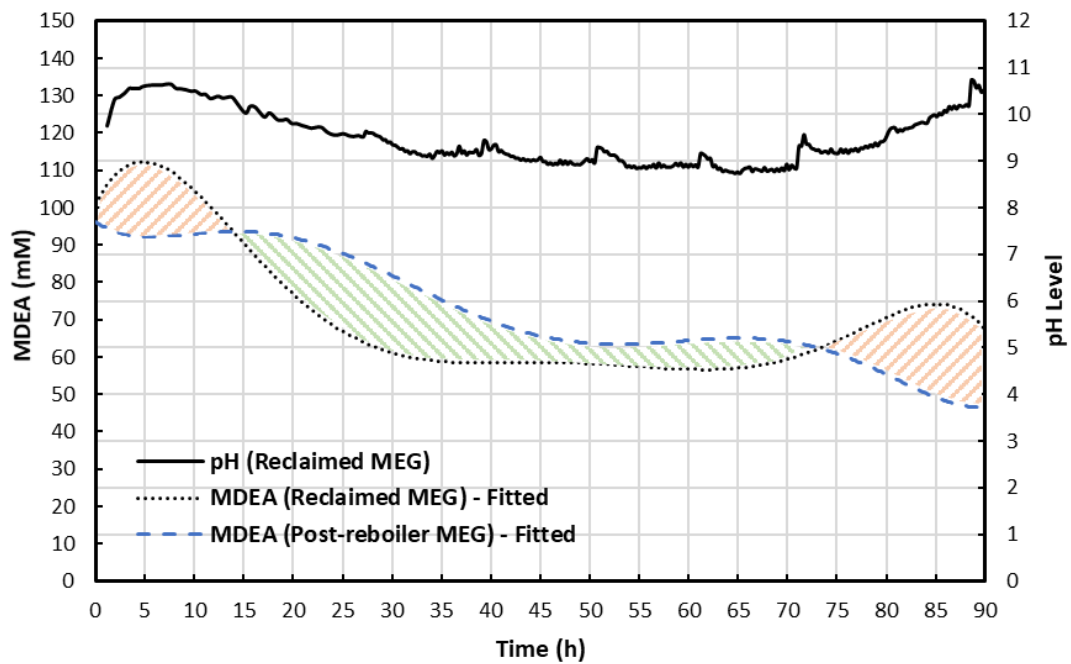


Figure 3.7: pH and MDEA concentration in post-reboiler and reclaimed MEG solutions as a function of time.

3.3.1.2 Effect of FFCI

The FFCI concentration in the feed to the reclamation unit compared with that in the reclaimed MEG solution is plotted in Figure 3.8. The results clearly show that FFCI was completely removed in the reclamation unit. No measurable FFCI was found in the reclaimed MEG solution (detection limit < 0.005 ppm). Further, FFCI is not a polymer (i.e., it is non-volatile), so full removal was expected. However, the removal of FFCI in the reclamation unit is not favourable when the adopted corrosion control method utilizes FFCI, as it requires constant reinjection of FFCI, which increases costs, albeit FFCI may be utilized in small quantities. Further, the pH range in the reclamation stream does not seem to influence the removal of FFCI. Figure 3.9 shows the gradual change in the salt slurry residues in the reclamation unit at various times during the experiment. Interestingly, FFCI accumulation in the reclamation unit results in a very different salt slurry residue compared with the harder, solid slurry residue that occurred when FFCI was not used. A discoloration of the residue within the reclamation unit was observed; the slurry was light brown initially and became very dark brown as the cycles progressed. Further, the viscosity at $t = 0$ h (i.e., 80 wt% MEG) was 8.97 mPa-s, while the viscosity of the final salt slurry residue, at $t = \sim 90$ h, was 1430.53 mPa-s, which corresponds to a ca. 159-fold increase in viscosity. The change in colour and increase in viscosity may have been caused by changes in the solution chemistry due to the degradation of products resulting from thermal oxidation and the accumulation of FFCI, MDEA, and organic acids in the slurry. The residue remained in liquid form but with a high viscosity (1430.53 mPa-s), whereas it was dry and solid when there was no FFCI in the solution. Detrimental side effects can occur with residue viscosity and hardness, as blockages in discharge lines can lead to sudden shutdowns of equipment. This indicates that the type of residue must be taken into account when considering design, especially when corrosion control methods switch, as varying chemical additives are utilized.

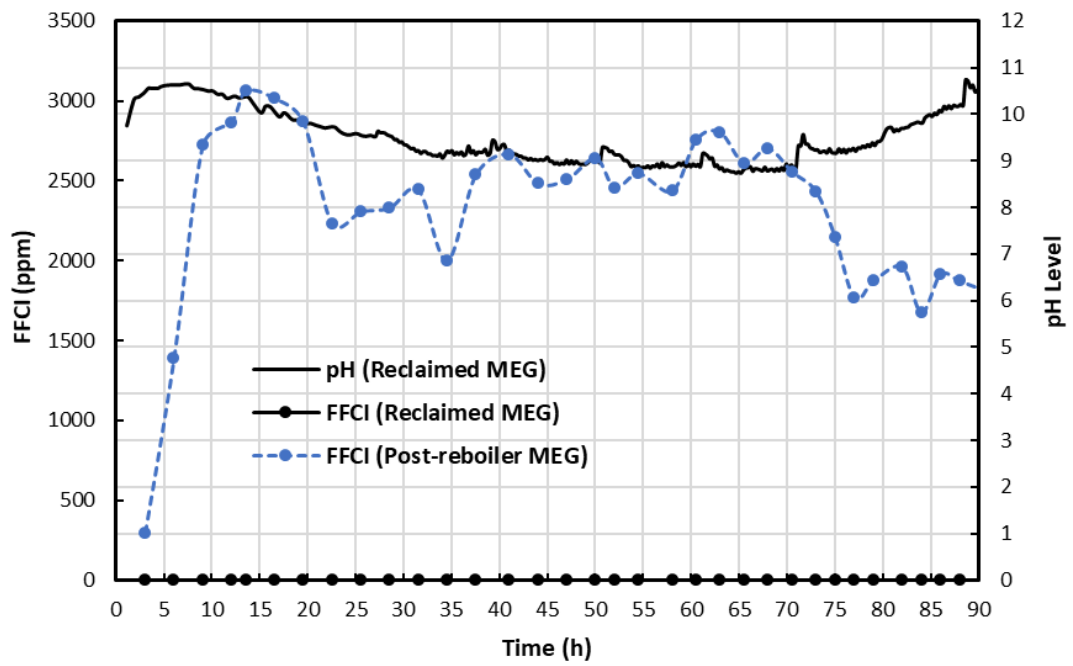


Figure 3.8: pH and FFCI concentration in post-reboiler and reclaimed MEG solutions as a function of time.

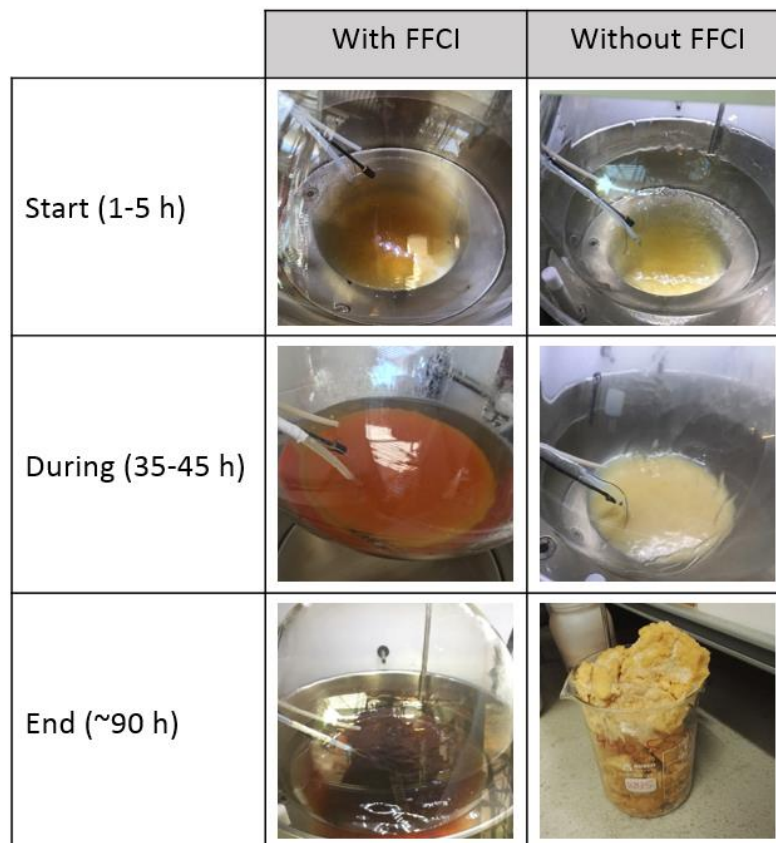


Figure 3.9: Physical and colour changes in salt slurry from the reclamation unit with and without FFCI.

3.3.1.3 Effect of pH on Acetic Acid Removal

Like MDEA removal, it is vitally important to remove acetic acid because of the increased corrosion risks involved. Acetic acid may accumulate in the MEG closed loop through the production of formation water (Latta et al., 2013) or if thermal oxidation of MEG occurs, as formic, glycolic, and acetic acids are produced (AlHarooni et al., 2015; Haque, 2012; Nazzer and Keogh, 2006). It is well known that acetic acid in the presence of CO₂ will increase corrosion of mild and carbon steel pipelines (Crolet et al., 1999; Ikeh et al., 2016; Liu et al., 2008), and increase top-of-the-line corrosion (Amri et al., 2009; Mendez et al., 2005; Svenningsen and Nyborg, 2014). Further, acetic acid may react with carbonate and bicarbonate present in the MEG stream to produce carbon dioxide, which lowers the pH and, thus, increases the corrosion rate (Halvorsen and Andersen, 2003; Lehmann et al., 2014).

The results show that there is a relationship between the reclaimed solution's pH and acetic acid concentration (see Figure 3.10). At pH levels above 10 ($t = 0-13.5$ h), there was no acetic acid present in the reclaimed MEG solution, but an average of 350 ppm of acetic acid was present in the input feed, indicating that the reclamation unit was effective in removing acetic acid. For $t = 13.5-22.5$ h, the pH steadily dropped to ~ 9.6 and acetic acid was removed at a rate of 39%. In contrast, at pH levels below ~ 9.6 ($t = 22.5-80$ h), the removal rate of acetic acid dropped to 29%. However, acetic acid concentration steadily decreased and tended toward zero, as the pH level started to increase above ~ 9.6 at $t \geq 80$ h, with a removal rate of 76%. The greater removal rate of acetic acid was due to the higher pH resulting in a high neutralization rate of acetic acid in the reclamation unit. Further, a lower pH level caused a decrease in the rate of the neutralization reaction between alkalinity and organic acids and, hence, lower removal rates were witnessed ($\text{pH} \leq 9.6$) over the period of $t = 22.5-80$ h (see Figure 3.10). It is clear that to remove organic acids such as acetic acid, the reclamation unit needs to be operated at high pH levels so that organic acids can be dissociated and then precipitated out of the reclaimed MEG solution in their salt form.

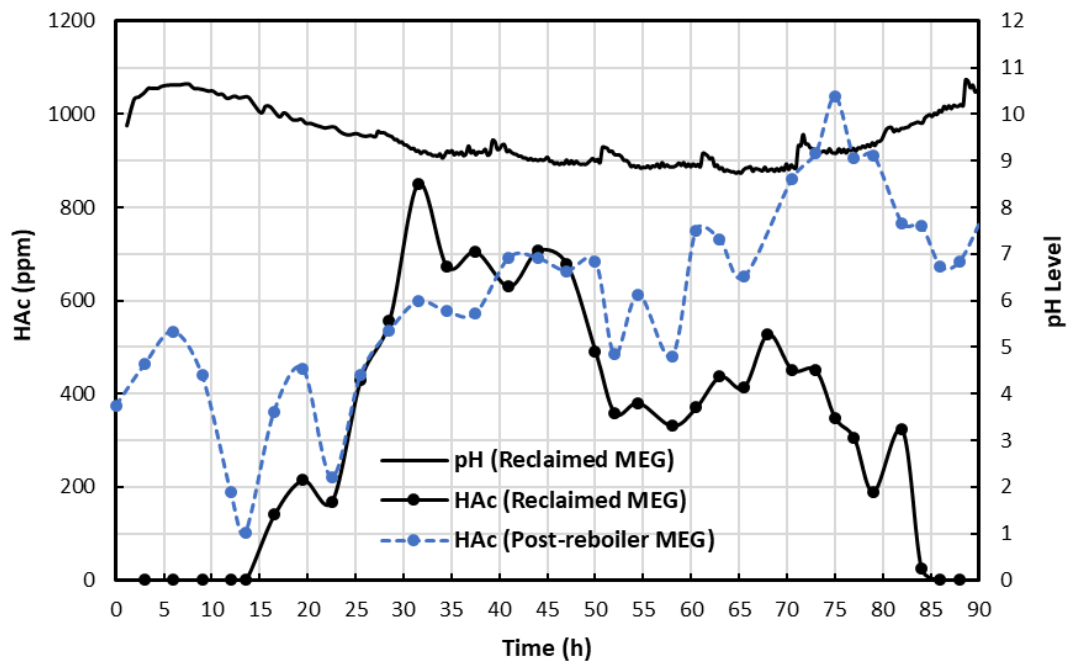


Figure 3.10: pH and acetic acid concentration in post-reboiler and reclaimed MEG solutions as a function of time.

3.3.1.4 Effect of pH on Divalent Salts Removal

The MEG pre-treatment unit was utilized to precipitate divalent salts, which prevents scale formation across the plant and downstream equipment (Baraka-Lokmane et al., 2013, 2012). For the precipitation reactions to occur, increased temperature, adequate residence time, and a sufficiently high pH must be established within the pre-treatment unit (Flaten, 2010; Montazaud, 2011). It was found that at $t = 0$ to ~ 62 h, the pH was below 8. At this pH level, the Ca^{2+} concentration was accumulating in the MEG inventory and was not being precipitated out in the pre-treatment unit as required. At $t = \sim 62$ h, NaOH was injected into the pre-treatment unit to increase the pH level to above 8, which resulted in very quick precipitation of divalent salts from the MEG inventory. Analysis showed that Ca^{2+} concentration dropped from 24 ppm to as low as 9 ppm while the Mg^{2+} concentration was not affected by the changes in pH.

3.3.2 Natural Gas Hydrate Inhibition

3.3.2.1 Preliminary Hydrate Testing

Preliminary hydrate testing was conducted, involving comparisons with the literature and prediction software, to determine apparatus accuracy and reliability of results. The

methane hydrate phase boundary was determined for a 30 wt% MEG solution over the pressure range of 8–18 MPa. The phase boundary is plotted in Figure 3.11, and the equilibria data points are tabulated in Table 3.4. Our results closely match the prediction results of Infochem's Multiflash (*Infochem Multiflash*, 2007), which utilizes the Association (CPA-Infochem) fluid phase model. The absolute average relative error (AARE) was calculated, using Eqn. (3.6), as 3.6%. Hydrate equilibria data obtained from the literature for the same system had a combined AARE of 4.7% (Haghighi et al., 2009b; Robinson and Ng, 1986). Thus, our results have low AAREs compared with the results from simulation and the existing literature, which suggests that our equilibria data are fairly accurate.

$$\text{AARE (T)} = \frac{100}{n} \sum_{i=1}^n \left| \frac{T_{calc} - T_{exp}}{T_{exp}} \right| \quad (3.6)$$

Table 3.4: Phase equilibrium data for 30 wt% MEG solution compared with Multiflash prediction and literature.

Methane + MEG (30 wt.%)		Multiflash CPA	Robinson and Ng (1986)	Haghighi et al. (2009)
P/MPa	T/°C	AARE/%	AARE/%	AARE/%
17.62	7.1	2.8	7.8	3.9
15.24	6.1	0.2	5.1	3.0
12.53	4.7	3.9	0.9	2.3
9.46	2.4	7.5	2.4	12.1
Average (AARE)		3.6	4.0	5.3

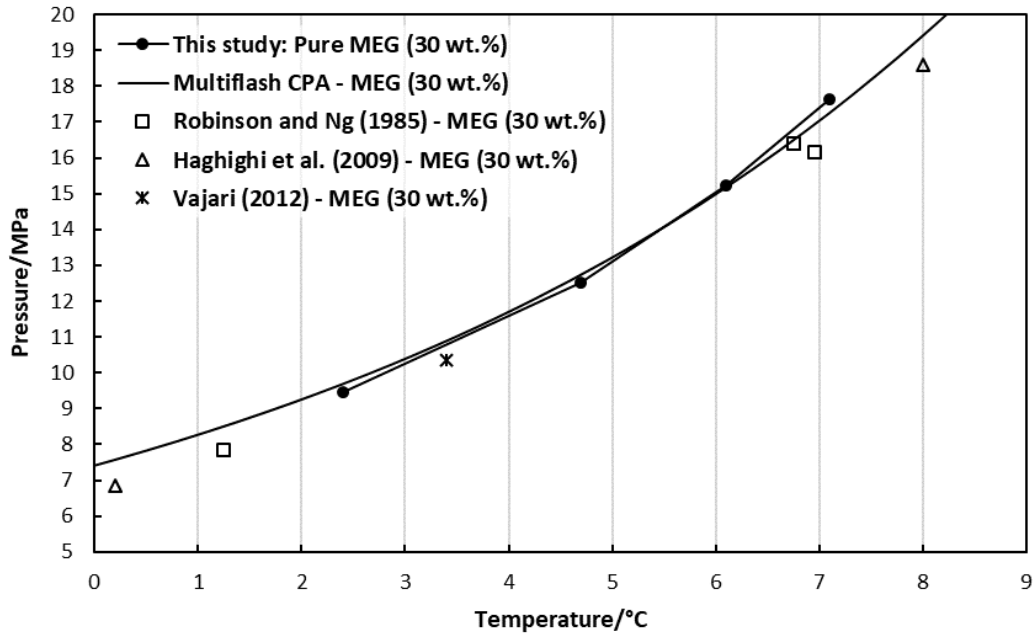


Figure 3.11: Methane hydrate phase boundary for 30 wt% MEG solution compared with Multiflash prediction and literature (Haghighi et al., 2009b; Robinson and Ng, 1986; Vajari, 2012).

3.3.2.2 Reclaimed MEG Hydrate Equilibria

The hydrate inhibition performance of the reclaimed MEG was evaluated by testing three samples (see Table 3.6) that came directly from the reclamation unit over the duration of the experiment. The test solutions were tested for natural gas hydrate inhibition, as opposed to pure methane, to ensure relevance to field scenarios, in which structure 2 (sII) hydrates are typically formed (the natural gas composition was given in Table 3.2). Hydrate formation and dissociation measurements were taken over the pressure range of 8-18 MPa and are tabulated in Table 3.5.

Table 3.5: Hydrate formation and dissociation (equilibria) data from this study.^a

Pure MEG – Natural Gas + MEG (35 wt.%)	
P/MPa	T/°C
18.16	10.5
14.94	9.7
12.61	8.9
8.57	7.3

Sample A – Natural Gas + MEG (35 wt.%)			
Formation		Dissociation	
P/MPa	T/°C	P/MPa	T/°C
17.65	3.7	17.12	9.5
15.76	3.4	14.87	9
12.23	2.5	13.02	8.5
9.87	1.6	8.93	7.1
Sample B – Natural Gas + MEG (35 wt.%)			
Formation		Dissociation	
P/MPa	T/°C	P/MPa	T/°C
17.44	6	18.24	11.2
15.73	5.6	15.41	10.4
12.76	4.5	12.34	9.5
9.78	2.9	8.67	8.1
Sample C – Natural Gas + MEG (35 wt.%)			
Formation		Dissociation	
P/MPa	T/°C	P/MPa	T/°C
17.93	6.4	17.71	10.8
15.34	5.9	15.24	10.1
12.83	5.3	12.45	9.3
9.14	3.1	9.32	8

^a Uncertainties are expanded uncertainties (U) calculated according to ISO's guidelines at a 95% level of confidence: U(P) = ±0.05 MPa; U(T) = ±0.03 °C (BIPM et al., 2008).

The left of the formation curve is known as the unstable zone, where spontaneous hydrate formation occurs. On the right-hand side of the dissociation/equilibrium curve, hydrate formation is impossible (Mullin, 2001). In the hydrate-stable region, hydrates may not form because of metastability, which refers to the persistence of the non-equilibrium state (Sloan Jr and Koh, 2007). Mullin (2001) described this region as one where spontaneous hydrate formation is improbable; however, in the presence of a hydrate crystal seed, growth will occur on the seed. Hydrate-stable regions were calculated from the formation and dissociation (equilibrium) curves using the definite

integral of the area under these curves, as per Eqn. (3.7):

$$\int_{P_{min}}^{P_{max}} (f_D(P) - f_F(P)) dP \quad (7)$$

where P_{max} and P_{min} denote the upper and lower boundaries for the area calculation, respectively, which were 8 and 18 MPa, respectively. The symbols $f_F(P)$ and $f_D(P)$ refer to the exponential fitted trend lines for the formation and dissociation experimental data, respectively.

Table 3.6: Reclaimed MEG samples (A-C) compositions, regression functions, and metastable regions.

Component	Sample A	Sample B	Sample C
Na (ppmw)	5.34	6.5	18.01
K (ppmw)	3.94	4.07	3.99
Ca (ppmw)	4.04	4.14	4.31
Mg (ppmw)	3.63	3.68	3.73
MDEA (mM)	38.83	24.73	31.12
Acetic acid (ppmw)	0	287.77	11.74
FFCI (ppmw)	0	0	0
MEG (wt.%)	35	35	35
Formation function (R^2)	$P = 6.287e^{0.274T}$ ($R^2 = 0.995$)	$P = 5.682e^{0.184T}$ ($R^2 = 0.995$)	$P = 4.864e^{0.196T}$ ($R^2 = 0.969$)
Dissociation function (R^2)	$P = 1.308e^{0.270T}$ ($R^2 = 0.999$)	$P = 1.234e^{0.242T}$ ($R^2 = 0.999$)	$P = 1.464e^{0.231T}$ ($R^2 = 0.999$)
Metastable region (MPa.°C)	58.53	52.65	44.58

Sample A represents the reclaimed MEG solution at the early stage of the experiment ($t = 6$ h). The hydrate phase boundary plotted in Figure 3.12 shows a leftward shift, representing enhanced hydrate inhibitory performance compared with a pure/fresh MEG sample of the same concentration. On average, a temperature shift of -0.47 °C was found relative to the equilibrium phase boundary calculated using Multiflash of 35 wt% pure MEG/deionized water solution. This leftward shift in the phase boundary

was due to the presence of MDEA in the MEG solution. Composition analysis of sample A show that 38.83 mM of MDEA was within the solution (see Table 3.6); the presence of MDEA was caused by the failure to remove it during reclamation (see Figure 3.7). Recent studies have suggested that MDEA may perform as a thermodynamic hydrate inhibitor. Thus, our results confirm that MDEA enhances the inhibition effect of 35 wt% MEG solution (Akhfash et al., 2017; AlHarooni et al., 2017). The metastable region for sample A is plotted in Figure 3.13. Compared with samples B and C, sample A had the greatest metastable region of 58.53 MPa °C, possibly as a result of less thermal exposure time and the added inhibition effect of MDEA with MEG (see Table 3.6).

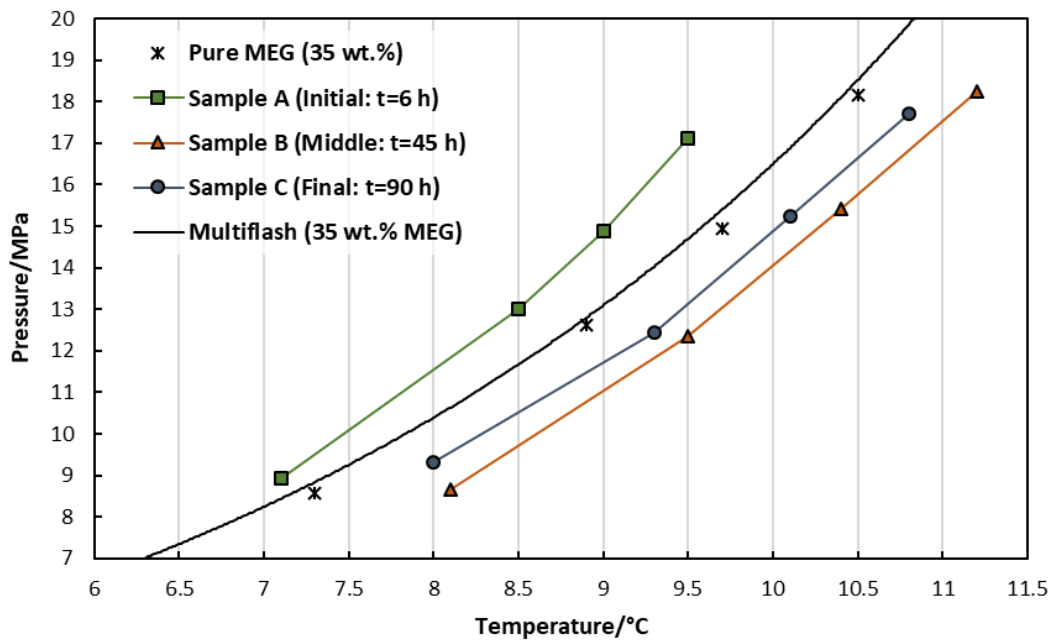


Figure 3.12: Natural gas hydrate phase boundaries for reclaimed MEG samples A-C.

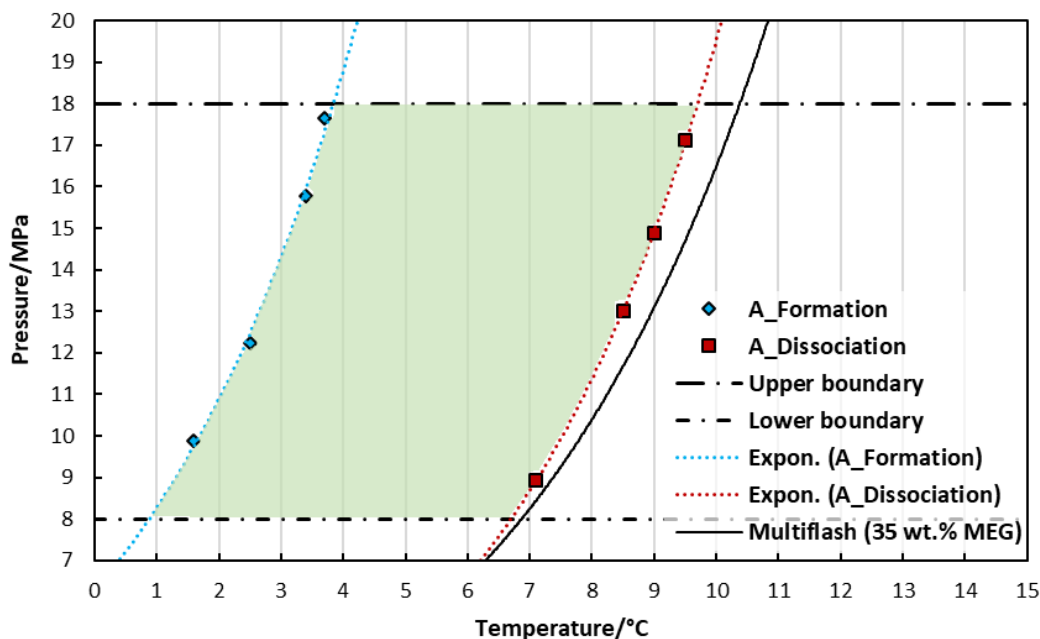


Figure 3.13: Hydrate metastable region for reclaimed MEG sample A.

Sample B represents the reclaimed MEG solution extracted during the middle stage of the experiment ($t = 45$ h). As shown in Figure 3.12, the hydrate phase boundary for sample B shifted rightward by 0.79 °C beyond the phase boundary of the pure MEG solution of the same concentration. This rightward shift in the hydrate phase boundary indicates a lower inhibitory performance due to the removal of MDEA from reclaimed MEG, as well as a hydrate promotion effect. Possible reasons for hydrate promotion are thermal degradation of the MEG and the presence of degradation products of MEG and MDEA. It is clear from Figure 3.7 that MDEA concentration decreased (equivalent concentration of 24.73 mM in 35 wt% MEG) because of lower pH conditions, which aid in the precipitation of MDEA out of the MEG solution. Thus, the added hydrate inhibitory performance from the proportional MDEA concentration in a 35 wt% MEG solution was diminished. Figure 3.10 shows that between $t = 30$ and 50 h, acetic acid concentration within the reclaimed MEG solution was accumulating because the pH level was below the high level required for the removal of acetic acid. Further, the acetic acid concentration increased beyond the input concentration found in the MEG stream from the reboiler, suggesting that MEG may have suffered thermal degradation. Several studies have determined the degradation products of MEG to be acetic, formic, and glycolic acids (AlHarooni et al., 2015; AlHarooni et al., 2016; Psarrou et al., 2011; Rossiter et al., 1985). AlHarooni et al. (2015) reported that MEG degradation

decreases the ability of MEG to act as a hydrate inhibitor after they exposed samples to high temperatures over 48 h (AlHarooni et al., 2015). However, our study was conducted at a temperature range of 130 ± 5 °C, over a total period of 45 h, as opposed to the high temperatures (165-200 °C) utilized by AlHarooni et al. (2015), suggesting that MEG degradation may also occur at lower temperatures or over a prolonged thermal exposure time. In terms of metastable regions, sample B has an area of 52.65 MPa °C, which is a 10% decrease compared with sample A (see Figure 3.14).

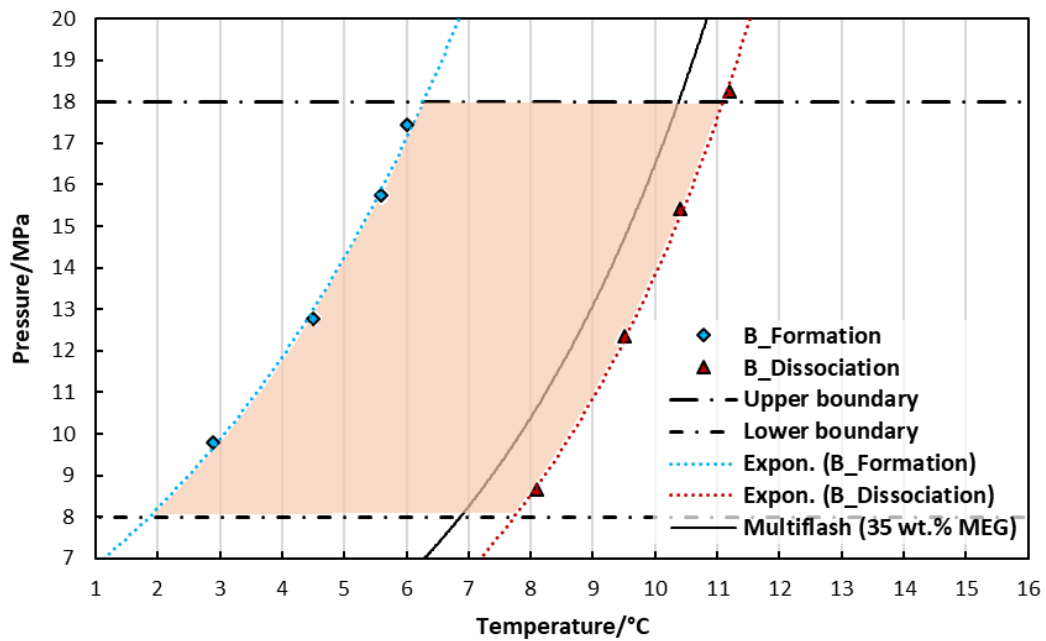


Figure 3.14: Hydrate metastable region for reclaimed MEG sample B.

Sample C represents the reclaimed MEG solution that was extracted at the end of the experiment ($t = 90$ h). Sample C had better hydrate inhibitory performance than sample B. The hydrate phase boundary shifted rightwards by 0.50 °C beyond the phase boundary of a pure MEG solution of the same concentration. The rightward shift may be due to the extended thermal exposure time (~ 90 h) and consequent accumulation of degradation products. Table 3.6 shows that sample C had a higher concentration of MDEA (hydrate inhibitor) than sample B, which explains the slightly better performance. In terms of the metastable regions, sample C has the smallest area of 44.58 MPa °C when compared with the areas of samples A and B (see Figure 3.15 and Table 3.6). This smaller metastable region is of concern and may be due to the extended thermal exposure time.

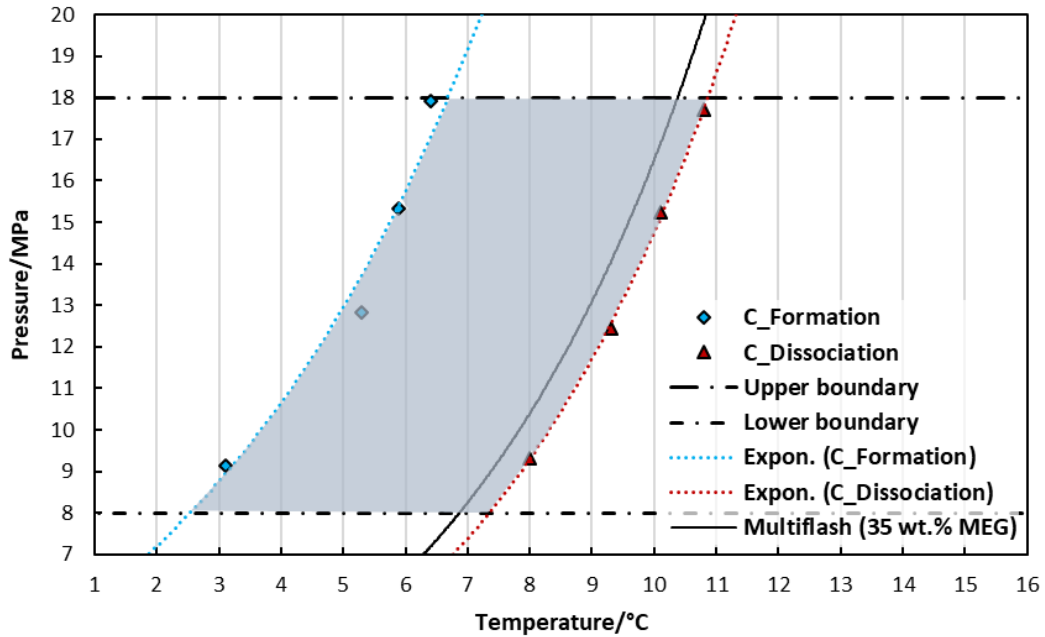


Figure 3.15: Hydrate metastable region for reclaimed MEG sample C.

3.4 Conclusion

Overall, the study confirms that operating the MEG loop system is dependent on a complex balance of pH between the different units involved. MDEA, acetic acid, and salts need to be progressively removed from the MEG inventory. If MDEA remained, there would be an increased potential for scale formation in the presence of formation water, as the barium and calcium ions appear. The study found that a pH of ≤ 9 was required to sufficiently remove MDEA in the reclamation unit. A pH of at least 9.6 was required to neutralize the acetic acid and remove it in its salt form in the reclamation unit. Further, a pH level above 8 was required in the pre-treatment unit to effectively precipitate out divalent salts. Ultimately, with the current plant configuration, the pH in the pre-treatment unit directly affects the pH in the consequent process units, including the reclamation unit. To address this issue, it is recommended that a new acid injection point be inserted after the pre-treatment unit, but before the regeneration unit, to decrease the pH, yet allow the pre-treatment unit to operate at the required pH. The acid injection will decrease the pH of the MEG solution entering the regeneration unit to levels below 7 and, thus, allow volatile acetic acid to be easily removed via the reflux drum alongside water. The consequent pH in the feed to the reclamation unit will be sufficiently low for MDEA to be successfully removed at a

greater rate than the 14% found with the current plant configuration. As for FFCI, the study has confirmed that pH conditions do not influence FFCI removal and that it was completely removed. Thus, complete FFCI loss in the slipstream to the reclamation unit can be expected. This may lead to increased costs because of the constant top up required, as FFCI is lost in the slipstream proportion. Further, FFCI accumulation in the reclamation slurry leads to a highly viscous residue (1430.53 mPa-s), which could potentially cause problems inside the reclamation unit, leading to downtime and increased maintenance. Therefore, the study recommends the consideration of designs to be put in place within facilities to handle chemical compounds such as FFCI accumulation.

The natural gas hydrate inhibition performance of reclaimed MEG from the initial, middle, and final stages of the experiment were evaluated. The initial sample showed the best performance because of the low thermal exposure time and the presence of MDEA which is known to act as a hydrate inhibitor. The middle sample showed the worst performance because of the prolonged thermal exposure (45 h), even though temperatures were kept around 130 °C, and the presence of smaller concentrations of MDEA. Interestingly, the final sample showed better performance than the middle sample but had the lowest metastable region of all three samples. The results suggest that MEG degradation may even occur at low temperatures over extended thermal exposure times and in low pH conditions.

Chapter 4 Effect of Salt-Laden Degraded MEG on Gas Hydrate Inhibition

This chapter is comprised of the following publication:

- **Alef, K.**, Barifcani, A., 2018. The Effect of Salt-Laden Degraded MEG on Gas Hydrate Inhibition. Presented at the SPE Kingdom of Saudi Arabia Annual Technical Symposium and Exhibition, Society of Petroleum Engineers. doi: 10.2118/192447-MS

In this study, MEG solution with realistic brine composition was tested for its gas hydrate inhibition performance. The typical lean-MEG solution was prepared by combining pure MEG in a brine solution based on common formation water salt composition. The degraded samples were extracted from a MEG recovery pilot plant that had undergone a complete recovery operation (~13 h) sustaining high exposure temperatures. Samples were then taken for gas hydrate testing using a high-pressure PVT cell. The isobaric hydrate testing method was employed for accurate hydrate equilibria results.

The new hydrate equilibria data revealed a hydrate promotion effect amongst the degraded MEG samples as opposed to pure non-degraded MEG. Although salt in the MEG solution improved hydrate inhibition, the results show that the inhibition effect was decreased as the extent of MEG degradation increased. Furthermore, MEG degradation products were identified to be acetic, formic, and glycolic acid. Observations reveal a colour change from colourless to slightly yellow depending on the extent of thermal degradation of the MEG samples. This contribution satisfies the thesis objectives (a), (b), and (d) while fulfilling the research gaps outlined in Section 1.3.

4.1 Introduction

Natural gas has increasingly become a profitable alternative to meet energy demands. However, the formation of gas hydrates continues to be a major challenge in the production and transportation of natural gas. For the least, hydrates can cause blockages in pipelines and thus severely disrupt gas production, and in some cases, they have the potential to even cause explosions in pipelines (Koh et al., 2011; Sloan Jr and Koh, 2007).

Hydrates are crystalline solids which are composed of molecules of gas and water. The gas molecules are known as ‘guest molecules’, become confined by the host; the host being cavities in the cage formed by water molecules. Common natural gas molecules include carbon dioxide, methane, ethane, and propane (Eslamimanesh et al., 2011; Sloan Jr and Koh, 2007). Such hydrates thus form in the presence of water and gas molecules at high pressure and low-temperature conditions (Zarinabadi and Samimi, 2011). These conditions commonly exist in subsea production and process lines, hence the need for hydrate inhibition. Certain techniques, if applied could eliminate at least one of these conditions: low temperatures can be eliminated by heating or thermal insulation; high pressures can be eliminated by depressurization, and water can be eliminated through natural gas dehydration by glycol or molecular sieves (Samimi, 2012). However, these techniques are not always applicable and may not be cost-effective (Sloan Jr and Koh, 2007; Son and Wallace, 2000).

Conventionally, thermodynamic hydrate inhibitors (THIs) are injected at the wellhead for the purpose of lowering the risk of hydrate related problems. THIs shift the hydrate equilibrium phase boundary to a higher pressure and lower temperature region thus allowing pipeline operating conditions to be within a hydrate-free region (Li et al., 2006). THIs are required in large volumes for an effective hydrate inhibition program. Common inhibitors that are utilized in the industry include methanol and monoethylene glycol (MEG). Although a larger volume of MEG is required as compared to methanol for the same hydrate formation temperature depression, MEG proves to be superior of the two. This is due to the lower volatility of MEG and lower solubility in gas, thus resulting in lower losses of MEG to the hydrocarbon phase as compared to methanol. Furthermore, the resulting water from a MEG system is cleaner than a methanol system, hence imposing no environmental concerns (Bikkina et al.,

2012). MEG also poses more benefits as an inhibitor than other glycols such as diethylene glycol (DEG) and tri-ethylene glycol (TEG), as MEG is more efficient in terms of weight to effectiveness ratio, and has little effect in changing the viscosity of water than other glycols (Hemmingsen et al., 2011). Furthermore, Brustad et al. (2005) suggest that MEG yields better suppression performance when compared to TEG due to lower molecular weight (Brustad et al., 2005). However, the greatest advantage of MEG over other THIs is the ability to be recovered using MEG regeneration units (MRUs) for continuous re-injection thus decreasing costs.

MRUs or the MEG recovery process is often established between offshore platforms (wellheads) and receiving facilities (onshore). The natural gas with associated condensate, produced water and used MEG also known as rich-MEG (MEG with contaminants from the production line) comes out of the well and into a production facility where phase separation will occur. The three-phase separator will then separate the fluid into gas, hydrocarbon liquid, produced water and rich-MEG. The rich-MEG stream will go through the MEG recovery process, whereas the produced gas and hydrocarbon liquid will be sent onshore for further processing. MEG recovery consists of two primary stages; regeneration and reclamation, and may sometimes include a MEG pre-treatment stage for the removal of potentially dangerous divalent salts. The MEG regeneration process involves the use of a reboiler and a distillation column to distil off unnecessary water to form the desired lean-MEG concentration (typically 80-90 wt%) required for re-injection (Psarrou et al., 2011). This process is performed under ambient pressure and at a temperature that is enough to boil water off but not MEG (typically >130 °C). This has been proved to be an effective process particularly in the beginning of production and where the water contains low total dissolved solids (TDS). However, as the field matures, there is an increase in the level of salt and other substances in the rich-MEG stream due to the production of formation water or remnant drilling fluids. These salts will pollute, accumulate and precipitate in the processing facility, and will not only increase MEG viscosity but may create fouling and deposition issues for the processing equipment (Bikkina et al., 2012). These salts will also lead the system to be more susceptible to corrosion. As for the reclamation stage of the process, it can be conducted in two modes; full-stream and slip-stream reclamation. This depends on the allowable amount of salt in the final lean-MEG solution ready for re-injection. In the slip-stream mode, a portion of the total output of

the MEG stream from the reboiler will undergo the reclamation stage. The reclamation stage consists of flashing the incoming MEG stream in a flash separator to remove soluble salts and non-volatile substances.

However, during the recoverability process, MEG may undergo multiple phases of thermal exposure. This will usually lead to the degradation of MEG which in-turn results in lower hydrate inhibition performance. Gas hydrates and prevention strategies have been researched extensively due to the detrimental consequences of hydrates in flow assurance. However, very little research exists that explores the effect of degradation of MEG on hydrate formation especially salt-laden MEG solutions. Thus, its behaviour in production and transportation systems need to be well researched to meet safety and production demands. In this study, rich-MEG samples which had undergone pre-treatment, regeneration and a slip-stream reclamation process were tested in a high-pressure PVT cell for the hydrate inhibition performance.

4.2 Methodology

MEG solution samples were extracted from the lean-glycol storage tank of a MEG regeneration/reclamation pilot plant (Figure 4.1). The MEG had undergone a pre-treatment stage where divalent or insoluble salts were removed from the salt-laden MEG solution which is typically performed to prevent scale formation within process facilities (Latta et al., 2013). The resulting solution was then regenerated to the required MEG concentration for reinjection into the wellhead – typically 70-90 wt% (Halvorsen et al., 2006; Nazzari and Keogh, 2006). The output solution which was still contaminated with soluble salts was then routed to the lean-glycol storage tank, whilst a slip-stream was routed to the reclamation unit (Son and Wallace, 2000). In the reclamation unit, the slip-stream portion was exposed to high temperatures to evaporate MEG and water whilst leaving behind the soluble salts in the reclaimer sump as waste. Once condensed, the reclaimed MEG solution was transferred to the lean-glycol storage tank. The composition of the final MEG solution is given in Table 4.1.

Table 4.1: Salt-laden MEG solution composition.

Component	Concentration (wt%)
MEG	80.20
Water	17.49
NaCl	1.75
KCl	0.55
Acetic acid	0.01

The hydrate testing of the MEG solution was conducted using a high-pressure PVT sapphire cell as shown in Figure 4.1. The isobaric hydrate testing method was employed with a step-cooling/step-heating rate of 1°C/h. At this rate, a homogenous and steady hydrate formation process was facilitated and thus accurate results were expected (Haghighi et al., 2009b). With this method, the gas hydrate equilibrium conditions are determined visually. Researchers that have used this method have attained accurate results when compared against results from other methods and prediction calculations (Chen et al., 2010; Mohebbi et al., 2012; Windmeier and Oellrich, 2014). The cell's chamber was cleaned with ethanol and deionized water prior to each test. A vacuum pump was then used to remove air and other gases from the cell to ensure there were no contaminants that could potentially affect the results. A sample (6 mL) of the MEG solution after dilution to 25 wt% MEG was then injected into the cell. The cell comes equipped with a magnetic stirrer that can operate at 500 rpm which helps in the continuous renewal of the water/gas surface to allow hydrate to form more readily and throughout the cell. The cell was then pressurized to the desired test pressure with methane via a piston pump with the aid of a pneumatic booster pump. Once, the test pressure was configured to be constant, the step-cooling system was activated. The pressure and temperature of the moment when first hydrate formation was detected were recorded. The cooling process was allowed to continue until after all visible liquid was converted to hydrate and the magnetic stirrer was brought to an abrupt stop due to hydrate blockage. At this stage, the step-heating process was commenced to determine the dissociation point (thermodynamic equilibrium) visually at the first sign of hydrate dissociation. These conditions were recorded for all tests for consequent analysis and comparison studies.

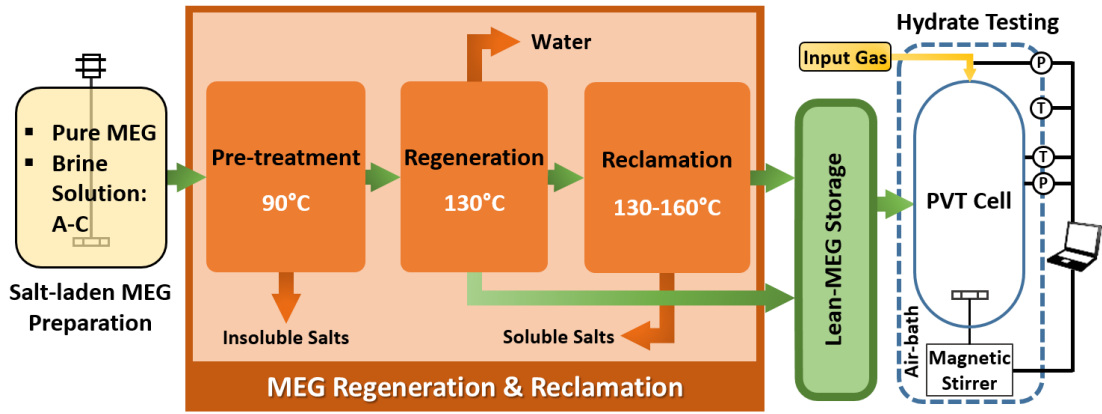


Figure 4.1: Basic schematic of the experimental apparatus utilized in this study including the PVT cell.

The materials utilized in this study are shown in Table 4.2. Deionized water was produced in-house via reverse osmosis with an electrical resistivity of $18 \text{ M}\Omega\cdot\text{cm}$ at $25.3 \text{ }^\circ\text{C}$. Nitrogen was also produced in the laboratory using a nitrogen generator with a purity of 99.997 %.

Table 4.2: Materials utilized in this study.

Chemical	Supplier	Purity (mol %)	CAS Number
Monoethylene glycol (MEG)	Sigma-Aldrich	99.8	107-21-1
Ethanol	Sigma-Aldrich	≥ 99.8	64-17-5
Methane	BOC (Australia)	99.995	74-82-8
Sodium chloride (NaCl)	Sigma-Aldrich	≥ 99.0	7647-14-5
Potassium Chloride (KCl)	Sigma-Aldrich	≥ 99	7447-40-7

4.3 Results and Discussion

Hydrate testing was conducted on pure water to check the accuracy of the results of the isobaric method and the experimental apparatus. The methane hydrate phase boundary of pure water (deionized) was determined over the pressure range of 70-130 bar. The equilibrium data is plotted in Figure 4.2 and tabulated in Table 4.3. Simulations of the hydrate experiments were conducted in HYSYS using the Peng-Robinson equation of state to provide a comparison (*Aspen HYSYS*, 2007). An average

absolute percentage deviation (AAPD) of 2.5 % was found between our experimental data and the HYSYS prediction. The formula for AAPD calculations is given in Eqn. (4.1). Furthermore, results from the literature were also compared to our data (Carroll, 2014; Lu and Sultan, 2008; Maekawa, 2001), and an AAPD of 1.3 % was found. Both AAPDs are relatively low in comparison to other literature and thus we can with confidence say that our experimental data is very accurate.

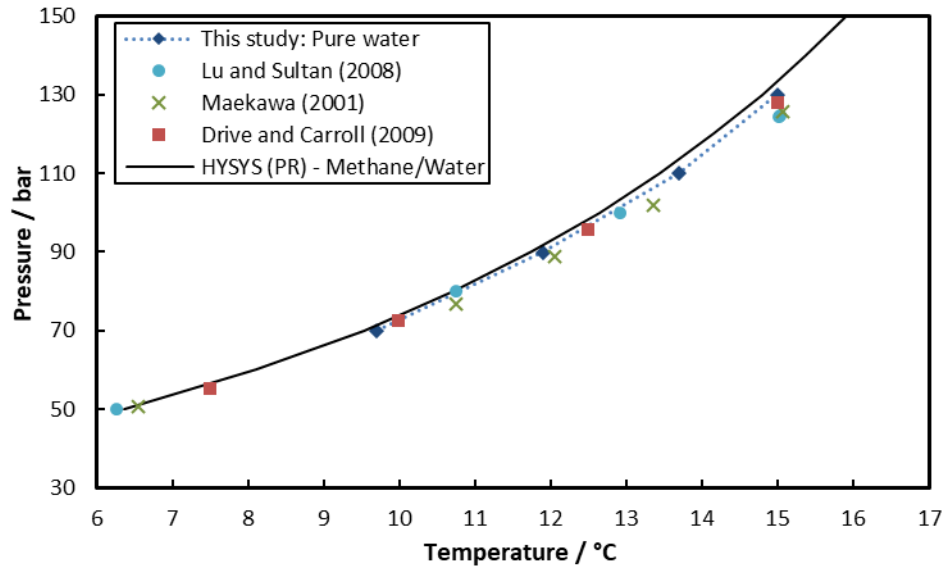


Figure 4.2: Methane hydrate phase boundary of pure water compared to literature and software.

$$AAPD = \sum_{i=1}^n \left| \frac{T_{calc} - T_{exp}}{T_{exp}} \right| \times \frac{100}{n} \quad (4.1)$$

4.3.1 Salt-laden MEG

To investigate the effect of MEG degradation on hydrate formation, two solutions were prepared. The first was prepared to provide a reference hydrate inhibition performance and was considered as a non-degraded MEG solution. The non-degraded solution was prepared with the same proportional salt composition as shown in Table 4.1 relative to a MEG concentration of 25 wt%.

The MEG solution from the lean-glycol tank still contained salt after the recovery process as only a slip-stream was fully reclaimed (Table 4.1). This solution was considered as degraded MEG as it had undergone one complete recovery process

whilst exposed to a temperature range of 130 – 160 °C between the reboiler and reclainer. The solution was prepared for hydrate testing by dilution to 25 wt% MEG with deionized water to match typical MEG concentrations found after injection into wellheads.

The hydrate phase boundaries for both solutions are plotted in Figure 4.3 and the equilibria data are provided in Table 4.3 with equilibrium temperature shifts.

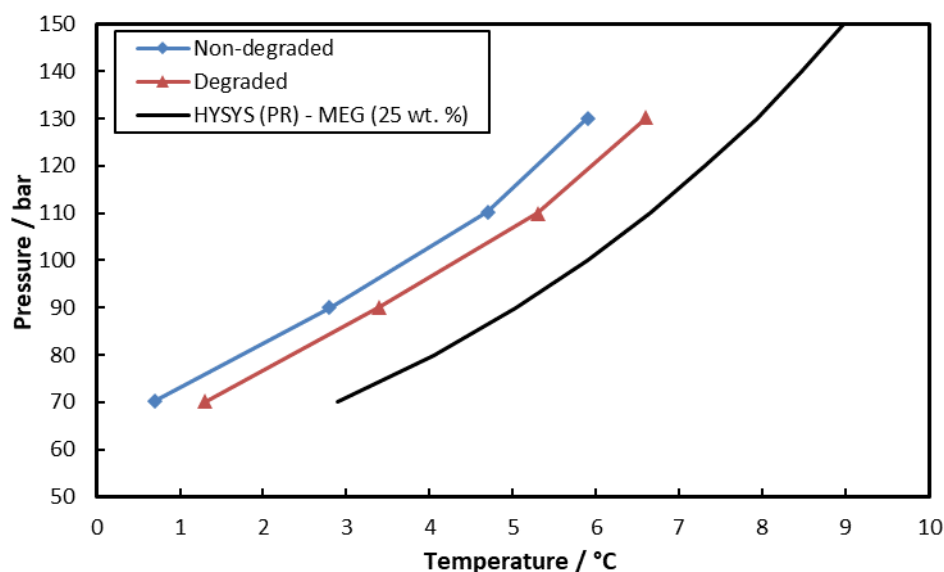


Figure 4.3: Hydrate phase boundaries for non-degraded and degraded MEG samples compared to HYSYS prediction.

Table 4.3: Methane equilibria data of this study with relative temperature shifts.

Pure water		Pure MEG (HYSYS-PR)		Non-degraded MEG			Degraded MEG		
P (bar)	T (°C)	P (bar)	T (°C)	P (bar)	T (°C)	Shift, ΔT (°C)	P (bar)	T (°C)	Shift, ΔT (°C)
70.0	9.7	70.0	3.0	70.3	0.7	2.3	70.1	1.3	1.7
89.9	11.9	80.0	4.0	90.0	2.8	1.2	90.2	3.4	0.6
110.1	13.7	110.0	6.6	110.2	4.7	1.9	110.0	5.3	1.3
130.0	15.0	130.0	7.9	130.1	5.9	2.0	130.2	6.6	1.3

The results show that the non-degraded MEG solution showed an enhanced hydrate inhibition performance as compared to a pure MEG solution without the presence of

salts. This can be explained by the added inhibitory effect of the electrolytes in the solution which produce an electrostatic force. It is established that salts such as sodium chloride or inorganic salts are thermodynamic hydrate inhibitors and thus will shift the hydrate phase boundary to lower temperature regions. This is due to the electrostatic force of the electrolytes which attract water molecules and thus deter them from forming a cage around gas molecules (Lu et al., 2001; Mohammadi and Richon, 2009). An average temperature suppression of 1.9 °C was determined as compared to a pure MEG sample with no added salts.

Figure 4.4 shows the gradual formation of gas hydrate in the PVT cell until hydrate blockage had occurred. It was observed that the magnetic stirrer would gradually come to a complete halt when all visible liquid had transformed into hydrate thus impeding freedom of stirrer to continue in motion.

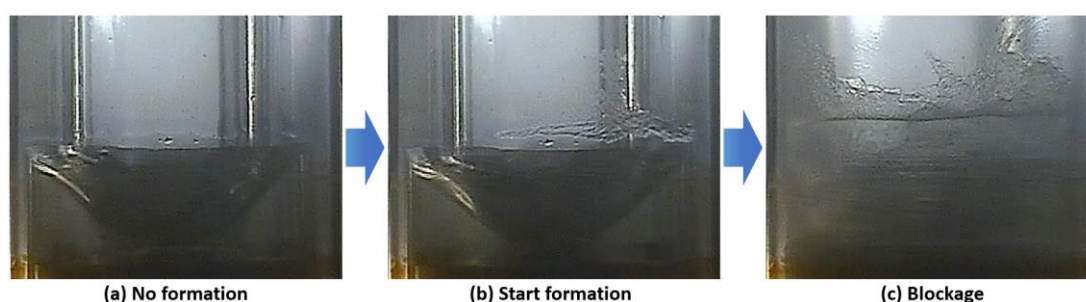


Figure 4.4: Gradual formation of methane hydrate in solution.

Interestingly, the hydrate phase boundary for the degraded MEG solution had shifted to the left of the PT diagram but not beyond that of the non-degraded solution. It showed a lower hydrate inhibition effect with an average temperature depression of 1.2 °C. This was due to the thermal oxidation of MEG, whilst MEG was going through the regeneration and reclamation process. This suggests that MEG exposed to high temperatures for even short amounts of time may drop in hydrate inhibition performance.

AlHarooni et al. (2015) explored MEG degradation at a temperature range of 135 – 200 °C using an autoclave system over a period of 4 – 48 h (AlHarooni et al., 2015). Their results show that the hydrate inhibitory performance decreased as temperature and time increased. The resulting MEG loses its inhibition quality and degradation products were identified as acetic, formic and glycolic acids. Although their research

was useful for investigating how heat affects the hydrate inhibitory performance of pure MEG, it did not properly represent the complex conditions present in typical regeneration and reclamation plants in terms of temperature-pressure and the chemistry of the various chemicals, impurities, and additives that are typically present in industrial applications. Latta et al. (2016) produced a detailed outline with regards to the various contaminants present in the different stages of the MEG recovery process (Latta et al., 2016). It is the lean-MEG solution which is the combination of the partial MEG stream which undergoes reclamation with a greater portion exiting the reboiler. Hence, the injected MEG will contain various contaminants carried over through the plant as well as MEG degradation products. The research by Psarrou et al. (2011) suggests that formic, acetic and glycolic acids are the main by-products of MEG degradation (Psarrou et al., 2011). In this study, we have shown that over the duration of ca. 13 hours, MEG will have a reduced hydrate inhibitory effect due to possible accumulation of contaminants in the MEG plant as well as thermal degradation of MEG and its by-products.

It has been suggested by many studies that it is important to minimize the level of dissolved oxygen in the MEG stream to prevent the conversion of iron carbonate into iron oxide for the purpose of not only preventing a high corrosion rate but to also prevent the thermal oxidation of MEG (Brustad et al., 2005; Latta et al., 2013). Furthermore, exposure to high temperatures and metal ions in solution will also contribute to accelerating the rate of MEG degradation.

Figure 4.5 shows the change in colour between the two solutions. As can be seen in Figure 4.5(b) that the colour of the solution is slightly yellow. This colour change was also observed by another researcher and was suggested that it is an indication of the degradation of MEG (Psarrou et al., 2011). This confirms that degradation had occurred in the MEG solution.

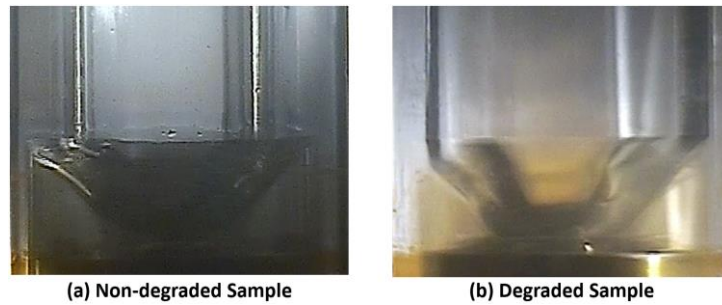


Figure 4.5: Change in colour between non-degraded and degraded MEG samples.

4.4 Conclusions

As there has only been a very limited amount of research done on the effect of degradation of salt-laden MEG on hydrate inhibition, this study comes in handy. Operators utilizing MEG, or flow assurance professionals using it as a hydrate inhibitor, and/or in other MEG applications will find the results of this study particularly useful. This study has produced new hydrate equilibria data of methane hydrate in the presence of MEG solutions. The results reveal that although dissolved salts may be present in the MEG solution which will provide an added inhibitory performance, it can be expected that MEG may degrade due to thermal oxidation in the recovery process which may ultimately decrease the quality and available quantity of MEG to perform as a hydrate inhibitor. Taking this into consideration is crucial to developing an optimum hydrate control program as well as addressing the dynamic risk of gas hydrate formation in pipelines.

Chapter 5 Hydrate Phase Equilibria for Methyldiethanolamine and Empirical Modelling for Prediction

This chapter is comprised of the following publication:

- **Alef, K.**, Iglauer, S., Gubner, R., Barifcani, A., 2018b. Hydrate Phase Equilibria for Methyldiethanolamine and Empirical Modelling for Prediction. *J. Chem. Eng. Data* 63, 3559–3565. doi: 10.1021/acs.jced.8b00440

The issue of gas hydrates in gas pipelines is commonly addressed by injecting hydrate inhibitors at the wellheads. Alongside these inhibitors, other chemical additives are also injected to address various concerns such as to reduce the risk of corrosion and scaling. However, it is not clear how the combined chemical cocktail affects gas hydrate formation over a wide pressure range. Methyldiethanolamine or N-methyldiethanolamine (MDEA) is a chemical typically found in the gas production context alongside hydrate inhibitors, and it is commonly used as part of the pH stabilization corrosion control method. The impact of MDEA on hydrate formation has not been studied well, nor has it been modelled. Thus, this chapter contributes a thorough study into the effect of MDEA on gas hydrate formation and the modelling of this effect. Empirically, an algorithm based on the experimental data collected in this study at a high-pressure range (7 to 20 MPa) was developed allowing for the prediction of hydrate phase equilibria in the presence of MDEA. This work will thus aid in the industrial application of hydrate inhibitors and improve gas hydrate prevention in production pipelines. This contribution satisfies the thesis objectives (g) and (h) while fulfilling the research gaps outlined in Section 1.3.

5.1 Introduction

The formation of ice-like solids known as gas hydrates is an ongoing issue in the production of valuable natural resources (Carroll, 2014; Hammerschmidt, 1934; Sloan Jr and Koh, 2007). Hydrates are crystalline solids which are composed of gas and water molecules; the gas molecules are known as “guest molecules” which become confined in cage-like cavities formed by water molecules (Eslamimanesh et al., 2011; Koh et al., 2002; Sloan Jr and Koh, 2007). High-pressure and low-temperature conditions, which are typically experienced within subsea production pipelines, can accelerate the rate of hydrate formation (Obanijesu et al., 2014). Conventional hydrate inhibition techniques such as thermal insulation, depressurization, and natural gas dehydration by glycol or molecular sieves may be impractical and not cost-effective (McIntyre et al., 2004).

Thus, chemical hydrate inhibitors are commonly utilized in the industry for hydrate inhibition and prevention of methane hydrate reformation (Jamaluddin and Kabir, 2012; Kim et al., 2017; Seo and Kang, 2012). They are classified as low-dosage hydrate inhibitors (LDHIs) and thermodynamic hydrate inhibitors (THIs) (Kelland, 2006). THIs work by moving the hydrate phase boundary toward lower temperatures and higher pressures, thus increasing the hydrate-safe region (Li et al., 2006). Monoethylene glycol (MEG) is one of the most commonly used thermodynamic hydrate inhibitors and is utilized in this study (Brustad et al., 2005; Sami et al., 2013).

Alongside hydrate formation, corrosion is another major issue leading to serious cost repercussions and downtime (Alef et al., 2018a; Olajire, 2015; Papavinasam et al., 2007). A corrosion control program may thus be adopted, which usually consists of using an amine such as methyldiethanolamine (MDEA) to increase the pH of the fluid system to initiate the precipitation of a stable iron carbonate layer on the inside of the pipeline for surface protection (pH stabilization) or by injecting corrosion inhibitors (Lehmann et al., 2016, 2014; Nyborg, 2009). The combined use of both gas hydrate and corrosion inhibitors is popular, and some compatibility studies have been conducted in terms of corrosion; however, the impact of different chemical additives on gas hydrate formation needs more work (Lehmann et al., 2014; Luna-Ortiz et al., 2014; Obanijesu et al., 2014). In this context, Obanijesu et al. (2014) studied the effect of different chemical additives such as corrosion inhibitors on the hydrate formation

temperature and found that corrosion inhibitors promote gas hydrate formation (Obanijesu et al., 2014). This may be detrimental as it can increase the risk of hydrate formation and production downtime. Others evaluated hydrate inhibitors as being able to perform as corrosion inhibitors, and in recent studies, hydrate and corrosion inhibitors were combined to form of a single polymer that can tackle both hydrate formation and corrosion issues simultaneously (Burgazli et al., 2005; Sheng et al., 2017). However, the combined injection of MDEA and MEG has not been fully explored at a high pressure range, which is, however, relevant for production (Akhfash et al., 2017). Chemical additives such as MDEA or corrosion inhibitors may lead to over-inhibition or even under-inhibition of gas hydrates in pipelines. Additionally, chemical compositions of inhibitors and additives are increasingly becoming proprietary due to the commercial appeal and preservation of a competitive edge (Achour and Kolts, 2015). This leads to an increasing lack of fundamental understanding and increasingly complex prediction models, or the lack thereof, of such prediction tools. Thus, in this investigation, the methane hydrate inhibition performance of one such chemical additive, MDEA, which is commonly injected in combination with MEG, was assessed at a high-pressure range (7–20 MPa) that has not been previously tested. Furthermore, an algorithm consisting of empirical models based on the experimental data of this study is provided due to the lack of software predictions for the hydrate inhibition performance of MDEA solutions. The models are based on a linear interpolation scheme between the hydrate phase boundaries of various concentrations of MDEA solutions to accurately predict the equilibrium temperature shift due to the presence of MDEA.

5.2 Methodology

5.2.1 Materials and Apparatus

The materials utilized in this study are given in Table 5.1. MEG was obtained from Chem-Supply with a purity of 99.477% (molar). MDEA was sourced from Sigma-Aldrich with a purity of $\geq 99\%$ (molar). Deionized (DI) water was conveniently produced within the laboratory using Hydro-Check 414R with an electrical resistivity of 18.18 M Ω ·cm (24 °C). The hydrate-forming gas was ultrahigh purity methane supplied by BOC with a purity of 99.995% (molar). Nitrogen for purging purposes was generated using an in-house nitrogen generator (AtlasCorpo, NGP10+) with a

purity of 99.9959% (molar).

Table 5.1: List of materials used in the experiments.

Material	Formula	Purity	Source
MEG	$C_2H_6O_2$	99.477 %	Chem-Supply
MDEA	$CH_3N(C_2H_4OH)_2$	≥ 99 %	Sigma-Aldrich
Deionized water	H_2O	18.18 $M\Omega \cdot cm$ (24 °C)	Hydro-Check 414R
Methane	CH_4	99.995 %	BOC
Nitrogen	N_2	99.9959 %	AtlasCorpo, NGP10+

A high-pressure PVT cell located in the Clean Gas Technology Australia (CGTA) laboratory, Curtin University, was utilized for the hydrate testing (Figure 5.1). The cell chamber (60 cm³) and tubing have a total volume of 86 cm³. Before each test run, the cell was cleaned with ethanol and thoroughly rinsed with deionized water. A vacuum pump was then utilized for drying the cell and to remove any remaining contaminants, and finally purged with nitrogen. The cell was equipped with a magnetic stirrer (up to 500 rpm stir rate) to promote mixing between the phases to facilitate hydrate formation and the prevention of a hydrate film to simply form at the gas–liquid surface (Alef et al., 2018c; Smith et al., 2015). Pressure sensors for measuring pressure and K-type thermocouples were installed for measuring the air bath, vapor, and liquid temperatures within the sapphire cell. The cell was mounted firmly within an air bath operated by a cooling/heating system. The inside of the cell was clearly visible from the outside and aided by a camera system with a light source to enhance the imagery.

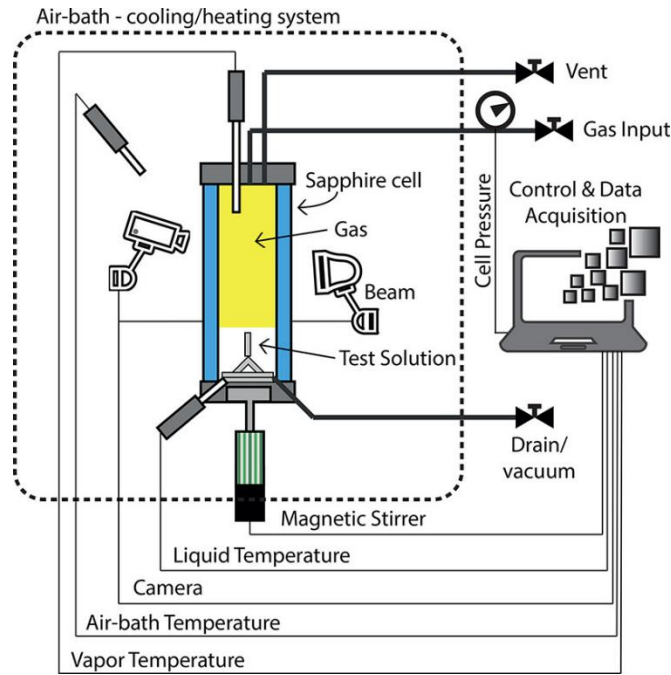


Figure 5.1: Schematic of the high-pressure PVT sapphire cell used in this study which is capable of performing hydrate inhibition testing.

5.2.2 Method

The well-known isochoric method was employed to accurately determine the hydrate phase equilibria (Sloan Jr and Koh, 2007). This method requires that the volume is kept constant while applying a step-cooling process (in this study: 2 °C/h) until hydrate blockage had occurred, and then applying a careful step-heating process (1 °C/h) to dissociate the gas hydrate. The intercept of the pressure–temperature curves from the cooling and heating processes gives the dissociation temperature also known as the thermodynamic equilibrium (Mech et al., 2015; Sloan Jr and Koh, 2007). Each test consisted of 4 experiments at varying pressures between 7 and 20 MPa to determine the full hydrate phase boundary. Table 5.2 contains the experimental test matrix for the isochoric hydrate tests conducted in this study. The test solutions were accurately prepared by precise mass measurement of the various components required using a highly accurate self-calibrated electronic balance with an accuracy of 0.09%. The test solutions were mixed in a beaker while being sparged with nitrogen and magnetically stirred for complete synthesis. An 8 mL sample was then injected into the PVT cell and mixed thoroughly by the magnetic stirrer before the test was initiated.

Table 5.2: Experimental matrix of hydrate inhibition tests conducted using the isochoric method.

Formulation	Composition (wt%)		
	Water	MDEA	MEG
Pure water	100	0	0
MDEA	97.5	2.5	0
MDEA	95	5	0
MDEA	92.5	7.5	0
Pure MEG	80	0	20
MEG-MDEA	77.5	2.5	20
MEG-MDEA	72.5	7.5	20

5.3 Results

Initial hydrate testing was conducted for the two reference systems, pure water, and water-MEG (20 wt%) samples to ascertain the accuracy of the results by comparing to the available literature and software data. Figure 5.2 illustrates the comparison, while the hydrate phase equilibria data are provided in Table 5.3 and Table 5.4. The tests were conducted three times under the same conditions for repeatability. The results had a standard deviation of 0.16 °C, indicating a very small deviation in the obtained data. Furthermore, the measured data were compared to software predictions using Soave–Redlich–Kwong (SRK), Peng–Robinson (PR), and CPA fluid packages in PVTsim, Multiflash, and CSMHYD (*Calsep PVTsim*, 2011; *Infochem Multiflash*, 2007; Sloan Jr and Koh, 2007). The measured data were also compared to similar literature data at the tested pressure range (Haghighi et al., 2009b; Marshall et al., 1964; McLeod and Campbell, 1961; Rock, 2002; Verma, 1974). An absolute average relative error (AARE) of 1.77% between the measured equilibria data of the different mixtures was found, confirming that our results match very well to published data and predictions. The absolute average relative error was calculated using Eqn. (5.1), where T_{exp} is the experimentally measured equilibrium temperature and T_{calc} is the equilibrium temperature predicted using software or obtained from literature.

$$\text{AARE (T)} = \frac{100}{n} \sum_{i=1}^n \left| \frac{T_{calc} - T_{exp}}{T_{exp}} \right| \quad (5.1)$$

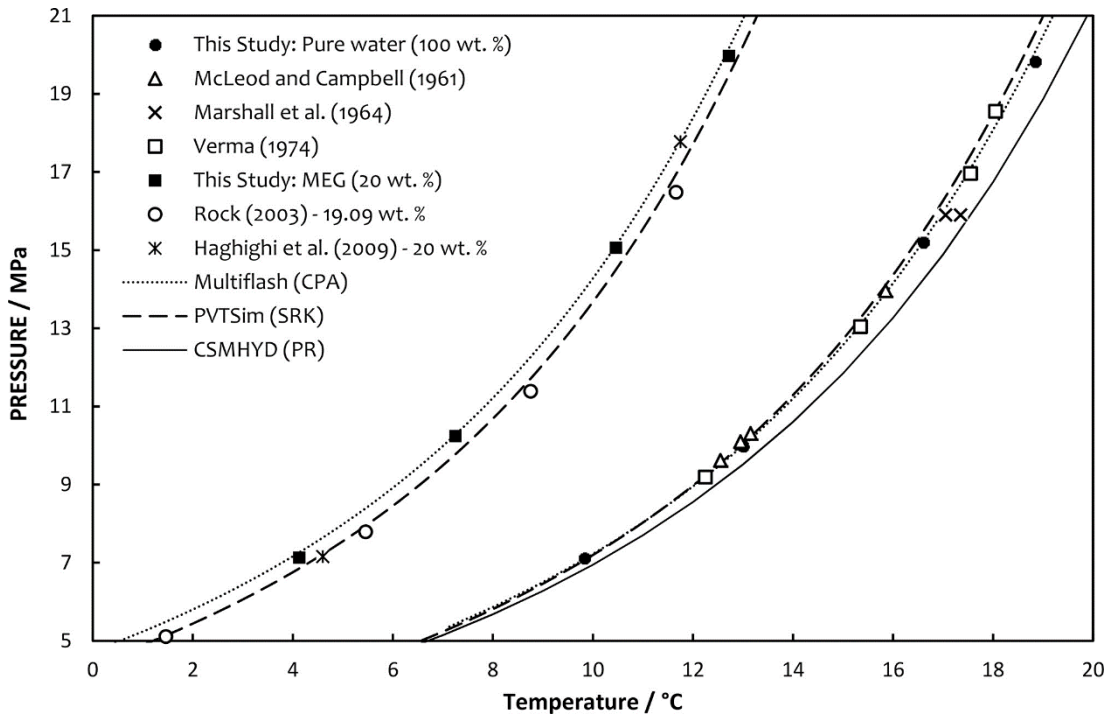


Figure 5.2: Methane hydrate phase boundaries for pure water and pure MEG (20 wt%) as compared to literature and software predictions.

5.3.1 Pure MDEA Tests

Samples of water–MDEA mixtures at MDEA concentrations of 2.5, 5, and 7.5 wt% were tested for methane hydrate inhibition. It was observed that the level of foaming increased as MDEA concentration increased. The newly obtained equilibria data are provided in Table 5.3. The hydrate phase boundaries for the MDEA samples are plotted in Figure 5.3. The hydrate phase boundaries as compared to that of pure water have shown an average leftward shift by 0.29, 0.58, and 0.82 °C, respectively. This leftward shift confirms that MDEA can act as a thermodynamic hydrate inhibitor even at higher pressures.

Table 5.3: Equilibria data for pure water and pure MDEA samples measured in this study.^a

Pure water		MDEA (2.5 wt%)		MDEA (5 wt%)		MDEA (7.5 wt%)	
P (MPa)	T (°C)	P (MPa)	T (°C)	P (MPa)	T (°C)	P (MPa)	T (°C)
7.11	9.83	7.36	9.85	7.42	9.63	7.66	9.64
9.98	13.00	10.07	12.76	9.96	12.28	10.84	12.85
15.20	16.61	15.29	16.40	14.98	16.03	15.24	15.89
19.83	18.84	19.93	18.57	20.26	18.49	20.02	18.18

^a Standard uncertainty in pressure and temperature measurements are ± 0.05 MPa and ± 0.03 °C, respectively.

The tests were simulated in Multiflash, and the results showed no change in the hydrate phase boundary as compared to the hydrate phase boundary of pure water, confirming that the effect of MDEA on the phase boundary has not been taken into account (Akhfash et al., 2017). The equivalent MEG concentrations required to yield the same amount of temperature suppression or shift in hydrate phase boundary caused by MDEA was determined by simulation in Multiflash (Figure 5.3). The results reveal that 2.5, 5, and 7.5 wt% of pure MDEA solutions are equivalent to 1.1, 2.1, and 3.3 wt% of pure MEG, respectively. This suggests that MEG is 2.31 times more effective than MDEA.

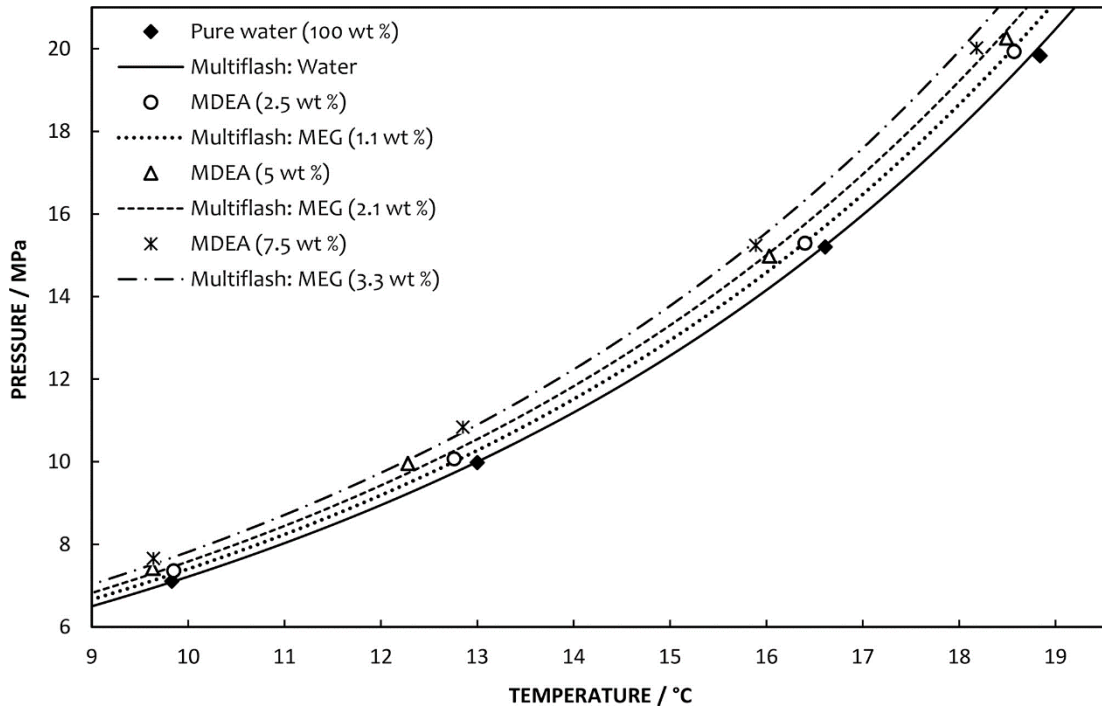


Figure 5.3: Methane hydrate phase boundaries for pure MDEA (2.5–7.5 wt%) and their equivalent MEG concentrations using Multiflash.

5.3.2 MEG Tests

MDEA was tested in a 20 wt% MEG solution to determine the combined hydrate inhibition performance at high pressures (7–20 MPa). Interestingly, during the cooling and hydrate nucleation phase, bubbling was observed instead of foaming (Figure 5.4). However, the foaming characteristic of MDEA samples was visible when the solution was stationary after stirring, as seen in the sample bottles in Figure 5.4.

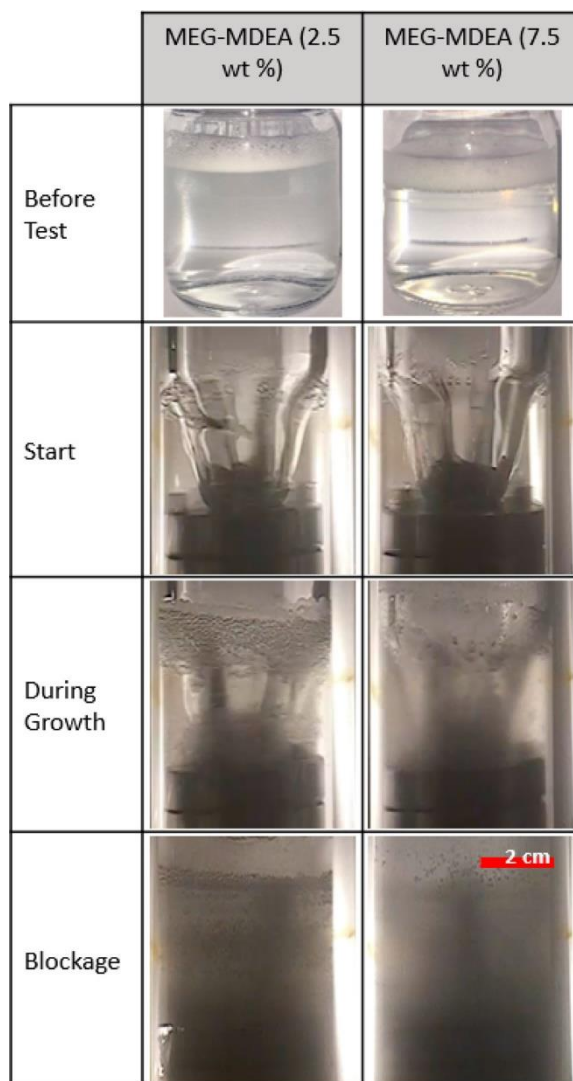


Figure 5.4: Stages of hydrate testing in MEG–MDEA (2.5 and 7.5 wt%) mixtures.

The hydrate phase boundaries are plotted in Figure 5.5, while equilibria data are provided in Table 5.4. The hydrate profiles for 20 wt% MEG with added MDEA at 2.5 and 7.5 wt% relative to deionized water show an enhanced hydrate inhibition performance as opposed to a 20 wt% pure MEG solution (Figure 5.5). At 2.5 wt% of MDEA concentration in the MEG solution, an average hydrate equilibrium temperature suppression of 0.13 °C was produced. While at a concentration of 7.5 wt% of MDEA, an average suppression of 0.46 °C was found. Interestingly, both samples showed a greater shift at higher pressures as opposed to lower pressures. The results clearly show that as the concentration of MDEA increases, there is a leftward shift in the hydrate profile, confirming that MDEA is contributing as a thermodynamic hydrate inhibitor even at higher pressures. The high solubility of MDEA in water is a

contributing factor to why the enhanced hydrate inhibitory performance is observed. MDEA and water merge by strong hydrogen bonding, thus making the water molecules less accessible to gaseous guest molecules, resulting in hydrate inhibition (Davoudi et al., 2014; Hossainpour, 2013). On the other hand, where carbon dioxide and acids are involved, MDEA has an exothermal reaction which generates heat, promoting dissociation of the gas hydrate (Park et al., 2006; Xiang et al., 2014). Furthermore, predictions for combined MDEA and MEG solutions using Multiflash showed an almost negligible temperature suppression as compared to our experimental data (Figure 5.5). The temperature shift that can be seen in the Multiflash predictions is simply the hydrate phase boundary of the same solution while ignoring the MDEA concentration, thus resulting in a higher MEG proportion. Therefore, the prediction is misleading as it produces results for a MEG solution of 21.6 wt% as opposed to the 20 wt% solution as defined by the user in the case of MEG–MDEA (7.5 wt%). It was assumed that the selected Multiflash configuration and equation of state (CPA) was not capable of recognizing MDEA's inhibition effect, so different equations of states (i.e., PR, SRK, modified PR, and modified SRK) were selected, but the results remained unhindered, suggesting that the added hydrate inhibitory performance of MDEA has not been taken into account in the Multiflash simulation model.

The combined effect of MEG (20 wt%) with MDEA at 2.5 and 7.5 wt% on the hydrate phase boundary was found to be equivalent to the hydrate performance of 20.28 and 20.95 wt% of pure MEG, respectively. The equivalent MEG concentration for the same MDEA concentration is higher for pure MDEA as opposed to combined mixtures of MEG–MDEA. This suggests that a mixture of MEG–MDEA showed a lesser performance as a hydrate inhibitor as compared to pure MDEA by a factor of 3.6.

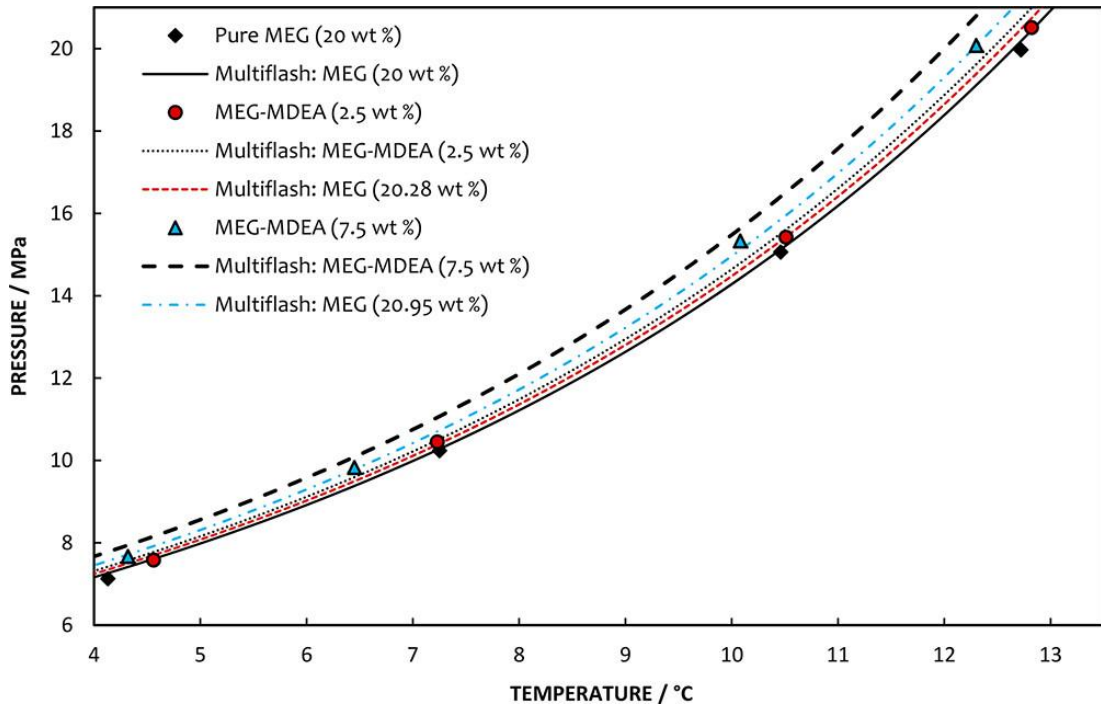


Figure 5.5: Measured and simulated phase boundaries for combined 20 wt% MEG with MDEA (2.5 and 7.5 wt%).

Table 5.4: New methane hydrate phase equilibria data for 20 wt% MEG/water–MDEA mixture.^a

Pure MEG (20 wt%)		MEG (20 wt%) -MDEA (2.5 wt%)		MEG (20 wt%) -MDEA (7.5 wt%)	
P (MPa)	T (°C)	P (MPa)	T (°C)	P (MPa)	T (°C)
7.13	4.13	7.58	4.56	7.67	4.32
10.24	7.25	10.45	7.23	9.83	6.45
15.06	10.46	15.42	10.51	15.33	10.08
19.97	12.72	20.51	12.82	20.08	12.3

^a Standard uncertainty in pressure and temperature measurements are ± 0.05 MPa and ± 0.03 °C, respectively.

5.3.3 Empirical Modelling

Simulations were conducted using Multiflash, which has an option to input MDEA concentration within the aqueous phase. However, the predicted hydrate phase boundaries of the MDEA solutions were identical to the results of pure water (100 wt%). This exposes the software's incapability to take into account the inhibitory

performance of MDEA. One of the goals of this study is to present an algorithm based on empirical modelling to allow for the prediction of equilibrium conditions of aqueous MDEA solutions with MEG. This is very useful since flow assurance software are not able to predict the hydrate inhibitory effect of MDEA. Thus, after establishing the hydrate inhibition performance of MDEA and MEG–MDEA solutions, the next step was to develop a relation between the experimentally measured equilibria data and MDEA concentration. This can be achieved through linear interpolation with the assumption that at a given pressure, the relationship between the thermodynamic equilibrium temperature and MDEA concentration is a linear one. Furthermore, Figure 5.3 and Figure 5.5 show that the equilibrium temperature decreases consistently with increasing MDEA concentration. Thus, a simple interpolation scheme that can determine the hydrate equilibrium conditions of MDEA and MEG–MDEA mixtures at different MDEA concentrations (x) based on the experimental data from this study is put forth.

Given that MDEA’s hydrate inhibition performance increases with increasing concentration, this increase will result in lower equilibrium temperature as compared to those of pure water ($x = 0$) or pure MEG ($x = 0$). This is expressed by Eqn. (5.2), where the first RHS term (T_0), which could also be called the reference term, denotes the equilibrium temperature of either deionized water or the pure MEG solution. The second RHS term, ΔT_x in Eqn. (5.2), is simply the temperature shift from T_0 to the equilibrium temperature (T_x) of a mixture of x wt% of MDEA.

$$T_x = T_0 - \Delta T_x \quad (5.2)$$

The reference term (T_0) for water is calculated by using a fitted exponential trendline on the experimental equilibrium data. The exponential function for the experimental data after correlation is given with pressure (P) as the subject. The equation can be rearranged in terms of T_0 as shown in Eqn. (5.3) (where a and b are constants of the exponential expression). The reference term for the pure MEG solution can also be predicted by an equation of state, thus allowing for a wider MEG concentration coverage compared to the 20 wt% MEG concentration adopted within this study.

$$T_0 = a \ln\left(\frac{P}{b}\right) \quad (5.3)$$

To derive the equilibrium temperature shift, ΔT_x involves developing a relationship to address the shift in hydrate phase boundaries of the reference system versus that of a high MDEA concentration mixture (upper boundary) as a function of pressure. In this study, the upper boundary was selected as the pure MDEA solution at a concentration of 7.5 wt%. The equilibrium temperature shift, $\Delta T_{7.5}$, between pure water as the reference, and pure MDEA (7.5 wt%) as the upper bound was determined over a varying pressure range (7–20 MPa) to account for the temperature dependence on pressure (Figure 5.6).

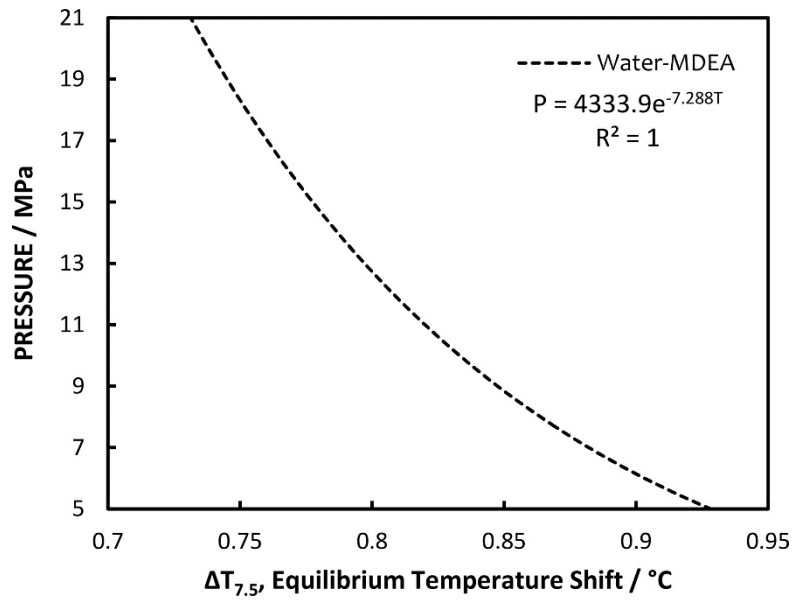


Figure 5.6: Pressure versus $\Delta T_{7.5}$, hydrate equilibrium temperature shift for between water and pure MDEA at 7.5 wt%.

The equation for $\Delta T_{7.5}$ can be derived from Figure 5.6, it is written here as Eqn. (5.4). However, to determine the equilibrium temperature shift for a mixture of x wt% concentration of MDEA (ΔT_x), the $\Delta T_{7.5}$ term can be used to interpolate by multiplying Eqn. (5.4) by $x/7.5$.

$$\Delta T_{7.5} = \left(\frac{1}{-7.288} \right) \ln \left(\frac{P}{4333.9} \right) \quad (5.4)$$

$$\Delta T_x = - \left(\frac{x}{7.5 \times 7.288} \right) \ln \left(\frac{P}{4333.9} \right) \quad (5.5)$$

By substituting Eqns. (5.3) and (5.5) into Eqn. (5.2), the general expression shown in Eqn. (5.6) for calculating equilibrium temperature, T , at a concentration of x wt% of

MDEA in pure water or MEG mixtures can be developed. The constants a and b were derived from the exponential expressions of the reference systems, while c and d for both pure MDEA and MEG solutions were obtained from the exponential expressions of the pressure versus equilibrium temperature shifts between the reference systems and high MDEA concentration solutions. These constants are given in Table 5.5.

$$T = a \ln\left(\frac{P}{b}\right) - c \ln\left(\frac{P}{d}\right) x \quad (5.6)$$

Table 5.5: Constants used in Eqn. (5.6) for pure MDEA and MEG–MDEA mixtures.

	a	b	c	d
MDEA	8.769	2.296	-0.0183	4333.9
MEG-MDEA	8.346	4.323	0.0104	0.031

The model was tested by comparing it with experimental data available in literature and data from this study (Akhfash et al., 2017). This comparison is shown in Figure 5.7 and Figure 5.8; it can be seen that the model fits very well. Most of the values predicted by the model are within 0.07 °C of the experimental data and have an average relative difference of 0.57% (Table 5.6). It can thus be established that the developed model accurately represents the effect of MDEA on the hydrate phase boundary for MDEA concentrations of 0–7.5 wt% and a pressure range of 7–20 MPa.

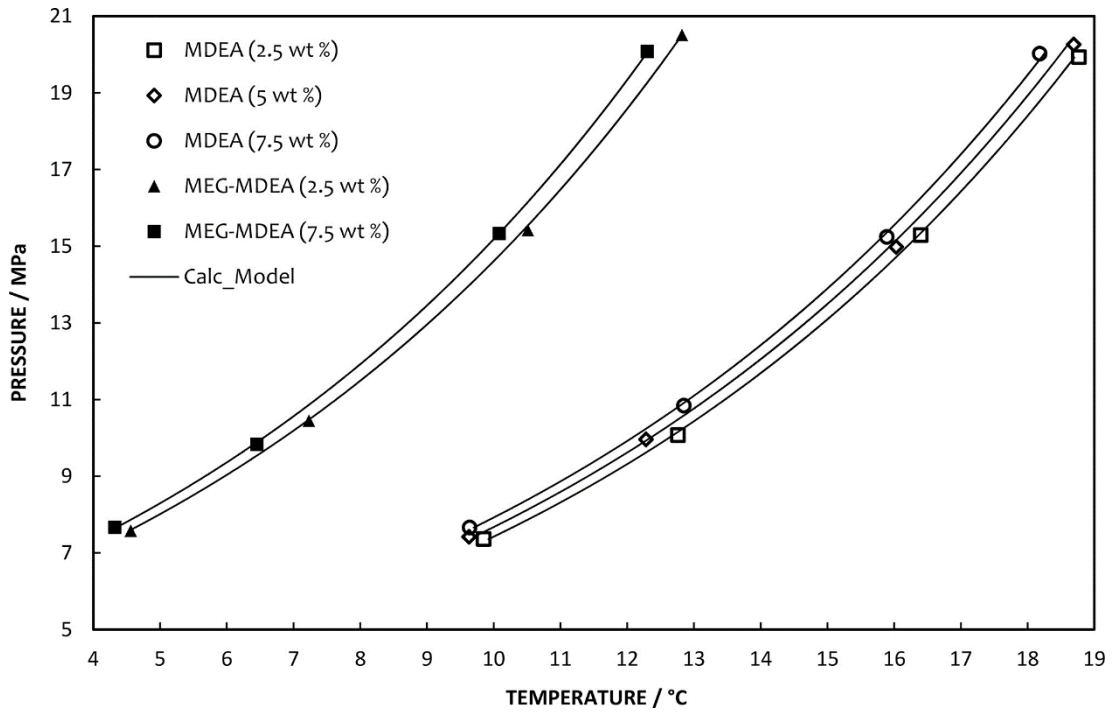


Figure 5.7: Comparison of predicted to experimental data for MDEA and MEG mixtures from this study.

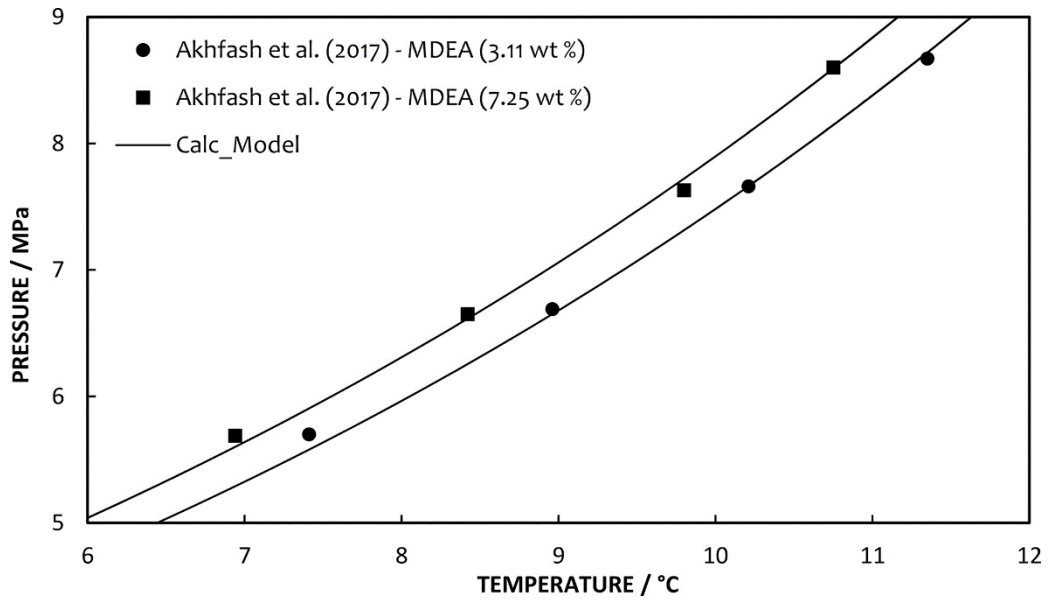


Figure 5.8: Comparison of predicted to experimental data for MDEA solutions from literature.

Table 5.6: Statistical comparison of model and experimental data.^a

Mixture	x^{MDEA} (wt%)	P (MPa)	T _{exp} (°C)	T _{calc} (°C) ^b	ΔT (°C)	RD (%) ^c	
This Study:	2.50	7.36	9.85	9.92	0.07	0.71	
Pure MDEA	2.50	10.07	12.76	12.69	0.07	0.55	
		15.29	16.40	16.37	0.03	0.18	
		19.93	18.77	18.70	0.07	0.37	
	5.00	7.42	9.63	9.70	0.07	0.73	
		9.96	12.28	12.31	0.03	0.24	
		14.98	16.03	15.93	0.10	0.62	
	7.50	20.26	18.69	18.60	0.09	0.48	
		7.66	9.64	9.70	0.06	0.62	
		10.84	12.85	12.79	0.06	0.47	
	Pure MDEA (Akhfash et al., 2017)	3.11	15.24	15.89	15.82	0.07	0.44
			20.02	18.18	18.25	0.07	0.39
			5.70	7.41	7.60	0.19	2.56
7.25		6.69	8.96	9.01	0.05	0.56	
		7.66	10.21	10.21	0.00	0.00	
		8.67	11.35	11.30	0.05	0.44	
This Study: MEG- MDEA	2.50	5.69	6.94	7.08	0.14	2.02	
		6.65	8.42	8.47	0.05	0.59	
		7.63	9.80	9.69	0.11	1.12	
	7.50	8.60	10.75	10.76	0.01	0.09	
		7.58	4.56	4.54	0.02	0.44	
This Study: MEG- MDEA	2.50	10.45	7.23	7.21	0.02	0.28	
		15.42	10.51	10.45	0.06	0.57	
		20.51	12.82	12.82	0.00	0.00	
	7.50	7.67	4.32	4.35	0.03	0.69	
		9.83	6.45	6.41	0.04	0.62	
		15.33	10.08	10.08	0.00	0.00	
	20.08	12.30	12.31	0.01	0.08		

^a Standard uncertainties in pressure and temperature measurements are ± 0.05 MPa and

± 0.03 °C, respectively.^b Model.^c Relative difference, $RD(T) = \frac{\text{abs}(T_{exp} - T_{calc})}{T_{exp}} \times 100$.

5.4 Conclusion

The combined use of MDEA and MEG is very common (Akhfash et al., 2017; Brustad et al., 2005; Davoudi et al., 2014; Glenat et al., 2004; Halvorsen et al., 2007; Lehmann et al., 2014; Nyborg and Dugstad, 2009). As such, the need for understanding how MDEA affects gas hydrate formation and the inhibition performance of MEG at a wide pressure range becomes important for the integrity of the hydrate control program. This study has produced new methane hydrate phase equilibria data for MEG and MDEA mixtures, confirming that MDEA can act as a thermodynamic hydrate inhibitor at high pressures (7–20 MPa), resulting in the suppression of the hydrate phase boundary. Pure MDEA showed an average equilibrium temperature shift of -0.82 °C at a concentration of 7.5 wt%. The combined effect of MDEA (7.5 wt%) with MEG (20 wt%) showed an equivalent hydrate performance of 20.95 wt% MEG. This shows that where MDEA and MEG are applied together for their respective purposes, the system may be slightly overinhibited due to the added hydrate inhibitory performance of MDEA. The study suggests that with the knowledge of the hydrate inhibitory performance of other chemical additives such as MDEA in the MEG injection stream, an added safety margin can be assumed. Furthermore, the study has presented an algorithm (provided in APPENDIX A. Outline of Algorithm, and MDEA Data) consisting of empirical models based on the experimental data of this study to provide an estimate for the added hydrate inhibitory effect of MDEA.

The hydrate phase equilibria data for MDEA illustrate that various chemical additives that are injected alongside hydrate inhibitors can potentially alter the expected hydrate inhibition performance of the adopted hydrate control program. In this case, it increased the hydrate-safe region and perhaps rendered the system into over-inhibition.

Chapter 6 Thermodynamic Modelling of Hydrate Phase Equilibria of Methyldiethanolamine

This chapter is comprised of the following publication:

- **Alef, K.**, Iglauer, S., Barifcani, A., 2019b. Thermodynamic Modeling of Hydrate Phase Equilibria in Methyldiethanolamine Solution in the Presence or Absence of Monoethylene Glycol. *J. Chem. Eng. Data* 64, 4148–4153. doi: 10.1021/acs.jced.9b00552

In recent studies, MDEA has been found to have an inhibiting effect on gas hydrate formation. This inhibitory effect is neither considered in field hydrate control programs nor in simulation software. To date, the effect has only been modelled empirically by the authors. In this study, thermodynamic modelling has been conducted using the cubic plus association equation of state (CPA EoS) combined with van der Waals and Platteuw's solid solution theory for hydrate phase equilibria. This application of the CPA EoS will allow for accurate prediction of hydrate equilibria of MDEA solutions used in the industry. Furthermore, new hydrate phase equilibria data for MDEA and MDEA–MEG systems have been produced. A good prediction by the proposed model (0.76% deviation) has been found across all available hydrate phase equilibria of MDEA systems with and without the presence of MEG in the literature.

This contribution satisfies the thesis objectives (g) and (h) while fulfilling the research gaps outlined in Section 1.3.

6.1 Introduction

A major challenge to gas production is the formation of gas hydrates which can cause blockages within gas pipelines leading to serious delays in production and increased maintenance costs (Alef et al., 2018c; Sloan Jr and Koh, 2007). Typical subsea conditions of high pressure and low temperature are optimum grounds for hydrate formation in pipelines, especially in the presence of abundant hydrate-forming gases. A popular solution to gas hydrate formation is the utilization of thermodynamic hydrate inhibitors, namely, monoethylene glycol (MEG), to shift the hydrate phase boundary to lower temperatures (Cha et al., 2013). This results in pipeline operating conditions to be within the hydrate-free region and thus effectively preventing/inhibiting hydrate formation (Figure 6.1). Further to the challenge of gas hydrates, pipelines and process facilities are also prone to corrosion, especially in the presence of produced water and chemical precipitation. To lower the risk of corrosion, amines such as methyldiethanolamine (MDEA) as part of a pH stabilization corrosion strategy may be injected into the system (Alef et al., 2019a). MDEA increases the overall pH level, thereby allowing for a stable iron carbonate layer to form a film along the pipeline, thus lowering the risk of corrosion (Alef et al., 2018a; Lehmann et al., 2014; Nyborg, 2009).

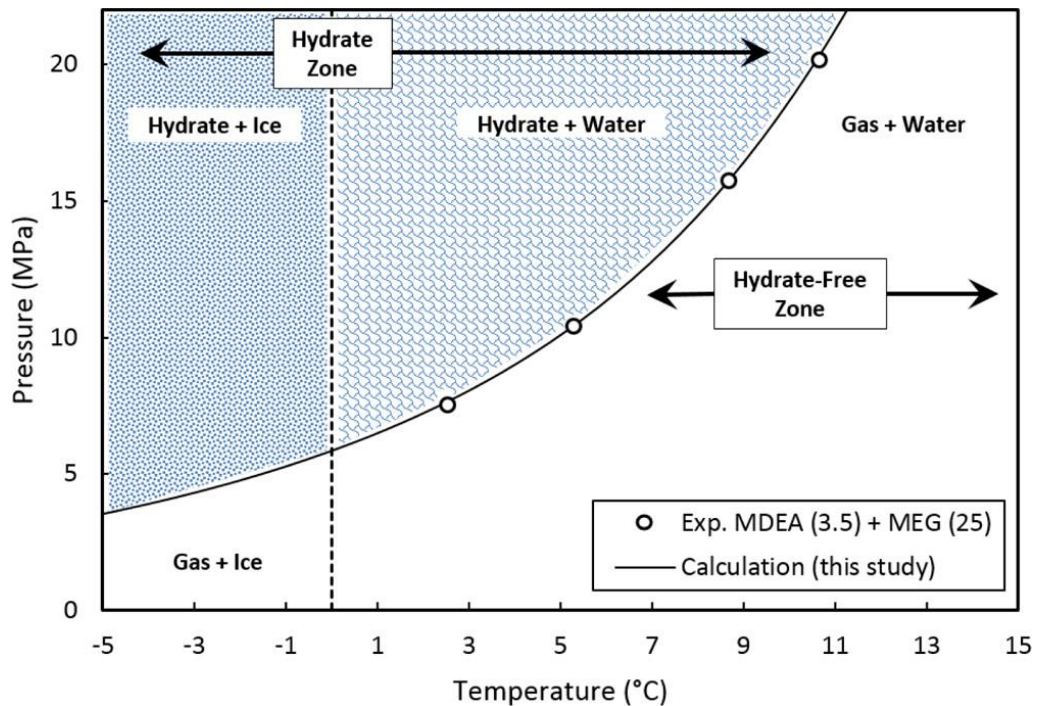


Figure 6.1: Hydrate phase diagram showing hydrate-free regions of quaternary mixture of water–methane–MEG–MDEA.

In recent studies, MDEA has been found to have an inhibiting effect on gas hydrate formation (Akhfash et al., 2017; Alef et al., 2018b; AlHarooni et al., 2016). AlHarooni et al. (2017) presented hydrate-formation pressure and temperature measurements as opposed to thermodynamic phase equilibria of MDEA solutions of 10 and 25 wt% at a pressure range of 5–20 MPa (AlHarooni et al., 2017). AlHarooni et al. (2016) also studied the effect of MDEA degradation among other oil field chemicals on hydrate formation (AlHarooni et al., 2016). Akhfash et al. (2017) presented hydrate phase equilibria data for MDEA solutions at concentrations of 3–7 vol % and a pressure range of 6–9 MPa, showing that MDEA can act as a thermodynamic hydrate inhibitor (Akhfash et al., 2017). Alef et al. presented hydrate phase equilibria data at a higher pressure range (7–20 MPa) and over a larger MDEA concentration range of 0–7.5 wt% (Alef et al., 2018b).

However, the inhibiting effect of MDEA has not been taken into account in gas hydrate control programs in the field, potentially rendering systems into over-inhibition. Furthermore, the inhibitory effect of MDEA has not been captured by flow assurance software or any thermodynamic model for hydrate phase equilibria in MDEA systems. Thus, Alef et al. developed an empirical model based on their experimentally obtained

phase equilibria to highlight the inhibitory effect of MDEA (Alef et al., 2018b). However, as is the case with most empirical models, they are based on a specific set of experimental data, and thus it is essential to develop a thermodynamic model which can describe MDEA systems over varying pressure and concentration ranges.

With that aim for this study, thermodynamic modelling was conducted based on the popular solid solution theory of van der Waals and Platteeuw and the algorithm produced by Parrish and Prausnitz for the prediction of hydrate phase equilibria (Parrish and Prausnitz, 1972; Van der Waals, 1959). The cubic plus association equation of state (CPA EoS) was applied to model MDEA systems and for the calculation of fugacity with the principle of uniformity in fugacity across the different fluid phases. The CPA EoS is preferred because of its ability to model associating compounds with non-associating compounds and ease of computation (Kontogeorgis and Folas, 2009). The model was then validated based on experimentally measured hydrate phase equilibria obtained in this study and from previous studies showing a very good fit (Akhfash et al., 2017; Alef et al., 2018b).

6.2 Methodology

6.2.1 Experimental Section

In order to test the developed model, experimental methane hydrate phase equilibria for two MDEA solution systems were attained. The well-known isochoric testing method was used for hydrate phase equilibrium temperature measurements with a step-cooling/heating rate of 1 °C/h (Alef et al., 2018b; Sloan Jr and Koh, 2007). The procedure has been described in depth in our previous articles (Alef et al., 2018c, 2018a, 2018b). A schematic for the experimental apparatus is shown in Figure 6.2, whereby a high-pressure cell containing the test solution and methane hydrate-forming gas was utilized.

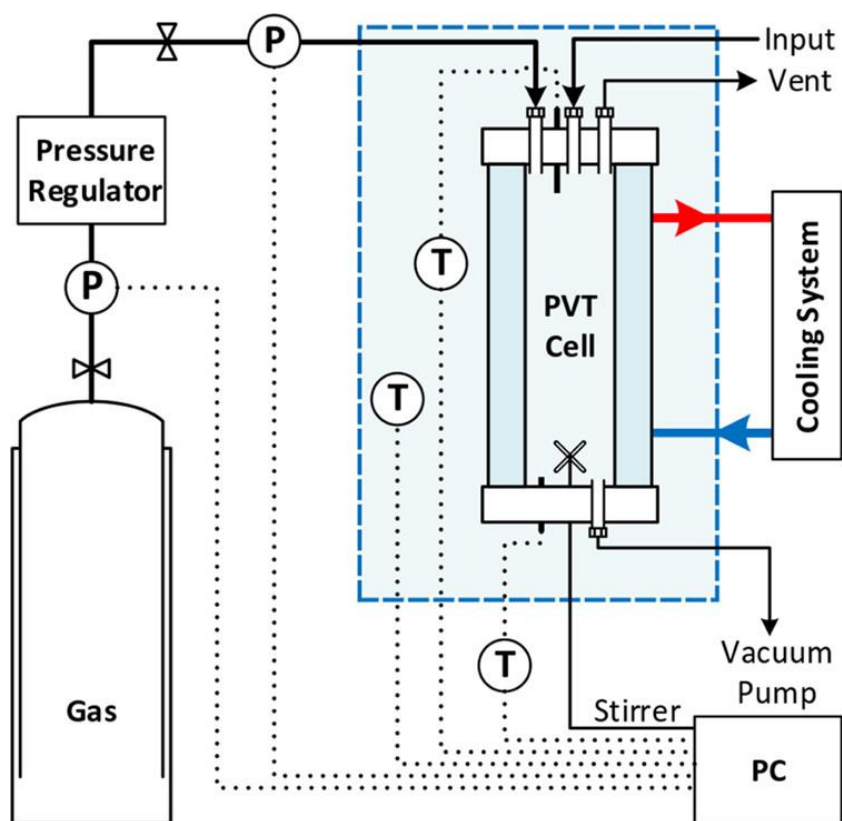
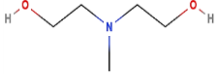


Figure 6.2: Schematic of the experimental apparatus used in this study.

The first of the two test solutions that were tested comprised 3.5 wt% MDEA in pure water. The second solution comprised both MDEA and MEG at 3.5 and 25 wt%, respectively, in pure water. The properties of the chemicals utilized in this study and their sources are tabulated in Table 6.1. The nitrogen used for purging purposes to prevent oxidative degradation of MEG was produced in-house using an Atlas Corpo, NGP10+ generator with a purity of 99.996 mol %. The deionized water used in the preparation of test solutions was produced in-house using a HydroCheck, 414R system with an electrical resistivity of 17.94 M Ω ·cm at 26 °C.

Table 6.1: Materials and their properties used in this study.^a

Material	Compound Formula	Mol. Wt. (g/mol)	Acentric Factor	T _c (K)	Purity (mol%)	CAS No.	Source
MDEA		119.164	1.242	677	≥99	105-59-9	Sigma-Aldrich
MEG		62.068	0.487	719.7	99.477	107-21-1	Chem-Supply
Methane		16.043	0.011	190.56	99.995	74-82-8	BOC

^a Data source: (Perry and Green, 1997; Zoghi et al., 2012).

6.2.2 Thermodynamic Modelling

In this study, the CPA EoS, as proposed by Kontogeorgis et al. (1999) was used for calculating the fugacity of each component in the fluid phase (Kontogeorgis et al., 1996, 1999). This equation of state works well to characterize the unusual thermodynamic behaviour of chemical species which form hydrogen bonding with molecules from the same species known as self-association or from different species known as cross-association. The CPA EoS model has been successfully employed in predicting the hydrate phase equilibria previously (Chapoy et al., 2010; Haghghi et al., 2009b, 2009a). It utilizes the widely used Soave–Redlich–Kwong (SRK) EoS to characterize the physical interactions while using the association term of statistical associating fluid theory to cater for varying types of hydrogen bonding compounds (Huang and Radosz, 1990). It can be written as follows in Eqn. (6.1) with pressure P as the subject (Kontogeorgis et al., 1999, 1996):

$$P = \frac{RT}{V_m - b} - \frac{a(T)}{V_m(V_m + b)} - \frac{RT}{2V_m} \left(1 + \rho \frac{\partial \ln(g)}{\partial \rho} \right) \sum_i x_i \sum_{A_i} (1 - X_{A_i}) \quad (6.1)$$

where R is the universal gas constant, T is the temperature, ρ is the molar density, V_m is the molar volume, and b is the covolume parameter of the EoS.

The energy parameter of the equation of state, $a(T)$, is defined by a Soave-type temperature dependency:

$$a(T) = a_0 \left(1 + c_1 \left(1 - \sqrt{\frac{T}{T_c}} \right) \right)^2 \quad (6.2)$$

where T_c is the critical temperature and a_0 and c_1 are two parameters of the SRK part of the EoS.

The association term of the CPA EoS mainly comprises X_{A_i} which denotes the fraction of nonbonded associating molecules, and x_i is the mole fraction of component i . X_{A_i} is defined as follows:

$$X_{A_i}^{-1} = \left(1 + \rho \sum_j x_j \sum_{B_j} X_{B_j} \Delta^{A_i B_j} \right) \quad (6.3)$$

where $\Delta^{A_i B_j}$ is the association strength, defined as follows:

$$\Delta^{A_i B_j} = g(\rho) b_{ij} \beta^{A_i B_j} \left[\exp\left(\frac{\varepsilon^{A_i B_j}}{RT}\right) - 1 \right] \quad (6.4)$$

where $\beta^{A_i B_j}$ is the association volume, $\varepsilon^{A_i B_j}$ is the association strength, and $g(\rho)$ is the radial distribution function given as:

$$g(\rho) = \frac{1}{1 - 1.9\eta}, \quad \eta = \frac{b\rho}{4}, \quad \rho = \frac{1}{V_m}, \quad \text{and} \quad b_{ij} = \frac{b_i + b_j}{2} \quad (6.5)$$

The parameters required for the CPA EoS for associating compounds (water, MEG, and MDEA) are typically obtained through regression of vapour–liquid-equilibrium (VLE) data. The parameters for the CPA EoS for water, MEG, and MDEA are given in Table 6.2. Since we are working with a mixture, the energy and covolume parameters of the SRK part of the EoS (i.e., a and b) must be modified as per the conventional mixing rules. The geometric mean rule is applied to the energy parameter:

$$a = \sum_i \sum_j x_i x_j a_{ij}, \quad \text{where} \quad a_{ij} = \sqrt{a_i a_j} (1 - k_{ij}) \quad (6.6)$$

$$b = \sum_i x_i b_i \quad (6.7)$$

where k_{ij} is the temperature-dependent interaction parameter and is the sole adjustable parameter.

Table 6.2: Parameters for the associating compounds in this study to be used in the CPA EoS.

	a_0 (bar L ² mol ⁻²)	b (L mol ⁻¹)	c_1	ϵ (bar L mol ⁻¹)	β	References
Water	1.2277	0.014515	0.67359	166.55	0.0692	(Kontogeorgis et al., 1999)
MEG	10.819	0.0514	0.6744	197.52	0.0141	(Derawi et al., 2003)
MDEA	21.659	0.11145	1.3371	161.59	0.03320	(Avlund et al., 2008)

Optimized values for the interaction parameter k_{ij} , which are temperature-dependent, are found in the literature and are given in Table 6.3. The expression for k_{ij} for MEG and MDEA are defined as shown in Eqn. (6.8).

$$\text{MEG: } k_{ij} = A + BT \quad \text{MDEA: } k_{ij} = A + BT + CT^2 \quad (6.8)$$

Table 6.3: Optimized values for interaction parameter k_{ij} for MEG and MDEA with non-associating compounds.^a

		Methane	Ethane	Propane	Carbon Dioxide
MEG	A	0.0004	0.1155	0.0002	-0.0002
	B [K ⁻¹]	0.0498	0	0.0348	0.1141
MDEA	A	-0.626	2.181	0.738	6.51
	B [10 ⁻³ K ⁻¹]	8.506	-9.183	-1.493	-40.4
	C [10 ⁻⁵ K ⁻²]	-1.383	1.065	0.072	68.7

^a Source: (Haghighi et al., 2009b; Wang et al., 2018, 2017)

The proposed optimized binary interaction parameters between the associating compounds (water–MEG, water–MDEA, and MEG–MDEA) are obtained from the literature and are based on the available experimental VLE data (Chang et al., 1993; Haghighi et al., 2009a; Voutsas et al., 2004; Yang et al., 2013; Zoghi et al., 2012). The coefficients for the temperature-dependent binary interaction parameters are provided in Table 6.4 as per Eqn. (6.8).

Table 6.4: Coefficients for optimized interaction parameters for water–MEG, water–MDEA, and MEG–MDEA mixtures.

Interaction	A	B [K ⁻¹]
Water-MEG	-0.2313	5.6294E-4
Water-MDEA	-0.635	0.00115
MEG-MDEA	-0.655	0.0011

As for the CPA parameters of the association term, combining rules are applied in the case of multiple associating compounds to determine the association strength. The combining rules of CR-1 and ECR are given below (Kontogeorgis and Folas, 2009):

$$\varepsilon^{A_i B_j} = \frac{\varepsilon^{A_i B_i} + \varepsilon^{A_j B_j}}{2} \quad \text{and} \quad \beta^{A_i B_j} = \sqrt{\beta^{A_i B_i} \beta^{A_j B_j}} \quad (6.9)$$

$$\Delta^{A_i B_j} = \sqrt{\Delta^{A_i B_i} \Delta^{A_j B_j}} \quad (6.10)$$

van der Waals and Platteeuw (1958) developed a model for gas hydrates similar to Langmuir for gas adsorption (Van der Waals, 1959). Parrish and Prausnitz (1972) implemented this model with an algorithm for the prediction of gas hydrate equilibria (Parrish and Prausnitz, 1972). Their method has been followed in this study with the following exception; the cell potential function has been extended across multiple shells as opposed to a single shell (Ballard, 2002). Hydrate phase equilibria can be determined by equating the fugacity of water in the hydrate phase to that of the liquid/vapor phase (Sloan Jr and Koh, 2007). In the hydrate phase, the fugacity of water, f_w^H , is calculated using Eqn. (6.11):

$$f_w^H = f_w^\beta e^{\left(-\frac{\Delta\mu_w^{\beta-H}}{RT}\right)} \quad (6.11)$$

where f_w^β is the fugacity of water in the hypothetical empty hydrate lattice and $\Delta\mu_w^{\beta-H}$ is the difference in the chemical potential of water between the hydrate, μ_w^H , and the empty hydrate lattice phases, μ_w^β . This difference is calculated by Eqn. (6.12):

$$\Delta\mu_w^{\beta-H} = \mu_w^\beta - \mu_w^H = RT \sum_{n=1}^2 v_n \ln \left(1 + \sum_i C_{n,i} f_i \right) \quad (6.12)$$

where v_n is the ratio of type n cavities and water molecules in a unit cell and f_i is the

fugacity of gaseous component i . $C_{n,i}$ represents the Langmuir constant for gaseous molecule i in cavity of type n , and it is calculated by Eqn. (6.13).

$$C_{n,i} = \frac{4\pi}{k_B T} \int_0^{R_n - a_i - \xi} e^{\left(-\frac{\sum_m \omega_{i,m}(r)}{k_B T}\right)} r^2 dr \quad (6.13)$$

where k_B is the Boltzman constant, R_n is the cavity radius, a_i is the hard sphere core diameter of gaseous molecule i , ξ is a small distance such as 0.0001 Å as suggested by Pratt et al. (2001) to avoid an overflow error at the integrand's limits (Pratt et al., 2001), and $\sum \omega_{i,m}(r)$ is the summation of the overall cell potential of all of the layers within cavity n . The cell potential is calculated using the equation derived by McKoy and Sinanoğlu and implemented as suggested by Ballard (2002) and Pratt et al. (2001) to avoid singularities, as shown in Eqn. (6.14) and (6.15) (Ballard, 2002; Pratt et al., 2001).

$$\omega_{i,m}(r) = 2\epsilon_i z_m \left[\frac{\sigma_i^{12}}{R_m^{11} r} \left(\delta_{i,m}^{10} + \frac{a_i}{R_m} \delta_{i,m}^{11} \right) - \frac{\sigma_i^6}{R_m^5 r} \left(\delta_{i,m}^4 + \frac{a_i}{R_m} \delta_{i,m}^5 \right) \right] \quad (6.14)$$

where

$$\delta_{i,m}^N = \frac{1}{N} \left[\left(1 - \frac{r}{R_m} - \frac{a_i}{R_m} \right)^{-N} - \left(1 + \frac{r}{R_m} - \frac{a_i}{R_m} \right)^{-N} \right] \quad (6.15)$$

and ϵ_i , σ_i , and a_i are the Kihara potential parameters and z_m is the coordination number for the type of hydrate structure as given by Ballard (2002).

To calculate the fugacity of water in the empty hydrate lattice, f_w^β , Eqn. (6.16) is used.

$$f_w^\beta = f_w^L e^{\left(\frac{\Delta\mu_w^{\beta-L}}{RT}\right)} \quad (6.16)$$

where f_w^L is the fugacity of water in the liquid phase and $\Delta\mu_w^{\beta-L}$ is the difference in the chemical potential of water between the liquid, $\Delta\mu_w^L$, and the empty hydrate lattice phases, $\Delta\mu_w^\beta$. This difference is calculated by Eqn. (6.17):

$$\frac{\Delta\mu_w^{\beta-L}}{RT} = \frac{\Delta\mu_w^0}{RT_0} - \int_{T_0}^T \frac{\Delta h_w^{\beta-L}}{RT^2} dT + \int_{P_0}^P \frac{\Delta v_w^{\beta-L}}{RT} dP \quad (6.17)$$

where $\Delta\mu_w^0$ is the difference in the chemical potential of water in the empty hydrate lattice and pure water at the reference state ($T_0 = 273.15$ K and $P_0 = 0$ MPa), while $\Delta h_w^{\beta-L}$ and $\Delta v_w^{\beta-L}$ are the differences in the molar enthalpy and volume between the

empty hydrate lattice and pure water. The $\Delta h_w^{\beta-L}$ term is calculated using Eqn. (6.18) (Anderson and Prausnitz, 1986; Holder et al., 1980).

$$\Delta h_w^{\beta-L} = \Delta h_w^0 + \int_{T_0}^T \Delta C_{Pw} dT \quad (6.18)$$

where Δh_w^0 and ΔC_{Pw} are the enthalpy and molar heat capacity differences between the empty hydrate lattice and pure water at the reference temperature and pressure. ΔC_{Pw} is calculated using Eqn. (6.19) as suggested by Holder et al. (1980) The reference properties that Holder et al. (1980) applied were used in this study (Dharmawardhana et al., 1980; Holder et al., 1980; Parrish and Prausnitz, 1972).

$$\Delta C_{Pw} = -37.32 + 0.179(T - T_0) \quad T > T_0 \quad (6.19)$$

6.3 Results

6.3.1 Experimental Phase Equilibria

The experimentally measured phase equilibria for the two MDEA solutions are tabulated in Table 6.5 and plotted in Figure 6.3 and Figure 6.4. Both solutions showed an inhibiting effect as expected. Pure MDEA (3.5 wt%) showed a depression of 0.31 °C in the hydrate equilibrium temperature as compared to pure water (Figure 6.3), whereas MDEA–MEG (3.5 wt%/25 wt%) solution showed a depression of 8.05 °C in hydrate equilibrium temperature as compared to a pure water solution (Figure 6.4).

The developed model was used to predict the experimentally tested systems, and the absolute average relative error (AARE) as per Eqn. (6.20) between the measured data and calculations were determined. The AARE for the pure MDEA system was 0.53%, whereas for the MEG–MDEA system, the AARE was 0.77%. The results indicate a very good consistency between the predicted and experimentally obtained hydrate phase equilibria.

$$\text{AAD (T in } ^\circ\text{C)} = \frac{100}{n} \sum_{i=1}^n \left| \frac{T_{\text{calc}} - T_{\text{exp}}}{T_{\text{exp}}} \right| \quad (6.20)$$

Table 6.5: AARE of model and experimental methane hydrate phase equilibria data for MDEA and MEG.^a

MDEA (3.5 wt%)			MDEA (3.5 wt%) + MEG (25 wt%)		
P [MPa]	T [°C]	AAD [%]	P [MPa]	T [°C]	AAD [%]
5.21	6.63	0.30	7.54	2.54	0.79
11.63	13.91	0.93	10.42	5.31	1.51
13.75	15.39	0.78	15.73	8.69	0.69
18.92	18.14	0.11	20.16	10.66	0.09

^a Standard uncertainty in pressure and temperature measurements are ± 0.05 MPa and ± 0.03 °C, respectively.

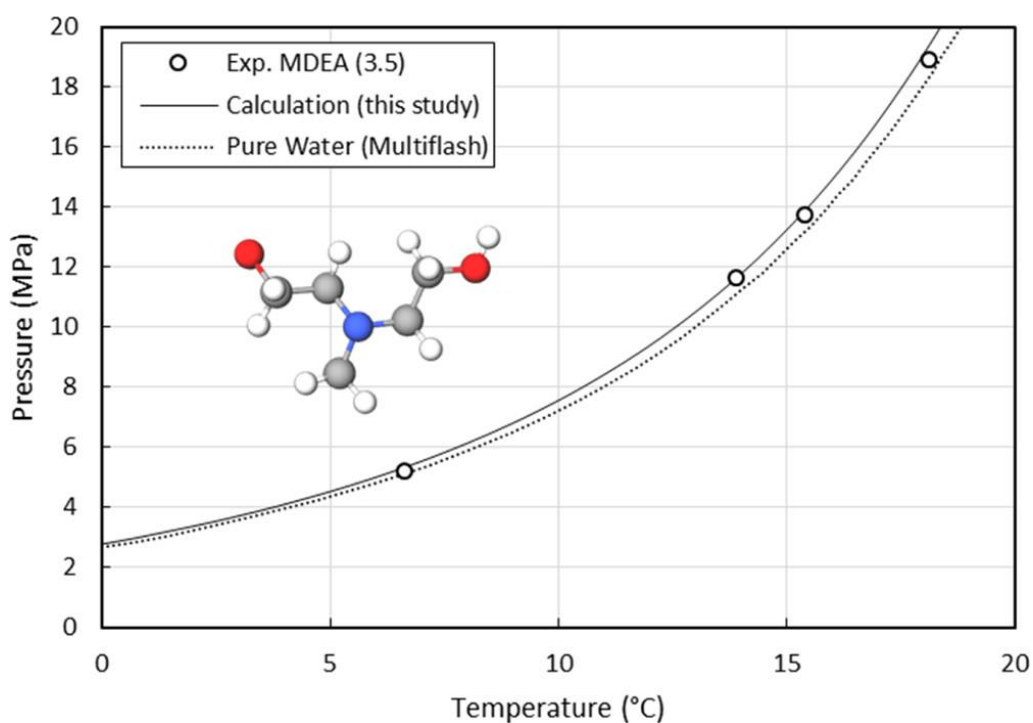


Figure 6.3: Methane hydrate equilibria for MDEA (3.5 wt%). The MDEA molecular structure is shown, where red = oxygen, blue = nitrogen, white = hydrogen, and grey = carbon.

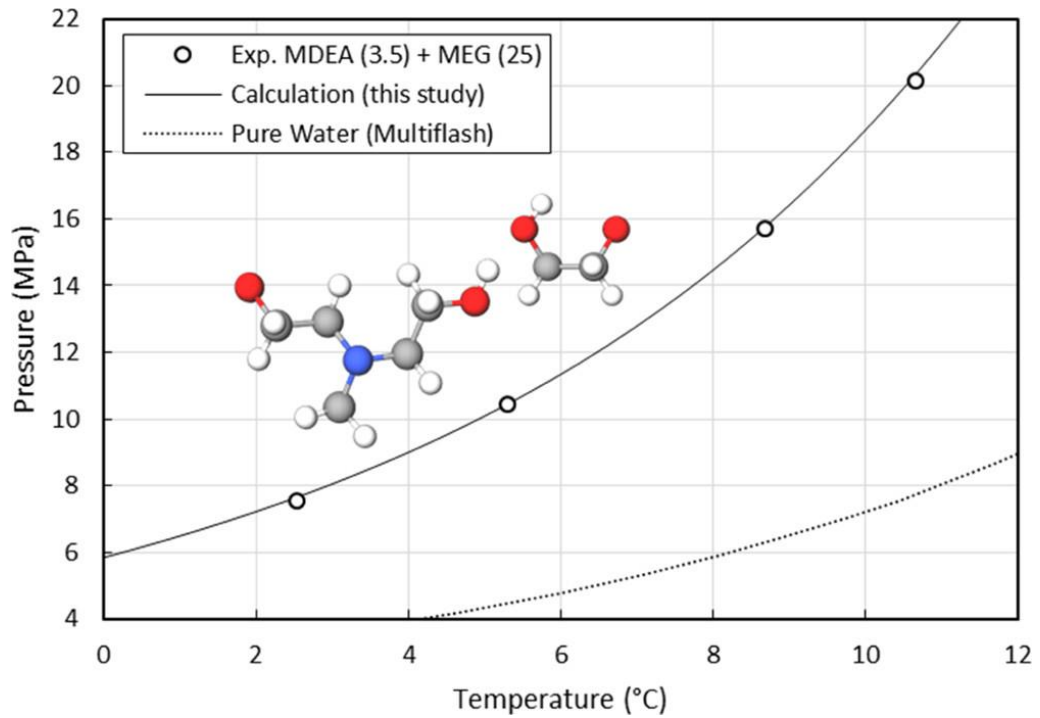


Figure 6.4: Methane hydrate equilibria for MDEA (3.5 wt%) combined with MEG (25 wt%). The MDEA and MEG molecular structures are shown, where red = oxygen, blue = nitrogen, white = hydrogen, and grey = carbon.

3.2. Model Validation

The model was tested against all available experimental hydrate phase equilibria data for MDEA systems (Table 6.6). The data published by Akhfash et al. (2017) explored a pressure range of 5.69–8.87 MPa and are plotted in Figure 6.5 alongside the calculated equilibria using our model. The calculated AARE is only 0.86% across all data, which indicates that the model is very accurate in predicting the hydrate phase equilibria across this pressure range and natural gas composition.

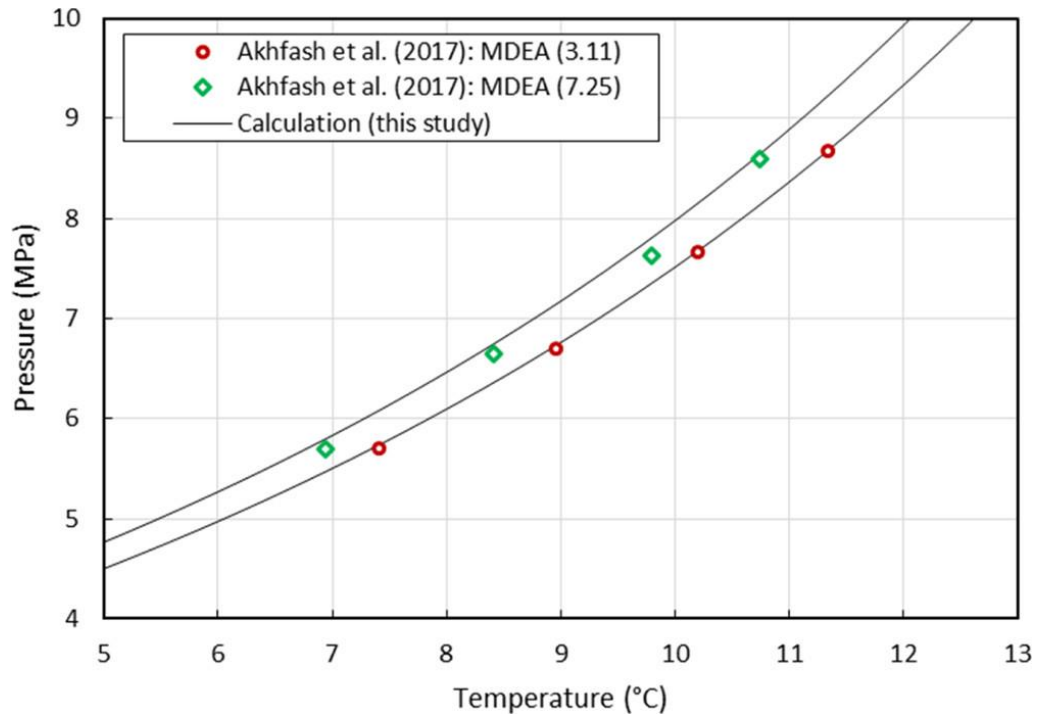


Figure 6.5: Comparison of model calculation to MDEA hydrate phase equilibria data from Akhfash et al. 2017.

Data produced by Alef et al. (2018) explored a pressure range of 7.36–20.26 MPa (Figure 6.6). The AARE between their data and the proposed model is 0.87%, which again indicates a very reliable prediction by the model.

Table 6.6: Comparison of published data with the proposed model.

Reference	T [°C]	P [MPa]	MDEA [wt%]	MEG [wt%]	No. Pts.	AARE [%]
(Akhfash et al., 2017)	6.94-17.27	5.69-8.87	3.11-7.25	0	8	0.86
	8.51-11.25	5.7-8.59	5.77-7.25	0-20.52	8	0.93
(Alef et al., 2018b)	9.63-18.57	7.36-20.26	2.5-7.5	0	12	0.87
	4.32-12.82	7.58-20.51	2.5-7.5	20	8	0.59
This Study	6.63-18.14	5.21-18.92	3.5	0	4	0.53
	2.54-10.66	7.54-20.16	3.5	25	4	0.77

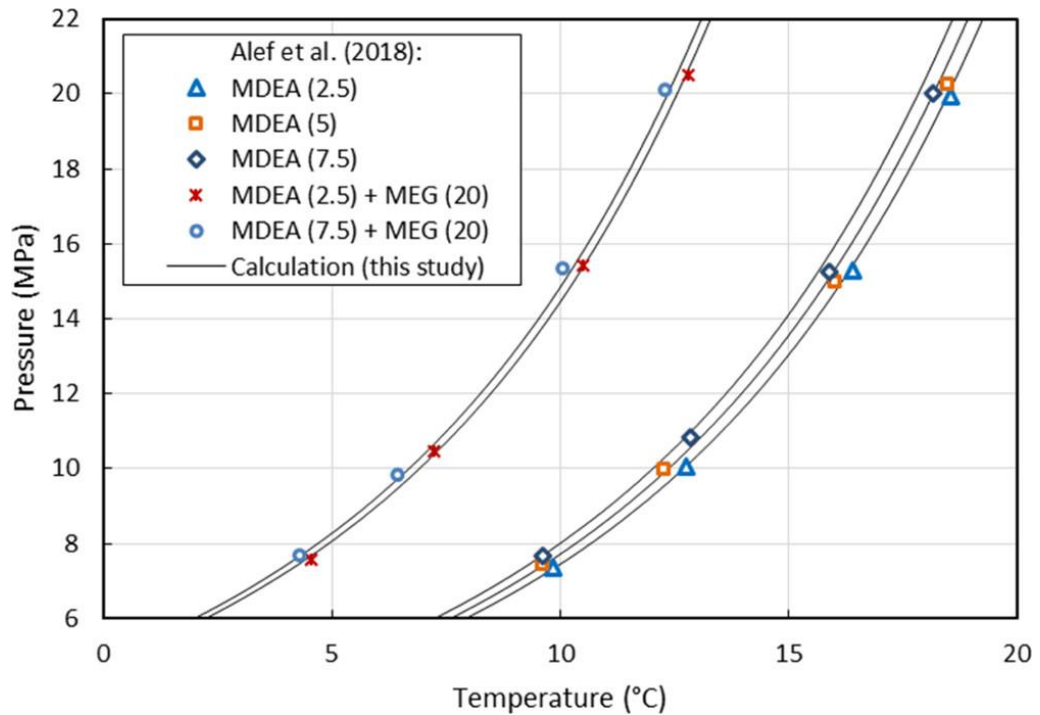


Figure 6.6: Comparison of model calculation to MDEA phase equilibria data from Alef et al. (2018).

6.4 Conclusions

The common use of MDEA as part of a corrosion strategy alongside a hydrate control program in oil and gas operations and transportation leads to the question of what the impact of MDEA upon hydrate formation is and how it could be modelled accurately. In this study, a thermodynamic model based on the CPA EoS is proposed for the calculation of hydrate phase equilibria of MDEA solutions even in the presence of MEG. Thus, this application of the CPA EoS to solve an industry problem serves as a resourceful example and will allow for MDEA integration into field hydrate programs and prediction software. The model was validated against all of the available hydrate phase equilibria data in the literature and the new phase equilibria data from this study. A total deviation of 0.76% was found, thus indicating a very good fit. Furthermore, the new hydrate phase equilibria data for MDEA at 3.5 wt% and MDEA–MEG at 3.5 and 25 wt% have been produced.

Chapter 7 Effect of Corrosion Inhibitors with Kinetic Hydrate Inhibitor on Gas Hydrate, and Empirical Modelling of MEG Degradation

This chapter is comprised of the following publication:

- **Alef, K.**, Barifcani, A., 2020. Effect of N-Methyl-Diethanolamine and Film Forming Corrosion Inhibitor on Gas Hydrate, and Empirical Modeling for Degradation. *Journal of Petroleum Science and Engineering* 184, 106522. doi: 10.1016/j.petrol.2019.106522

This chapter aims to cover two important topics. Firstly, the study aims to explore and quantify the effect of film forming corrosion inhibitor (FFCI) and MDEA in the presence of the two types of hydrate inhibitors; MEG and an LDHI such as KHI. It was found that both the chemicals increase the overall hydrate inhibition performance of the mixture as opposed to pure KHI solution. However, it was found that MDEA caused a slight decrease in the growth time as opposed to the pure KHI and KHI+FFCI solutions. In terms of the effect of FFCI on MEG, it was found that FFCI serves as a hydrate inhibitor albeit not as effective as MEG. Secondly, the study has developed two empirical models for hydrate phase equilibria prediction of MEG-only and MDEA+MEG solutions that have underwent thermal degradation as a function of exposure temperature. Moreover, an algorithm bringing together all of the empirical models produced in this study and as part of Chapters 2 and 4 has been developed. This contribution satisfies the thesis objectives (i) and (e) while fulfilling the research gaps outlined in Section 1.3.

7.1 Introduction

The occurrence of gas hydrates within gas pipelines could at the least, cause blockages leading to production down-time (Carroll, 2014). Gas hydrates are made up of a network of water cages that enclose gaseous molecules (Sloan Jr and Koh, 2007). Common pressure and temperature conditions of subsea systems promote the formation of gas hydrates (i.e., high pressures and low temperatures). The pressure/temperature from the well to the production facilities must be monitored to ensure the operation is within the hydrate-safe region. The inhibition of gas hydrates can be achieved via several techniques such as depressurization, thermal insulation and dehydration, however, these techniques may/may not be aligned with the cost/design limits of the project (McIntyre et al., 2004).

A popular method for hydrate inhibition in the industry is the use of chemical hydrate inhibitors (Kim et al., 2017; Seo and Kang, 2012). These inhibitors are further classified into two categories thermodynamic hydrate inhibitors (THIs) and low-dosage hydrate inhibitors (LDHIs) (Kelland, 2006). The way by which THIs cause the inhibition of gas hydrates is by shifting the thermodynamic hydrate phase equilibrium towards a lower temperature, thereby extending the hydrate-safe region for operations (Li et al., 2006). A very common THI is monoethylene glycol (MEG) which is favoured above all other THIs due to its ability to be safely and cost-effectively recovered at a high efficiency (Brustad et al., 2005). However, during the recovery process, MEG and other chemical additives may undergo thermal degradation which ultimately decreases the quality of MEG (Alef et al., 2019a, 2018c). On the other hand, LDHIs are a new and promising type of inhibitors which are required in very small concentrations, usually less than 1 wt% as compared to 15-50 wt% for THIs (Sloan et al., 1998). This may result in LDHIs becoming a more cost-effective option due to the smaller quantities required, however, LDHIs are less likely to be recovered for subsequent re-use. LDHIs are further classified into, kinetic hydrate inhibitors (KHIs) and anti-agglomerates (AAs). KHIs act to delay the nucleation and growth of hydrates giving enough time for safe transportation to occur. In essence, KHIs are effective if residence time in the pipeline is lower than the induction time. AAs disrupt agglomeration of hydrate crystals causing a transportable slurry; the slurry is considered transportable if the slurry viscosity is not considerably high to avoid

causing excessive pressure drops (Kelland et al., 2000).

Common to gas hydrate formation within pipelines, the risk of corrosion is alike, which may result in high production downtime, loss of equipment/facilities and cost (Aljourani et al., 2009; Garverick, 1994; López et al., 2003; Olajire, 2015; Papavinasam et al., 2007). The corrosion risk is generally addressed via the pH stabilization method whereby the artificial increase of the pH level in the fluid system promotes the growth of a stable layer composing of iron carbonate on the inner walls of the production flowline (Nyborg, 2009); or the injection of corrosion inhibitors such as a film forming corrosion inhibitor (FFCI) (Lehmann et al., 2016, 2014).

While the joint use of gas hydrate inhibitors and corrosion inhibitors is popular, the effect of these chemicals on gas hydrate formation has not been evaluated. There exists studies that are cantered on corrosion but lack the hydrate facet, and more specifically the use of low dosage hydrate inhibitors (Lehmann et al., 2014; Luna-Ortiz et al., 2014; Obanijesu et al., 2014). Alef et al. (2018b), studied the effect of MDEA on gas hydrate formation and developed an empirical model to allow for hydrate phase temperature prediction (Alef et al., 2018b). As a result, it is clear that chemical additives like MDEA and FFCI may lead to over-inhibition or even under-inhibition of gas hydrates, which may lead to additional costs or an increased risk. To achieve a safe balance, empirical data is of utmost importance to help understand the mechanism involved and build predictive models that will allow for hydrate phase equilibrium temperatures to be estimated. In this study, the inhibitory performance of FFCI was assessed at high pressures (7-20 MPa) in conjunction with MEG. Moreover, MDEA and FFCI were tested with KHI to give insight into how they influence the hydrate inhibition performance of KHIs. Furthermore, two empirical models were built to allow for the prediction of hydrate equilibrium temperature shift of MEG and MDEA + MEG solutions that have undergone thermal degradation simulating the MEG recovery process. These empirical models play an important role due to the lack of software predictions for the hydrate inhibition performance of degraded MEG/MDEA solutions. The models are based on a linear interpolation scheme between the hydrate phase equilibria of two boundary conditions of MEG and MDEA + MEG solutions to accurately predict the equilibrium temperature shift.

7.2 Methodology

7.2.1 Materials & Apparatus

In this study, methane (CAS no. 74-82-8) supplied from BOC with a purity of 99.995 mol % was selected as the hydrate forming gas. For thermodynamic hydrate inhibition, MEG (CAS no. 107-21-1) was utilized which was acquired from Chem-Supply having a purity of 99.477 mol %. As for kinetic hydrate inhibition, a commercially used (proprietary) KHI was utilized. As for corrosion inhibitors that were tested alongside the hydrate inhibitors were a pH stabilizer known as MDEA (CAS no. 105-59-9) which was obtained from Sigma-Aldrich having a purity of ≥ 99 mol %, and a commercially-used (proprietary) FFCI. The deionized water utilized in this study was produced in-house with an electrical resistivity of 19.40 M Ω cm at 23.5 °C. Nitrogen utilized for purging was generated in-house (NGP10+) having a purity of 99.9959 mol %.

The experimental apparatus utilized for hydrate testing has been thoroughly explained in our previous studies (Alef et al., 2018a; Alef and Barifcani, 2019). A PVT system capable of high pressures (up to 50 MPa) and low temperatures was utilized (Figure 7.1). The inner volume of the cell is 60 cm³ while having an additional 26 cm³ due to tubing volume. Prior to conducting an experimental test, the cell was washed with ethanol/acetone and thoroughly cleaned with deionized water followed by a vacuum drain pump. This ensured water and contaminants were removed from the cell. It was then finally connected to the nitrogen purging line and allowed to purge for an hour. A renewed surface between the liquid and vapour phases within the cell was achieved via consistent stirring that was provided by the in-built magnetic stirrer. Moreover, the cell was equipped with temperature and pressure sensors that were controlled via a computer system for heating/cooling and gas injection purposes.

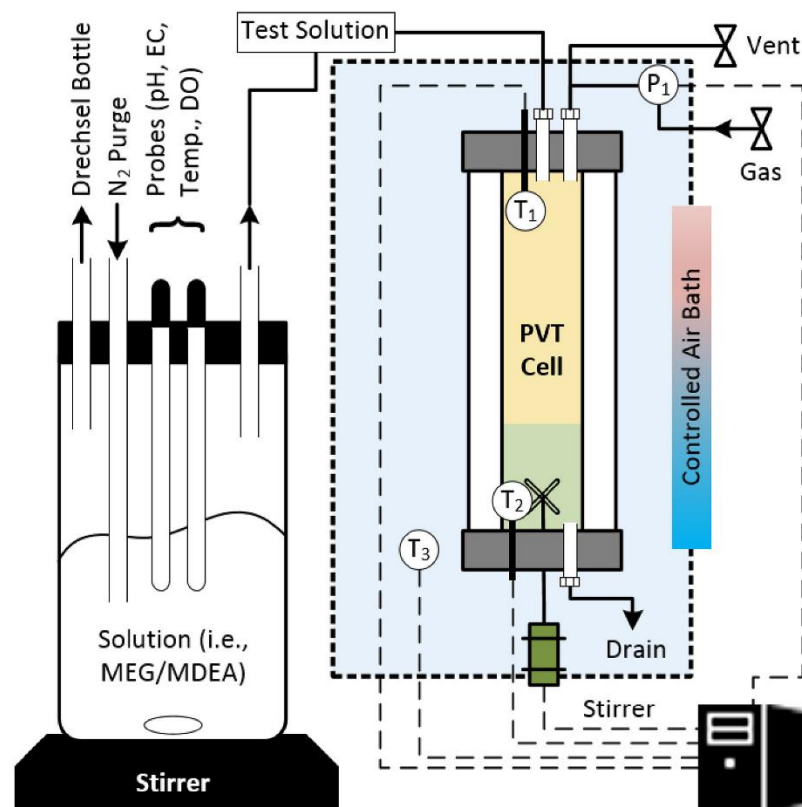


Figure 7.1: The apparatus used for solution preparation, and hydrate testing using a high-pressure PVT cell in this study. P_1 denotes cell pressure, while T_1 , T_2 , T_3 denote temperatures of vapor phase, liquid phase and air bath respectively.

The samples for the hydrate tests were meticulously prepared to avoid any oxidative degradation of MEG and to prevent impurities within solutions. A setup comprising of a 1 L beaker that was constantly purged with nitrogen and stirred via a magnetic stirrer was used for the test solution preparation as depicted in Figure 7.1. After complete synthesis, an 8 mL sample was carefully injected into the test chamber and allowed to be stirred prior to commencement of hydrate testing.

7.2.2 Isochoric Method

The isochoric method that was employed in this study to determine hydrate phase equilibria data is a well-known accurate hydrate testing method. In addition to holding the volume of the system constant, the rates for step-cooling and step-heating were 2 °C/hour and 1 °C/hour respectively. The thermodynamic equilibrium point is calculated using the recorded pressure and temperature data of the test (Sloan Jr and Koh, 2007). Figure 7.2 shows the pressure-temperature curves of the cooling and step-

heating process as part of the isochoric method to determine the hydrate dissociation (thermodynamic equilibrium) point of a 20 wt% MEG solution at ~10 MPa. The pressure and temperature curve show the nucleation, growth and dissociation stages. The initial conditions (point A) are outside of the hydrate formation conditions (indicated by point B). As the temperature decreases to point B, hydrate begins to form until point C is reached where the critical hydrate size lies. Applying heat at point C reaches a point where dissociation commences and traverses a path that will eventually cross the cooling path (point A to B). The intersection of the cooling and heating curves (indicated as blue and red respectively) is the resulting thermodynamic equilibrium temperature which can be compared against literature, or predictions via equation of state software packages. For each test solution, 4 tests were conducted at varying pressures ranging from 7 to 20 MPa to allow for plotting the hydrate phase boundary. Table 7.1 gives the experiment matrix for all the isochoric tests that were conducted as part of this study.

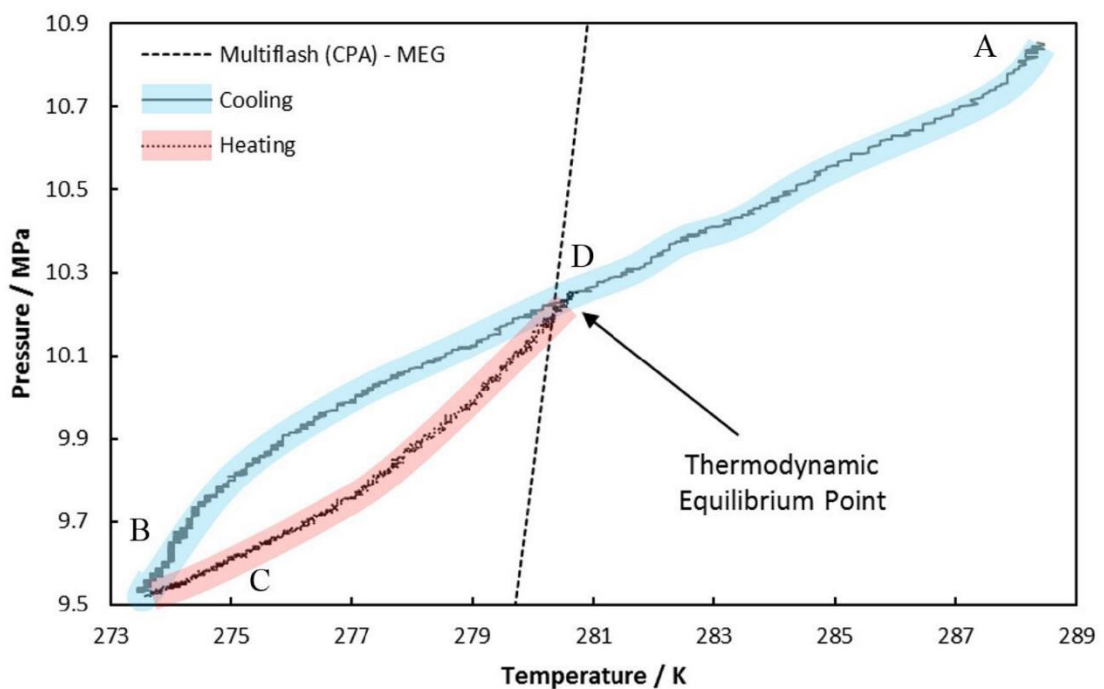


Figure 7.2: Pressure-temperature curves for the cooling and heating stages of the isochoric method for 20 wt% MEG solution. Methane hydrate phase boundary simulated in Multiflash is plotted as a dashed curve.

Table 7.1: Experimental matrix for tests using the isochoric hydrate testing method.

Test Description	Composition (wt%)		
	DI water	FFCI	MEG
FFCI	99.5	0.5	0
FFCI	97	3	0
FFCI	96	4	0
FFCI+MEG	77	3	20

7.2.3 Isothermal method

The hydrate inhibition performance of the kinetic hydrate inhibitor, as well as the combined KHI + MDEA and KHI + FFCI mixtures, were assessed using the high-pressure PVT cell (experimental matrix is given in Table 7.2). The method employed was the isothermal method which requires that the temperature remain constant after cooling to the required sub-cooling temperature. This method is very popular and has been used for assessing hydrate inhibition performance of KHIs (Lone and Kelland, 2013; Natarajan et al., 1994; Nerheim, 1993; Vysniauskas and Bishnoi, 1983; Wu and Zhang, 2010). After the sample was prepared using the aforementioned procedure, it was loaded into the PVT cell. When the air-bath temperature was stable at about 17 °C, the cell was then pressurized using methane to a pressure of ~12 MPa and then stirred at a rate of 500 rpm. The cell was then rapidly cooled to the desired temperature of ~4 °C (a sub-cooling of ~10 °C) at 0.5 °C/min, after which the cell was held at a constant temperature to measure hydrate induction and growth times from the acquired pressure-temperature data. The induction time (t_i) was defined as the time from the beginning of the cooling process to the first instance of hydrate formation (Bishnoi and Natarajan, 1996; Jensen et al., 2008; Skovborg et al., 1993). The growth time (t_g) was defined as the time from the first instance of hydrate formation until hydrate blockage had occurred in the chamber forcing the stirrer to come to a complete stop. Both t_i and t_g can be determined from the pressure-temperature data as a result of the experiment. Initially, as the cooling process was initiated, the temperature and pressure of the closed system decreased due to the cooling and gas consumption into the liquid phase. During the hold time, first hydrate formation was signified by a pressure drop (>0.2 MPa), and an increase in temperature due to hydrate formation being an

exothermic process (Daraboina et al., 2013).

The memory effect of water as described in numerous literature publications was also considered in this study, since the hydrate induction and growth times are found to be lower in water that has undergone a hydrate formation event as opposed to that in fresh water that has not (Duchateau et al., 2009; Lee and Englezos, 2005; Moon et al., 2003; Zeng et al., 2006). The tests were conducted on fresh samples (water with no memory) and memory samples (water that had already experienced a hydrate formation event). Furthermore, the tests were repeated at the same conditions three times for repeatability.

Table 7.2: The experimental matrix of hydrate inhibition tests conducted using the isothermal method.

Test Description	Composition (wt%)			
	DI water	MDEA	FFCI	KHI
KHI	99.5	0	0	0.5
KHI+MDEA	97	2.5	0	0.5
KHI+FFCI	96.5	0	3	0.5

7.3 Results and Discussion

7.3.1 FFCI and FFCI + MEG mixtures

FFCI (0.5, 3 and 4 wt%) samples with the balance being deionized water were tested for methane hydrate inhibition. The newly obtained equilibria data have been tabulated in Table 7.3. It was observed that FFCI samples showed a slight change in colour where the solution turned slightly yellow. The hydrate phase boundaries for the FFCI samples are plotted in Figure 7.3. Interestingly, FFCI showed a leftward shift in the hydrate phase boundary. The three samples (0.5, 3 and 4 wt%) as compared to pure water showed an equilibrium temperature shift of -0.1, -0.54 and -0.87 °C respectively. Thus, this leftward shift confirms that FFCI can also act as a thermodynamic hydrate inhibitor by shifting the hydrate phase boundary to that of lower temperatures and higher pressures. This hydrate inhibitory effect may be due to the high solubility of FFCI in water as both join by strong hydrogen bonds thus decreasing the amount of available water molecules to form cages around gaseous molecules, causing hydrate

inhibition (Davoudi et al., 2014; Hossainpour, 2013). Furthermore, FFCIs are considered as mixed inhibitors whereby they decelerate both the anodic and cathodic reactions. They typically have numerous functional groups with polar heads, and contain imidazoline, quaternary ammonium compounds, polymerizable acetylenic alcohols, oxyalkylated amines, various nitrogen heterocycles and surfactants to help with dispersion in the fluid and to create a film/barrier between the fluid and the surface of the pipeline (Barmatov et al., 2015, 2012). These constituents and polar heads may cause a hydrostatic force or through hydrogen bonding attract more and more water molecules away from forming cage structures around gaseous molecules. Their long chain of hydrocarbon assists in adhering to the surface of the pipeline, and may also adhere to a hydrate surface preventing it from growing to its critical size after which hydrate growth readily occurs.

Table 7.3: Equilibria data for pure FFCI solutions and MEG mixture measured in this study.^a

0.5 wt% FFCI		3 wt% FFCI		4 wt% FFCI		3 wt% FFCI+MEG	
P (MPa)	T (°C)	P (MPa)	T (°C)	P (MPa)	T (°C)	P (MPa)	T (°C)
7.45	10.25	7.55	9.95	7.39	9.35	7.41	2.95
9.7	12.75	10.13	12.55	9.75	11.95	10.59	6.25
15.06	16.35	15.67	16.15	15.19	15.61	15.23	9.35
20.14	18.65	20.38	18.54	20.37	18.21	19.84	11.25

^a Standard uncertainty in pressure and temperature measurements are ± 0.05 MPa and ± 0.03 °C respectively.

The equivalent MEG concentrations required to yield the same amount of temperature suppression or shift in hydrate phase boundary caused by FFCI was determined by simulation in Multiflash (Figure 7.3). The results reveal that FFCI solutions of concentrations 0.5, 3 and 4 wt% are equivalent to 0.6, 2.68 and 3.21 wt% of MEG respectively. This suggests that FFCI is an effective thermodynamic hydrate inhibitor albeit not as effective as MEG.

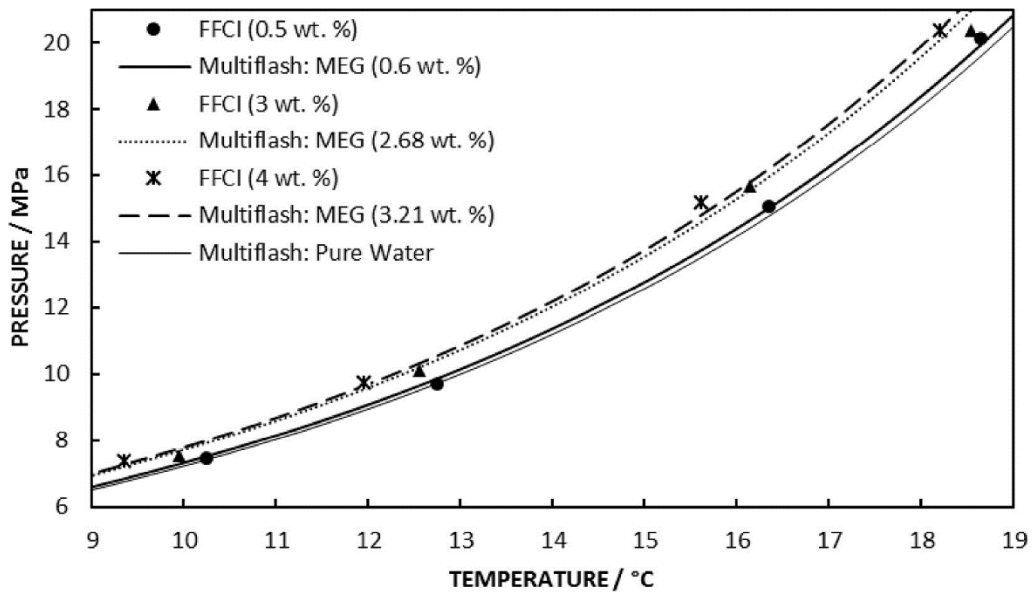


Figure 7.3: Methane hydrate phase boundaries for aqueous FFCI (0.5, 3 and 4 wt%) and their equivalent MEG concentration using Multiflash.

FFCI (3 wt%) combined with MEG (20 wt%) was tested to determine the combined effect on the hydrate phase boundary as shown in Figure 7.4. A temperature suppression of $-1.55\text{ }^{\circ}\text{C}$ was produced relative to 20 wt% pure MEG without any additives. Furthermore, the amount of pure MEG required to produce the equivalent temperature suppression of FFCI + MEG solution was found to be 23.12 wt% of MEG. This increased hydrate inhibitory performance may be attributed to the synergistic hydrate inhibition effect of both MEG and FFCI. Hence, where FFCI is used alongside MEG, an enhanced hydrate inhibitory performance can be expected.

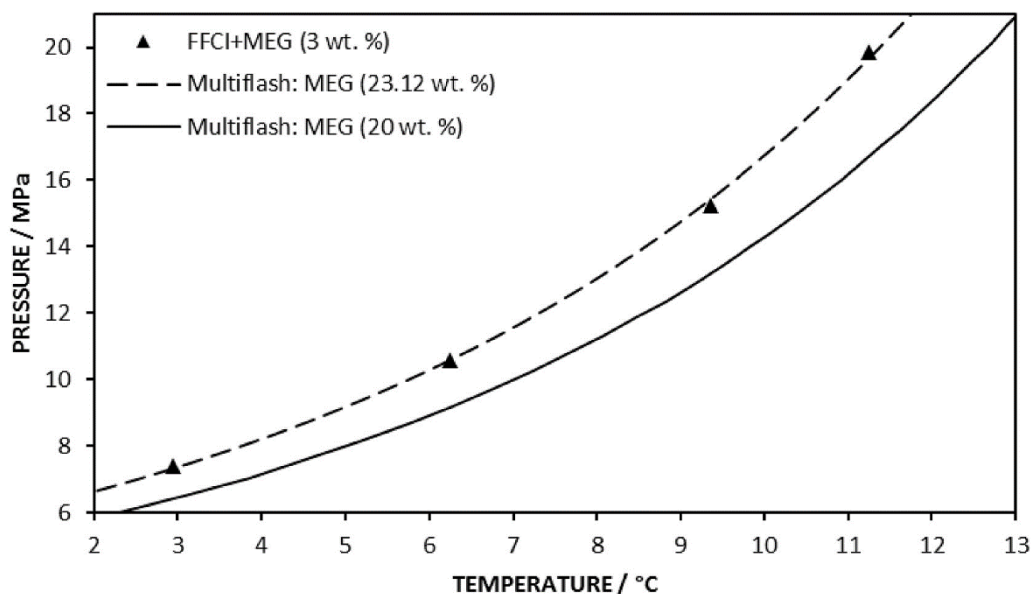


Figure 7.4: Hydrate phase boundary for the combined mixture of 3 wt% FFCI with 20 wt% MEG compared with a 20 wt% MEG only solution.

7.3.2 KHI Mixtures

Kinetic hydrate inhibitors act to slow down the process of hydrate nucleation rather than shift the thermodynamic equilibrium to lower temperatures and higher pressures. For this reason, conventional hydrate testing techniques cannot be used to assess the performance of KHIs. In this study the induction and growth times at a sub-cooling of $\sim 10^{\circ}\text{C}$ for methane hydrate formation in samples that contained 0.5 wt% KHI with and without additives of MDEA (2.5 wt%) and FFCI (3 wt%) were measured. During the induction phase of the 0.5 wt% KHI sample with no additives, it was observed to have waves of bubbles circulating at the surface (Figure 7.5). While samples with MDEA and FFCI did not show such behaviour during induction. An explanation for such behaviour is perhaps due to the different way by which the gas dissolves within the varying samples. During the growth phase, samples with additives showed slightly deranged larger hydrate solids forming initially, while the pure KHI sample had smaller and more agglomerated hydrate solids being formed (Figure 7.5). This observation can be explained due to the separate compounds within the solution adhering to hydrate solids preventing further growth as explained later in this section.

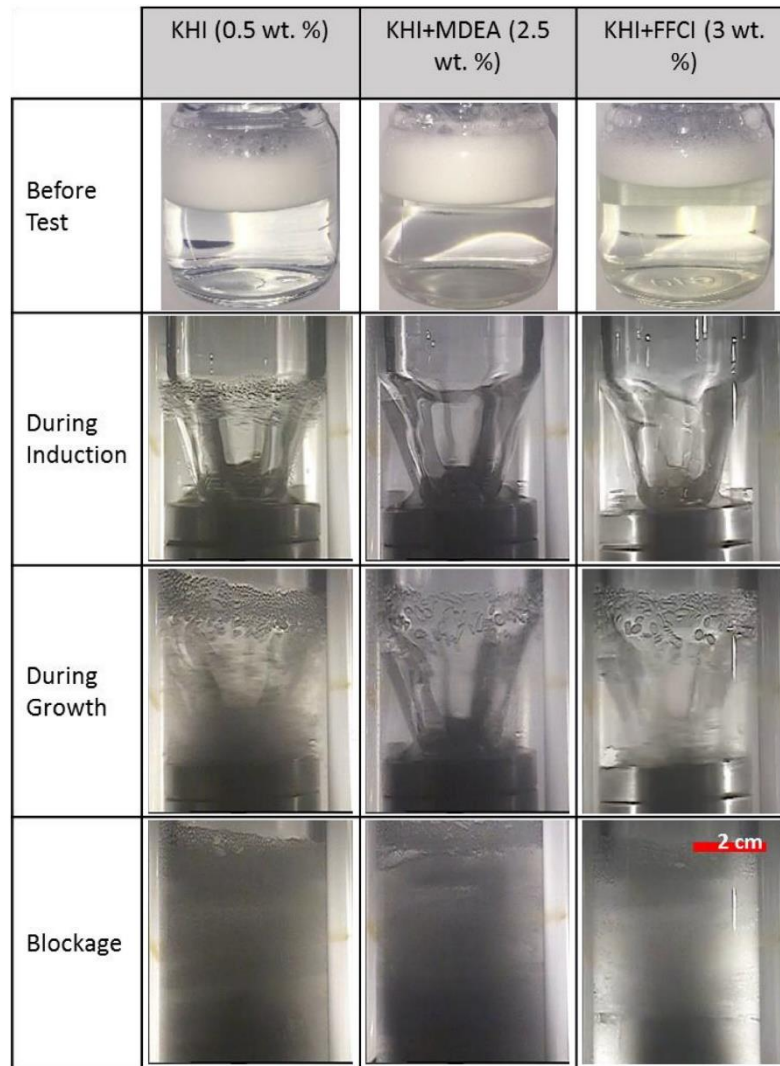


Figure 7.5: Stages of hydrate testing of KHI in the presence of MDEA and FFCI.

The measured induction and growth times for the three samples are plotted in Figure 7.6 and Figure 7.7, and are tabulated in Table 7.4. The degree of sub-cooling was kept constant at $10\text{ }^{\circ}\text{C} \pm 1\text{ }^{\circ}\text{C}$ for all tests to ensure comparable results. The results reveal that the induction time for KHI + MDEA was the highest (224 min) followed by KHI + FFCI (179 min) and finally the KHI only sample (155 min). In terms of growth times, the KHI + FFCI sample had the highest time (55 min) followed by KHI only sample (38 min) and finally KHI + MDEA (32 min).

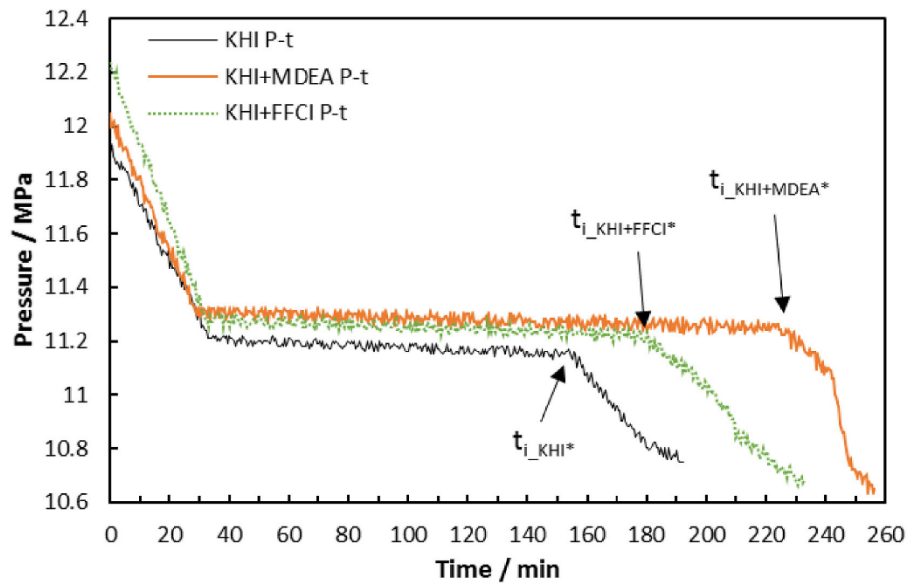


Figure 7.6: Pressure drop curves against time for KHI with MDEA and FFCI in memory water.

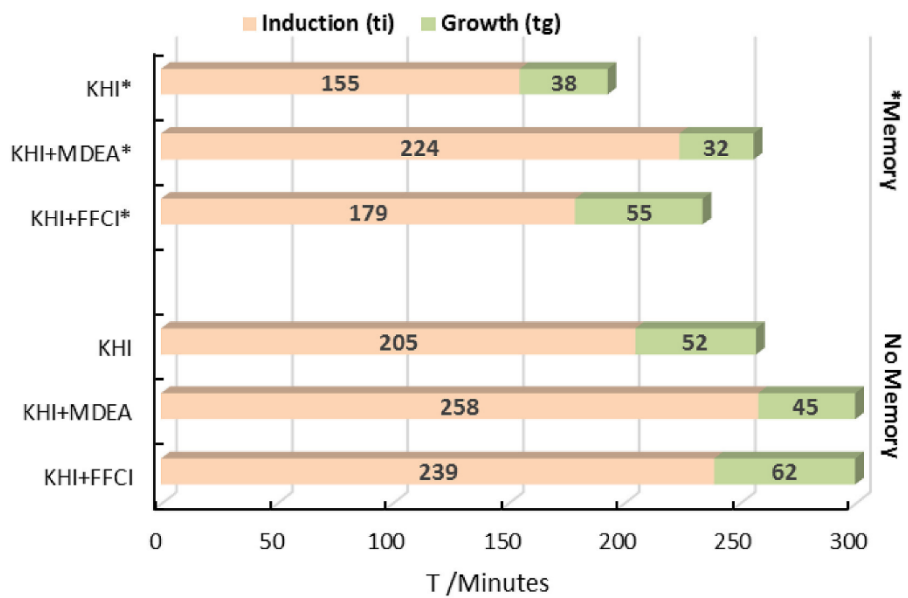


Figure 7.7: Induction and growth times for KHI with/without MDEA and FFCI.

It is known that hydrophobic and hydrophilic tails of KHIs can alter their hydrate inhibitory performance (Wang et al., 2019). In one such study, Park et al. (2017), combined a KHI with a corrosion inhibitor, and found the chemical to function as both hydrate and corrosion inhibitor (Park et al., 2017). Typical KHIs employed in the industry such as vinyl lactam monomers (PVP and PVCap) and lactam monomer-based copolymers are water-soluble. These chemicals are made-up of polyvinyl

backbones with varying cyclic amide groups (Kamal et al., 2016). The backbone and additional groups may have numerous oxygen atoms (double-bond and single-bond) that carry large charge densities attracting hydrogen atoms from nearby water molecules. By attracting the water molecules, they are prevented from forming caged structures around gaseous molecules. This also increases the chance for the backbone of the KHI to rest flat upon the hydrate surface preventing further hydrate crystal growth. Thus, a hydrate slurry is formed which can be transported at least as opposed to complete hydrate blockage in the pipeline. Hence, KHIs affect induction and growth times via the mechanism of bonding and adsorption of their inner groups upon the hydrate crystal surface and with water molecules. This in turn decreases the rate of agglomeration of hydrate crystals as well as preventing water molecules to form cage structures around gas molecules. Ultimately, this averts the hydrate crystal nucleus from growing to the critical size as importantly required for spontaneous hydrate formation (Sloan Jr and Koh, 2007).

In terms of MDEA (2.5 wt%) combined with KHI (0.5 wt%), an increase of 44.5% was found in the induction time (from 155 to 224 min), whilst the growth time dropped by 15.8% from 38 min to 32 min. This suggests that MDEA increases the induction time drastically, however, the downside is that growth time was decreased. This increase in the induction time due to MDEA can also be explained due to MDEA decreasing the thermodynamic hydrate phase boundary thus requiring an even lower hydrate formation temperature as compared to that of the base solution. The high induction times for the combined solutions of KHI with additives such as MDEA and FFCI can be attributed to the hydrophilic nature of these chemicals and the thermodynamic hydrate inhibition quality of FFCI (as established earlier in this study) and MDEA as described in our earlier works (Alef et al., 2019b, 2018b). The shift in hydrate equilibrium curve results in a higher sub-cooling range for the KHI with MDEA or FFCI, and thus at the degree of sub-cooling at which the samples were tested, the combined solution had a higher potential than the KHI-only sample. An increase in both the induction time (15.5%) and growth time (44.7%) for FFCI (3 wt%) with KHI (0.5 wt%) was found. The highest growth time was found for the KHI + FFCI sample which may be attributed to the long chains of hydrocarbons present in the FFCI which increase the chance for them to adhere to the hydrate surface preventing further hydrate crystal growth. Hydrate crystals must reach a critical size

before they can grow to their potential size. By increasing the growth time, this also suggests that FFCI in the system alongside KHI can increase the effectivity of the hydrate inhibition program by enlarging the hydrate safety window of the operation.

Table 7.4: Experimental data for KHI, MDEA and FFCI solutions under a sub-cooling of ~ 10 °C.^{ab}

KHI (wt%)	MDEA (wt%)	FFCI (wt%)	P_{exp} (MPa)	T_{exp} (°C)	Sub-cooling ΔT (°C)	T_i (min)	T_g (min)
0.5	0	0	11.32	3.24	10.66	205	52
0.5 ^b	0	0	11.19	3.14	10.65	155	38
0.5	2.5	0	11.12	3.62	10.11	258	45
0.5 ^b	2.5	0	11.28	3.75	10.11	224	32
0.5	0	3	11.24	3.59	10.24	239	62
0.5 ^b	0	3	11.25	3.64	10.20	179	55

^a Standard uncertainty in pressure and temperature measurements are ± 0.05 MPa and ± 0.03 °C respectively.

^b Denotes samples were tested in memory water.

7.3.3 Empirical Modelling

In the MEG recovery process, there exists numerous sub-processes that may cause thermal degradation of MEG and other chemicals alongside MEG due to the high operating temperatures. Namely, the re-boiler and reclamation units of the MEG recovery unit can result in the highest thermal exposure. Alef et al. (2018c), studied the cycling effect of MEG regeneration on hydrate inhibition performance, and subsequently developed an empirical model for temperature shift prediction (Alef et al., 2018c). Similarly, Alef et al. (2018b), developed an empirical model for hydrate phase equilibria prediction in pure MDEA and MDEA + MEG solutions (Alef et al., 2019b, 2018b). However, there does not exist an empirical model to predict the hydrate phase equilibria for MEG-only or MDEA + MEG solutions that have undergone thermal degradation for a specific period of time. In this section, available literature data has been utilized to develop and verify two empirical models to fill the gap in the literature and build a foundation for MEG and MDEA + MEG degradation modelling research work.

The boundary conditions for the models are given in Table 7.6 (as denoted by tick marks). To develop a mathematical relation between the experimentally obtained hydrate phase equilibria and thermal exposure temperature, a simple linear interpolation across the phase boundaries corresponding to the varying thermal exposure temperatures was applied. The assumption being that at any given pressure, there exists a linear relation between the phase boundary temperature and thermal exposure temperature. Since MEG/MDEA + MEG degradation causes a decrease in the hydrate inhibitory performance of MEG (i.e., shifting the hydrate phase boundary to the right) as shown in (Figure 7.8), an interpolation scheme across the thermal exposure temperature and corresponding hydrate phase boundaries is developed. The models were based on two boundary conditions; the lower limit boundary which corresponds to the equilibrium temperature of the unexposed solution, and the upper limit boundary corresponding to the equilibrium temperature of the exposed solution (maximum thermal exposure). It is thus, expected that higher thermal exposure temperatures ($t_{exposure}$) will result in higher phase equilibrium temperatures ($T_{exposed}$). This can be expressed by the addition of the shift in temperature due to degradation ($\Delta T_{exposed}$) to the temperature of the unexposed solution ($T_{unexposed}$) as shown in Eqn. (7.1).

$$T_{exposed} = T_{unexposed} + \Delta T_{exposed} \quad (7.1)$$

The lower limit or the unexposed solution phase equilibrium boundary ($T_{unexposed}$) is determined by fitting an exponential function to the experimental data. The exponential function is then re-arranged so that temperature is the subject of the function as given in Eqn. (7.2) where P denotes the equilibrium pressure, while a and b are the constants of the exponential function.

$$T_{unexposed} = a \ln\left(\frac{P}{b}\right) \quad (7.2)$$

To derive the shift in temperature due to degradation ($\Delta T_{exposed}$) involves developing a relationship between the shift in equilibrium temperature of the lower boundary and the upper boundary versus equilibrium pressure (P). In terms of MEG-only solutions, the equilibrium temperature shift with unexposed MEG as the lower limit, and a MEG solution exposed to 200 °C for 48 h as the upper limit was determined over a varying pressure range (0–30 MPa) to account for the temperature dependence on pressure

(Figure 7.8). While for MDEA + MEG solutions, the equilibrium temperature shift with unexposed MDEA + MEG as the lower limit, and a MDEA + MEG solution exposed to 200 °C for 240 h as the upper limit was determined over a varying pressure range (0-30 MPa) to account for the temperature dependence on pressure (Figure 7.8). Thus, the equations for $\Delta T_{exposed, 200^\circ C}$ for the two systems are simply the exponential functions as derived from Figure 7.8 as given in Eqns. (7.3), (7.4). To determine $\Delta T_{exposed, x}$, a linear interpolation is applied to Eqns. (7.3), (7.4) by multiplying the entire term by $(x-22)/200$, resulting in Eqns. (7.5), (7.6) where x is the desired exposure temperature, while the 22 and 200 °C refers to the unexposed and exposed solution exposure temperatures respectively.

$$\text{MEG:} \quad \Delta T_{exposed, 200^\circ C} = \left(\frac{1}{-3.157} \right) \ln \left(\frac{P}{2591.4} \right) \quad (7.3)$$

$$\begin{array}{l} \text{MDEA} \\ \text{+ MEG:} \end{array} \quad \Delta T_{exposed, 200^\circ C} = \left(\frac{1}{-2.651} \right) \ln \left(\frac{P}{407.11} \right) \quad (7.4)$$

$$\text{MEG:} \quad \Delta T_{exposed, x} = \left(\frac{1}{-3.157(200 - 22)} \right) \ln \left(\frac{P}{2591.4} \right) (x - 22) \quad (7.5)$$

$$\begin{array}{l} \text{MDEA} \\ \text{+ MEG:} \end{array} \quad \Delta T_{exposed, x} = \left(\frac{1}{-3.157(200 - 22)} \right) \ln \left(\frac{P}{2591.4} \right) (x - 22) \quad (7.6)$$

To develop a general expression for the two systems, equation pairs (2–5) and (2–6) can be substituted into Eqn. (7.1) separately, to calculate hydrate equilibrium temperature at a specified thermal exposure temperature. The overall expression for MEG-only and MDEA + MEG systems is then given in Eqn. (7.7), and the corresponding constants (a , b , c , d) for both systems are given in Table 7.5.

$$T_{exposed, x} = a \ln \left(\frac{P}{b} \right) + c \ln \left(\frac{P}{d} \right) (x - 22) \quad (7.7)$$

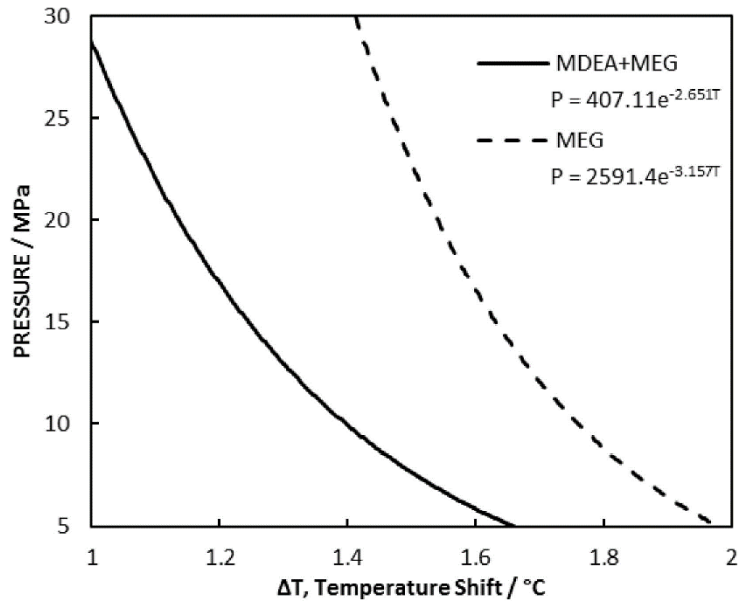


Figure 7.8: Hydrate equilibrium temperature shift for MEG and MDEA + MEG degraded solutions.

Table 7.5: Constants to be used in Eqn. (7.7) for aqueous MEG and MDEA + MEG mixtures.

	a	b	c	d
MEG	7.6805	6.6764	-1.78E-03	2591.4
MDEA+MEG	7.8678	4.3161	-2.12E-03	407.11

7.3.3.1 Model Validation

The models were validated against available literature data to see how well they predicted the hydrate phase equilibrium temperature of degraded MEG and MDEA + MEG samples. The comparison of MEG solutions exposed to 165 °C and 180 °C are shown in Figure 7.9. While, the comparison of MDEA + MEG solutions exposed to varying temperatures are given in Figure 7.10. The absolute average relative error (AARE) between the model calculated values and the experimental data were determined as per Eqn. (7.8) are given in Table 7.6. The comparisons indicate that the model generally predicted well with an AARE between 2.7 and 3.4%. The model showed a larger deviation at lower pressures. In regards to the MDEA + MEG sample that was exposed to 135 °C, the model showed a higher deviation such that the

experimental data showed a greater temperature shift. It is recommended that the model is tuned with more experimental data once available to further increase the accuracy of the model and to cater for lower pressure ranges.

$$AARE (\%, T \text{ in } ^\circ C) = \frac{100}{N} \sum_{i=1}^N \left| \frac{T_{model} - T_{exp}}{T_{exp}} \right| \quad (7.8)$$

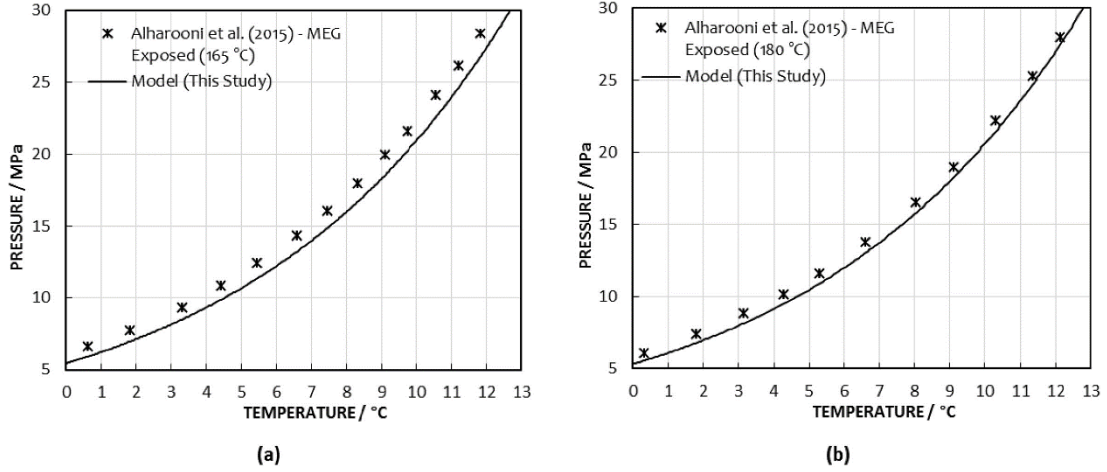


Figure 7.9: Comparison of calculations using model compared to experimental data for MDEA solutions exposed to 165 °C and 180 °C.

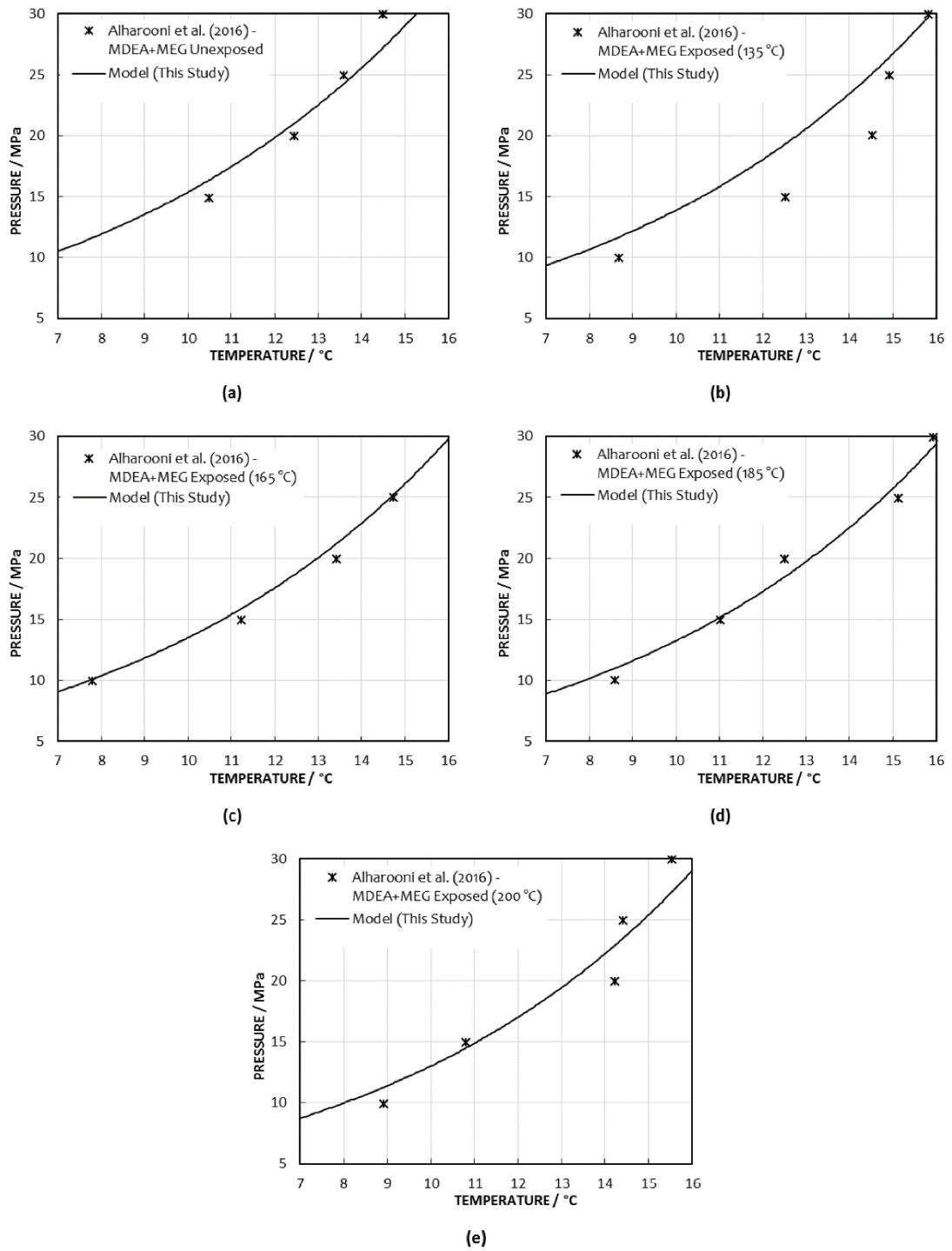


Figure 7.10: Comparison of calculations using model compared to experimental data for MDEA + MEG solutions exposed to 135, 165, 185 and 200 °C.

Table 7.6: Calculations using model compared to experimental data for MEG and MDEA + MEG mixtures from literature.

Mixture	T _{Exposure} (° C)	Exposure Time (h)	P (MPa)	T _{exp} (° C)	Model Bound.	AARE (%) ^a
MDEA (2 wt%)	22	0	10-30.0	7.0-14.5		4.32
+MEG (20 wt%)	22	0	P = 43.161e ^{0.1271T}		✓	0.01
(AlHarooni et al., 2016)	135	240	5.0-30.0	2.2-15.8		7.72
	135	240	P = 35.434e ^{0.126T}			7.15
	165	240	9.9-30.0	7.8-16.4		2.31
	165	240	P = 42.389e ^{0.1174T}			2.61
	185	240	10.0-30.0	8.6-15.9		3.52
	185	240	P = 36.77e ^{0.1294T}			0.60
	200	240	9.9-30.0	8.9-15.5		5.59
	200	240	P = 34.329e ^{0.1335T}		✓	0.03
MEG (25 wt%)	22	0	7.0-30.5	0.4-11.7	✓	0.21
(AlHarooni et al., 2015)	165	48	14.3-30.3	6.6-12.3		5.65
	180	48	10.1-30.2	4.2-12.8		4.55
	200	48	5.7-30.0	0.8-13.0	✓	0.33

^a AARE was calculated as per Eqn. (7.8).

Moreover, a useful algorithm or grouping of the empirical models produced in this study for the degradation effect of MEG and MDEA + MEG solutions in conjunction with models produced in our earlier works has been developed (Figure 7.11). The algorithm covers the simulation needs of MEG regeneration and degradation, and MDEA inhibitory effect as well as degradation. These aspects of MEG and MDEA in the context of gas hydrate control has not been modelled in hydrate simulation software, thus the algorithm serves an important role. The inputs to the algorithm are solution composition (concentrations), pressure and temperature conditions. The output is hydrate phase equilibrium conditions (pressure and temperature).

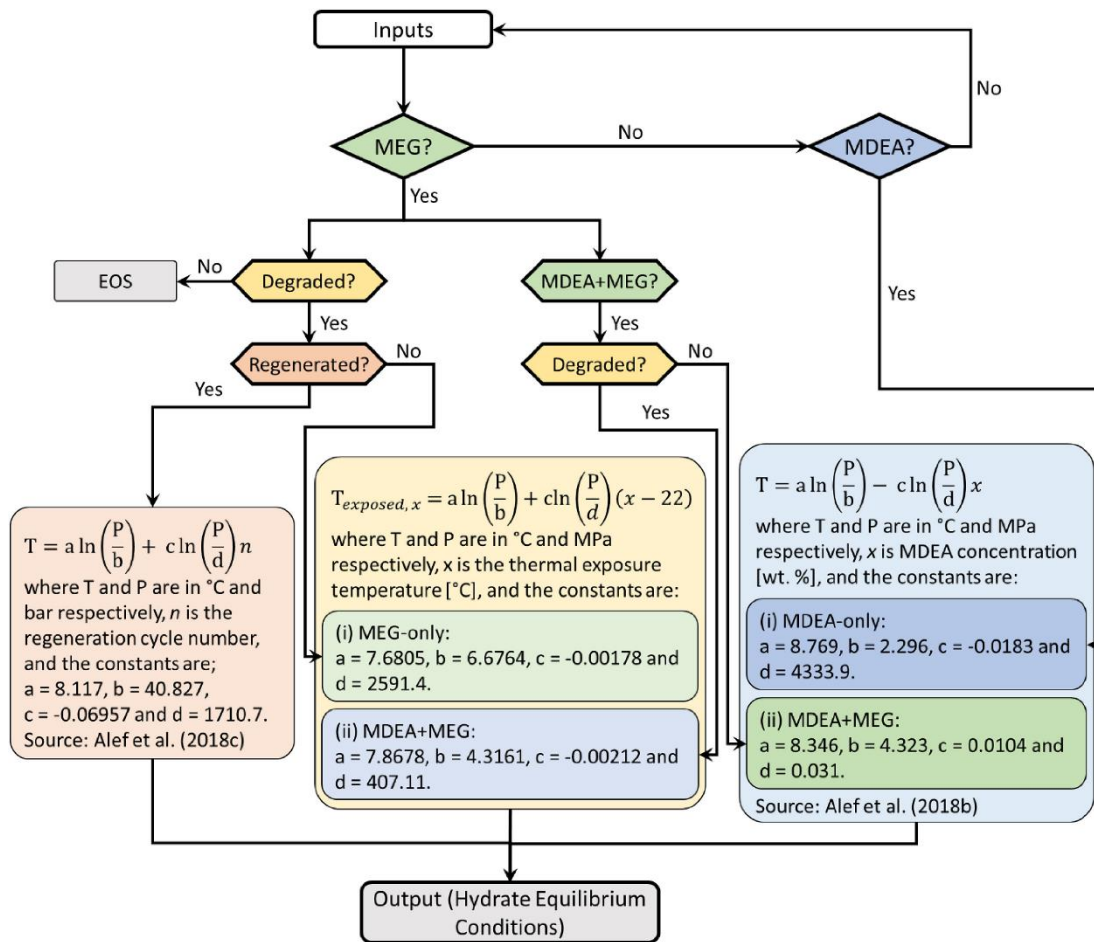


Figure 7.11: The algorithm to determine equilibrium temperature of aqueous MDEA, and MDEA + MEG solutions at varying concentrations.

7.4 Conclusion

The study evaluated the hydrate inhibitory performance of MEG with FFCI, finding that FFCI showed good hydrate inhibitory performance. It was found that only 3 wt% of FFCI in a 20 wt% MEG solution showed an equivalent hydrate inhibition performance of a 23.12 wt% MEG solution. MDEA and FFCI were also found to enhance the inhibitory performance of solutions containing KHI. The experimental equilibria data from this study for both MDEA and FFCI illustrate that various chemical additives that are injected alongside hydrate inhibitors can potentially produce a higher hydrate inhibition performance than otherwise expected. In this case, it increased the hydrate-safe region, and perhaps rendered the system into over-inhibition. However, other chemical additives may have a hydrate promoting effect which could render the system under-inhibited and prone to risk if not adequately

addressed.

New experimental data for FFCI, FFCI + MEG, KHI + MDEA and KHI + FFCI have been developed. Empirical modelling for degraded MEG and MDEA + MEG samples were conducted to bridge the gap in literature for such models to cater for the degradation effect. An algorithm based on these empirical models and previous models is given to help estimate the hydrate phase equilibrium conditions of MDEA, degraded MEG and MDEA + MEG solutions. This is much needed as there are no software simulation models available, to the best of the authors' knowledge, that properly take into account the degradation effect.

Chapter 8 Effect of Dissolved Oxygen, Sodium Bisulfite, and Oxygen Scavengers on Methane Hydrate Inhibition

This chapter is comprised of the following publication:

- **Alef, K.**, Iglauer, S., Barifcani, A., 2018a. Effect of Dissolved Oxygen, Sodium Bisulfite, and Oxygen Scavengers on Methane Hydrate Inhibition. *J. Chem. Eng. Data* 63, 1821–1826. doi: 10.1021/acs.jced.8b00150

Numerous chemical additives are added to monoethylene glycol (MEG) injection streams to maintain and protect assets as well as to ensure steady production of hydrocarbons. Dissolved oxygen levels are monitored due to the serious corrosion risks that it poses. These levels are kept within the acceptable and safe limit by the injection of oxygen scavengers. Since these chemical additives are injected into gas production systems, it is important to understand how they impact gas hydrate formation; whether they promote or inhibit gas hydrates. The study found dissolved oxygen may promote gas hydrate formation and thus should be kept to a minimum as already prescribed for mitigating corrosion. Oxygen scavengers generally served to slightly increase hydrate inhibition, except for one oxygen scavenger that showed otherwise. Suggesting that hydrate control programs can be improved by ensuring the compatibility of all chemical additives are ascertained and that they all serve their purposes without adversely affecting other processes. This chapter focuses on the effect of dissolved oxygen and various oxygen scavengers on gas hydrate formation. This contribution satisfies the thesis objective (j) while fulfilling the research gaps outlined in Section 1.3.

8.1 Introduction

Gas hydrate formation and corrosion are flow assurance issues which adversely affect gas processing and transportation. Chemical additives such as hydrate inhibitors are commonly injected to shift hydrate formation conditions so that pipeline operating conditions are within the hydrate-safe region, or to postpone hydrate nucleation, or to prevent the agglomeration of hydrate particles thus preventing hydrate plugging (Cha et al., 2013; Kelland, 2006; Sloan Jr and Koh, 2007). Monoethylene glycol (MEG) is a popular thermodynamic hydrate inhibitor due to its recoverability using closed-loop MEG regeneration and reclamation facilities (Brustad et al., 2005). Preventing or lowering the risk of corrosion in gas pipelines is commonly achieved by pH stabilization or the injection of film forming corrosion inhibitors (Latta et al., 2013; Lehmann et al., 2014). The pH stabilization method requires that pH is adjusted using an amine to precipitate a stable protective iron carbonate film (Dugstad and Seiersten, 2004; Halvorsen et al., 2007). However, dissolved oxygen (DO) even in small concentrations within lean-MEG injection lines, gas pipelines, downstream and well-head equipment, and MEG regeneration facilities also poses serious corrosion and operational risks (Ivonye, 2014; Joosten et al., 2007; Kvarekval et al., 2002; Salasi et al., 2017; Wang et al., 2013; Wang and Wylde, 2010). Dissolved oxygen can cause serious pitting corrosion to carbon steel and certain corrosion resistant alloy (CRA) pipelines especially in the presence of MEG (Joosten et al., 2007; Lehmann et al., 2014). Dissolved oxygen also increases the rate of carbon dioxide corrosion of carbon steel (John et al., 2009; Martin, 2001; Xiang et al., 2014). Furthermore, DO may hinder the effectivity of film forming corrosion inhibitors as well as the stability of iron carbonate films on the inner walls of pipelines (Gulbrandsen et al., 2005; Xiang et al., 2014).

Oxygen ingress is typically addressed by either purging using an inert gas for the removal of dissolved oxygen or the injection of specific chemicals known as oxygen scavengers (typically sulfites) to react with dissolved oxygen, lowering levels to <20 ppb (Braga, 1987; Kelland, 2009; Kundu and Seiersten, 2017). Due to the low level of dissolved oxygen required to prevent corrosion, industrial-grade nitrogen cannot be used for purging as the sole method (unless ultrapure nitrogen is feasible) due to the high oxygen contamination levels (>3%) (Lehmann et al., 2014). A combined

approach where nitrogen purging in storage vessels alongside the injection of oxygen scavengers is commonly implemented to not only reduce the dissolved oxygen concentration but to do so in a short duration of time (Braga, 1987). Even small amounts of dissolved oxygen over an extended period could result in nucleation of corrosion pits and consequent autocatalytic propagation (Salasi et al., 2017).

In terms of gas hydrate inhibition, it is important to understand how the added chemicals or oxygen scavengers will affect the hydrate inhibition performance of MEG. These chemicals must be assessed to ensure there are no opposing effects on the desired hydrate inhibition performance owing to dissociation products, by-products of side-reactions, impedance to MEG's inhibition kinetics, and incompatibilities. The tendency for these side-reactions to occur are further enhanced by the high operational temperatures applied in MEG closed loops, and thus build-up of by-products and chemical additives in the MEG closed loop may play a role in hydrate inhibition. In this study, the methane hydrate inhibition performance of MEG combined with various oxygen scavengers was investigated. Oxygen scavengers are required in large concentrations to have an effective result (Lehmann et al., 2014). Optimally, oxygen scavengers should be non-volatile, allowing for removal with salts during the reclamation process, preventing unnecessary build-up and fouling of the MEG closed loop (Lehmann et al., 2014). However, MEG operations may not have a reclamation stage, or may have slip-stream reclamation depending on the allowable salt tolerance in the final lean-MEG solution to be injected at the wellhead, so oxygen scavengers may not be removed at all, or are removed from only a portion of the MEG inventory. Thus, knowing whether they perform as hydrate promoters or inhibitors is crucial to a successful hydrate flow assurance program.

8.2 Experimental Methodology

8.2.1 Materials and Chemicals

The chemicals utilized in this study were sourced from various high-grade vendors and are reported in Table 8.1. MEG was sourced from Chem-Supply (99.477 mol %), and deionized water was effectively produced within the laboratory (electrical resistivity of $18 \text{ M}\Omega\cdot\text{cm}$ at $24 \text{ }^\circ\text{C}$). Ultrahigh purity methane (99.995 mol %) supplied by BOC was used as the hydrate forming gas, while ultrahigh purity nitrogen (99.9959 mol %)

was produced in-house using a nitrogen generator for purging and to maintain a nitrogen blanket in all experiments.

The oxygen scavengers tested in this study for their hydrate inhibitory performance were sodium bisulfite (NaHSO_3), a proprietary oxygen scavenger (hereafter referred to as OS-P), and finally a nonsulfite oxygen scavenger (IFEox2) developed by Kundu and Seiersten which is erythorbic acid-based (Kundu and Seiersten, 2017). The use of transition-metal ions as catalysts in aqueous solutions to increase the rate of sulfite-oxidation is well-known (Podkrajšek et al., 2004; Salasi et al., 2017). Salasi et al. (2017) evaluated the use of transition-metal ions such as Co(II), Fe(II), Mn(II), and Ni(II) in MEG solutions and suggested Mn(II) ions in the form of its chloride salt as an effective catalyst. Therefore, sodium bisulfite test solutions were prepared using manganese chloride. The composition of the nonsulfite-based oxygen scavenger was based on the publication of Kundu and Seiersten (2017). The composition of the nonsulfite oxygen scavenger, and the dosages used in the test solutions are reported in Table 8.2 and Table 8.3.

Table 8.1: Materials utilized in this study.

Material	Formula	Purity (mol%)	Supplier
Monoethylene glycol	$\text{C}_2\text{H}_6\text{O}_2$	99.477	Chem-Supply
Methane	CH_4	99.995	BOC
Nitrogen	N_2	99.9959	NGP10+
Sodium bisulfite	NaHSO_3	>99.5	Sigma-Aldrich

Table 8.2: Composition of the oxygen scavenger developed by Kundu and Seiersten (2017).

Material	Formula	Concentration (wt%)	Purity (mol%)	Supplier
Erythorbic Acid	$\text{C}_6\text{H}_8\text{O}_6$	17	≥ 99.0	Sigma-Aldrich
Diethylaminoethanol (DEAE)	$\text{C}_6\text{H}_{15}\text{NO}$	25	≥ 99.5	Sigma-Aldrich
Manganese chloride	$\text{MnCl}_2 \cdot 4\text{H}_2\text{O}$	0.5	>98.0	Chem-Supply
Deionized water	H_2O	57.5	- ^a	Produced in lab

^a Produced in the laboratory and sparged with nitrogen.

8.2.2 Test Apparatus and Experimental Procedure

The MEG solutions were carefully prepared with oxygen scavengers as shown in Figure 8.1. The composition and oxygen scavenger dosage for each test solution are reported in Table 8.3. An airtight glass vessel of 1 L volume upon a magnetic stirrer was used for mixing the solution. A ThermoScientific Orion 5-Star pH probe (accuracy of ± 0.002) was used for measuring the pH within the cell, and for dissolved oxygen measurements, the In-Pro 6850i ($\pm 1\% + 6$ ppb) was utilized. Both probes were connected to Mettler Toledo M800 devices for continuous monitoring. The cell was connected to a nitrogen/air retractable inlet which was controlled via a two-way valve. This allowed for purging the mixture within the cell and to provide a nitrogen blanket throughout the experiment to minimize oxygen intrusion. Gas flow meters were used to control the flow of inlet gas, and an outlet connected to a gas wash bottle was installed to prevent over pressurization in the glass vessel.

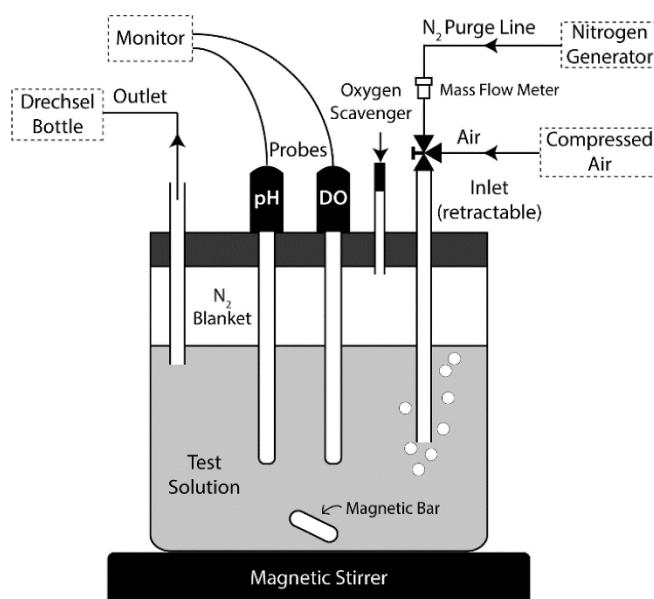


Figure 8.1: Schematic of the test apparatus used for the preparation of MEG/oxygen scavenger solutions.

Table 8.3: Oxygen scavenger dosage in each test solution.

Test Solution	MEG (wt%)	Oxygen Scavenger	Catalyst (ppm)	Dissolved Oxygen (ppb)
---------------	-----------	------------------	----------------	------------------------

(wt%)				
Blank	20	-	-	<20
Blank	20	-	-	>7500
Sodium Bisulfite (NaHSO ₃)	0	0.01 (100 ppm)	1	<20
		0.1		
		1		
		10		
	20	0.01 (100 ppm)		
		0.1		
		1		
		10		
OS-P	20	0.025 (250 ppm)	-	<20
IFEox2	20	0.01 (100 ppm)	-	<20

The gas hydrate inhibition testing was conducted using a high-pressure PVT cell. The isochoric method was adopted for determining the hydrate phase equilibria applying a 1 °C/hour step-heating and step-cooling rate (Sloan Jr and Koh, 2007). At each step of the procedure, the system was allowed to reach equilibrium before resuming the process. The preliminary experiments were conducted three times to test repeatability. Details of the procedure and test apparatus for hydrate testing were explained in our previous research studies (Alef et al., 2018c; Smith et al., 2016, 2015).

8.3 Results

Preliminary experiments to establish data accuracy were conducted for the methane hydrate phase boundary for 20 wt% MEG solution with the balance being deionized water. Data from literature and predictions from HYSYS using the Peng–Robinson equation of state were compared to the measured hydrate phase boundary (Figure 8.2). The measured data revealed an absolute average relative error (AARE) of 2.6% from literature and 2.2% from software calculations. Taking into consideration experimental error margins from previous publications, the statistical analysis indicates that the measured data in this study are accurate and show a good agreement with the reference data (*Aspen HYSYS*, 2007; Eichholz et al., 2004; Haghighi et al., 2009b; Rock, 2002). AARE was calculated using Eqn. (8.1).

$$\text{AARE (T)} = \frac{100}{n} \sum_{i=1}^n \left| \frac{T_{\text{calculated}} - T_{\text{measured}}}{T_{\text{measured}}} \right| \quad (8.1)$$

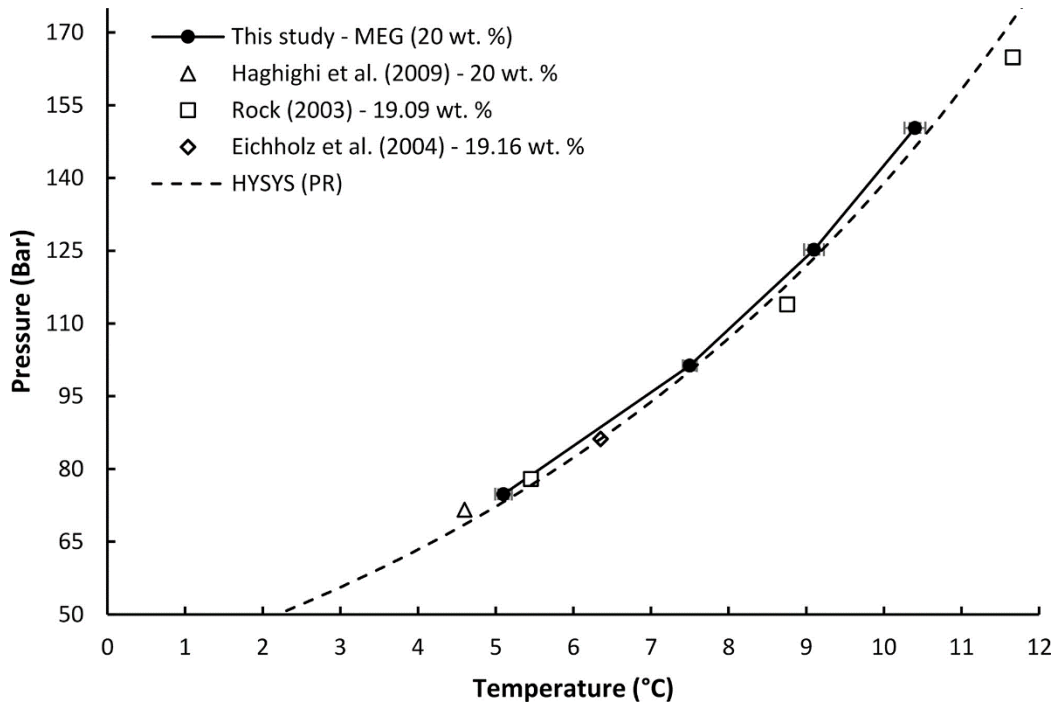


Figure 8.2: Methane hydrate phase boundary for 20 wt% MEG + 80 wt% water solution.

8.3.1 Effect of Dissolved Oxygen

MEG solutions containing high and low dissolved oxygen concentrations were tested to determine their influence on hydrate inhibitory performance. The measured phase boundaries are plotted in Figure 8.3. It was found that with increased exposure to oxygen (i.e., at dissolved oxygen levels of >7500 ppb), the hydrate phase boundary shifted to the right by an average of 0.4 °C. This suggests that dissolved oxygen increases the thermodynamic equilibrium temperature for MEG solutions and thus promotes hydrate formation. The increase in hydrate formation temperature may be caused due to the reaction of oxygen with minute particles of iron carbonate which could be present in manufactured MEG solutions. The product of this reaction is iron oxide, which leads to a reduction in MEG quality (Brustad et al., 2005; Lehmann et al., 2014). Furthermore, oxygen contributes to degradation of MEG through oxidation which ultimately decreases MEG quality. Degradation of MEG and the effect it has on

hydrate inhibition is an area that has not been well researched to date. Rossiter et al. committed to MEG degradation research and showed that the products of MEG degradation consisted of oxalic, formic, and glycolic acids (Rossiter et al., 1985). The mechanism by which thermal oxidation of MEG occurs involves complex free radicals (Bamford et al., 1980). Other researchers also found similar products of MEG degradation through the use of high-performance liquid chromatography (HPLC) and ion chromatography (IC) (AlHarooni et al., 2015; Madera et al., 2003). AlHarooni et al. (2015) found that the hydrate inhibitory performance of MEG decreased due to thermal oxidation while also showing that fresh samples of MEG exposed to oxygen showed similar degradation products when analysed using HPLC and IC analysis techniques. The degradation of MEG or glycols in general occur through a thermal oxidative reaction, and hence, the removal of oxygen could prevent unnecessary degradation of MEG, which will in turn prevent the drop in hydrate inhibition performance (Rossiter et al., 1985).

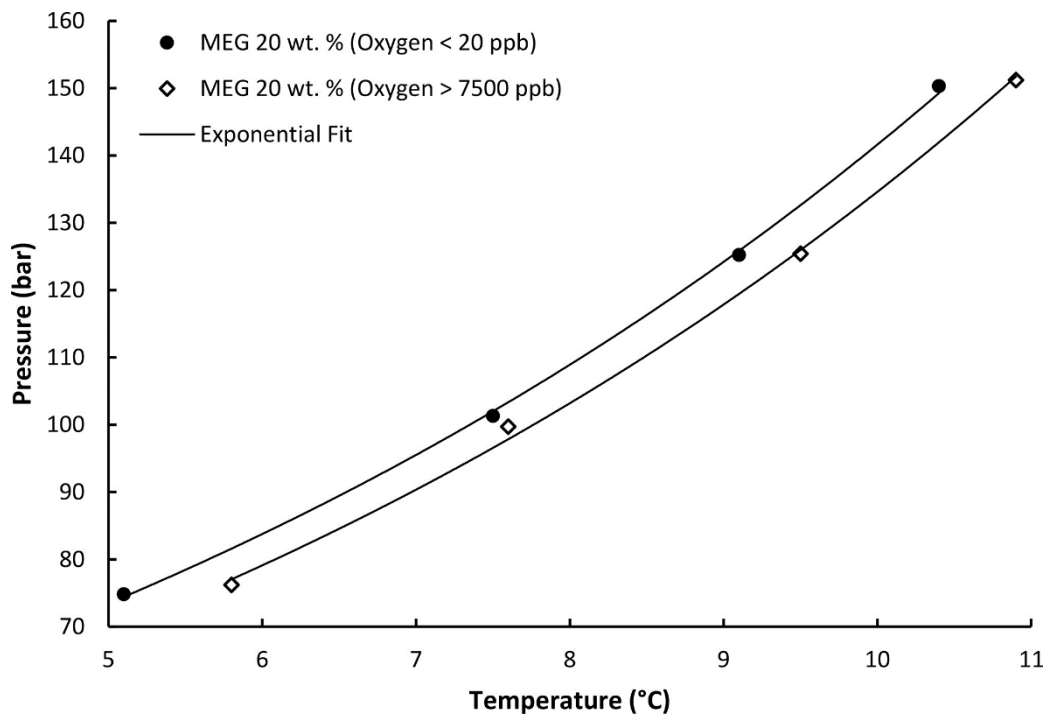


Figure 8.3: Hydrate phase boundaries of 20 wt% MEG solution with low (<20 ppb) and high (>7500 ppb) oxygen content.

8.3.2 Effect of Sodium Bisulfite

Oxygen scavengers are utilized in low concentrations in industrial applications,

usually in concentrations of 200 to 500 ppm within lean-MEG (80 wt%). In this work, a range of concentrations was applied to investigate the shift in hydrate phase boundary due to oxygen scavenger concentration. Varying concentrations of aqueous sodium bisulfite (0.01, 0.1, 1, and 10 wt%) solutions were tested for methane hydrate inhibition. Hydrate phase boundaries were obtained with and without hydrate inhibitor (MEG 20 wt%). The results are shown in Table 8.4 and are illustrated in Figure 8.4 and Figure 8.5.

Table 8.4: Methane hydrate equilibria data for sodium bisulfite solutions.^a

NaHSO₃ (0.01 wt%)		NaHSO₃ (0.1 wt%)		NaHSO₃ (1 wt%)	
P/bar	T/°C	P/bar	T/°C	P/bar	T/°C
75.8	10.4	75.3	10.2	73.6	9.6
99.5	12.8	100.7	12.9	101.1	12.5
125.9	14.9	124.4	14.7	123.3	14.3
151.1	16.6	150.9	16.5	151.2	16.2
NaHSO₃ (10 wt%)		MEG (20 wt%) + DI Water		MEG + NaHSO₃ (0.01 wt%)	
P/bar	T/°C	P/bar	T/°C	P/bar	T/°C
77.6	7.2	74.8	5.1	73.8	4.9
96.5	9.3	101.3	7.5	98.8	7.2
126.3	11.5	125.2	9.1	125.4	9.1
145.5	12.7	150.3	10.4	149.1	10.3
MEG + NaHSO₃ (0.1 wt%)		MEG + NaHSO₃ (1 wt%)		MEG + NaHSO₃ (10 wt%)	
P/bar	T/°C	P/bar	T/°C	P/bar	T/°C
75.5	4.9	73.9	3.8	91.2	0.4
99.7	7.1	98.2	6.2	103.1	1.12
126.2	9	123	8.2	121.4	2.38
149.6	10.3	151.5	9.9	144	3.67

^a All uncertainties are expanded uncertainties (U) at 95% level of confidence: $U(P) = \pm 0.5$ bar; $U(T) = \pm 0.03$ °C.

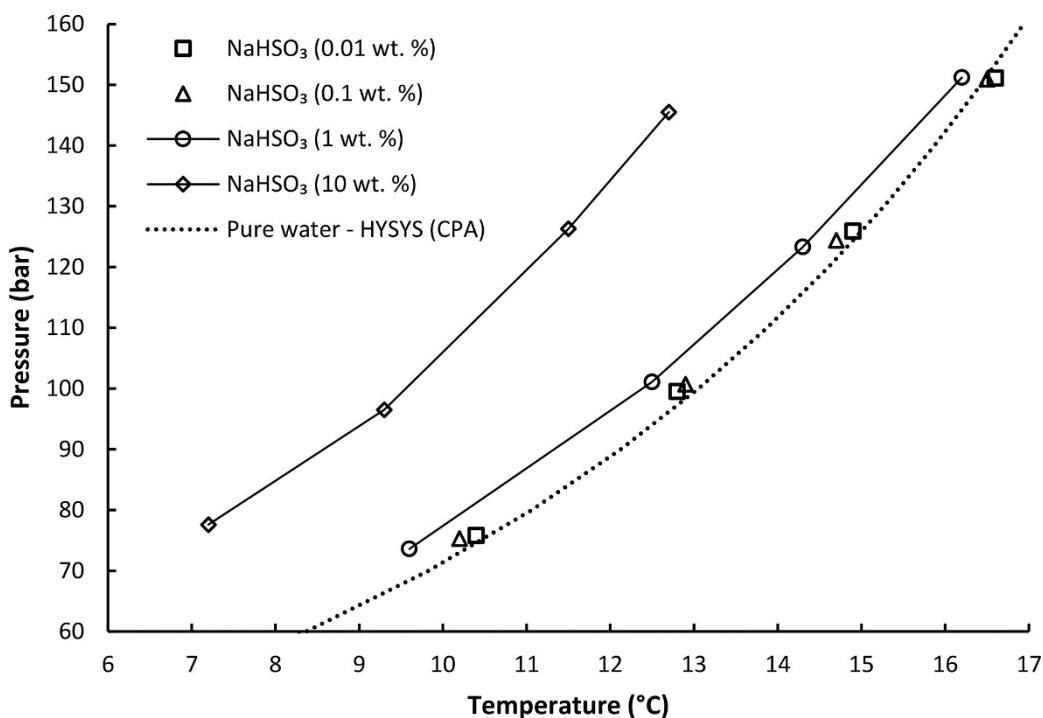


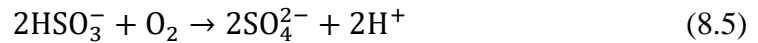
Figure 8.4: Hydrate phase boundaries for aqueous NaHSO₃ solutions.

The hydrate phase boundaries of aqueous NaHSO₃ solutions show no inhibitory effect for a concentration of 0.01 wt% and produced a small depression of ~0.1 °C at 0.1 wt% when compared to the phase boundary of pure water. However, the hydrate phase boundary was shifted to lower temperatures by ~0.4 °C on average at a concentration of 1 wt%. While at 10 wt% of NaHSO₃ in pure water, the hydrate phase boundary was shifted by ~3.4 °C, showing the greatest inhibition effect.

The hydrate phase boundary for MEG/NaHSO₃ mixtures at NaHSO₃ concentrations of 0.01, 0.1, 1, and 10 wt% in 20 wt% MEG showed a temperature depression of 0.1, 0.2, 0.9, and 6.4 °C, respectively. At higher NaHSO₃ concentrations of 1 and 10 wt%, an increased hydrate inhibitory performance was observed, suggesting it performs as a thermodynamic hydrate inhibitor to a greater extent than when NaHSO₃ is present in smaller concentrations. In the presence of MEG, NaHSO₃ has a greater temperature depression (88% increase), which may be due to the synergistic effect caused by combining MEG with NaHSO₃ and the decrease in the number of water molecules available for hydrate cage formation.

A water molecule consists of hydrogen atoms which have a positive dipole charge, whereas the oxygen atom has a negative charge, and these oppositely charged dipoles

allow water molecules to easily cage together around a host molecule by forming hydrogen bonds (Tohidi et al., 2000). Sodium bisulfite dissociates in water into Na^+ and HSO_3^- ions as per Eqns. (8.2) to (8.5). These dissolved ions as well as the catalyst manganese ions in the aqueous salt solution interact with the negatively and positively charged dipoles of available water molecules. This strong electrostatic attraction between a salt ion and water molecule is stronger than the hydrogen bonding that occurs between water molecules. This weakens the hydrogen bonding between water molecules and shifts the thermodynamic equilibrium to lower temperatures, which ultimately inhibits hydrate formation by preventing the gaseous molecule to be encaged by water molecules (Nguyen and Nguyen, 2015; Sun et al., 2017). The strength of electrostatic attraction is characterized by the charge and atomic radius of the ion. In the case of a cation, the strength is directly proportional to charge and inversely proportional to the radius (Cha et al., 2016; Lv et al., 2018).



The results reveal that at NaHSO_3 concentrations of 0.01–0.1 wt% (equivalent to 100–1000 ppm) show no change in the hydrate phase boundary and thus have no impact on the inhibitory performance of MEG. This concentration range is inclusive of the typical concentrations of oxygen scavengers that are required to remove oxygen. Therefore, no additional hydrate inhibitory performance, but also no hydrate promotion, are expected at the stated NaHSO_3 concentrations.

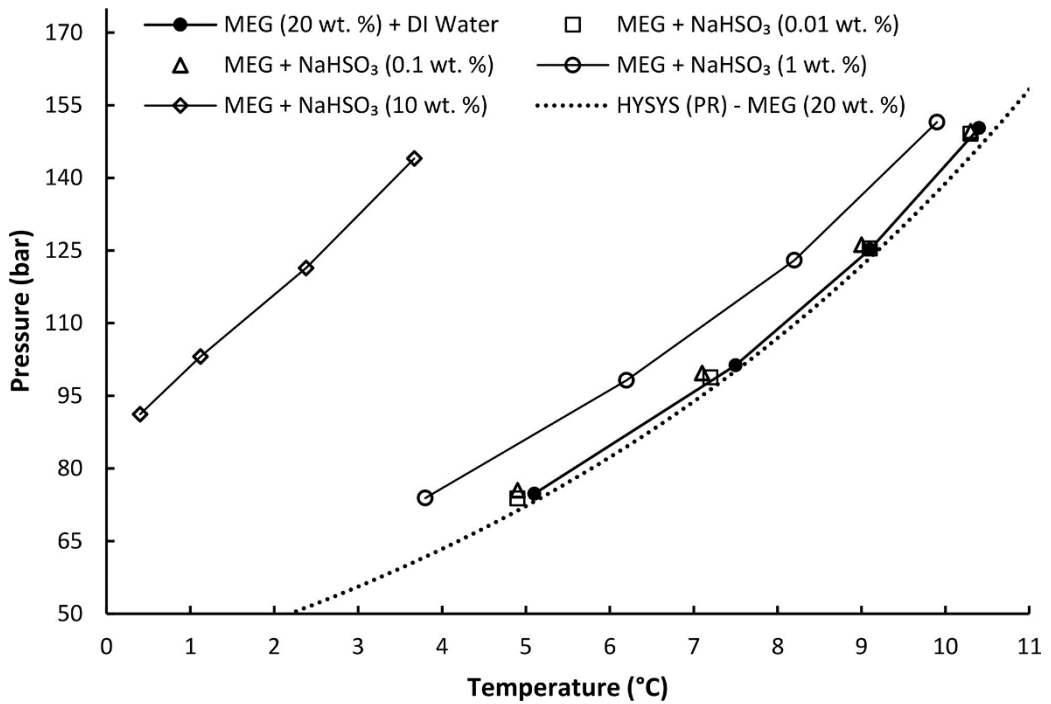


Figure 8.5: Hydrate phase boundaries for aqueous NaHSO₃ + MEG solutions.

8.3.3 Effect of Proprietary Oxygen Scavenger (OS-P)

A proprietary oxygen scavenger (OS-P) used in the oil and gas industry was combined with 20 wt% MEG solution in the recommended concentration range by the manufacturer. The hydrate phase boundary was measured and is plotted in Figure 8.6. The hydrate phase boundary as compared to a 20 wt% pure MEG solution has been shifted to higher temperature by ~ 0.3 °C, which signifies hydrate promotion. Although hydrate promotion was identified, only a very small concentration of OS-P (up to 0.05 wt%) is usually utilized within lean-MEG (typically >80 wt%). This hydrate promotion may be overlooked, but due to the small dosage of the chemical as well as the various other proprietary chemical additives used in the industry may result in detrimental effects. We conclude that proprietary chemical additives designed and created for specific purposes may have negative consequences on other flow assurance issues.

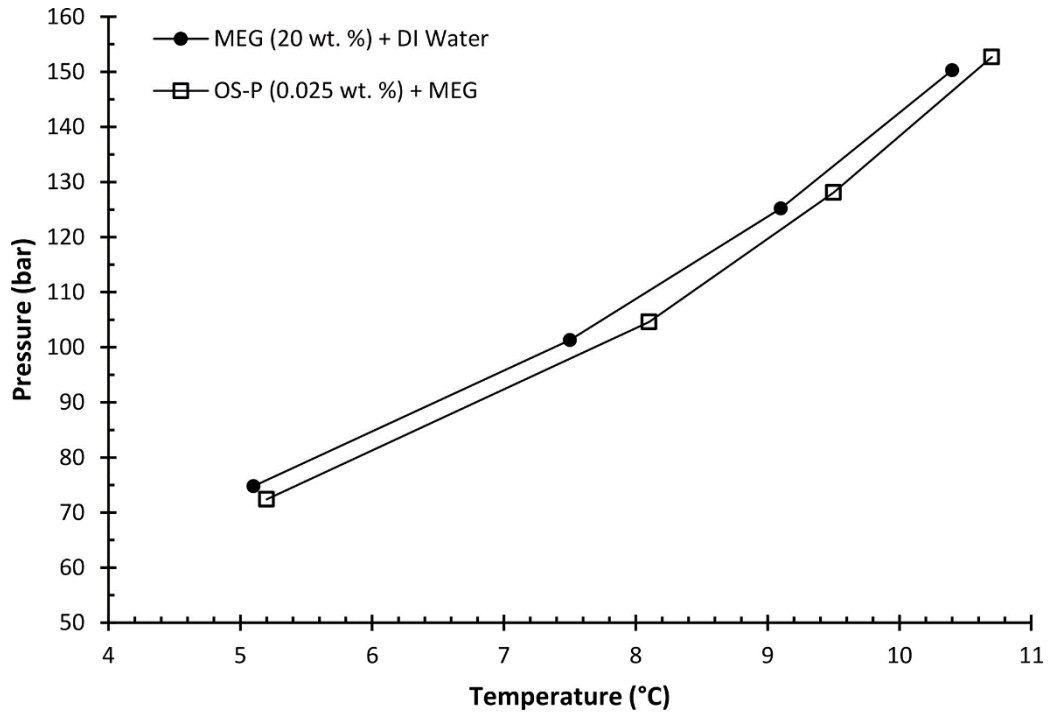


Figure 8.6: Hydrate phase boundary of proprietary oxygen scavenger, OS-P (0.025 wt%) in 20 wt% MEG solution.

8.3.4 Effect of Nonsulfite-Based Oxygen Scavenger (IFEox2)

The nonsulfite oxygen scavenger (IFEox2) developed by Kundu and Seiersten was investigated in this study which comprises erythorbic acid, diethylaminoethanol (DEAE), and a manganese catalyst. It was tested to realize its influence on gas hydrate formation in the presence of 20 wt% MEG solution. The measured hydrate phase boundary is plotted in Figure 8.7. The results show that the phase boundary has shifted to the left by ~ 0.1 °C, suggesting this oxygen scavenger acted as a hydrate inhibitor. This slight inhibition performance could be related to hydrogen bonding of some water molecules with the remaining hydroxyl groups of erythorbic acid, DEAE, and erythorbate salt. Erythorbate salt is a result of the postneutralization reaction by DEAE with erythorbic acid (Figure 8.8).

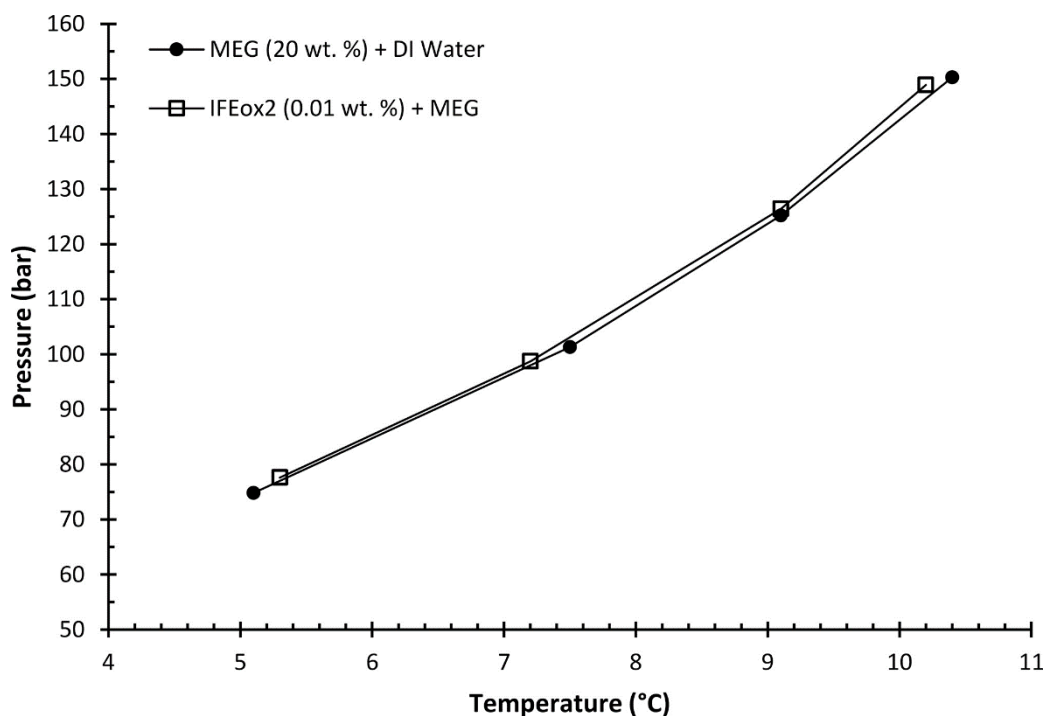


Figure 8.7: Hydrate phase boundary of IFEox2 (0.01 wt%) in 20 wt% MEG solution.

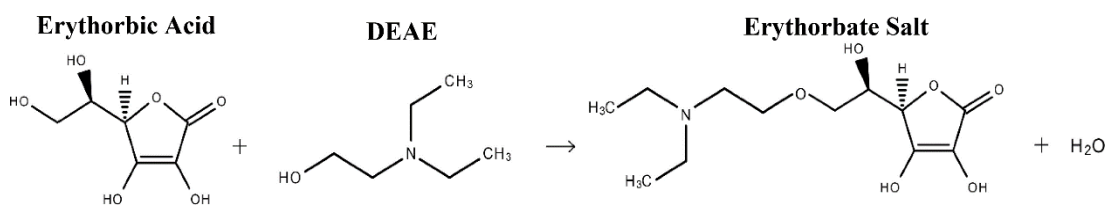


Figure 8.8: Conversion of erythorbic acid to erythorbate salt by neutralization reaction by DEAE.

8.4 Conclusions

The influence of dissolved oxygen and various oxygen scavengers on gas hydrate formation was studied. Gas hydrates can cause dangerous consequences, and thus, it is important to understand how the various chemical additives that are injected alongside MEG behave and distort the hydrate inhibition performance. The study produced new hydrate equilibria data for sodium bisulfite solutions (0.01–10 wt%) with and without the presence of MEG. Results show greater inhibition at higher concentrations as opposed to commonly used dosages for oxygen scavenging applications. However, a proprietary oxygen scavenger promoted hydrate formation, which suggests that chemical additives should be thoroughly assessed for compatibility with other chemicals as well as tested to determine any potential negative

consequences. A nonsulfite oxygen scavenger showed inhibition performance but may not surmount to any benefit due to the small dosages required. Furthermore, the study has revealed that dissolved oxygen, while it already negatively affects corrosion risk, may have a hydrate promotion effect as well, which increases the risk of gas hydrate formation. Clearly, dissolved oxygen levels should be kept to a minimum.

Chapter 9 Hydrate Phase Equilibria of Phosphonate Scale Inhibitors, Amines, and Ethylene Glycol

This chapter is comprised of the following publication:

- **Alef, K.**, Barifcani, A., 2019. Hydrate Phase Equilibria of Phosphonate Scale Inhibitors, Amines, and Ethylene Glycol. *J. Chem. Eng. Data* 64, 3205–3210. doi: 10.1021/acs.jced.9b00366

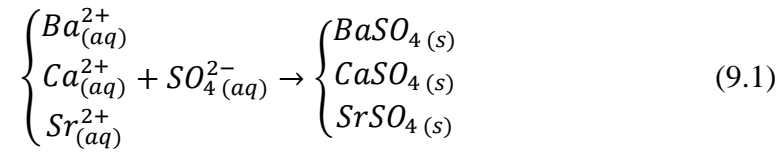
This chapter contributes new hydrate phase equilibria data for various scale inhibitors and amines. Scale formation risks arise due to formation water production posing serious concerns in valves, pumps, and production equipment. Scale inhibitors are injected to prevent scale formation. These chemicals have not been modelled in hydrate simulators nor have their impact upon gas hydrate been studied experimentally. Thus, in this study, various phosphonate scale inhibitors such as iminodi (methylene) phosphonate, nitrilotris (methylene) phosphonate, and diethylenetriaminepenta (methylene) phosphonate, and two amines, monoethanolamine (MEA) and diethanolamine (DEA) were tested using the isochoric hydrate testing method for their hydrate inhibition performance. The average temperature depression for each chemical as mentioned in the aforementioned order was found to be 0.06, 0.15, and 0.2 K for the scale inhibitors at a concentration of 350 ppm. This suggests that scale inhibitors may also inhibit hydrate formation, albeit at limited extent, but more importantly, they do not serve to promote hydrate formation; thus, they are not disturbing the hydrate control program. While for the amines, an average temperature depression of 0.2 and 0.47 K was found for MEA and DEA at a concentration of 5 wt% respectively. Suggesting that such amines when used alongside MEG may bring about an additional hydrate inhibitory performance. This contribution satisfies the thesis objective (k) while fulfilling the research gaps outlined in Section 1.3.

9.1 Introduction

Gas hydrates are ice-like structures that form above the ice formation temperature. It is a phenomenon whereby water through hydrogen bonding encapsulates gaseous molecules forming a caged structure (Sloan Jr and Koh, 2007). Typical low temperature subsea conditions of high pressure serve the right conditions for increased hydrate formation in the presence of natural gas in pipelines (Koh et al., 2002). The formation of gas hydrates in gas pipelines can, for the least, stop valuable gas production due to blockage leading to loss in production time and increased costs due to immediate hydrate removal works. Conventionally, the industry injects chemical additives known as gas hydrate inhibitors to lower the thermodynamic hydrate equilibrium (i.e., MEG—monoethylene glycol), to prevent agglomeration of hydrate solids, or to prolong the hydrate induction and nucleation period (Kelland, 2006; Li et al., 2006).

Alongside the gas hydrate challenge in pipelines, there is the tendency for scale deposition to occur in the presence of formation water, seawater, or injected water (Crowe et al., 1994). Scaling can cause serious complications in pumps, valves, and other production equipment while increasing inner surface roughness, decreasing the pipeline diameter thus causing a pressure drop or complete flow blockage leading to loss in production time (Bratland, 2010; Olajire, 2015). Typical scales that occur in oilfield production are calcium sulfate (CaSO_4), barium sulfate (BaSO_4), strontium sulfate (SrSO_4), and calcium carbonate (CaCO_3). (8,9) Scales of the sulfate type occur due to the mingling of different waters that are chemically incompatible such as formation water, seawater, or injection water as given in Eqn. (9.1), while carbonate scales have a tendency to form due to pressure reduction or an increase in pH caused by escaping CO_2 (Bratland, 2010; Liu et al., 2009). In some fields, formation of water production occurs later in the life of the field, thus increasing the risk of scale formation. At this time, the use of amines such as methyldiethanolamine (MDEA) for corrosion control via the pH stabilization method can no longer be employed because of the high risk of scale formation (Alef et al., 2018b; Olsen and Halvorsen, 2015). Thus, there is a change in the corrosion control method, whereby a film-forming corrosion inhibitor is utilized, while the use of a scale inhibitor (typically phosphonates) becomes incumbent to protect the system and to prevent/reduce scale

formation in pipelines (Halvorsen et al., 2009, 2006).



Amines are commonly used in the natural gas processing industry as well as used for corrosion control through the pH stabilization method. Amines in the form of monoethanolamine (MEA) and diethanolamine (DEA) are utilized in amine gas treating, while MDEA serves as an excellent chemical absorbent to favourably remove H₂S and CO₂ from sour gas streams during natural gas processing (Closmann et al., 2009; Idem et al., 2006; Lawson and Garst, 1976; Weiland et al., 1997).

The aforementioned chemicals are amongst numerous other chemical additives that are usually injected alongside MEG or that are found in the gas production system or processing facilities for which their impact on gas hydrate formation, whether positive or negative, is unknown. The hydrate phase equilibria for these chemicals have never been determined. In this study, a selection of these chemicals have been thoroughly tested at relevant dosage amounts to characterize their impact on methane gas hydrate formation, thus contributing valuable hydrate phase equilibria data.

9.2 Methodology

9.2.1 Materials

The chemicals and materials utilized in this study were sourced from high-grade vendors and are listed in Table 9.1. The commonly applied hydrate inhibitor, MEG, was sourced from Chem-Supply at a purity of 99.477 mol %. Deionized water was abundantly produced within the research laboratory with an electrical resistivity of 16 MΩ·cm at room temperature. The hydrate-forming gas that was used for hydrate testing was selected as ultrahigh purity methane supplied by BOC at a purity of 99.995 mol %. Ultrahigh purity nitrogen (99.9959 mol %) for purging the test apparatus and maintaining a nitrogen blanket in all sample preparation procedures was abundantly produced using a nitrogen generator (AtlasCopco, NGP10+) within the research laboratory. Three phosphonates were selected as the scale inhibitors that were utilized in this study consisting of iminodi(methylene) phosphonate (IDMP), nitrilotris(methylene) phosphonate (NTMP), and diethylenetriaminepenta(methylene)

phosphonate (DTPMP), all sourced from Sigma-Aldrich. As for the amines, MEA and DEA were used in this study and were sourced from Sigma-Aldrich.

Table 9.1: List of chemicals utilized in this study.

Chemical	Formula	CAS Reg. No.	Concentration	Source
MEG	C ₂ H ₆ O ₂	107-21-1	99.477%	Chem-Supply
Methane	CH ₄	74-82-8	99.995%	BOC
IDMP	C ₂ H ₉ NO ₆ P ₂	17261-34-6	97%	Sigma-Aldrich
NTMP	C ₃ H ₁₂ NO ₉ P ₃	6419-19-8	97%	Sigma-Aldrich
DTPMP	C ₉ H ₂₈ N ₃ O ₁₅ P ₅	15827-60-8	50% + 15% HCl + 35% H ₂ O	Sigma-Aldrich
MEA	C ₂ H ₇ NO	141-43-5	≥99%	Sigma-Aldrich
DEA	C ₄ H ₁₁ NO ₂	111-42-2	≥99%	Sigma-Aldrich

9.2.2 Experimental Method

The isochoric hydrate testing method was employed across all tests with a step-heating and cooling rate of 1 K/h to determine the hydrate phase equilibria data. All test solutions were carefully prepared in a sealed glass vessel purged with nitrogen to prevent oxygen ingress and stirred using a magnetic stirrer for complete synthesis as shown in Figure 9.1 (Alef et al., 2019c). An initial test was conducted on a pure MEG solution of 5 wt% for comparison to simulation results from Multiflash and PVTsim software. Then, test solutions comprising chemicals as per the experimental test matrix (Table 9.2) with the balance being deionized water were carefully prepared taking into account the varying initial concentrations. Samples of the test solutions (7 mL) were precisely injected into a clean high-pressure PVT cell as depicted in Figure 9.1. Chemical dosage amounts that are relevant to the industry were adopted in this study. Typically, scale inhibitors are injected at very low dosages (i.e., 5–300 ppm), while amines such as MDEA are typically injected at 3–7 wt% (Alef et al., 2018b; Dugstad and Seiersten, 2004; Jordan et al., 2019; Lehmann et al., 2014; Shaw et al., 2012; Shaw and Sorbie, 2015; Vetter, 1972). The procedure for the sample preparation and hydrate testing has been given in more detail in previous studies (Alef et al., 2018b, 2018a).

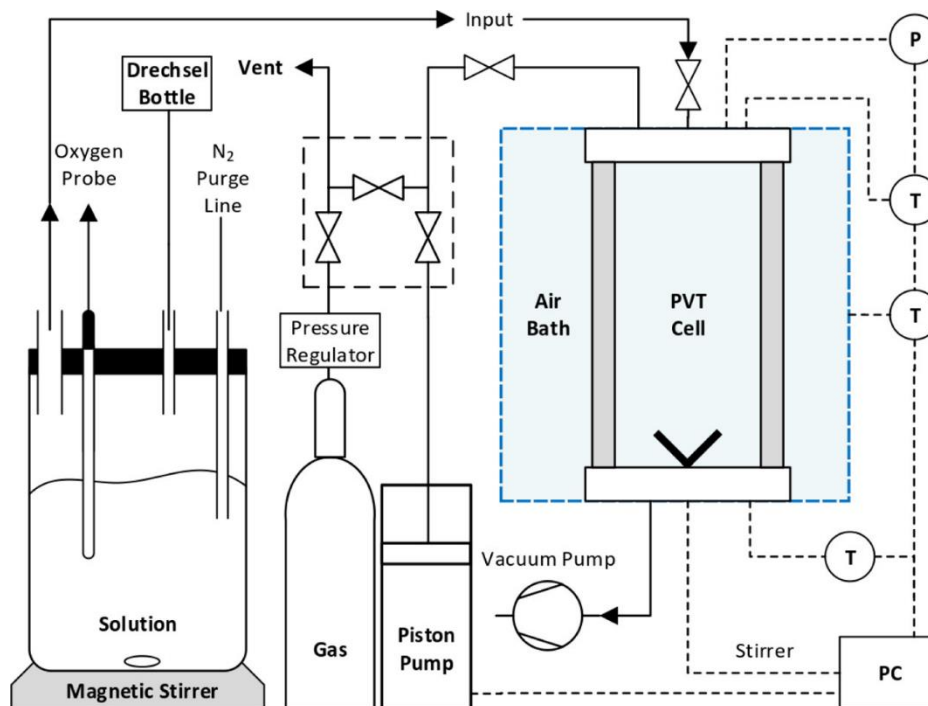
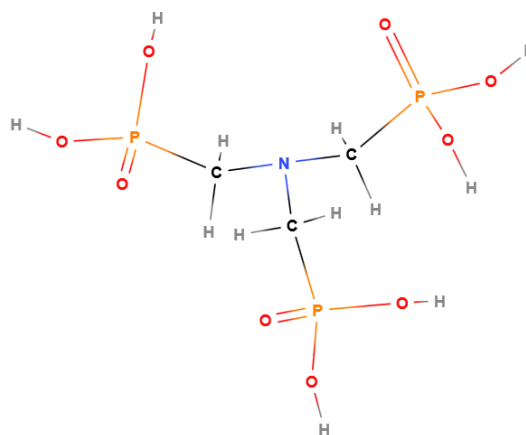


Figure 9.1: High-pressure PVT cell used in this study for performing hydrate inhibition testing.

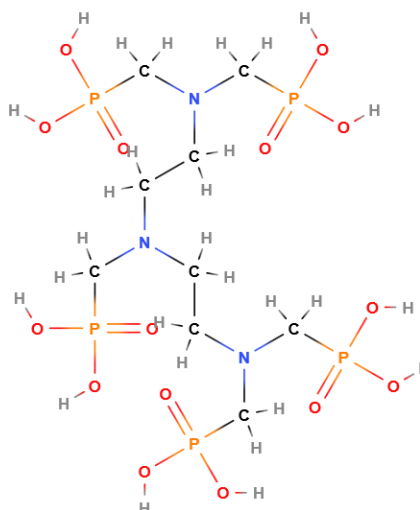
Table 9.2: Experimental test matrix and chemical structures.

Test	Dosage	Chemical Structure
MEG	5 wt%	<chem>CCOCC</chem>
IDMP	35 ppm 350 ppm	<chem>CC(C)OP(=O)(C)OP(=O)(C)C</chem>
NTMP	35 ppm	

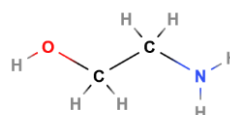
350 ppm



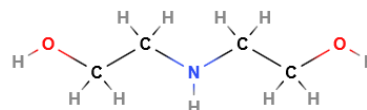
DTPMP 35 ppm
350 ppm



MEA 5 wt%



DEA 5 wt%



9.3 Results

The hydrate phase equilibria boundary of pure MEG (5 wt%) is given in Figure 9.2 and Table 9.2. As expected, the thermodynamic hydrate inhibitor (MEG) shifted the hydrate phase boundary to the left by 1.07 K in reference to the simulated hydrate phase boundary of pure water. The absolute average relative error as per Eqn. (9.2) between the experimentally measured equilibrium temperature (T_{meas}) and the

equilibrium temperature predicted using software (T_{pred}) was found to be 1.7% for Cubic Plus Association equation of state in Multiflash and 1.4% for Soave–Redlich–Kwong Peneloux equation of state in PVTsim, indicating that the error is small and that the results are accurate in terms of hydrate testing.

$$AARE (T) = \frac{100}{n} \sum_{i=1}^n \left| \frac{T_{pred} - T_{meas}}{T_{meas}} \right| \quad (9.2)$$

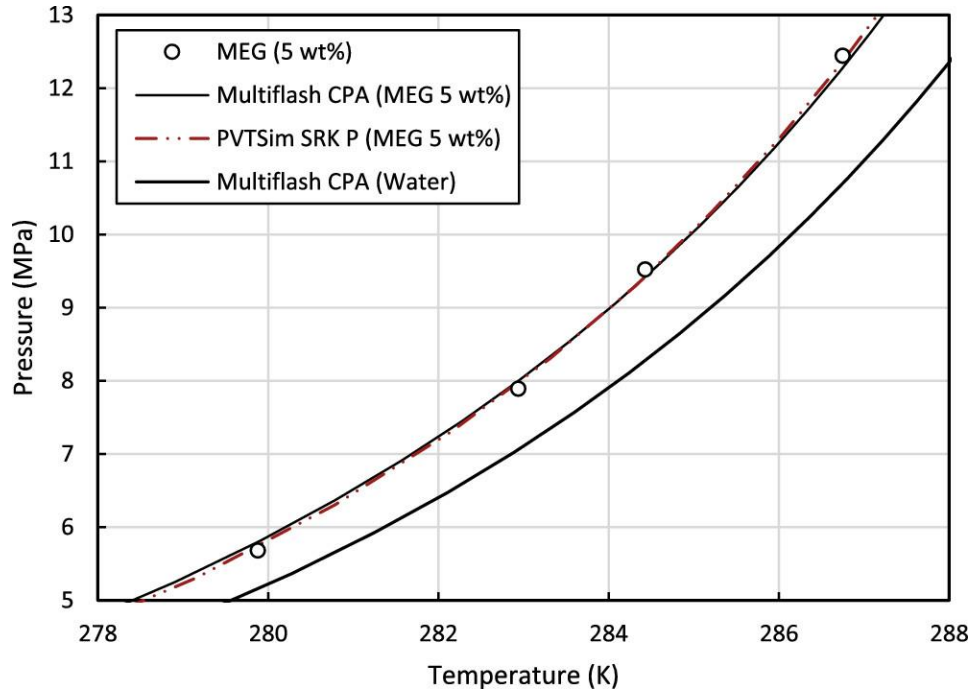


Figure 9.2: Hydrate phase boundary for pure MEG (5 wt%) compared to software predictions.

9.3.1 Scale Inhibitors

The hydrate phase boundaries of the scale inhibitors (IDMP, NTMP, and DTPMP) at a concentration of 35 ppm were determined as plotted in Figure 9.3 and given in Table 9.3. The hydrate inhibitory performance of all three as compared to pure water is almost negligible, albeit acting as hydrate inhibitors. The average temperature depression caused by each was 0.03, 0.05, and 0.05 K, respectively, whereby the temperature depression caused by IDMP was almost negligible taking into consideration the uncertainty of measurement. However, the same scale inhibitors at a concentration of 350 ppm have shown varying and slightly more pronounced hydrate inhibitory performances (Figure 9.4). At higher concentrations, the average

temperature depression caused by each was 0.06, 0.15, and 0.20 K, respectively.

The best performer in terms of hydrate inhibition is DTPMP followed by NTMP, which may be related to the size of the chemical structure (DTPMP > NTMP > IDMP) and the number of hydroxyl groups, whereby there exists 10 [OH⁻] groups for DTPMP >6 [OH⁻] for NTMP >2 [OH⁻] for IDMP (Table 9.2). The hydroxyl groups form hydrogen bonds with water molecules, thus reducing the quantity of water molecules that are available to form a cage structure around gaseous molecules, thus reducing hydrate formation. Furthermore, DTPMP contains 15% HCl which dissociates in water into H⁺ and Cl⁻ ions. The ions will electrostatically attract to the oppositely charged dipoles of water molecules preventing them to form water cages around gaseous molecules (Nguyen and Nguyen, 2015; Sun et al., 2017; Tohidi et al., 2000). Thus, shifting the thermodynamic equilibrium point to a lower temperature leads to increased hydrate inhibition.

Moreover, the results suggest that at the typical scale inhibitor concentration range applied in the field will not bring about a significant shift in the hydrate phase boundary at the upper end of the concentration range, despite there being a negligible effect at the lower end of the concentration range. Thus, scale inhibitors unless utilized in much higher dosages do not raise concerns to the effectivity of the hydrate control program nor do they necessarily contribute an added safety margin nor serve to potentially reduce MEG injection.

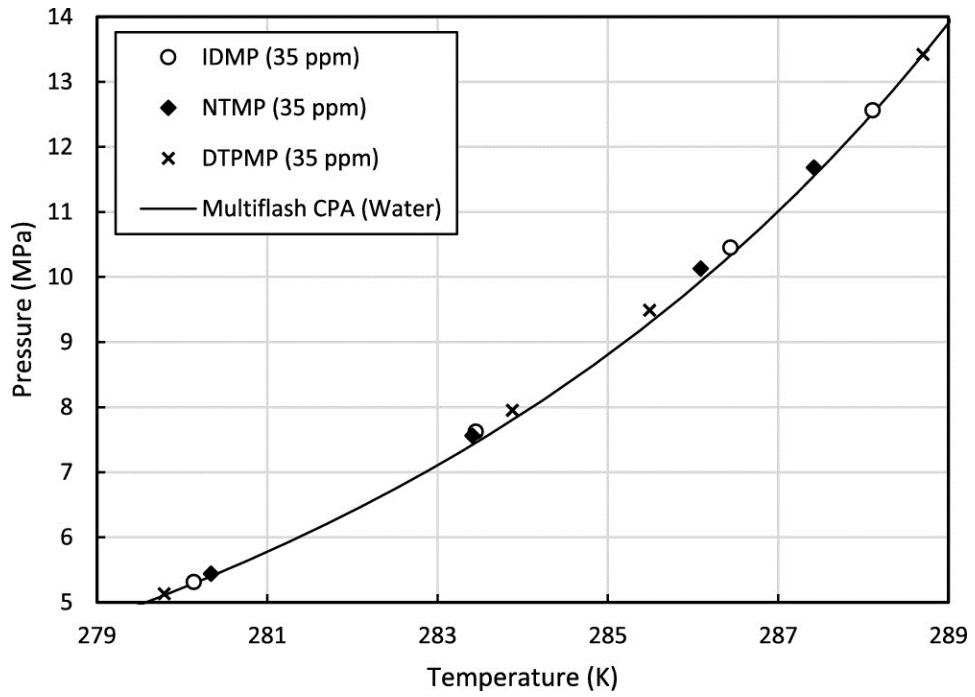


Figure 9.3: Hydrate phase boundaries for scale inhibitors (IDMP, NTMP, and DTPMP) at 35 ppm compared pure water.

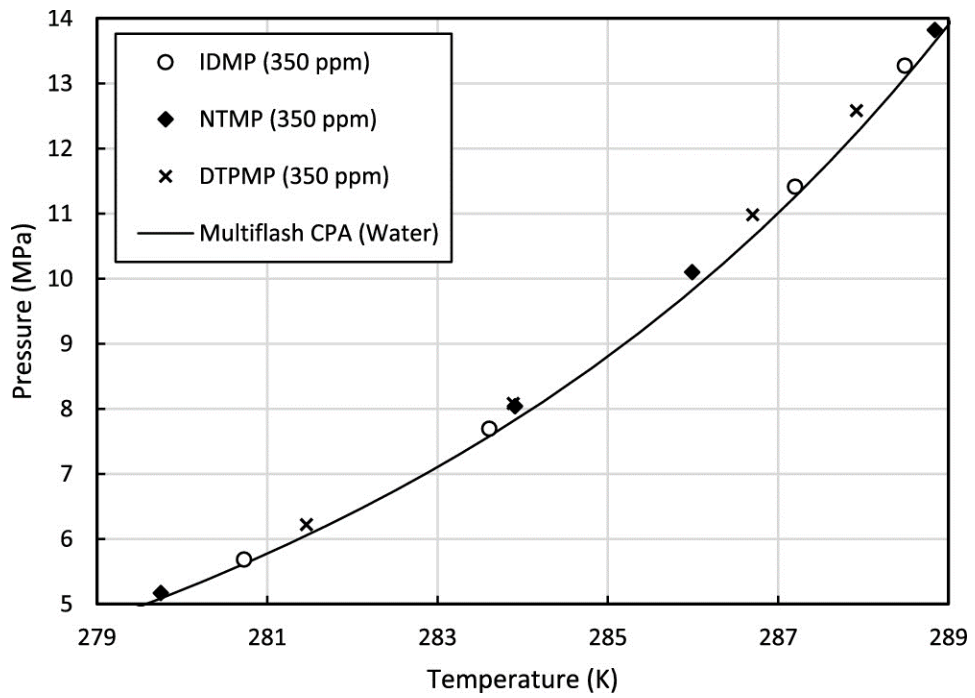


Figure 9.4: Hydrate phase boundaries for scale inhibitors (IDMP, NTMP, and DTPMP) at 350 ppm compared pure water.

9.3.2 Amines (MEA and DEA)

The hydrate phase boundaries for the amines (MEA and DEA) at a concentration of 5 wt% were determined as plotted in Figure 9.5 and given in Table 9.3. Both MEA and DEA exhibited hydrate inhibitor qualities by shifting the hydrate phase boundary to the left. Average temperature depressions of 0.2 and 0.47 K were found. MEA and DEA are completely miscible in water while having hydrophilic properties and hydroxyl groups which are able to establish hydrogen bonding with water molecules. Through this mechanism, both chemicals are able to decrease the amount of available water molecules that could potentially encage gaseous molecules (Davoudi et al., 2014; Hossainpour, 2013). Another factor that leads to the dissociation of the hydrate may be due to the heat released from the exothermal reaction in CO₂/H₂S systems containing an amine (Park et al., 2006; Xiang et al., 2014).

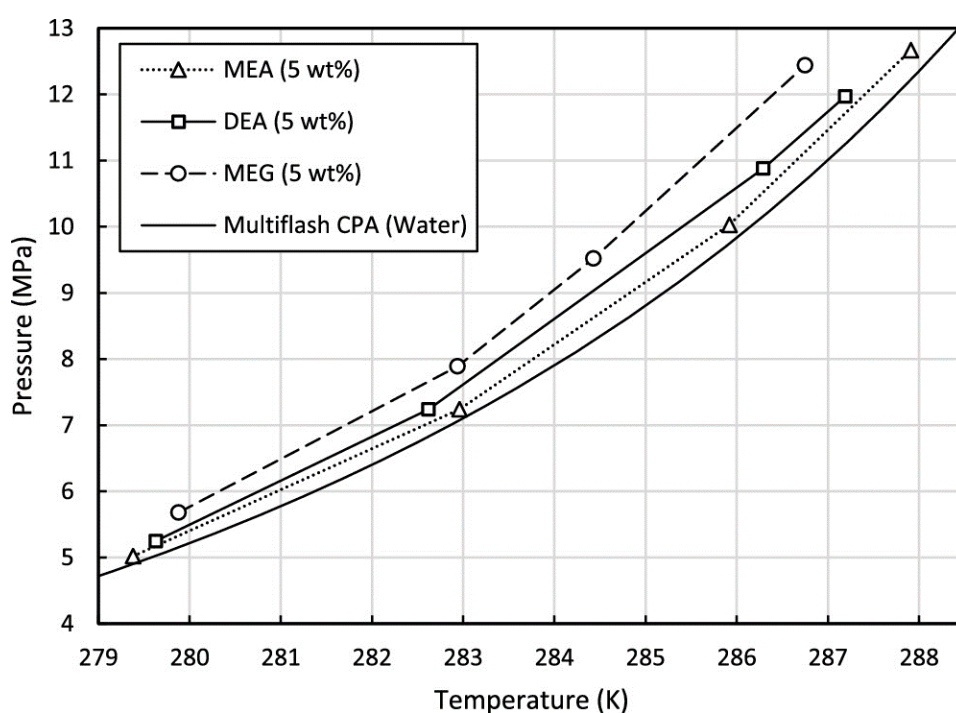


Figure 9.5: Hydrate phase boundaries of MEA, DEA, and MEG at 5 wt% as compared to pure water.

MEG was found to be 3.8 and 2.1 times more effective as compared to MEA and DEA of the same concentration with the reference being the hydrate phase boundary of pure water, respectively. The equivalent amount of MEG was determined as 1.3 wt% for 5 wt% MEA and 2.4 wt% for 5 wt% DEA via simulation using Multiflash as shown in (Figure 9.6).

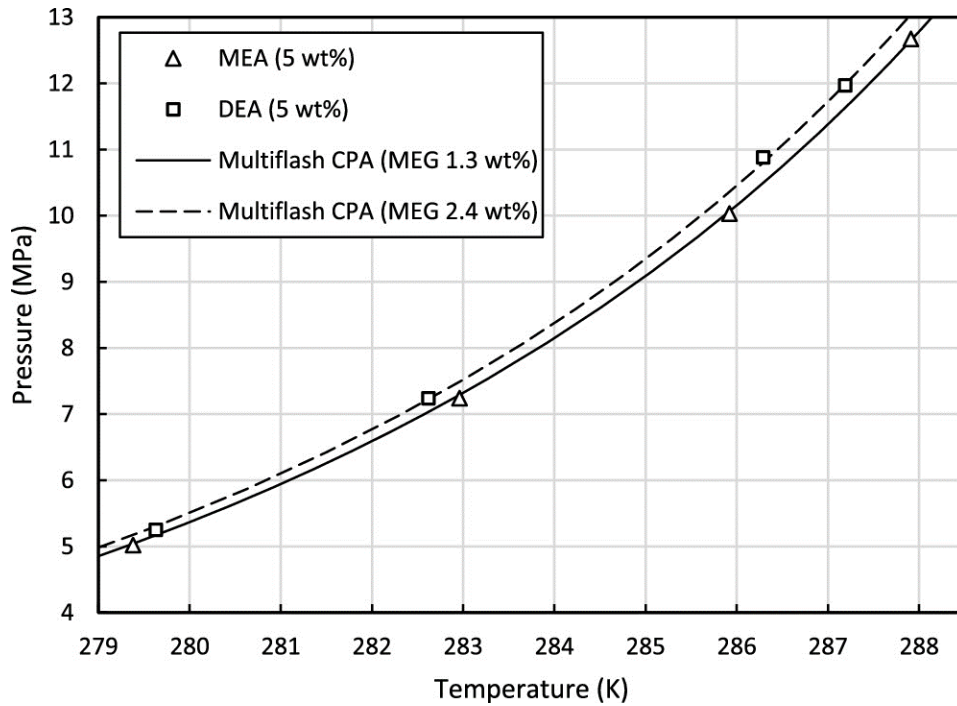


Figure 9.6: Hydrate phase boundaries for MEA and DEA at 5 wt% and their equivalent MEG concentrations using Multiflash.

Table 9.3: Equilibria data produced in this study for meg, scale inhibitors (IDMP, NTMP, and DTPMP), and amines (MEA and DEA).^a

MEG (5 wt%)		MEA (5 wt%)		DEA (5 wt%)	
T/K	P/MPa	T/K	P/MPa	T/K	P/MPa
279.88	5.68	279.38	5.02	279.63	5.25
282.94	7.89	282.96	7.24	282.62	7.24
284.43	9.52	285.92	10.03	286.29	10.88
286.75	12.44	287.91	12.67	287.19	11.97
IDMP (35 ppm)		NTMP (35 ppm)		DTPMP (35 ppm)	
T/K	P/MPa	T/K	P/MPa	T/K	P/MPa
280.14	5.31	280.34	5.44	279.79	5.13
283.45	7.62	283.41	7.56	283.88	7.95
286.44	10.45	286.09	10.13	285.49	9.49
288.11	12.56	287.42	11.68	288.7	13.42

IDMP (350 ppm)		NTMP (350 ppm)		DTPMP (350 ppm)	
T/K	P/MPa	T/K	P/MPa	T/K	P/MPa
280.73	5.68	279.75	5.17	281.46	6.22
283.61	7.69	283.91	8.04	283.89	8.08
287.2	11.41	285.99	10.1	286.7	10.98
288.49	13.27	288.84	13.82	287.92	12.58

^a Standard uncertainty in pressure and temperature measurements are ± 0.05 MPa and ± 0.03 K, respectively.

9.4 Conclusions

There are numerous chemical additives that are commonly injected into gas pipelines, gas production systems, or processing facilities for various reasons such as hydrate, wax, scale, emulsion, and corrosion inhibition. Such chemicals have not been studied as to their impact on gas hydrate formation, whether positive or negative. Hence, in this study, three commonly used phosphonates or scale inhibitors (IDMP, NTMP, and DTPMP) as well as two amines (MEA and DEA) were tested for hydrate formation, and their hydrate phase boundaries were determined.

The scale inhibitors, although utilized at very small dosage in the field, did not show significant hydrate inhibition performance, whereby showing a maximum depression of 0.2 K. The amines showed pronounced hydrate inhibitory qualities with a maximum temperature depression of 0.47 K which is equivalent to MEG concentration of 2.4 wt% in the case of DEA. On the other hand, both types of chemicals—scale inhibitors and amines did not raise concerns in terms of hydrate formation; thus, the integrity of the hydrate control program can be expected to be intact.

Chapter 10 Utilization of MEG Pilot Plant and MEG Degradation

Methods

This chapter is comprised of the following publications:

- **Alef, K.**, Iglauer, S., Barifcani, A., 2017. An Innovative Approach to Assessing Gas Hydrate Inhibition and Corrosion Control Strategies, In One Curtin International Postgraduate Conference (OCPC), Miri, Sarawak, Malaysia: Curtin.
- **Alef, K.**, Iglauer, S., Barifcani, A., 2019c. Degradation and Hydrate Phase Equilibria Measurement Methods of Monoethylene Glycol. *MethodsX* 6, 6–14. doi: 10.1016/j.mex.2018.12.004

This chapter delves into the innovative use of the MEG pilot plant utilized in this project for MEG operations, realistic fluid simulation, production chemicals compatibility studies, switching of corrosion strategies, salt removal and hydrate testing of regenerated MEG. Moreover, the chapter also covers the developed sample preparation, degradation and hydrate phase equilibria measurement methods of monoethylene glycol. Detailed procedures are given for accurate sample preparation and MEG degradation processes via the reclamation unit and the autoclave mimicking field-like MEG degradation. A detailed procedure for hydrate testing using a high-pressure PVT cell employing the isochoric hydrate testing method. A computer script was developed for quickly determining the hydrate equilibria temperature from the acquired pressure-temperature data from experiments. This contribution satisfies the thesis objectives (a) and (f) while fulfilling the research gaps outlined in Section 1.3.

10.1 An Innovative Approach to Assessing Gas Hydrate Inhibition and Corrosion Control Strategies

As the scarcity of oil increases, natural gas has become a favourable alternative which is available abundantly in many parts of the world. Projects in the hundreds that are focused on the extraction and processing of natural gas have sprung up throughout the world, this has secured natural gas as a key alternative to oil/coal and has brought about large-scale distribution as a source of energy (Stanek and Bialecki, 2014). A major concern in the production and transportation of natural gas is the formation of gas hydrates, due to the presence of water which under typical subsea conditions of high pressure and low temperature, freezes, resulting in blockages and plugging in pipes, which often become dangerous projectiles (Koh et al., 2011; Sloan Jr and Koh, 2007). The consequences of gas hydrates may cause a disastrous loss of containment of gas, which can be highly expensive, very damaging to our environments, and poses great threats to the health and safety of project personnel (Camargo et al., 2011; Englezos, 1993).

Natural gas hydrates also known as clathrate hydrates, are crystal-lattice structures similar to ice, composed of host and guest molecules where the host is water molecules capturing common gas molecules found in natural gas (Koh, 2002; Sloan Jr and Koh, 2007). Methods utilized in the industry to prevent/inhibit gas hydrates include depressurization, thermal insulation of the pipeline, dehydration, or the most common, to inject a hydrate inhibitor such as methanol or monoethylene glycol (MEG) (Son and Wallace, 2000). MEG is highly favourable due to its high boiling and flash point, low volatility, and it being safer for the environment as opposed to methanol (Brustad et al., 2005; Chapoy and Tohidi, 2012; Grzelak and Stenhaug, 2016). The other advantage of MEG is that it can easily be regenerated due to its high boiling point thus saving costs in terms of constant replenishment.

Whilst gas hydrates remain a challenge, corrosion and scaling are also major challenges facing oil and gas facilities resulting in severe cost implications (Aljourani et al., 2009; Garverick, 1994; López et al., 2003; Papavinasam et al., 2007). A corrosion management strategy may be put in place, which usually consists of injecting corrosion inhibitors (Lehmann et al., 2016, 2014), or artificially adjusting pH levels so that a stable iron carbonate layer can be precipitated upon the internals of the pipelines

(Nyborg, 2009). Corrosion strategies may need to be switched especially due to associated formation water production which increases the risk of corrosion and scale formation (Latta et al., 2016, 2013).

Due to the large operations involved, it is difficult for companies to assess or to make a decision on how to effectively change from one strategy to another without completely shutting down the plant. Or, to analyse how different chemical additives will behave in a MEG regeneration plant, and consequently their impact on the hydrate inhibition performance. Companies are wanting to understand the effect of reclamation on gas hydrate inhibition to be able to maintain continuous operation and to predict potential future issues from the continual recycling of MEG. This article presents an innovative approach to providing a basis for testing and running simulations that solve relevant problems companies may have. The approach involves mimicking typical MEG regeneration and reclamation process seen in the industry via an innovative bench-scale MEG pilot plant to allow for realistic yet cost-effective testing of various scenarios to find practical solutions. A high-pressure PVT cell is then used to test the hydrate inhibition performance of the MEG samples from the bench-scale operation. At the same time, experimental results can be compared to the results of simulations from a range of flow assurance software such as Aspen's HYSYS, Infochem's Multiflash and Calsep's PVTsim. With all the data on hand, empirical modelling can be used to produce meaningful relationships to help with the prediction that software packages cannot achieve. Furthermore, the experimental data that the models are built upon are relevant to field-specific cases.

10.1.1 MEG Operation

Typical MEG hydrate inhibition operations begin with an injection of lean-MEG at the offshore wellheads, where it thoroughly mixes with the production fluids thus allowing for thermodynamic hydrate inhibition (Son and Wallace, 2000). As the production fluids arrive onshore, a three-phase separator is utilized. The resulting aqueous phase composing of MEG and water, as well as other contaminants such as organic compounds and salts, are taken through a pre-treatment process to separate insoluble contaminants and hydrocarbons. The MEG solution is then re-concentrated via a reboiler operating above the boiling point of water to remove unwanted water. Finally, a portion of or all of the resulting solution may be sent through a flash separator

operating at the vaporization temperature of MEG thus allowing soluble contaminants to be left behind (Psarrou et al., 2011; Teixeira et al., 2015). The final solution is now considered lean-MEG ready to be reinjected at offshore wellheads (Nazzer and Keogh, 2006).

In this study, a brief outline of a MEG bench-scale facility to be used for simulating actual field operations is proposed. It can be designed as a MEG regeneration and reclamation closed loop system with a processing capacity of up to 5 kg/hr of lean-MEG. There are 5 main processes that need to be designed and built using stainless steel tanks, heating mechanisms, mass flow meters, various measuring probes and a programmable logic controller to record and monitor:

1. Simulating formation water: Formation water and other contaminants that are found in the production fluids in the field are to be prepared so as to match field conditions as accurately as possible. Once the composition of the field formation water is available then the required salts, acids and other contaminants are sourced and mixed with de-ionized water to produce simulated formation water (Figure 10.1). The water can be stored in the formation water tank (FWT) that is continuously sparged with nitrogen to prevent oxygen ingress.

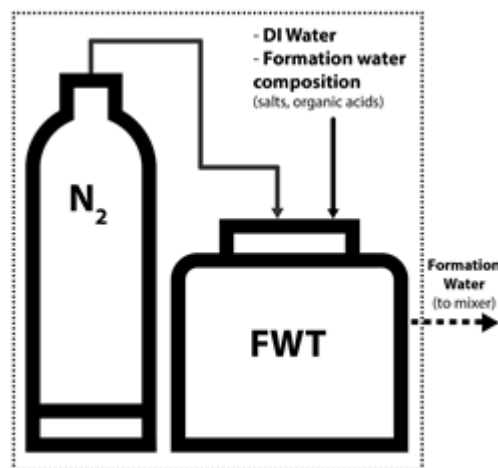


Figure 10.1: Simulation of field formation water.

2. Preparation of contaminated MEG: contaminated MEG refers to MEG that has been separated from the production fluids (i.e. containing salts from formation water). Based on the field concentration of contaminated MEG, appropriate

amount of lean-MEG from the lean-MEG tank (LMT), formation water and any other chemical additives such as corrosion inhibitors are to be mixed using a high-speed mixer (Figure 10.2). This allows for proper mixing under high shear stress simulating turbulent pipeline flow.

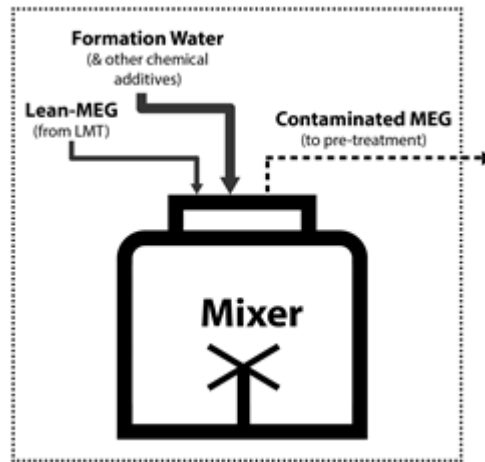


Figure 10.2: Simulation of pipeline conditions to create contaminated MEG solution.

3. Pre-treatment of MEG: Now that contaminated MEG has been simulated it can undergo pre-treatment. A pre-treatment vessel heats the solution to high temperatures, and where the alkalinity can be adjusted as required to promote precipitation of divalent salts (insoluble contaminants) (Figure 10.3). The alkalinity can be adjusted by using sodium hydroxide (NaOH) or hydrochloric acid (HCl). Finding the fine balance of pH level in the pre-treatment unit is very difficult, as this will impact the pH in the other sections of the MEG plant where a certain pH level may be critical. A constant recycle loop keeps the suspended solids in motion. The solution is then sent to the contaminated MEG tank (CMT) for storage.

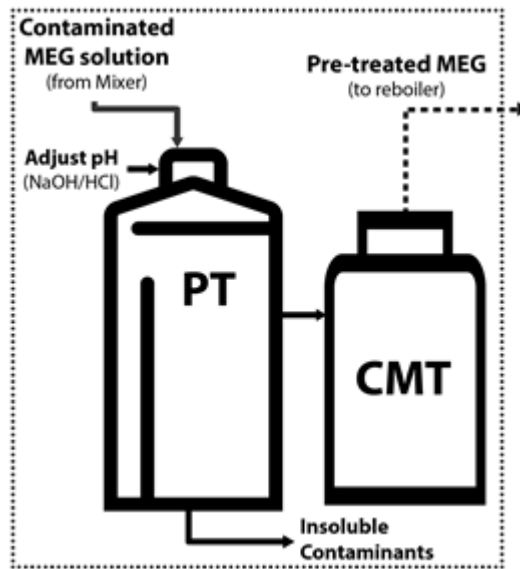


Figure 10.3: Contaminated MEG going through pre-treatment to remove insoluble contaminants.

4. Re-concentration of MEG: The contaminated MEG (now free from insoluble contaminants) from the pre-treatment vessel is allowed to settle in the CMT to remove suspended solids. An additional 10 μm filter downstream of the tank removes any remaining particles before the MEG is routed through to the reboiler and distillation column (RBD) as shown in Figure 10.4. It is heated to a temperature above the boiling point of water but below the boiling point of MEG so only water can be removed. The amount of water removed is based on the required concentration for re-injection at offshore wellheads (typically 80% volume MEG/water). The resulting solution is stored in the lean-MEG tank (LMT) whilst a slip-stream depending on the allowable salt limit within lean-MEG as prescribed by field conditions is sent to the MEG reclamation unit (MRU).

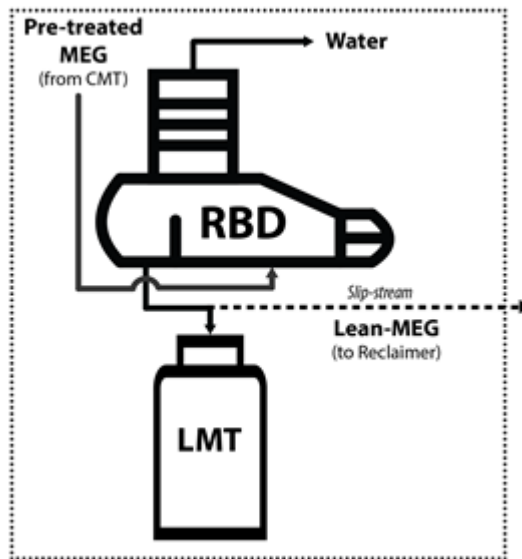


Figure 10.4: MEG from CMT arrives at the reboiler and distillation (RBD) where water is removed thus increasing MEG concentration.

5. Reclamation of MEG: A slipstream (or all produced salt loaded lean-MEG) can be “reclaimed” using a rotary evaporator operating in continuous mode. The salt loaded lean-MEG solution can be flashed in the vacuum flask which can be operated at 100 mBar. The unit should be operating at vacuum conditions in order to avoid exposing MEG to temperatures ($>135\text{ }^{\circ}\text{C}$) that could cause degradation (AlHarooni et al., 2015). The rotary flask is above an oil bath heated to high temperatures allowing for uniform heat distribution due to rotation of flask. The resulting flashed vapor will rise to the condenser and can be collected as salt-free lean-MEG in the receiving flask to be sent to the lean-MEG tank for storage (Figure 10.5).

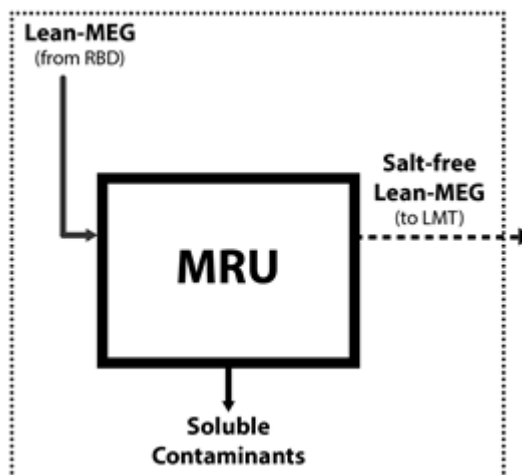


Figure 10.5: The MEG reclamation unit (MRU) removes soluble contaminants from the incoming MEG solution.

10.1.2 Gas Hydrate Testing

In parallel to the MEG operation, samples of MEG at any stage of the process can be taken to test for hydrate inhibition performance. A well-recognized and commonly used tool for determining the gas hydrate formation, dissociation and equilibrium points, as well as gas consumption, is a high-pressure PVT cell. Varying gas mixtures can be introduced into the chamber and sample solutions containing required hydrate inhibitors can be injected. Common methods of determining the hydrate phase equilibria can be employed such as isochoric, isobaric and isothermal methods.

A typical high-pressure PVT cell (Figure 10.6) is made out of sapphire material so a complete visual of the internals of the chamber is available for detailed visual observations. The cell is equipped with a magnetic stirrer to produce an agitation rate that helps in complete transformation of the liquid water phase to hydrate, and encourages the renewal of the surface (Sloan Jr and Koh, 2007). The cell is equipped with pressure and temperature sensors to capture PVT data for analysis.

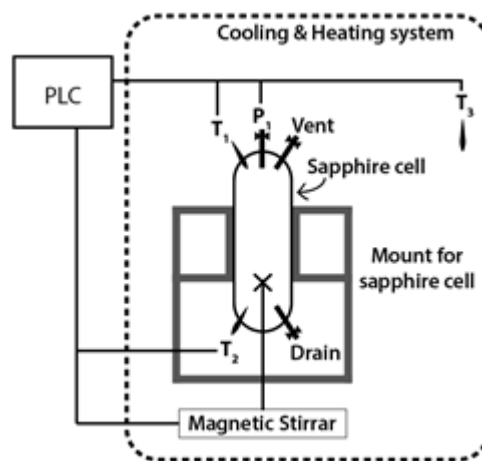


Figure 10.6: Basic schematic of a high-pressure PVT cell apparatus capable of gas hydrate testing.

10.1.2.1 Flow Assurance Software

Flow assurance software packages are increasingly becoming more advanced as technology develops. The use of these software packages in the context of gas hydrates

allow for prediction of formation conditions, validation of experimental data, and to improve/build upon numerical models that have been experimentally derived. Hydrate formation and phase equilibria conditions can be estimated using thermodynamic equations of state and correlations (Smith et al., 2016, 2015). Although, these simulation tools can quickly and fairly accurately determine hydrate conditions, it is to be noted that no model can perfectly determine the measured hydrate phase equilibria and thus this needs to be considered in the analysis of the differences and deviations (AlHarooni et al., 2016; AlHarooni et al., 2016).

10.1.2.2 Empirical Modelling

As chemical additives that are used in the industry are increasingly becoming proprietary, flow assurance software fails to predict or provide meaningful analysis. This is due to the unknown compositions of these chemical additives. This approach capitalizes on the experimental data specific to a field scenario by developing empirical relationships that can determine the specific information. This can be as simple as a linear interpolation between a range of experimental data relevant to the problem at hand. As shown in Figure 10.7, if a pattern is recognized between a set of hydrate phase equilibria data of varying concentration of a hydrate inhibitor, a simple interpolation scheme can be developed to interpolate between the measured data.

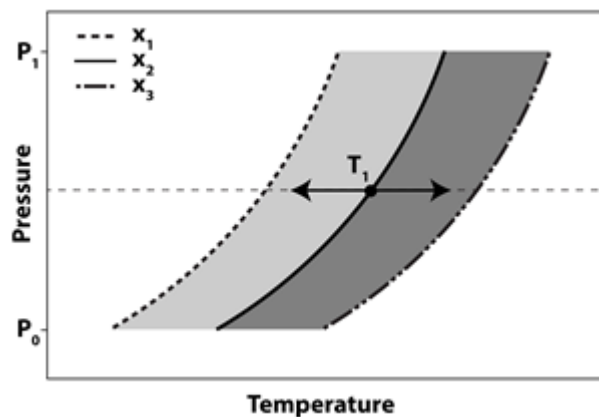


Figure 10.7: Example of interpolation of a gas hydrate profile shift, showing multiple concentrations.

10.1.3 Use Cases

Some of the capabilities and uses of the approach outlined in this article which

combines a bench-scale MEG regeneration facility with gas hydrate inhibition testing include but not limited to:

- Simulation of realistic production fluids, such as condensate mixtures and simulated formation of water/brines. Verifying production chemical additive compatibility.
- Simulating the effects of well clean-ups providing valuable insights and analysis before actual field activity.
- Simulating the effects of switching from one corrosion management strategy to another (e.g. switching between the film forming corrosion inhibitor to pH stabilization, and vice versa).
- Providing input into methods for optimising salt removal.
- Study corrosion and scale formation throughout the MEG regeneration plant.
- Providing gas hydrate inhibition performance for all of the above uses. Using the measured data to develop empirical models to help industry personnel predict hydrate formation conditions where it is not possible to determine using traditional flow assurance software.

Protection of the production gas pipelines from internal corrosion is conventionally achieved using one of two methods: pH stabilization or injecting a film forming corrosion inhibitor (FFCI). The MEG bench-scale facility can be used to simulate the procedures for switching between corrosion management strategies and the following key objectives can be achieved:

- Distribution/partitioning of chemicals/corrosion inhibitors in the various sections of the MEG facility.
- The behaviour of the pre-treatment, regeneration and reclamation units, and the removal efficiency of injected chemicals.
- Confirm feasibility of switchover procedures, identify potential gaps and improvement opportunities.
- Document observations and lessons learned.

A primary corrosion control method that is usually implemented is pH stabilization, whereby a base - Methyl diethanolamine (MDEA) is added to the lean MEG onshore, increasing the pH, lowering the corrosion rate and encouraging the formation of a

protective FeCO_3 scale on the pipeline wall (Latta et al., 2013). pH stabilization is a very effective method of controlling internal corrosion and reducing the production of corrosion products from the flowline which has a tendency to foul downstream equipment. However, pH stabilization increases the risk of scaling in the subsea architecture, particularly in the choke module and well jumpers, and cannot be used once formation water breakthrough occurs, or initially when remnant completion fluids may pose a scale risk. So FFCI is employed as an alternative corrosion control method, used when pH stabilization is not feasible due to scale formation risk (Halvorsen et al., 2007). FFCI adsorbs to the pipeline wall, forming a protective film which prevents corrosion. Risks associated with the use of FFCI are an increased risk of emulsions, under deposit corrosion, top of line corrosion and fouling of inlet liquid filters, separators, and the rich MEG processing unit (Latta et al., 2016). FFCI protection is a less robust corrosion protection method and is intended to be employed only for a limited period. The switchover to pH stabilization mode will occur once all wells have unloaded the majority of leftover completion fluid, rich MEG chemistry has stabilized, and the risk of scaling is deemed to be low. The decision to switchover may also be driven by unfavourable conditions caused by operation in FFCI modes, such as emulsion formation, excessive corrosion rates or equipment fouling. The reverse switchover from pH stabilization back to FFCI mode may be required if field-wide formation water production is unmanageable through alternative means such as production reallocation or scale inhibitor injection. The decision to switchover may also be driven by unfavourable conditions caused by operation in pH stabilization mode.

10.1.4 Conclusion

With the above approach, companies can invest in developing a bench-scale MEG pilot plant that matches their actual field design at a fraction of the cost, allowing field case scenarios to be tested beforehand, where best practices and lessons learned are documented for actual field use. Operations that would otherwise take months or years to occur in the field can be scaled down to a matter of days with this approach yet yield accurate insights to help improve the design and operation in the field. Furthermore, gas hydrate inhibition performance can be evaluated simultaneously at various stages of the MEG regeneration process giving insights into how the inhibition performance

is influenced by other chemical additives, or the process itself (i.e. continual recycling of MEG). Future work of the authors' aims to show a working a facility with actual field use cases to showcase this approach.

10.2 Degradation and Hydrate Phase Equilibria Measurements of Monoethylene Glycol

10.2.1 Method Details

To meet energy demands, Natural gas has increasingly become a profitable alternative. However, a serious challenge is the formation of gas hydrates. The traditional technique to inhibit hydrate formation in pipelines is the injection of a thermodynamic hydrate inhibitor to shift the hydrate phase equilibrium boundary to lower temperatures, thus leaving the operating conditions of pipelines to be within a hydrate-safe region (Sloan Jr and Koh, 2007). For the least, hydrates can cause blockages in pipelines, severely disrupting gas production, and also have the potential to cause explosions in pipelines. A common hydrate inhibitor that is utilized is Monoethylene glycol (MEG), it is mainly favourable due to its high recoverability. However, during the recoverability process MEG undergoes multiple phases of thermal exposure. This usually leads to thermal degradation in the MEG solution which results in an overall lower hydrate inhibitory performance (Alef et al., 2018c).

In-order to understand how degradation occurs, its products, the impact on the equipment, and the hydrate inhibition performance of MEG, a method to degrade and test MEG is proposed in-detail. A study conducted by the authors that successfully utilized this method reported on the effect of regenerated MEG over multiple cycles (Alef et al., 2018c). The method essentially comprises of three stages; a) Degradation of MEG, b) Analysis of degraded MEG, and c) Hydrate testing of degraded MEG.

10.2.2 Degradation of MEG

The utilization of MEG as a continuous hydrate inhibitor necessitates ongoing regeneration to remove impurities such as produced water, reservoir fluids, salts, corrosion products and production/drilling chemicals that have a tendency to accumulate within the MEG solution (Alef et al., 2018a; Nazzari and Keogh, 2006; Son and Wallace, 2000; Teixeira et al., 2015). Reclamation is the process in which non-

volatile chemicals and monovalent salts are removed from the MEG solution through processing a stream of re-concentrated MEG solution from the regeneration process. The process occurs in a flash separator operating in vacuum where the input solution (MEG-water-contaminants) are boiled off at a temperature greater than the boiling point of water and MEG. Both, the water and MEG will evaporate while leaving behind salts and other chemicals that can then be removed from the system (Brustad et al., 2005). Care needs to be taken to ensure temperatures do not rise beyond the thermal degradation temperature of MEG, even though degradation of MEG has been shown to be possible at reclaimer operating conditions which are considerably lower (Alef et al., 2018c; Psarrou et al., 2011).

Two experimental apparatuses within the laboratory (reclamation unit and autoclave system) will be illustrated and their procedures to produce degraded MEG samples will be outlined. The reclamation process typically implemented in the field was reproduced by a rotary evaporator essentially a vacuum distillation unit (Figure 10.8). Laboratory scale rotary evaporators are designed for different reclamation processes with vacuum control with slight modifications based on specific requirements. The rotary evaporator is utilized to carry out the separation of MEG from monovalent salts and insoluble contaminants where salt-laden MEG as an input solution is distilled by removing the salts as a crystalized residue, and pure lean-MEG is collected as condensate product. To achieve optimum operating conditions, a vacuum pump is utilized to avoid MEG degradation due to high temperatures while increasing the salt removal efficiency. The reclamation unit comprises of an overhead condenser, a vacuum flask partially submerged in an oil bath, a vacuum system, a liquid receiver and an integrated control box. Modifications have been made to allow for sparging with nitrogen (99.999 mol%) to ensure there is no oxygen contamination. To ensure operating temperatures remain within tolerable and desired levels, several K-type thermocouples were retrofitted to measure the temperatures of the vapor and liquid-slurry phases, while being connected to the Programmable Logical Controller (PLC). A level sensor was utilized to control the flow of lean MEG into the evaporator flask based on the desired slip stream portion from the input (or from the regeneration unit in the case of field application). Other instruments were utilized to monitor the system in terms of pH, pressure, flowrates, electrical conductivity (EC), dissolved oxygen (DO).

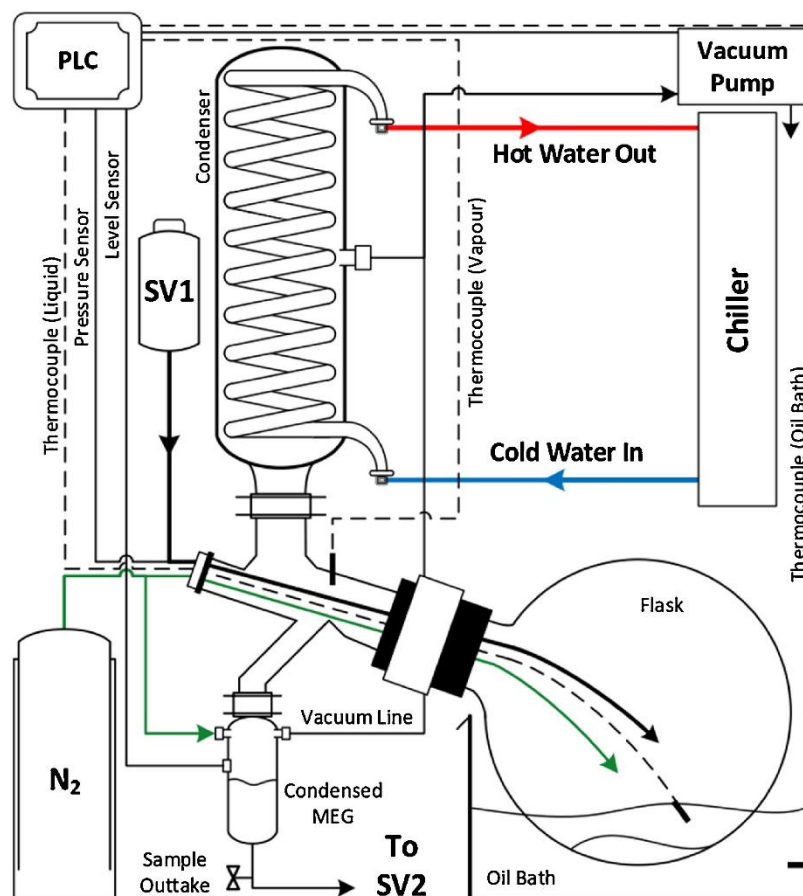


Figure 10.8: Schematic for the suggested experimental set-up of the reclamation unit.

Procedure for the preparation and degradation of test solution is as follows:

1. Preparation of initial solution (non-degraded salt-laden MEG solution)
 - a. Set-up the air-tight beaker system as shown in Figure 10.9(a). The magnetic stirrer is used to mix and keep the solution in constant synthesis. Probes can be installed to measure pH, electrical conductivity and dissolved oxygen of the solution. Connect the nitrogen line to ensure there is minimum oxygen ingress.
 - b. Prepare and transfer a salt-laden MEG solution according to desired concentration (typically MEG at 80 wt%) and volume based on experiment design into the beaker.
 - c. Give the solution sufficient time (6 h) for dissolved O₂ levels to reach (≤ 20 ppb) and for complete synthesis.
2. Analysis of prepared solution representing non-degraded MEG.
 - a. Record all the measurements such as pH, EC, O₂, colour (photo) and

mixing behaviour.

- b. Extract a smaller sample for IC to determine MEG degradation products (acetic, formic, glycolic acid).
- c. Extract another sample in order to prepare a diluted MEG solution to a concentration of 20–40 wt% (typical field MEG injection concentration) for hydrate testing. Use Eqns. (10.1) and (10.2) to determine the required additional water (ΔM) to reach the desired MEG concentration for testing.

$$M_1 C_1 = M_2 C_2 \quad (10.1)$$

$$\Delta M = M_2 - M_1 \quad (10.2)$$

where M_1 and M_2 are the masses of the initial (undiluted solution) and final (diluted solution) in g respectively, C_1 and C_2 are the concentrations of the initial and final solutions respectively, and ΔM is the additional water required to reach the desired concentration (C_2) in g.

After careful preparation of the test solution, it is ready for the degradation process as follows:

3. Degradation of prepared solution using the reclamation unit (Figure 10.8).
 - a. Transfer the initial solution to storage vessel 1 (SV1).
 - b. Power on the main PLC computer and in-line sensors such as pH, EC, DO, pressure and temperature.
 - c. Activate the nitrogen purge line to all vessels and the rotary flask to prevent unnecessary oxygen ingress.
 - d. Power on the cooling system and configure the temperature to around $\sim 4\text{--}6\text{ }^\circ\text{C}$.
 - e. Power on the liquid dosage pump from vessel 1 to start dosing into the rotary flask.
 - f. Power on the reclamation unit. The unit should be preconfigured to the desired refill, drain and condensate time as per experiment design.
 - g. Set-up the required vacuum pressure (10–15 kPa), oil bath temperature (depending on the required vapor temperature in the experiment design)

- and flask rotation speed (20–30 rpm).
- h. Initiate the reclamation process and the flask shall start to receive salt-laden MEG at the preconfigured dosage pump flowrate.
 - i. After sufficient drain and condensate time has occurred, the processed solution will be sent to storage vessel 2 (SV2).
 - j. MEG samples may be taken at any time from SV1/SV2 at the sample outtake valve for further analysis of degradation products and hydrate testing according to step 2.
 - k. When the volume level of SV1 is at 15%, activate the pump to transfer the contents of SV2 to SV1 so that the process can repeat until the total operation time for reclamation has been fulfilled according to the experiment design.
 - l. To shut-down the apparatus, drain the contents of the rotary flask and power off all equipment.
 - m. When sufficient cooling of the flask has occurred, extract the salt residue left at the bottom of the flask, and store it if required for future analysis (i.e. viscosity, SEM/ECM and particle analysis).
 - n. Extract the degraded MEG solution (contents of SV1 and SV2) for further analysis as outlined in step 2.
4. A slightly more simplified approach to attaining degraded MEG samples is the use of typical stainless steel high pressure/temperature autoclaves requiring no modifications (Figure 10.9(b)). The procedure for MEG degradation using an autoclave is as follows:
- a. Thoroughly clean the autoclave with ethanol and deionized water.
 - b. Transfer the prepared solution (step 1) to the autoclave using a pump to avoid unnecessary contamination of the autoclave.
 - c. Purge the autoclave for 2 h with nitrogen to ensure there is no oxygen contamination.
 - d. Place the autoclave in its heating jacket and activate the required temperature via the control panel.
 - e. Enable the pre-installed stirrer if required.
 - f. After the required operation time has passed, deactivate the system via the control panel and allow for the autoclave to cool down.

- g. Once cool, extract the degraded MEG solution for further analysis as outlined in step 2.

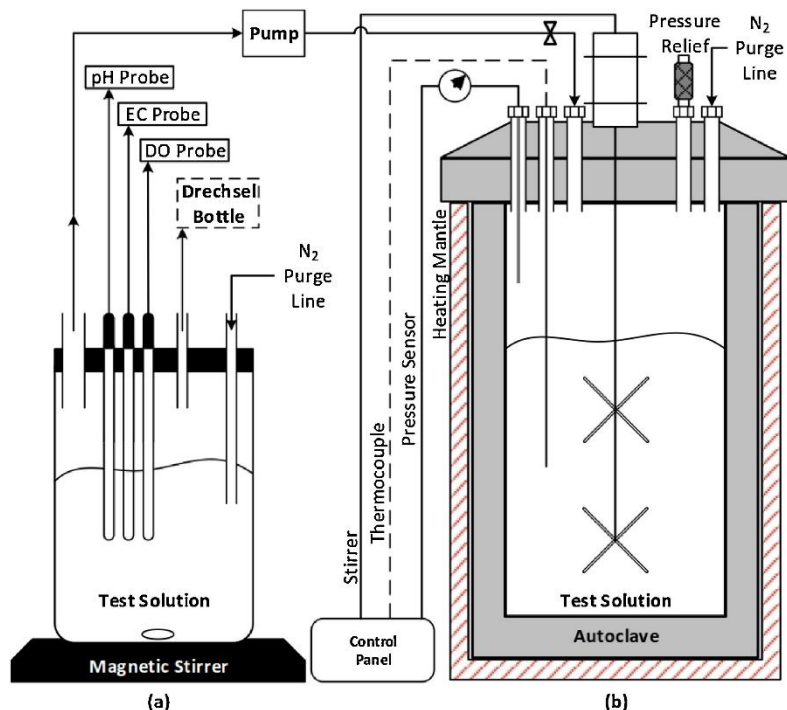


Figure 10.9: Schematic for the preparation of the test solution and autoclave set.

10.2.3 Hydrate Testing of Degraded MEG

To determine the hydrate phase equilibria of the degraded and non-degraded samples, a high-pressure PVT Sapphire Cell can be utilized. The desired gas mixture can be introduced into the chamber according to the experimental design and the type of hydrate structure under study. Common methods of determining the hydrate phase equilibria can be employed such as the isochoric, isobaric and isothermal methods. A typical high-pressure PVT cell (Figure 10.10) is made out of sapphire material so a complete visual of the internals of the chamber is available for detailed visual observations. The cell has been designed with an inner volume of 60 cm³ to allow for sufficient gas and liquid to form hydrate. An automated magnetic stirrer fitted to the cell produced an agitation rate that helps in the complete transformation of the liquid water phase to hydrate, and encourages the renewal of the surface where there is a higher tendency for hydrate film to form. The recommended stirrer rate to be applied is 400–500 rpm. The cell is equipped with pressure and temperature sensors to capture PVT data for further analysis.

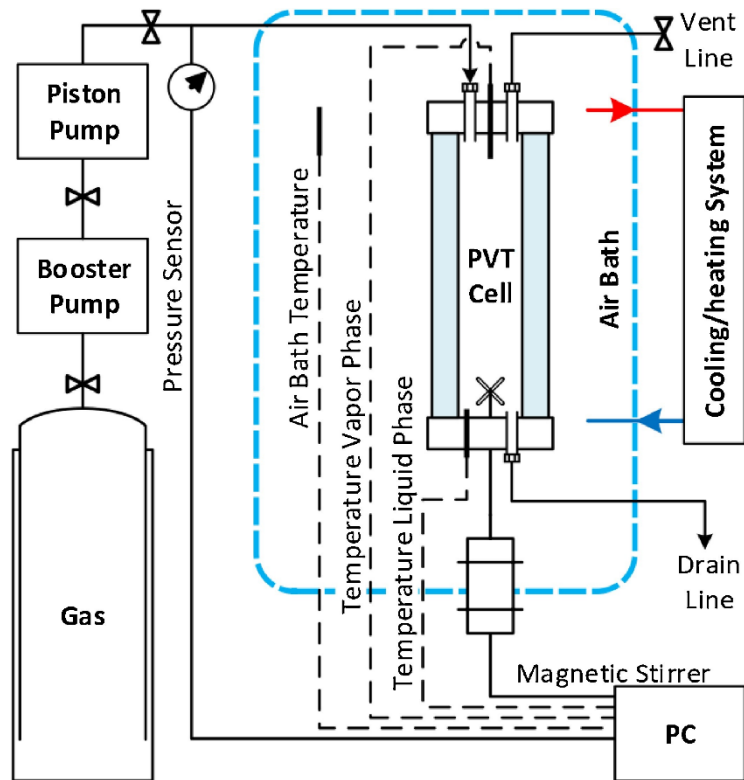


Figure 10.10: Schematic of experimental set-up for hydrate testing using PVT Cell.

5. Method to determine the phase equilibria for degraded MEG solution

- a. Thoroughly rinse the inside of the PVT cell with ethanol/acetone, and then with deionized water.
- b. Close all valves and power on the vacuum pump to ensure there are no contaminants within the cell.
- c. Inject a 7 mL sample of the test solution through the inlet valve into the cell.
- d. Power on the PVT system (control computer, piston pump, magnetic stirrer, air circulation fan and cooling system).
- e. Ensure the gas supply is ready and firmly connected to the manifold then open the gas input line into the cell.
- f. Enable the piston pump via the control software to inject gas into the chamber and to increase the pressure to the desired pressure for the first point on the hydrate phase boundary. Close the gas input valve once desired pressure is achieved.
- g. Enable the heating system to heat up the sample to 35 °C to destroy any water memory profiles, then turn off the heater.

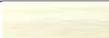
- h. Enable data acquisition and ensure temperature, pressure and stirrer rate data are being recorded (at 5 s intervals).
- i. Begin video recording using the camera and light beam focused on the sample within the cell.
- j. Enable the cooling process to begin and set the cooling rate to 1 °C/h via the control software.
- k. Carefully note visual observations such as the growth, agglomeration and behaviour of hydrate formation; the inter-phase conditions (i.e., clear, foaming, bubbling, grey or cloudy), film formation on the inner walls of the cell; the temperature at which the first hydrate particle is formed, the point at which the stirrer stops moving due to impeding hydrate solids, and the rate of reduction of the solution in the cell.
- l. When all visible liquid has transformed into hydrate, continue the cooling process for a further 3 °C but avoid going below 0 °C (i.e., ice formation region).
- m. Begin the slow step-wise heating process at a rate of 0.5 °C/h with a maximum rate of 1 °C/h so that a sufficient time is available for equilibrium to be achieved. The process can be ended when all visible hydrate solids are converted to liquid.
- n. The PVT system can now be cleaned and shut-down.
- o. From the acquired temperature and pressure data for the cooling and heating processes, the hydrate thermodynamic equilibrium point may then be determined from the intercept of the two curves. Use the computer script provided in the Supporting information for automated processing of data logs to determine the hydrate phase equilibria conditions.
- p. Repeat the entire process (5) for at least another 3 more pressure points in order to plot the hydrate phase boundary.

10.2.4 Method Validation

The degradation of MEG can be identified by the presence of by-products. Studies from literature that investigated degradation of MEG have found the by-products of MEG degradation to be formic, glycolic, acetic and oxalic (Clifton et al., 1985; Madera

et al., 2003; Monticelli et al., 1988; Ranjbar and Abasi, 2013; Rossiter et al., 1985, 1983). Numerous studies have been conducted by our laboratory using our method which are outlined in Table 10.1 (Alef et al., 2018c; AlHarooni et al., 2015; AlHarooni et al., 2016). The results clearly show the presence of degradation products such as acetic acid between degraded and non-degraded samples. A study conducted by Psarrou et al. (2011) has reported that a sign of degradation in the reclamation process is the colour of the solution where it changes to more of a yellow colour (Psarrou et al., 2011). The colour changes have also been reported in Table 10.1, and it can be seen that the colour has changed from clear to yellow to dark brown as the degradation amount increases amongst the MEG solution samples. Furthermore, the effect of MEG degradation on the hydrate phase boundary can be studied using this method. A pure MEG solution of 25 wt% was prepared and degraded for 100 h using this method. The changes in colour, pH, EC and the shift in hydrate phase boundary have been reported in Table 10.1 and Figure 10.11. It can be confirmed that degradation products and promotion of hydrate formation was found.

Table 10.1: Experimental data of degraded and non-degraded MEG solutions using reported methods.

Solution	Exposure Temp. (° C)	Exposure Time (h)	ΔT_{Hyd} (° C) ^a	Colour	ΔpH ^a	ΔEC ($\mu S/cm$) ^a	Acetic acid (ppm)	Source
MEG (25 wt%)	23.6 ^b	- ^b	0		0	0	3	- ^c
	100	100	0.18		-0.15	43	10	
MEG (25 wt%)	135	48	-		-	-	12	(AlHarooni et al., 2015)
	165	48	0.72		-	-	18	
	185	48	1.07		-	-	21	
	200	48	1.62	-	-	-	-	
MEG (20 wt%) + MDEA (2 wt%)	22 ^b	- ^b	0		0	2	10	(AlHarooni et al., 2016)
	135	240	1.7		-0.29	50.1	36	
	165	240	1		-0.43	78.9	56	
	185	240	1.1		-0.45	112.0	62	
	200	240	1.3		-0.56	141.3	71	
MEG (20 wt%)	≤ 126	11	0.13		-	-	6.5	(Alef et al., 2018c)
	≤ 126	56	1		-	-	82.7	

Solution	Exposure Temp. (° C)	Exposure Time (h)	ΔT_{Hyd} (° C) ^a	Colour	ΔpH ^a	ΔEC ($\mu S/cm$) ^a	Acetic acid (ppm)	Source
+ Brine	≤ 126	97	1.7		-	-	139.3	

^a Shift from a non-degraded sample of the same solution. ^b Room conditions. ^c This study.

Experiments were conducted to determine the methane-water hydrate phase boundary using the set-up reported in this study. The phase equilibria data are plotted in Figure 10.11. The results were compared to the widely available literature data (Jhaveri and Robinson, 1965; McLeod and Campbell, 1961; Verma, 1974). An absolute average relative error (AARE) of 0.98% was found, which confirms that our apparatus and procedure are highly accurate in determining hydrate phase equilibria (Figure 10.11).

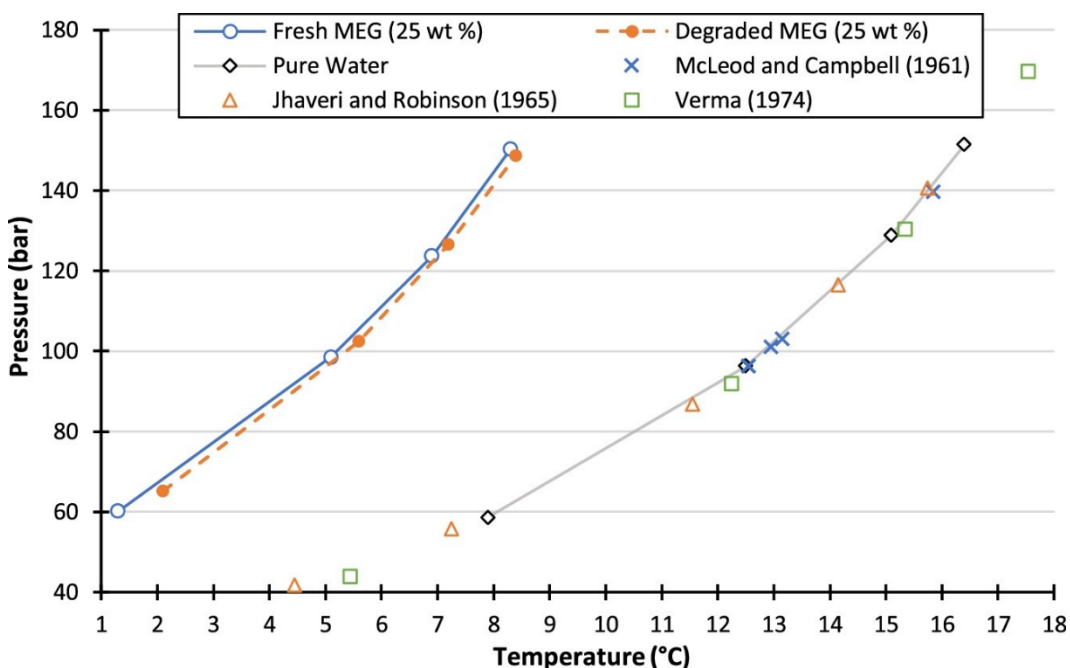


Figure 10.11: Comparison of degraded MEG with fresh MEG, and literature comparison of methane-water hydrate.

10.2.5 Conclusion

Flow assurance challenges such as gas hydrates and corrosion are a serious concern for the oil and gas industry. An array of chemicals (i.e., hydrate, corrosion, scale, wax inhibitors and oxygen scavengers) are injected into the hydrocarbon production and process pipelines to prevent, decrease and or mitigate these concerns. MEG is a

conventional hydrate inhibitor that is commonly used in the industry due to its reusability. However, MEG may undergo degradation in the reboiler and reclamation units of a MEG regeneration plant. Thus, to study the effects of degradation of MEG especially in the presence of other chemical additives upon the adopted hydrate inhibition program becomes important. This study has outlined the necessary methods to mimic field-like degradation of MEG and analysis in terms of hydrate inhibition performance and degradation products.

Chapter 11 Summary and Conclusions

In this thesis, extensive hydrate testing of MEG samples was conducted to investigate the hydrate kinetics and phase equilibria of said samples. MEG regeneration and reclamation was evaluated. Empirical and thermodynamic modelling was conducted to allow for prediction of gas hydrate phase equilibria. Specifically, the following conclusions were made:

- Effect of regenerated MEG on gas hydrate, and empirical modelling for prediction:
 - ❖ Field-like MEG regeneration and reclamation operation was reproduced using the MEG pilot plant for the first time.
 - ❖ The samples from each cycle were analysed for their composition and tested using a PVT cell for hydrate inhibition performance.
 - ❖ The study found a rightward shift in the hydrate phase boundary for MEG suggesting a promotion in hydrate formation as the number of cycles of MEG regeneration increased. It found an average equilibrium temperature shift of 1.7 °C for cycle 9 as compared to pure MEG (20 wt% MEG).
 - ❖ High performance liquid chromatography analysis revealed degradation products increased with cycle number.
 - ❖ The study has found that thermal degradation of MEG can occur even if MEG is not exposed to its known degradation temperature range.
 - ❖ Empirical model was developed for prediction based on the results of this study for the benefit of industry personnel and MEG end-users.
- Evaluation of MEG reclamation and natural gas hydrate inhibition during corrosion control switchover:
 - ❖ MDEA and acetic acid cannot be removed in the reclamation unit simultaneously due to contrasting pH required.
 - ❖ FFCI and MDEA caused a very viscous residue in the reclamation unit and caused discoloration.
 - ❖ New natural gas hydrate equilibria data for reclaimed MEG have been reported alongside metastable regions.
 - ❖ The performance of reclaimed MEG varied compared with that of pure

MEG, and was lower at the end of the experiment.

- Effect of methyldiethanolamine on gas hydrate, and modelling for prediction:
 - ❖ Hydrate phase equilibria for MDEA solutions at a high-pressure range (7 – 20 MPa) were produced.
 - ❖ Pure MDEA showed an average equilibrium temperature shift of -0.82 °C at a concentration of 7.5 wt%. The combined effect of MDEA (7.5 wt%) with MEG (20 wt%) showed an equivalent hydrate performance of 20.95 wt% MEG.
 - ❖ Empirical modelling for hydrate phase equilibria was developed for prediction.
 - ❖ Thermodynamic model based on the CPA equation of state was developed for the calculation of hydrate phase equilibria of MDEA solutions even in the presence of MEG for numerous hydrate formers.
- Effect of corrosion inhibitors with kinetic hydrate inhibitor on gas hydrate, and empirical modelling of meg degradation:
 - ❖ The study evaluated the hydrate inhibitory performance of MEG with FFCI, finding that FFCI showed good hydrate inhibitory performance. It was found that only 3 wt% of FFCI in a 20 wt% MEG solution showed an equivalent hydrate inhibition performance of a 23.12 wt% MEG solution.
 - ❖ MDEA and FFCI were also found to enhance the inhibitory performance of solutions containing KHI.
 - ❖ The study suggests other chemical additives can provide increased hydrate inhibitory performance than previously expected.
 - ❖ Empirical modelling to determine the equilibrium temperature suppression of MEG and MDEA+MEG degraded solutions have been developed.
- Effect of dissolved oxygen, sodium bisulfite, and oxygen scavengers on methane hydrate inhibition:
 - ❖ The study produced new hydrate phase equilibria data for sodium bisulfite solutions (0.01–10 wt%) with and without the presence of MEG. Results show greater inhibition at higher concentrations as opposed to commonly used dosages for oxygen scavenging

applications.

- ❖ However, a proprietary oxygen scavenger promoted hydrate formation, which suggests that chemical additives should be thoroughly assessed for compatibility with other chemicals as well as tested to determine any potential negative consequences.
 - ❖ A non-sulfite oxygen scavenger showed inhibition performance but may not surmount to any benefit due to the small dosages required.
 - ❖ Furthermore, the study has revealed that dissolved oxygen may also increase the risk of gas hydrate formation despite the fact that it already negatively affects corrosion risk. Clearly, dissolved oxygen levels should be kept to a minimum.
- Hydrate phase equilibria of phosphonate scale inhibitors, amines, and ethylene glycol:
 - ❖ Three commonly used phosphonates or scale inhibitors (IDMP, NTMP, and DTPMP) as well as two amines (MEA and DEA) were tested for hydrate formation, and their hydrate phase boundaries were determined.
 - ❖ The scale inhibitors, although utilized at very small dosage in the field, did not show significant hydrate inhibition performance, whereby showing a maximum depression of 0.2 °C.
 - ❖ The amines showed pronounced hydrate inhibitory qualities with a maximum temperature depression of 0.47 °C which is equivalent to MEG concentration of 2.4 wt% in the case of DEA.
 - ❖ On the other hand, both types of chemicals; scale inhibitors and amines; did not raise concerns in terms of hydrate formation; thus, the integrity of the hydrate control program can be expected to be intact.
 - Utilization of MEG pilot plant and MEG degradation methods:
 - ❖ With the MEG pilot plant approach, companies can invest in developing an operation that matches their actual field design at a fraction of the cost, allowing field case scenarios to be tested beforehand, where best practices and lessons learned are documented for actual field use.
 - ❖ Operations that would otherwise take months or years to occur in the

field can be scaled down to a matter of days with this approach yet yielding accurate insights to help improve the design and operation in the field.

- ❖ Procedure to prepare accurate MEG solutions avoiding oxidative degradation of MEG (i.e., controlling oxygen ingress).
- ❖ Two methods are suggested to mimic field-like degradation of MEG solutions (i.e., degradation by reclamation and autoclave).
- ❖ Adoption of the isochoric hydrate testing method while using a high-pressure PVT cell with the aid of a computer script to accurately evaluate hydrate phase equilibria conditions.

11.1 Further Research Potential

The following are recommended future extensions to the above work:

- Improve the developed models for MEG degradation by conducting more MEG regeneration experiments that mimic the actual field operations and formation water compositions.
- Study the effect of time on MEG degradation and subsequently, its hydrate inhibition performance.
- Similarly, study the effect of MEG degradation on its hydrate inhibitory performance in solutions with higher MEG concentrations.
- How the metastable regions differ in other test cells with varying rate of cooling and mixing rates.
- Utilize a flow loop for hydrate testing that is directly connected to the MEG pilot plant for real-time hydrate testing at specific operating pressures and temperatures, which shall allow for tuning the developed models for higher accuracy.
- For chemical compatibility studies, it is recommended that demulsifiers and asphaltene inhibitors are also tested for their effect on gas hydrate formation.

BIBLIOGRAPHY

- Achour, M., Kolts, J., 2015. Corrosion Control by Inhibition Part I: Corrosion Control by Film Forming Inhibitors. Presented at the CORROSION 2015, NACE International.
- Akhfash, M., Arjmandi, M., Aman, Z.M., Boxall, J.A., May, E.F., 2017. Gas Hydrate Thermodynamic Inhibition with MDEA for Reduced MEG Circulation. *J. Chem. Eng. Data* 62, 2578–2583. <https://doi.org/10.1021/acs.jced.7b00072>
- Al Dhafeeri, M.A., 2007. Identifying sources key to detailed troubleshooting of amine foaming. *Oil & Gas Journal* 105, 56–56.
- Alef, K., Barifcani, A., 2020. Effect of N-methyl-diethanolamine and film forming corrosion inhibitor on gas hydrate, and empirical modeling for degradation. *Journal of Petroleum Science and Engineering* 184, 106522. <https://doi.org/10.1016/j.petrol.2019.106522>
- Alef, K., Barifcani, A., 2019. Hydrate Phase Equilibria of Phosphonate Scale Inhibitors, Amines, and Ethylene Glycol. *J. Chem. Eng. Data* 64, 3205–3210. <https://doi.org/10.1021/acs.jced.9b00366>
- Alef, K., Barifcani, A., 2018. The Effect of Salt-Laden Degraded MEG on Gas Hydrate Inhibition. Presented at the SPE Kingdom of Saudi Arabia Annual Technical Symposium and Exhibition, Society of Petroleum Engineers. <https://doi.org/10.2118/192447-MS>
- Alef, K., Gubner, R., Iglauer, S., Barifcani, A., 2019a. Evaluation of MEG reclamation and natural gas hydrate inhibition during corrosion control switchover. *Journal of Petroleum Science and Engineering* 176, 1175–1186. <https://doi.org/10.1016/j.petrol.2018.08.052>
- Alef, K., Iglauer, S., Barifcani, A., 2019b. Thermodynamic Modeling of Hydrate Phase Equilibria in Methyldiethanolamine Solution in the Presence or Absence of Monoethylene Glycol. *J. Chem. Eng. Data* 64, 4148–4153. <https://doi.org/10.1021/acs.jced.9b00552>
- Alef, K., Iglauer, S., Barifcani, A., 2019c. Degradation and hydrate phase equilibria measurement methods of monoethylene glycol. *MethodsX* 6, 6–14. <https://doi.org/10.1016/j.mex.2018.12.004>
- Alef, K., Iglauer, S., Barifcani, A., 2018a. Effect of Dissolved Oxygen, Sodium Bisulfite, and Oxygen Scavengers on Methane Hydrate Inhibition. *J. Chem. Eng. Data* 63, 1821–1826. <https://doi.org/10.1021/acs.jced.8b00150>
- Alef, K., Iglauer, S., Gubner, R., Barifcani, A., 2018b. Hydrate Phase Equilibria for Methyldiethanolamine and Empirical Modeling for Prediction. *J. Chem. Eng. Data* 63, 3559–3565. <https://doi.org/10.1021/acs.jced.8b00440>
- Alef, K., Smith, C., Iglauer, S., Gubner, R., Barifcani, A., 2018c. The effect of regenerated MEG on hydrate inhibition performance over multiple regeneration cycles. *Fuel* 222, 638–647. <https://doi.org/10.1016/j.fuel.2018.02.190>
- AlHarooni, K., Barifcani, A., Pack, D., Gubner, R., Ghodkay, V., 2015. Inhibition effects of thermally degraded MEG on hydrate formation for gas systems. *Journal of Petroleum Science and Engineering* 135, 608–617. <https://doi.org/10.1016/j.petrol.2015.10.001>
- AlHarooni, K., Pack, D., Iglauer, S., Gubner, R., Ghodkay, V., Barifcani, A., 2017. Effects of Thermally Degraded Monoethylene Glycol with Methyl Diethanolamine and Film-Forming Corrosion Inhibitor on Gas Hydrate

- Kinetics. Energy Fuels 31, 6397–6412.
<https://doi.org/10.1021/acs.energyfuels.7b00733>
- AlHarooni, K., Pack, D., Iglauer, S., Gubner, R., Ghodkay, V., Barifcani, A., 2016. Analytical Techniques for Analyzing Thermally Degraded Monoethylene Glycol with Methyl Diethanolamine and Film Formation Corrosion Inhibitor. Energy Fuels 30, 10937–10949.
<https://doi.org/10.1021/acs.energyfuels.6b02116>
- AlHarooni, K.M., Barifcani, A., Pack, D., Iglauer, S., 2016. Evaluation of Different Hydrate Prediction Software and Impact of Different MEG Products on Gas Hydrate Formation and Inhibition. Presented at the Offshore Technology Conference Asia, Offshore Technology Conference.
<https://doi.org/10.4043/26768-MS>
- Aljourani, J., Raeissi, K., Golozar, M.A., 2009. Benzimidazole and its derivatives as corrosion inhibitors for mild steel in 1M HCl solution. Corrosion Science 51, 1836–1843. <https://doi.org/10.1016/j.corsci.2009.05.011>
- Amri, J., Gulbrandsen, E., Nogueira, R.P., 2009. Effect Of Acetic Acid On Propagation And Stifling Of Localized Attacks In CO2 Corrosion Of Carbon Steel. Presented at the CORROSION 2009, NACE International.
- Anderson, B.J., Bazant, M.Z., Tester, J.W., Trout, B.L., 2005. Application of the Cell Potential Method To Predict Phase Equilibria of Multicomponent Gas Hydrate Systems. J. Phys. Chem. B 109, 8153–8163.
<https://doi.org/10.1021/jp045551g>
- Anderson, F.E., Prausnitz, J.M., 1986. Inhibition of gas hydrates by methanol. AIChE Journal 32, 1321–1333. <https://doi.org/10.1002/aic.690320810>
- Aspen HYSYS, 2007. . AspenTech, Calgary.
- Avlund, A.S., Kontogeorgis, G.M., Michelsen, M.L., 2008. Modeling Systems Containing Alkanolamines with the CPA Equation of State. Ind. Eng. Chem. Res. 47, 7441–7446. <https://doi.org/10.1021/ie800040g>
- Ballard, A.L., 2002. Non-ideal hydrate solid solution model for a multi-phase equilibria program, A (PhD Thesis). Colorado School of Mines. Arthur Lakes Library.
- Ballard, A.L., Sloan Jr, E.D., 2002. The next generation of hydrate prediction: I. Hydrate standard states and incorporation of spectroscopy. Fluid Phase Equilibria, Proceedings of the Ninth International Conference on Properties and Phase Equilibria for Product and Process Design 194–197, 371–383. [https://doi.org/10.1016/S0378-3812\(01\)00697-5](https://doi.org/10.1016/S0378-3812(01)00697-5)
- Ballard, L., Sloan, E.D., 2004. The next generation of hydrate prediction IV: A comparison of available hydrate prediction programs. Fluid Phase Equilibria 216, 257–270. <https://doi.org/10.1016/j.fluid.2003.11.004>
- Bamford, C.H., Compton, R.G., Tipper†, C.F.H., 1980. Liquid Phase Oxidation. Elsevier.
- Bandyopadhyay, A.A., Klauda, J.B., 2011. Gas Hydrate Structure and Pressure Predictions Based on an Updated Fugacity-Based Model with the PSRK Equation of State. Ind. Eng. Chem. Res. 50, 148–157.
<https://doi.org/10.1021/ie100440s>
- Bansal, V., 1994. Kinetic study of clathrate hydrates (PhD Thesis). Colorado School of Mines.
- Baraka-Lokmane, S., Hurtevent, C., Ohanessian, J.-L., Rousseau, G., Seiersten, M.E., Deshmush, S., 2012. Prediction of Mineral Scaling in a MEG Loop System of

- a Gas Production Offshore. Presented at the SPE International Conference on Oilfield Scale, Society of Petroleum Engineers. <https://doi.org/10.2118/155124-MS>
- Baraka-Lokmane, S., Hurtevent, Ch., Seiersten, M., Flaten, E., Farrell, M., Bradshaw, O., Hare, S., Bonis, M., Jacob, F., Carles, N., 2013. Technical challenges and solutions in a closed loop MEG regeneration system for gas field offshore, UK. Presented at the MULTIPHASE FLOW 2013, A Coruña, Spain, pp. 511–522. <https://doi.org/10.2495/MPF130421>
- Barmatov, E., Geddes, J., Hughes, T., Nagl, M., 2012. Research On Corrosion Inhibitors For Acid Stimulation. Presented at the CORROSION 2012, NACE International.
- Barmatov, E., Hughes, T., Nagl, M., 2015. Efficiency of film-forming corrosion inhibitors in strong hydrochloric acid under laminar and turbulent flow conditions. *Corrosion Science* 92, 85–94. <https://doi.org/10.1016/j.corsci.2014.11.038>
- Barrer, R.M., Stuart, W.I., 1957. Non-stoichiometric clathrate compounds of water. *Proceedings of the Royal Society of London. Series A. Mathematical and Physical Sciences* 243, 172–189. <https://doi.org/10.1098/rspa.1957.0213>
- Bates, R.G., 1964. Determination of pH: theory and practice. *Determination of pH: theory and practice*.
- Bikkina, C., Radhakrishnan, N., Jaiswal, S., Harrington, R., Charlesworth, M., 2012. Development of MEG Regeneration Unit Compatible Corrosion Inhibitor for Wet Gas Systems. Presented at the SPE Asia Pacific Oil and Gas Conference and Exhibition, Society of Petroleum Engineers. <https://doi.org/10.2118/160301-MS>
- BIPM, I., IFCC, I., IUPAC, I., ISO, O., 2008. Evaluation of measurement data—guide for the expression of uncertainty in measurement. *JCGM 100: 2008*. Citado en las 167.
- Bishnoi, P.R., Gupta, A.K., Englezos, P., Kalogerakis, N., 1989. Multiphase equilibrium flash calculations for systems containing gas hydrates. *Fluid Phase Equilibria, Proceedings of the Fifth International Conference* 53, 97–104. [https://doi.org/10.1016/0378-3812\(89\)80076-7](https://doi.org/10.1016/0378-3812(89)80076-7)
- Bishnoi, P.R., Natarajan, V., 1996. Formation and decomposition of gas hydrates. *Fluid Phase Equilibria, Proceedings of the Seventh International Conference on Fluid Properties and Phase Equilibria for Chemical Process Design* 117, 168–177. [https://doi.org/10.1016/0378-3812\(95\)02950-8](https://doi.org/10.1016/0378-3812(95)02950-8)
- Blackman, A.G., Gahan, author.), Lawrence R., 2014. *Aylward and Findlay's SI chemical data*, 7th edition. ed. Milton, Qld : John Wiley & Sons Australia.
- Braga, T.G., 1987. Effects of Commonly, Used Oilfield Chemicals on the Rate of Oxygen Scavenging by Sulfite/Bisulfite. *SPE Production Engineering* 2, 137–142. <https://doi.org/10.2118/13556-PA>
- Bratland, O., 2010. *Pipe Flow 2: Multi-Phase Flow Assurance*. Ove Bratland Flow Assurance Consulting, Chonburi, Thailand.
- Brkić, D., Tanasković, T.I., 2008. Systematic approach to natural gas usage for domestic heating in urban areas. *Energy* 33, 1738–1753. <https://doi.org/10.1016/j.energy.2008.08.009>
- Brown, P.W., Rossiter, W.J., Galuk, K.G., 1986. A mass spectrometric investigation of the thermal oxidative reactivity of ethylene glycol. *Solar Energy Materials* 13, 197–202. [https://doi.org/10.1016/0165-1633\(86\)90018-3](https://doi.org/10.1016/0165-1633(86)90018-3)

- Brustad, S., Løken, K.-P., Waalman, J.G., 2005. Hydrate Prevention using MEG instead of MeOH: Impact of experience from major Norwegian developments on technology selection for injection and recovery of MEG. Presented at the Offshore Technology Conference, Offshore Technology Conference. <https://doi.org/10.4043/17355-MS>
- Burgazli, C.R., Navarrete, R.C., Mead, S.L., 2005. New Dual Purpose Chemistry for Gas Hydrate and Corrosion Inhibition. *Journal of Canadian Petroleum Technology* 44. <https://doi.org/10.2118/05-11-04>
- Byk, S.S., Fomina, V.I., 1968. Gas Hydrates. *Russ. Chem. Rev.* 37, 469. <https://doi.org/10.1070/RC1968v037n06ABEH001654>
- Calsep PVTsim, 2011. . CALSEP A/S, Houston, Texas.
- Camargo, R., Gonçalves, M., Barreto, C., Faraco, R., Nieckele, A.O., 2011. On The Safety Of Hydrate Remediation By One-Sided Depressurization, in: *Proc. 7th Int. Conf. on Gas Hydrates*.
- Cao, Z., Tester, J.W., Trout, B.L., 2002. Sensitivity Analysis of Hydrate Thermodynamic Reference Properties Using Experimental Data and ab Initio Methods. *J. Phys. Chem. B* 106, 7681–7687. <https://doi.org/10.1021/jp0207376>
- Carroll, J., 2014. *Natural Gas Hydrates: A Guide for Engineers*. Gulf Professional Publishing.
- Carson, D.B., Katz, D.L., 1942. Natural Gas Hydrates. *Transactions of the AIME* 146, 150–158. <https://doi.org/10.2118/942150-G>
- Cha, M., Hu, Y., Sum, A.K., 2016. Methane hydrate phase equilibria for systems containing NaCl, KCl, and NH₄Cl. *Fluid Phase Equilibria, Special Issue: Gas Hydrates and Semiclathrate Hydrates* 413, 2–9. <https://doi.org/10.1016/j.fluid.2015.08.010>
- Cha, M., Shin, K., Kim, J., Chang, D., Seo, Y., Lee, H., Kang, S.-P., 2013. Thermodynamic and kinetic hydrate inhibition performance of aqueous ethylene glycol solutions for natural gas. *Chemical Engineering Science* 99, 184–190. <https://doi.org/10.1016/j.ces.2013.05.060>
- Chang, H.T., Posey, M., Rochelle, G.T., 1993. Thermodynamics of alkanolamine-water solutions from freezing point measurements. *Ind. Eng. Chem. Res.* 32, 2324–2335. <https://doi.org/10.1021/ie00022a016>
- Chapoy, A., Haghighi, H., Burgass, R., Tohidi, B., 2010. Gas hydrates in low water content gases: Experimental measurements and modelling using the CPA equation of state. *Fluid Phase Equilibria, Colloquium Dominique Richon* 296, 9–14. <https://doi.org/10.1016/j.fluid.2009.11.026>
- Chapoy, A., Tohidi, B., 2012. Hydrates in high MEG concentration systems, in: *Proceeding of the 3rd International Gas Processing Symposium*. pp. 5–7.
- Chatti, I., Delahaye, A., Fournaison, L., Petitet, J.-P., 2005. Benefits and drawbacks of clathrate hydrates: a review of their areas of interest. *Energy Conversion and Management* 46, 1333–1343. <https://doi.org/10.1016/j.enconman.2004.06.032>
- Chen, L.-T., Sun, C.-Y., Chen, G.-J., Zuo, J.Y., Ng, H.-J., 2010. Assessment of hydrate kinetic inhibitors with visual observations. *Fluid Phase Equilibria* 298, 143–149. <https://doi.org/10.1016/j.fluid.2010.07.024>
- Child, W.C., 1964. Molecular interactions in clathrates: a comparison with other condensed phases. *Q. Rev. Chem. Soc.* 18, 321–346. <https://doi.org/10.1039/QR9641800321>
- Chin, H.-Y., Hsieh, M.-K., Chen, Y.-P., Chen, P.-C., Lin, S.-T., Chen, L.-J., 2013.

- Prediction of phase equilibrium for gas hydrate in the presence of organic inhibitors and electrolytes by using an explicit pressure-dependent Langmuir adsorption constant in the van der Waals–Platteeuw model. *The Journal of Chemical Thermodynamics* 66, 34–43. <https://doi.org/10.1016/j.jct.2013.06.014>
- Christiansen, R.L., Sloan, E.D.J., 1995. A compact model for hydrate formation.
- Clifton, J.R., Rossiter, W.J., Brown, P.W., 1985. Degraded aqueous glycol solutions: pH values and the effects of common ions on suppressing pH decreases. *Solar Energy Materials* 12, 77–86. [https://doi.org/10.1016/0165-1633\(85\)90026-7](https://doi.org/10.1016/0165-1633(85)90026-7)
- Closmann, F., Nguyen, T., Rochelle, G.T., 2009. MDEA/Piperazine as a solvent for CO₂ capture. *Energy Procedia, Greenhouse Gas Control Technologies* 9 1, 1351–1357. <https://doi.org/10.1016/j.egypro.2009.01.177>
- Crolet, J.L., Thevenot, N., Dugstad, A., 1999. Role of Free Acetic Acid on the CO₂ Corrosion of Steels. Presented at the CORROSION 99, NACE International.
- Crowe, C., McConnell, S.B., Hinkel, J.J., Chapman, K., 1994. Scale Inhibition in Wellbores. Presented at the University of Tulsa Centennial Petroleum Engineering Symposium, Society of Petroleum Engineers. <https://doi.org/10.2118/27996-MS>
- Daraboina, N., Malmos, C., von Solms, N., 2013. Investigation of Kinetic Hydrate Inhibition Using a High Pressure Micro Differential Scanning Calorimeter. *Energy Fuels* 27, 5779–5786. <https://doi.org/10.1021/ef401042h>
- Davies, S.R., Selim, M.S., Sloan, E.D., Bollavaram, P., Peters, D.J., 2006. Hydrate plug dissociation. *AIChE Journal* 52, 4016–4027. <https://doi.org/10.1002/aic.11005>
- Davoudi, M., Heidari, Y., Safadoost, A., Samieirad, S., 2014. Chemical injection policy for internal corrosion prevention of South Pars sea-pipeline: A case study. *Journal of Natural Gas Science and Engineering* 21, 592–599. <https://doi.org/10.1016/j.jngse.2014.09.017>
- Davy, H., 1832. On a combination of oxymuriatic gas and oxygen gas. *Abstracts of the Papers Printed in the Philosophical Transactions of the Royal Society of London* 1, 393–394. <https://doi.org/10.1098/rspl.1800.0221>
- Dehaghani, A.H.S., Karami, B., 2018. A new predictive thermodynamic framework for phase behavior of gas hydrate. *Fuel* 216, 796–809. <https://doi.org/10.1016/j.fuel.2017.11.128>
- Derawi, S.O., Michelsen, M.L., Kontogeorgis, G.M., Stenby, E.H., 2003. Application of the CPA equation of state to glycol/hydrocarbons liquid–liquid equilibria. *Fluid Phase Equilibria* 209, 163–184. [https://doi.org/10.1016/S0378-3812\(03\)00056-6](https://doi.org/10.1016/S0378-3812(03)00056-6)
- Dharmawardhana, P.B., Parrish, W.R., Sloan, E.D., 1980. Experimental Thermodynamic Parameters for the Prediction of Natural Gas Hydrate Dissociation Conditions. *Ind. Eng. Chem. Fund.* 19, 410–414. <https://doi.org/10.1021/i160076a015>
- Duchateau, C., Peytavy, J.-L., Glénat, P., Pou, T.-E., Hidalgo, M., Dicharry, C., 2009. Laboratory Evaluation of Kinetic Hydrate Inhibitors: A Procedure for Enhancing the Repeatability of Test Results. *Energy Fuels* 23, 962–966. <https://doi.org/10.1021/ef800710x>
- Dugstad, A., Seiersten, M., 2004. pH-stabilisation, a Reliable Method for Corrosion Control of Wet Gas Pipelines. Presented at the SPE International Symposium on Oilfield Corrosion, Society of Petroleum Engineers.

<https://doi.org/10.2118/87560-MS>

- Dugstad, A., Seiersten, M., Nyborg, R., 2003. Flow Assurance of pH Stabilized Wet Gas Pipelines. Presented at the CORROSION 2003, NACE International.
- Dwyer, D.F., Tiedje, J.M., 1983. Degradation of ethylene glycol and polyethylene glycols by methanogenic consortia. *Appl. Environ. Microbiol.* 46, 185–190.
- Eichholz, C., Majumdar, A., Clarke, M.A., Oellrich, L.R., Bishnoi, P.R., 2004. Experimental Investigation and Calculation of Methane Hydrate Formation Conditions in the Presence of Ethylene Glycol and Sodium Chloride. *J. Chem. Eng. Data* 49, 847–851. <https://doi.org/10.1021/je034179f>
- El Meragawi, S., Diamantonis, N.I., Tsimpanogiannis, I.N., Economou, I.G., 2016. Hydrate – fluid phase equilibria modeling using PC-SAFT and Peng–Robinson equations of state. *Fluid Phase Equilibria, Special Issue: Gas Hydrates and Semiclathrate Hydrates* 413, 209–219. <https://doi.org/10.1016/j.fluid.2015.12.003>
- Englezos, P., 1993. Clathrate hydrates. *Ind. Eng. Chem. Res.* 32, 1251–1274. <https://doi.org/10.1021/ie00019a001>
- Eslamimanesh, A., Mohammadi, A.H., Richon, D., 2011. Thermodynamic model for predicting phase equilibria of simple clathrate hydrates of refrigerants. *Chemical Engineering Science* 66, 5439–5445. <https://doi.org/10.1016/j.ces.2011.06.062>
- Evans, W.H., David, E.J., 1974. Biodegradation of mono-, di- and triethylene glycols in river waters under controlled laboratory conditions. *Water Research* 8, 97–100. [https://doi.org/10.1016/0043-1354\(74\)90132-8](https://doi.org/10.1016/0043-1354(74)90132-8)
- Ezrin, M., Zepke, A., Helwig, J., Lavigne, G., Dudley, M., 2000. Plastics failure due to oxidative degradation in processing and service, in: *SPE ANTEC Proceedings*.
- Flaten, E.M., 2010. The effect of MEG (mono ethyleneglycol) on the precipitation kinetics of calcium carbonate related to natural gas production from subsea wells. NTNU.
- Flaten, E.M., Watterud, G., Andreassen, J.-P., Seiersten, M.E., 2008. Precipitation of Iron and Calcium Carbonate in Pipelines at Varying MEG Contents. Presented at the SPE International Oilfield Scale Conference, Society of Petroleum Engineers. <https://doi.org/10.2118/114089-MS>
- Franks, F., Darlington, J., Schenz, T., Mathias, S.F., Slade, L., Levine, H., 1987. Antifreeze activity of Antarctic fish glycoprotein and a synthetic polymer. *Nature* 325, 146–147. <https://doi.org/10.1038/325146a0>
- Freitas, A.M., Lobão, A.C., Cardoso, C.B., 2002. Hydrate Blockages in Flowlines and Subsea Equipment in Campos Basin. Presented at the Offshore Technology Conference, Offshore Technology Conference. <https://doi.org/10.4043/14257-MS>
- Fujioka, Y., Takeuchi, K., Shindo, Y., Komiyama, H., 1994. Shrinkage of liquid CO₂ droplets in water. *International Journal of Energy Research* 18, 765–769. <https://doi.org/10.1002/er.4440180807>
- Garverick, L., 1994. *Corrosion in the Petrochemical Industry*. ASM International.
- Gazzard, J., 2008. *Aviation and climate change: Can alternative fuel save the day?* Aviation Environment Federation, London, UK.
- Giavarini, C., Hester, K., 2011. *Gas Hydrates: Immense Energy Potential and Environmental Challenges*. Springer Science & Business Media.
- Glenat, P., Peytavy, J.-L., Holland-Jones, N., Grainger, M., 2004. *South-Pars Phases*

- 2 and 3: The Kinetic Hydrate Inhibitor (KHI) Experience Applied at Field Start-up. Presented at the Abu Dhabi International Conference and Exhibition, Society of Petroleum Engineers. <https://doi.org/10.2118/88751-MS>
- Grzelak, E.M., Stenhaug, M., 2016. A More Efficient Use of MEG to Fully Inhibit Hydrates with Reduced Cost. Presented at the Offshore Technology Conference Asia, Offshore Technology Conference. <https://doi.org/10.4043/26854-MS>
- Gulbrandsen, E., Kvarekvål, J., Miland, H., 2005. Effect of Oxygen Contamination on Inhibition Studies in Carbon Dioxide Corrosion. *CORROSION* 61, 1086–1097. <https://doi.org/10.5006/1.3280625>
- Hagerup, O., Olsen, S., 2003. Corrosion Control by pH Stabilizer, Materials and Corrosion Monitoring in 160 km Multiphase Offshore Pipeline. Presented at the CORROSION 2003, NACE International.
- Haghighi, H., Chapoy, A., Burgess, R., Mazloum, S., Tohidi, B., 2009a. Phase equilibria for petroleum reservoir fluids containing water and aqueous methanol solutions: Experimental measurements and modelling using the CPA equation of state. *Fluid Phase Equilibria* 278, 109–116. <https://doi.org/10.1016/j.fluid.2009.01.009>
- Haghighi, H., Chapoy, A., Burgess, R., Tohidi, B., 2009b. Experimental and thermodynamic modelling of systems containing water and ethylene glycol: Application to flow assurance and gas processing. *Fluid Phase Equilibria* 276, 24–30. <https://doi.org/10.1016/j.fluid.2008.10.006>
- Haghtalab, A., Zare, M., Ahmadi, A.N., Nazari, K., 2012. Prediction of hydrate equilibrium conditions using Electrolyte Cubic Square-Well Equation of State. *Fluid Phase Equilibria* 333, 74–86. <https://doi.org/10.1016/j.fluid.2012.07.022>
- Halvorsen, A.M.K., Andersen, T.R., 2003. PH Stabilization for Internal Corrosion Protection of Pipeline Carrying Wet Gas With CO₂ and Acetic Acid. Presented at the CORROSION 2003, NACE International.
- Halvorsen, A.M.K., Andersen, T.R., Halvorsen, E.N., Kojen, G.P., Skar, J.I., Biørnstad, C., Fitje, H., 2007. The Relationship Between Internal Corrosion Control Method, Scale Control And Meg Handling Of A Multiphase Carbon Steel Pipeline Carrying Wet Gas With CO₂ And Cetic Acid. Presented at the CORROSION 2007, NACE International.
- Halvorsen, E.N., Halvorsen, A.M.K., Andersen, T.R., Biørnstad, C., Reiersolmen, K., 2009. Qualification of Scale Inhibitors for Subsea Tiebacks With MEG Injection. Presented at the SPE International Symposium on Oilfield Chemistry, Society of Petroleum Engineers. <https://doi.org/10.2118/121665-MS>
- Halvorsen, E.N., Halvorsen, A.M.K., Ramstad, K., Tydal, T., Biørnstad, C., 2006. Scale Inhibitor Testing for Multiphase Pipelines in a Subsea to Shore Development with a Closed MEG-loop System. Presented at the SPE International Oilfield Scale Symposium, Society of Petroleum Engineers. <https://doi.org/10.2118/100662-MS>
- Hammerschmidt, E.G., 1934. Formation of Gas Hydrates in Natural Gas Transmission Lines. *Ind. Eng. Chem.* 26, 851–855. <https://doi.org/10.1021/ie50296a010>
- Haque, M.E., 2012. Ethylene Glycol Regeneration Plan: A Systematic Approach to Troubleshoot the Common Problems. *Journal of Chemical Engineering* 27, 21–26. <https://doi.org/10.3329/jce.v27i1.15853>
- Heidaryan, E., Salarabadi, A., Moghadasi, J., Dourbash, A., 2010. A new high

- performance gas hydrate inhibitor. *Journal of Natural Gas Chemistry* 19, 323–326. [https://doi.org/10.1016/S1003-9953\(09\)60060-8](https://doi.org/10.1016/S1003-9953(09)60060-8)
- Hemmingsen, P.V., Burgass, R., Pedersen, K.S., Kinnari, K., Sørensen, H., 2011. Hydrate temperature depression of MEG solutions at concentrations up to 60wt%. Experimental data and simulation results. *Fluid Phase Equilibria* 307, 175–179. <https://doi.org/10.1016/j.fluid.2011.05.010>
- Holder, G.D., Corbin, G., Papadopoulos, K.D., 1980. Thermodynamic and Molecular Properties of Gas Hydrates from Mixtures Containing Methane, Argon, and Krypton. *Ind. Eng. Chem. Fund.* 19, 282–286. <https://doi.org/10.1021/i160075a008>
- Holz, F., Richter, P.M., Egging, R., 2015. A Global Perspective on the Future of Natural Gas: Resources, Trade, and Climate Constraints. *Rev Environ Econ Policy* 9, 85–106. <https://doi.org/10.1093/reep/reu016>
- Hossainpour, R., 2013. Catalysts for Enhanced CO₂-CH₄ Exchange in Natural Gas Hydrates. An experimental feasibility study of exchange enhancement by use of chemical additives (Thesis). The University of Bergen.
- Hsieh, M.-K., Ting, W.-Y., Chen, Y.-P., Chen, P.-C., Lin, S.-T., Chen, L.-J., 2012. Explicit pressure dependence of the Langmuir adsorption constant in the van der Waals–Platteeuw model for the equilibrium conditions of clathrate hydrates. *Fluid Phase Equilibria* 325, 80–89. <https://doi.org/10.1016/j.fluid.2012.04.012>
- Huang, S.H., Radosz, M., 1990. Equation of state for small, large, polydisperse, and associating molecules. *Ind. Eng. Chem. Res.* 29, 2284–2294. <https://doi.org/10.1021/ie00107a014>
- Huo, Z., Freer, E., Lamar, M., Sannigrahi, B., Knauss, D.M., Sloan, E.D., 2001. Hydrate plug prevention by anti-agglomeration. *Chemical Engineering Science* 56, 4979–4991. [https://doi.org/10.1016/S0009-2509\(01\)00188-9](https://doi.org/10.1016/S0009-2509(01)00188-9)
- Idem, R., Wilson, M., Tontiwachwuthikul, P., Chakma, A., Veawab, A., Aroonwilas, A., Gelowitz, D., 2006. Pilot Plant Studies of the CO₂ Capture Performance of Aqueous MEA and Mixed MEA/MDEA Solvents at the University of Regina CO₂ Capture Technology Development Plant and the Boundary Dam CO₂ Capture Demonstration Plant. *Ind. Eng. Chem. Res.* 45, 2414–2420. <https://doi.org/10.1021/ie050569e>
- Ikeh, L., Enyi, G.C., Nasr, G.G., 2016. Inhibition Performance of Mild Steel Corrosion in the Presence of CO₂, HAc and MEG. Presented at the SPE International Oilfield Corrosion Conference and Exhibition, Society of Petroleum Engineers. <https://doi.org/10.2118/179942-MS>
- Infochem Multiflash, 2007. . Infochem Computer Services Ltd., London, U.K.
- Ivonye, I.C., 2014. Corrosion processes and mechanisms in the presence of MonoEthylene Glycol (MEG) (phd). University of Leeds.
- Jamaluddin, A.K.M., Kabir, C.S., 2012. Flow assurance: Managing flow dynamics and production chemistry. *Journal of Petroleum Science and Engineering* 100, 106–116. <https://doi.org/10.1016/j.petrol.2012.11.017>
- Jaramillo, P., Griffin, W.M., Matthews, H.S., 2007. Comparative Life-Cycle Air Emissions of Coal, Domestic Natural Gas, LNG, and SNG for Electricity Generation. *Environ. Sci. Technol.* 41, 6290–6296. <https://doi.org/10.1021/es063031o>
- Jeffrey, G.A., McMullan, R.K., 2007. The Clathrate Hydrates, in: *Progress in Inorganic Chemistry*. John Wiley & Sons, Ltd, pp. 43–108.

- <https://doi.org/10.1002/9780470166093.ch2>
- Jensen, L., Thomsen, K., von Solms, N., 2008. Propane hydrate nucleation: Experimental investigation and correlation. *Chemical Engineering Science* 63, 3069–3080. <https://doi.org/10.1016/j.ces.2008.03.006>
- Jhaveri, J., Robinson, D.B., 1965. Hydrates in the methane-nitrogen system. *The Canadian Journal of Chemical Engineering* 43, 75–78. <https://doi.org/10.1002/cjce.5450430207>
- John, D., Kinsella, B., Bailey, S., De Marco, R., 2009. Flow Dependence of Carbon Dioxide Corrosion Using Short Electrodes by Jet Impingement. *CORROSION* 65, 771–777. <https://doi.org/10.5006/1.3319103>
- John, V.T., Papadopoulos, K.D., Holder, G.D., 1985. A generalized model for predicting equilibrium conditions for gas hydrates. *AIChE Journal* 31, 252–259. <https://doi.org/10.1002/aic.690310212>
- Joosten, M.W., Tier, B., Seiersten, M., Wintermark, C., 2007. Materials Considerations for MEG (Mono Ethylene Glycol) Reclamation Systems. Presented at the CORROSION 2007, NACE International.
- Jordan, M., Temple, E., Sham, A., Williams, H., McCallum, C., 2019. Investigation into the Synergistic Interaction of a Range of Generic Scale Inhibitors for Improved Sulphate Scale Control in North Sea Topside Processes. Presented at the SPE International Conference on Oilfield Chemistry, Society of Petroleum Engineers. <https://doi.org/10.2118/193613-MS>
- Jordan, M.M., Feasey, N.D., Johnston, C., 2005. Inorganic Scale Control Within MEG/Methanol Treated Produced Fluids. Presented at the SPE International Symposium on Oilfield Scale, Society of Petroleum Engineers. <https://doi.org/10.2118/95034-MS>
- Kamal, M.S., Hussein, I.A., Sultan, A.S., von Solms, N., 2016. Application of various water soluble polymers in gas hydrate inhibition. *Renewable and Sustainable Energy Reviews* 60, 206–225. <https://doi.org/10.1016/j.rser.2016.01.092>
- Kamimura, A., Guerra, S.M.G., Sauer, I.L., 2006. On the substitution of energy sources: Prospective of the natural gas market share in the Brazilian urban transportation and dwelling sectors. *Energy Policy* 34, 3583–3590. <https://doi.org/10.1016/j.enpol.2005.07.020>
- Kan, A.T., Fu, G., Tomson, M.B., 2002a. Effect of Methanol on Carbonate Equilibrium and Calcite Solubility in a Gas/Methanol/Water/Salt Mixed System. *Langmuir* 18, 9713–9725. <https://doi.org/10.1021/la025620n>
- Kan, A.T., Fu, G., Watson, M.A., Tomson, M.B., 2002b. Effect of Hydrate Inhibitors on Oilfield Scale Formation and Inhibition. Presented at the International Symposium on Oilfield Scale, Society of Petroleum Engineers. <https://doi.org/10.2118/74657-MS>
- Karamoddin, M., Varaminian, F., 2013. Experimental measurement of phase equilibrium for gas hydrates of refrigerants, and thermodynamic modeling by SRK, VPT and CPA EOSs. *The Journal of Chemical Thermodynamics* 65, 213–219. <https://doi.org/10.1016/j.jct.2013.06.001>
- Kashchiev, D., Firoozabadi, A., 2002. Nucleation of gas hydrates. *Journal of Crystal Growth* 243, 476–489. [https://doi.org/10.1016/S0022-0248\(02\)01576-2](https://doi.org/10.1016/S0022-0248(02)01576-2)
- Katz, D.L., 1945. Prediction of Conditions for Hydrate Formation in Natural Gases. *Transactions of the AIME* 160, 140–149. <https://doi.org/10.2118/945140-G>
- Kelland, M.A., 2009. *Production chemicals for the oil and gas industry*. Boca Raton : CRC Press.

- Kelland, M.A., 2006. History of the Development of Low Dosage Hydrate Inhibitors. *Energy Fuels* 20, 825–847. <https://doi.org/10.1021/ef050427x>
- Kelland, M.A., Svartaas, T.M., Øvsthus, J., Namba, T., 2000. A New Class of Kinetic Hydrate Inhibitor. *Annals of the New York Academy of Sciences* 912, 281–293. <https://doi.org/10.1111/j.1749-6632.2000.tb06782.x>
- Khan, M.N., Warriar, P., Peters, C.J., Koh, C.A., 2018. Advancements in hydrate phase equilibria and modeling of gas hydrates systems. *Fluid Phase Equilibria* 463, 48–61. <https://doi.org/10.1016/j.fluid.2018.01.014>
- Kim, H., Yoo, W., Lim, Y., Seo, Y., 2018. Economic evaluation of MEG injection and regeneration process for oil FPSO. *Journal of Petroleum Science and Engineering* 164, 417–426. <https://doi.org/10.1016/j.petrol.2018.01.071>
- Kim, J., Kim, H., Sohn, Y. hoon, Chang, D., Seo, Y., Kang, S.-P., 2017. Prevention of methane hydrate re-formation in transport pipeline using thermodynamic and kinetic hydrate inhibitors. *Journal of Petroleum Science and Engineering* 154, 114–125. <https://doi.org/10.1016/j.petrol.2017.04.011>
- Kim, Jakyung, Shin, K., Kim, Juneyoung, Chang, D., Seo, Y., Chang, K.P., 2014. Kinetic Hydrate Inhibition Performance of MEG in Under-Inhibition System: Reduction Opportunities of MEG Injection for Offshore Gas Field Developments. Presented at the Offshore Technology Conference-Asia, Offshore Technology Conference. <https://doi.org/10.4043/24961-MS>
- Kimuro, H., Yamaguchi, F., Ohtsubo, K., Kusayanagi, T., Morishita, M., 1993. CO₂ clathrate formation and its properties in a simulated deep ocean. *Energy Conversion and Management, Proceedings of the International Energy Agency Carbon Dioxide Disposal Symposium* 34, 1089–1094. [https://doi.org/10.1016/0196-8904\(93\)90057-H](https://doi.org/10.1016/0196-8904(93)90057-H)
- Kirchner, M.T., Boese, R., Billups, W.E., Norman, L.R., 2004. Gas Hydrate Single-Crystal Structure Analyses. *J. Am. Chem. Soc.* 126, 9407–9412. <https://doi.org/10.1021/ja049247c>
- Kitaigorodsky, A.I., 1984. Particle Packing in a Crystal, in: Kitaigorodsky, A.I. (Ed.), *Mixed Crystals*, Springer Series in Solid-State Sciences. Springer Berlin Heidelberg, Berlin, Heidelberg, pp. 49–84. https://doi.org/10.1007/978-3-642-81672-7_3
- Klauda, J., Sandler, S., 2003. Phase behavior of clathrate hydrates: a model for single and multiple gas component hydrates. *Chemical Engineering Science* 58, 27–41. [https://doi.org/10.1016/S0009-2509\(02\)00435-9](https://doi.org/10.1016/S0009-2509(02)00435-9)
- Knott, T., 2001. Holding hydrates at bay. *Offshore Engineer* 45, 29–34.
- Koh, C.A., 2002. Towards a fundamental understanding of natural gas hydrates. *Chem. Soc. Rev.* 31, 157–167. <https://doi.org/10.1039/B008672J>
- Koh, C.A., Sloan, E.D., Sum, A.K., Wu, D.T., 2011. Fundamentals and Applications of Gas Hydrates. *Annual Review of Chemical and Biomolecular Engineering* 2, 237–257. <https://doi.org/10.1146/annurev-chembioeng-061010-114152>
- Koh, C.A., Westacott, R.E., Zhang, W., Hirachand, K., Creek, J.L., Soper, A.K., 2002. Mechanisms of gas hydrate formation and inhibition. *Fluid Phase Equilibria, Proceedings of the Ninth International Conference on Properties and Phase Equilibria for Product and Process Design* 194–197, 143–151. [https://doi.org/10.1016/S0378-3812\(01\)00660-4](https://doi.org/10.1016/S0378-3812(01)00660-4)
- Kohl, A.L., Nielsen, R., 1997. *Gas Purification*. Elsevier.
- Kontogeorgis, G.M., Folas, G.K., 2009. *Thermodynamic Models for Industrial Applications: From Classical and Advanced Mixing Rules to Association*

- Theories. John Wiley & Sons.
- Kontogeorgis, G.M., V. Yakoumis, I., Meijer, H., Hendriks, E., Moorwood, T., 1999. Multicomponent phase equilibrium calculations for water–methanol–alkane mixtures. *Fluid Phase Equilibria* 158–160, 201–209. [https://doi.org/10.1016/S0378-3812\(99\)00060-6](https://doi.org/10.1016/S0378-3812(99)00060-6)
- Kontogeorgis, G.M., Voutsas, E.C., Yakoumis, I.V., Tassios, D.P., 1996. An Equation of State for Associating Fluids. *Ind. Eng. Chem. Res.* 35, 4310–4318. <https://doi.org/10.1021/ie9600203>
- Kundu, S.S., Seiersten, M., 2017. Development of a non-sulphite oxygen scavenger for monoethylene glycol (MEG) used as gas hydrate inhibitor. *Journal of Petroleum Science and Engineering* 158, 120–128. <https://doi.org/10.1016/j.petrol.2017.07.041>
- Kvamme, B., Kuznetsova, T., Aasoldsen, K., 2005. Molecular dynamics simulations for selection of kinetic hydrate inhibitors. *Journal of Molecular Graphics and Modelling* 23, 524–536. <https://doi.org/10.1016/j.jmkgm.2005.04.001>
- Kvarekval, J., Nyborg, R., Seiersten, M., 2002. Corrosion Product Films on Carbon Steel in Semi-Sour CO₂/H₂S Environments. Presented at the CORROSION 2002, NACE International.
- Latta, T.M., Palejwala, A.A., Tipson, S.K., Haigh, N.P., 2016. Design Considerations for Mitigating the Impact of Contaminants in Rich MEG on Monoethylene Glycol Recovery Unit MRU Performance. Presented at the Offshore Technology Conference Asia, Offshore Technology Conference. <https://doi.org/10.4043/26456-MS>
- Latta, T.M., Seiersten, M.E., Bufton, S.A., 2013. Flow Assurance Impacts on Lean/Rich MEG Circuit Chemistry and MEG Regenerator/Reclaimer Design. Presented at the Offshore Technology Conference, Offshore Technology Conference. <https://doi.org/10.4043/24177-MS>
- Lawson, J.D., Garst, A.W., 1976. Gas sweetening data: equilibrium solubility of hydrogen sulfide and carbon dioxide in aqueous monoethanolamine and aqueous diethanolamine solutions. *J. Chem. Eng. Data* 21, 20–30. <https://doi.org/10.1021/je60068a010>
- Lee, J.D., Englezos, P., 2005. Enhancement of the performance of gas hydrate kinetic inhibitors with polyethylene oxide. *Chemical Engineering Science* 60, 5323–5330. <https://doi.org/10.1016/j.ces.2005.05.023>
- Lee, S.-Y., Holder, G.D., 2002. Model for gas hydrate equilibria using a variable reference chemical potential: Part 1. *AIChE Journal* 48, 161–167. <https://doi.org/10.1002/aic.690480116>
- Lehmann, M.N., Bowman, C.W., Mok, W.Y., Barr, N.J., 2016. Application of oxygen scavengers to glycol systems. US9249516B2.
- Lehmann, M.N., Lamm, A., Nguyen, H.M., Bowman, C.W., Mok, W.Y., Salasi, M., Gubner, R., 2014. Corrosion Inhibitor and Oxygen Scavenger for use as MEG Additives in the Inhibition of Wet Gas Pipelines. Presented at the Offshore Technology Conference-Asia, Offshore Technology Conference. <https://doi.org/10.4043/25070-MS>
- Li, X.-S., Wu, H.-J., Englezos, P., 2006. Prediction of Gas Hydrate Formation Conditions in the Presence of Methanol, Glycerol, Ethylene Glycol, and Triethylene Glycol with the Statistical Associating Fluid Theory Equation of State. *Ind. Eng. Chem. Res.* 45, 2131–2137. <https://doi.org/10.1021/ie051204x>
- Liu, D., Chen, Z., Guo, X., 2008. The effect of acetic acid and acetate on CO₂

- corrosion of carbon steel. *Anti-Corrosion Methods and Materials*. <https://doi.org/10.1108/00035590810870437>
- Liu, X., Jungang, L., Qianya, Z., Jinlai, F., Yingli, L., Jingxin, S., 2009. The analysis and prediction of scale accumulation for water-injection pipelines in the Daqing Oilfield. *Journal of Petroleum Science and Engineering* 66, 161–164. <https://doi.org/10.1016/j.petrol.2009.02.007>
- Liu, Yucheng, Wu, D., Chen, M., Zhang, B., Chen, J., Liu, Yuanzhi, 2015. Identification of Methyldiethanolamine Degradation Products and Their Influence on Foaming Properties during the Desulfurization Process for High-Sulfurous Natural Gas. *Ind. Eng. Chem. Res.* 54, 5836–5841. <https://doi.org/10.1021/ie504432d>
- Loken, K., Li, X., Austvik, T., 1998. The hydrate control strategy for the Asgard field and hydrate plug melting using the bundle heating method, in: BHR Group Conference Series. Professional Engineering Publishing, Bury St. Edmunds, pp. 491–506.
- Lone, A., Kelland, M.A., 2013. Exploring Kinetic Hydrate Inhibitor Test Methods and Conditions Using a Multicell Steel Rocker Rig. *Energy Fuels* 27, 2536–2547. <https://doi.org/10.1021/ef400321z>
- Long, J.P., Sloan, E.D., 1996. Hydrates in the ocean and evidence for the location of hydrate formation. *Int J Thermophys* 17, 1–13. <https://doi.org/10.1007/BF01448204>
- López, D.A., Pérez, T., Simison, S.N., 2003. The influence of microstructure and chemical composition of carbon and low alloy steels in CO₂ corrosion. A state-of-the-art appraisal. *Materials & Design* 24, 561–575. [https://doi.org/10.1016/S0261-3069\(03\)00158-4](https://doi.org/10.1016/S0261-3069(03)00158-4)
- Lu, H., Matsumoto, R., Tsuji, Y., Oda, H., 2001. Anion plays a more important role than cation in affecting gas hydrate stability in electrolyte solution? — a recognition from experimental results. *Fluid Phase Equilibria* 178, 225–232. [https://doi.org/10.1016/S0378-3812\(00\)00464-7](https://doi.org/10.1016/S0378-3812(00)00464-7)
- Lu, Z., Sultan, N., 2008. Empirical expressions for gas hydrate stability law, its volume fraction and mass-density at temperatures 273.15K to 290.15K. *Geochemical Journal* 42, 163–175. <https://doi.org/10.2343/geochemj.42.163>
- Luna-Ortiz, E., Healey, M., Anderson, R., Sørhaug, E., 2014. Crystal Growth Inhibition Studies for the Qualification of a Kinetic Hydrate Inhibitor under Flowing and Shut-In Conditions. *Energy Fuels* 28, 2902–2913. <https://doi.org/10.1021/ef402493x>
- Lv, Q., Zang, X., Li, X., Li, G., 2018. Effect of seawater ions on cyclopentane-methane hydrate phase equilibrium. *Fluid Phase Equilibria* 458, 272–277. <https://doi.org/10.1016/j.fluid.2017.11.031>
- Madera, M., Höflinger, W., Kadnar, R., 2003. Ion chromatographic identification and quantification of glycol degradation products. *Journal of Chromatography A, 15th International Ion Chromatography Symposium* 997, 279–284. [https://doi.org/10.1016/S0021-9673\(03\)00060-8](https://doi.org/10.1016/S0021-9673(03)00060-8)
- Maekawa, T., 2001. Equilibrium conditions for gas hydrates of methane and ethane mixtures in pure water and sodium chloride solution. *Geochemical Journal* 35, 59–66. <https://doi.org/10.2343/geochemj.35.59>
- Makogon, T.Y., Larsen, R., Knight, C.A., Dendy Sloan, E., 1997. Melt growth of tetrahydrofuran clathrate hydrate and its inhibition: method and first results. *Journal of Crystal Growth* 179, 258–262. [212](https://doi.org/10.1016/S0022-</p>
</div>
<div data-bbox=)

- Makogon, Y.F., 1965. A gas hydrate formation in the gas saturated layers under low temperature. *Gas Industry* 5, 14–15.
- Malegaonkar, M.B., Dholabhai, P.D., Bishnoi, P.R., 1997. Kinetics of carbon dioxide and methane hydrate formation. *The Canadian Journal of Chemical Engineering* 75, 1090–1099. <https://doi.org/10.1002/cjce.5450750612>
- Marshall, D.R., Saito, S., Kobayashi, R., 1964. Hydrates at high pressures: Part I. Methane-water, argon-water, and nitrogen-water systems. *AIChE Journal* 10, 202–205. <https://doi.org/10.1002/aic.690100214>
- Martin, R.L., 2001. Corrosion Consequences of Oxygen Entry Into Sweet Oilfield Fluids. Presented at the SPE Annual Technical Conference and Exhibition, Society of Petroleum Engineers. <https://doi.org/10.2118/71470-MS>
- McGinnis, B.D., Adams, V.D., Middlebrooks, E.J., 2000. Degradation of ethylene glycol in photo Fenton systems. *Water Research* 34, 2346–2354. [https://doi.org/10.1016/S0043-1354\(99\)00387-5](https://doi.org/10.1016/S0043-1354(99)00387-5)
- McIntyre, G., Hlavinka, M., Hernandez, V., Bryan, T., 2004. Hydrate Inhibition with Methanol—A Review and New Concerns over Experimental Data Presentation, in: 83rd Annual GPA Convention, New Orleans.
- McKoy, V., Sinanoğlu, O., 1963. Theory of Dissociation Pressures of Some Gas Hydrates. *J. Chem. Phys.* 38, 2946–2956. <https://doi.org/10.1063/1.1733625>
- McLeod, H.O.J., Campbell, J.M., 1961. Natural Gas Hydrates at Pressures to 10,000 psia. *Journal of Petroleum Technology* 13, 590–594. <https://doi.org/10.2118/1566-G-PA>
- Mech, D., Pandey, G., Sangwai, J.S., 2015. Effect of Molecular Weight of Polyethylene Glycol on the Equilibrium Dissociation Pressures of Methane Hydrate System. *J. Chem. Eng. Data* 60, 1878–1885. <https://doi.org/10.1021/acs.jced.5b00088>
- Mehta, A.P., Hebert, P.B., Cadena, E.R., Weatherman, J.P., 2002. Fulfilling the Promise of Low Dosage Hydrate Inhibitors: Journey from Academic Curiosity to Successful Field Implementation. Presented at the Offshore Technology Conference, Offshore Technology Conference. <https://doi.org/10.4043/14057-MS>
- Mendez, C., Singer, M., Comacho, A., Nesic, S., Hernandez, S., Sun, Y., Gunaltun, Y., Joosten, M.W., 2005. Effect of Acetic Acid, pH and MEG on the CO₂ Top of the Line Corrosion. Presented at the CORROSION 2005, NACE International.
- Mohammadi, A.H., Richon, D., 2009. Methane hydrate phase equilibrium in the presence of salt (NaCl, KCl, or CaCl₂)+ethylene glycol or salt (NaCl, KCl, or CaCl₂)+methanol aqueous solution: Experimental determination of dissociation condition. *The Journal of Chemical Thermodynamics* 41, 1374–1377. <https://doi.org/10.1016/j.jct.2009.06.012>
- Mohebbi, V., Naderifar, A., Behbahani, R.M., Moshfeghian, M., 2012. Investigation of kinetics of methane hydrate formation during isobaric and isochoric processes in an agitated reactor. *Chemical Engineering Science* 76, 58–65. <https://doi.org/10.1016/j.ces.2012.04.016>
- Montazaud, T., 2011. Precipitation of carbonates in the pretreatment process for regeneration of ethylene glycol (Master's Thesis). Institut for kjemisk prosessteknologi.
- Monticelli, C., Brunoro, G., Frignani, A., Zucchi, F., 1988. Corrosion behaviour of

- AA 6351 in glycol/water solutions degraded at elevated temperature 39, 379–384.
- Moon, C., Taylor, P.C., Rodger, P.M., 2003. Molecular Dynamics Study of Gas Hydrate Formation. *J. Am. Chem. Soc.* 125, 4706–4707. <https://doi.org/10.1021/ja028537v>
- Mori, Y.H., 1998. Clathrate hydrate formation at the interface between liquid CO₂ and water phases—a review of rival models characterizing “hydrate films.” *Energy Conversion and Management* 39, 1537–1557. [https://doi.org/10.1016/S0196-8904\(98\)00029-6](https://doi.org/10.1016/S0196-8904(98)00029-6)
- Mullin, J.W., 2001. *Crystallization*. Elsevier.
- Mussini, P.R., Marcolungo, I., Rondinini, S., Longhi, P., 1991. Acid-base equilibria and acidity scales in ethylene glycol/water solvent mixtures: Recommended reference-value ph-metric standards and ionization constants for ophthalmic acid at normal and subzero temperatures. *Chimica e l’Industria* 73, 262–268.
- Nagata, I., Kobayashi, R., 1966. Calculation of Dissociation Pressures of Gas Hydrates Using Kihara Model. *Ind. Eng. Chem. Fund.* 5, 344–348. <https://doi.org/10.1021/i160019a009>
- Natarajan, V., Bishnoi, P.R., Kalogerakis, N., 1994. Induction phenomena in gas hydrate nucleation. *Chemical Engineering Science* 49, 2075–2087. [https://doi.org/10.1016/0009-2509\(94\)E0026-M](https://doi.org/10.1016/0009-2509(94)E0026-M)
- Nazzer, C.A., Keogh, J., 2006. *Advances in Glycol Reclamation Technology*. Presented at the Offshore Technology Conference, Offshore Technology Conference. <https://doi.org/10.4043/18010-MS>
- Nerheim, A.R., 1993. Investigation of gas hydrate formation kinetics by laser light scattering.
- Nguyen, N.N., Nguyen, A.V., 2015. The dual effect of sodium halides on the formation of methane gas hydrate. *Fuel* 156, 87–95. <https://doi.org/10.1016/j.fuel.2015.04.022>
- Nyborg, R., 2009. Pipeline corrosion prevention by ph stabilization or corrosion inhibitors, in: *Rio Pipeline Conference and Exposition*.
- Nyborg, R., Dugstad, A., 2009. Flow Assurance of Wet Gas Pipelines From a Corrosion Viewpoint. Presented at the ASME 2002 21st International Conference on Offshore Mechanics and Arctic Engineering, American Society of Mechanical Engineers Digital Collection, pp. 125–132. <https://doi.org/10.1115/OMAE2002-28294>
- Obanijesu, E.O., Akindeju, M.K., Vishnu, P., Tade, M.O., 2011. Modelling the Natural Gas Pipeline Internal Corrosion Rate Resulting from Hydrate Formation, in: Pistikopoulos, E.N., Georgiadis, M.C., Kokossis, A.C. (Eds.), *Computer Aided Chemical Engineering, 21 European Symposium on Computer Aided Process Engineering*. Elsevier, pp. 1160–1164. <https://doi.org/10.1016/B978-0-444-54298-4.50011-8>
- Obanijesu, E.O., Gubner, R., Barifcani, A., Pareek, V., Tade, M.O., 2014. The influence of corrosion inhibitors on hydrate formation temperature along the subsea natural gas pipelines. *Journal of Petroleum Science and Engineering* 120, 239–252. <https://doi.org/10.1016/j.petrol.2014.05.025>
- Olajire, A.A., 2015. A review of oilfield scale management technology for oil and gas production. *Journal of Petroleum Science and Engineering* 135, 723–737. <https://doi.org/10.1016/j.petrol.2015.09.011>
- Olsen, S., 2006. *Corrosion Control by Inhibition, Environmental Aspects, and pH*

- Control: Part II: Corrosion Control by pH Stabilization. Presented at the CORROSION 2006, NACE International.
- Olsen, S., Halvorsen, A.M.K., 2015. Corrosion Control by pH Stabilization. Presented at the CORROSION 2015, NACE International.
- Østergaard, K.K., Tohidi, B., Burgass, R.W., Danesh, A., Todd, A.C., 2001. Hydrate Equilibrium Data of Multicomponent Systems in the Presence of Structure-II and Structure-H Heavy Hydrate Formers. *J. Chem. Eng. Data* 46, 703–708. <https://doi.org/10.1021/je0003086>
- Papavinasam, S., Doiron, A., Panneerselvam, T., Revie, R.W., 2007. Effect of Hydrocarbons on the Internal Corrosion of Oil and Gas Pipelines. *CORROSION* 63, 704–712. <https://doi.org/10.5006/1.3278419>
- Park, J., Kim, H., Sheng, Q., Wood, C.D., Seo, Y., 2017. Kinetic Hydrate Inhibition Performance of Poly(vinyl caprolactam) Modified with Corrosion Inhibitor Groups. *Energy Fuels* 31, 9363–9373. <https://doi.org/10.1021/acs.energyfuels.7b01956>
- Park, S.-W., Lee, Joon-Wook, Choi, B.-S., Lee, Jae-Wook, 2006. Absorption of carbon dioxide into non-aqueous solutions of N-methyldiethanolamine. *Korean J. Chem. Eng.* 23, 806–811. <https://doi.org/10.1007/BF02705932>
- Parrish, W.R., Prausnitz, J.M., 1972. Dissociation Pressures of Gas Hydrates Formed by Gas Mixtures. *Ind. Eng. Chem. Proc. Des. Dev.* 11, 26–35. <https://doi.org/10.1021/i260041a006>
- Perry, H., Green, D., 1997. *Perry's Chemical Engineers Handbook*. Mc-Graw Hill Inc, New York.
- Peters, D., Selim, M.S., Sloan, E.D., 2000. Hydrate Dissociation in Pipelines by Two-Sided Depressurization: Experiment and Model. *Annals of the New York Academy of Sciences* 912, 304–313. <https://doi.org/10.1111/j.1749-6632.2000.tb06784.x>
- Platteeuw, J.C., Waals, J.H. van der, 1958. Thermodynamic properties of gas hydrates. *Molecular Physics* 1, 91–96. <https://doi.org/10.1080/00268975800100111>
- Podkrajšek, B., Berčič, G., Turšič, J., Grgič, I., 2004. Aqueous Oxidation of Sulfur(IV) Catalyzed by Manganese(II): A Generalized Simple Kinetic Model. *Journal of Atmospheric Chemistry* 47, 287–303. <https://doi.org/10.1023/B:JOCH.0000021157.14292.a2>
- Pratt, R.M., Ballard, A.L., Sloan, E.D., 2001. Beware of singularities when calculating clathrate hydrate cell potentials! *AIChE Journal* 47, 1897–1898. <https://doi.org/10.1002/aic.690470820>
- Psarrou, M.N., Jøsang, L.O., Sandengen, K., Østvold, T., 2011. Carbon Dioxide Solubility and Monoethylene Glycol (MEG) Degradation at MEG Reclaiming/Regeneration Conditions. *J. Chem. Eng. Data* 56, 4720–4724. <https://doi.org/10.1021/je200709h>
- Radhakrishnan, R., Trout, B.L., 2002. A new approach for studying nucleation phenomena using molecular simulations: Application to CO₂ hydrate clathrates. *J. Chem. Phys.* 117, 1786–1796. <https://doi.org/10.1063/1.1485962>
- Ranjbar, K., Abasi, A., 2013. Failure assessment of crude oil preheating tubes in mono ethylene glycol–water mixture solution. *Engineering Failure Analysis* 31, 161–167. <https://doi.org/10.1016/j.engfailanal.2013.01.048>
- Ripmeester, J.A., Tse, J.S., Ratcliffe, C.I., Powell, B.M., 1987. A new clathrate hydrate structure. *Nature* 325, 135–136. <https://doi.org/10.1038/325135a0>
- Robinson, D., Ng, H.J., 1986. Hydrate formation and inhibition in gas or gas

- condensate streams. *Journal of Canadian Petroleum Technology* 25.
- Rock, A., 2002. Experimentelle und theoretische Untersuchung zur Hydratbildung aus Gasgemischen in inhibitorhaltigen wässrigen Lösungen. Universität Karlsruhe (TH), Karlsruhe, Germany.
- Rodger, P.Mark., 1990. Stability of gas hydrates. *J. Phys. Chem.* 94, 6080–6089. <https://doi.org/10.1021/j100378a082>
- Ross, J.R.H., van Keulen, A.N.J., Hegarty, M.E.S., Seshan, K., 1996. The catalytic conversion of natural gas to useful products. *Catalysis Today, Proceedings of the 1st Global Conference of Young Chinese Scientist on Catalysis Science and Technology* 30, 193–199. [https://doi.org/10.1016/0920-5861\(96\)00035-1](https://doi.org/10.1016/0920-5861(96)00035-1)
- Rossiter, W.J., Brown, P.W., Godette, M., 1983. The determination of acidic degradation products in aqueous ethylene glycol and propylene glycol solutions using ion chromatography. *Solar Energy Materials* 9, 267–279. [https://doi.org/10.1016/0165-1633\(83\)90049-7](https://doi.org/10.1016/0165-1633(83)90049-7)
- Rossiter, W.J., Godette, M., Brown, P.W., Galuk, K.G., 1985. An investigation of the degradation of aqueous ethylene glycol and propylene glycol solutions using ion chromatography. *Solar Energy Materials* 11, 455–467. [https://doi.org/10.1016/0165-1633\(85\)90016-4](https://doi.org/10.1016/0165-1633(85)90016-4)
- Rudenko, A.I., Gershuni, A.N., Kalabina, L.V., 1997. Some characteristics of ethylene glycol as a heat-transfer agent for closed two-phase systems. *J Eng Phys Thermophys* 70, 799–804. <https://doi.org/10.1007/BF02657642>
- Sadeq, D., Iglauer, S., Lebedev, M., Smith, C., Barifcani, A., 2017. Experimental determination of hydrate phase equilibrium for different gas mixtures containing methane, carbon dioxide and nitrogen with motor current measurements. *Journal of Natural Gas Science and Engineering* 38, 59–73. <https://doi.org/10.1016/j.jngse.2016.12.025>
- Saeedi Dehaghani, A.H., Badizad, M.H., 2017. Inhibiting asphaltene precipitation from Iranian crude oil using various dispersants: Experimental investigation through viscometry and thermodynamic modelling. *Fluid Phase Equilibria* 442, 104–118. <https://doi.org/10.1016/j.fluid.2017.03.020>
- Salasi, M., Pojtanabuntoeng, T., Wong, S., Lehmann, M., 2017. Efficacy of Bisulfite Ions as an Oxygen Scavenger in Monoethylene Glycol (At Least 20 wt%)/Water Mixtures. *SPE Journal* 22, 1,467-1,477. <https://doi.org/10.2118/185944-PA>
- Sami, N.A., Das, K., Sangwai, J.S., Balasubramanian, N., 2013. Phase equilibria of methane and carbon dioxide clathrate hydrates in the presence of (methanol+MgCl₂) and (ethylene glycol+MgCl₂) aqueous solutions. *The Journal of Chemical Thermodynamics* 65, 198–203. <https://doi.org/10.1016/j.jct.2013.05.050>
- Samimi, A., 2012. Preventing Hydrate Formation in Gas Transporting Pipe Lines with Synthetic Inhibitors. *International Journal of Science and Investigations, France* 48–50.
- Sandengen, K., 2006. Prediction of mineral scale formation in wet gas condensate pipelines and in meg (mono ethylene glycol) regeneration plants. Fakultet for naturvitenskap og teknologi.
- Sandengen, K., Kaasa, B., Østvold, T., 2007. pH Measurements in Monoethylene Glycol (MEG) + Water Solutions. *Ind. Eng. Chem. Res.* 46, 4734–4739. <https://doi.org/10.1021/ie061305a>
- Scott, D.W., Villalobos, A., Kwok, C.K., Scott, W.F., 2016. Hydrate Management

- Analysis Applying MEG Injection for Gas and Condensate Fields: A Dynamic Approach. Presented at the Abu Dhabi International Petroleum Exhibition & Conference, Society of Petroleum Engineers. <https://doi.org/10.2118/183553-MS>
- Seo, Y., Kang, S.-P., 2012. Inhibition of methane hydrate re-formation in offshore pipelines with a kinetic hydrate inhibitor. *Journal of Petroleum Science and Engineering, Unconventional hydrocarbons exploration and production Challenges* 88–89, 61–66. <https://doi.org/10.1016/j.petrol.2011.11.001>
- Shaw, S., Welton, T.D., Sorbie, K.S., 2012. The Relation Between Barite Inhibition by Phosphonate Scale Inhibitors and the Structures of Phosphonate-Metal Complexes. Presented at the SPE International Conference on Oilfield Scale, Society of Petroleum Engineers. <https://doi.org/10.2118/155114-MS>
- Shaw, S.S., Sorbie, K., 2015. Synergistic Properties of Phosphonate and Polymeric Scale-Inhibitor Blends for Barium Sulfate Scale Inhibition. *SPE Production & Operations* 30, 16–25. <https://doi.org/10.2118/169752-PA>
- Sheng, Q., Silveira, K.C. da, Tian, W., Fong, C., Maeda, N., Gubner, R., Wood, C.D., 2017. Simultaneous Hydrate and Corrosion Inhibition with Modified Poly(vinyl caprolactam) Polymers. *Energy Fuels* 31, 6724–6731. <https://doi.org/10.1021/acs.energyfuels.7b00525>
- Shukla, P.R., Dhar, S., Victor, D.G., Jackson, M., 2009. Assessment of demand for natural gas from the electricity sector in India. *Energy Policy, New Zealand Energy Strategy* 37, 3520–3534. <https://doi.org/10.1016/j.enpol.2009.03.067>
- Skovborg, P., Ng, H.J., Rasmussen, P., Mohn, U., 1993. Measurement of induction times for the formation of methane and ethane gas hydrates. *Chemical Engineering Science* 48, 445–453. [https://doi.org/10.1016/0009-2509\(93\)80299-6](https://doi.org/10.1016/0009-2509(93)80299-6)
- Skovborg, P., Rasmussen, P., 1994. A mass transport limited model for the growth of methane and ethane gas hydrates. *Chemical Engineering Science* 49, 1131–1143. [https://doi.org/10.1016/0009-2509\(94\)85085-2](https://doi.org/10.1016/0009-2509(94)85085-2)
- Sloan, E.D., 2005. A changing hydrate paradigm—from apprehension to avoidance to risk management. *Fluid Phase Equilibria, PPEPPD 2004 Proceedings* 228–229, 67–74. <https://doi.org/10.1016/j.fluid.2004.08.009>
- Sloan, E.D., Subramanian, S., Matthews, P.N., Lederhos, J.P., Khokhar, A.A., 1998. Quantifying Hydrate Formation and Kinetic Inhibition. *Ind. Eng. Chem. Res.* 37, 3124–3132. <https://doi.org/10.1021/ie970902h>
- Sloan Jr, E.D., Koh, C.A., 2007. *Clathrate Hydrates of Natural Gases*. CRC Press.
- Smelik, E.A., King, H.E., 2015. Crystal-growth studies of natural gas clathrate hydrates using a pressurized optical cell. *American Mineralogist* 82, 88–98. <https://doi.org/10.2138/am-1997-1-211>
- Smith, C., Barifcani, A., Pack, D., 2016. Helium substitution of natural gas hydrocarbons in the analysis of their hydrate. *Journal of Natural Gas Science and Engineering* 35, 1293–1300. <https://doi.org/10.1016/j.jngse.2016.09.033>
- Smith, C., Barifcani, A., Pack, D., 2015. Gas hydrate formation and dissociation numerical modelling with nitrogen and carbon dioxide. *Journal of Natural Gas Science and Engineering* 27, 1118–1128. <https://doi.org/10.1016/j.jngse.2015.09.055>
- Son, K.V., Wallace, C., 2000. Reclamation/regeneration of glycols used for hydrate inhibition. *Deep Offshore Technology*.
- Stanek, W., Bialecki, R., 2014. Can natural gas warm the climate more than coal? *Fuel*

- 136, 341–348. <https://doi.org/10.1016/j.fuel.2014.07.075>
- Sun, Q., Chen, B., Li, X., Guo, X., Yang, L., 2017. The investigation of phase equilibria and kinetics of CH₄ hydrate in the presence of bio-additives. *Fluid Phase Equilibria* 452, 143–147. <https://doi.org/10.1016/j.fluid.2017.09.002>
- Svenningsen, G., Nyborg, R., 2014. Modeling of Top of Line Corrosion with Organic Acid and Glycol. Presented at the CORROSION 2014, NACE International.
- Taylor, C.J., 2007. Adhesion force between hydrate particles and macroscopic investigation of hydrate film growth at the hydrocarbon / water interface (Thesis). Colorado School of Mines. Arthur Lakes Library.
- Teixeira, A.M., Medeiros, J.L., Araújo, O.Q.F., 2015. Offshore Monoethylene Glycol Recovery Units: The Importance of Choice of MEG State in the Reference Environment for Effective Exergy Analysis. Presented at the OTC Brasil, Offshore Technology Conference. <https://doi.org/10.4043/26135-MS>
- Tohidi, B., Burgass, R.W., Danesh, A., Østergaard, K.K., Todd, A.C., 2000. Improving the Accuracy of Gas Hydrate Dissociation Point Measurements. *Annals of the New York Academy of Sciences* 912, 924–931. <https://doi.org/10.1111/j.1749-6632.2000.tb06846.x>
- Turner, D.J., 2005. Clathrate hydrate formation in water-in-oil dispersions.
- Uchida, T., Ebinuma, T., Kawabata, J., Narita, H., 1999. Microscopic observations of formation processes of clathrate-hydrate films at an interface between water and carbon dioxide. *Journal of Crystal Growth* 204, 348–356. [https://doi.org/10.1016/S0022-0248\(99\)00178-5](https://doi.org/10.1016/S0022-0248(99)00178-5)
- Udachin, K.A., Ratcliffe, C.I., Ripmeester, J.A., 2001. Structure, Composition, and Thermal Expansion of CO₂ Hydrate from Single Crystal X-ray Diffraction Measurements. *J. Phys. Chem. B* 105, 4200–4204. <https://doi.org/10.1021/jp004389o>
- Urdahl, O., Børnes, A.H., Kinnari, K.J., Holme, R., 2003. Operational Experience by Applying Direct Electrical Heating for Hydrate Prevention. Presented at the Offshore Technology Conference, Offshore Technology Conference. <https://doi.org/10.4043/15189-MS>
- Vajari, S.M., 2012. Development of hydrate inhibition monitoring and initial formation detection techniques (Thesis). Heriot-Watt University.
- Van der Waals, J.H., 1959. Clathrate solutions. *Adv. Chem. Phys.* 2, 1–57.
- Verma, V.K., 1974. Gas hydrates from liquid hydrocarbon-water systems (PhD Thesis). University of Michigan.
- Vetter, O.J., 1972. An Evaluation of Scale Inhibitors. *Journal of Petroleum Technology* 24, 997–1,006. <https://doi.org/10.2118/3188-PA>
- Villard, P., 1888. Sur quelques nouveaux hydrates de gaz. *Compt. Rend* 106, 1602–1603.
- Voutsas, E., Vrachnos, A., Magoulas, K., 2004. Measurement and thermodynamic modeling of the phase equilibrium of aqueous N-methyldiethanolamine solutions. *Fluid Phase Equilibria* 224, 193–197. <https://doi.org/10.1016/j.fluid.2004.05.012>
- Vysniauskas, A., Bishnoi, P.R., 1983. A kinetic study of methane hydrate formation. *Chemical Engineering Science* 38, 1061–1072. [https://doi.org/10.1016/0009-2509\(83\)80027-X](https://doi.org/10.1016/0009-2509(83)80027-X)
- Wang, C., Hu, X., Ivonye, I., Neville, A., 2013. Corrosion Study of Carbon Steel in the Presence of Monoethylene Glycol (MEG) and Corrosion Inhibitors in Acid. Presented at the CORROSION 2013, NACE International.

- Wang, H., Wylde, J., 2010. Corrosion Inhibitor Development For Slight Sour Environment With Oxygen Intrusion Issue. Presented at the CORROSION 2010, NACE International.
- Wang, T., El Ahmar, E., Coquelet, C., 2017. Alkane solubilities in aqueous alkanolamine solutions with CPA EoS. *Fluid Phase Equilibria* 434, 93–101. <https://doi.org/10.1016/j.fluid.2016.11.025>
- Wang, T., El Ahmar, E., Coquelet, C., Kontogeorgis, G.M., 2018. Improvement of the PR-CPA equation of state for modelling of acid gases solubilities in aqueous alkanolamine solutions. *Fluid Phase Equilibria* 471, 74–87. <https://doi.org/10.1016/j.fluid.2018.04.019>
- Wang, Y., Fan, S., Lang, X., 2019. Reviews of gas hydrate inhibitors in gas-dominant pipelines and application of kinetic hydrate inhibitors in China. *Chinese Journal of Chemical Engineering*. <https://doi.org/10.1016/j.cjche.2019.02.023>
- Weiland, R.H., Dingman, J.C., Cronin, D.B., 1997. Heat Capacity of Aqueous Monoethanolamine, Diethanolamine, N-Methyldiethanolamine, and N-Methyldiethanolamine-Based Blends with Carbon Dioxide. *J. Chem. Eng. Data* 42, 1004–1006. <https://doi.org/10.1021/je960314v>
- Windmeier, C., Oellrich, L.R., 2014. Experimental Methane Hydrate Dissociation Conditions in Aqueous Solutions of Lithium Salts. *J. Chem. Eng. Data* 59, 516–518. <https://doi.org/10.1021/je4010036>
- Wu, Q., Zhang, B., 2010. Memory effect on the pressure-temperature condition and induction time of gas hydrate nucleation. *Journal of Natural Gas Chemistry* 19, 446–451. [https://doi.org/10.1016/S1003-9953\(09\)60086-4](https://doi.org/10.1016/S1003-9953(09)60086-4)
- Xiang, Y., Choi, Y.-S., Yang, Y., Nešić, S., 2014. Corrosion of Carbon Steel in MDEA-Based CO₂ Capture Plants Under Regenerator Conditions: Effects of O₂ and Heat-Stable Salts. *CORROSION* 71, 30–37. <https://doi.org/10.5006/1354>
- Yang, C., Feng, Y., Cheng, B., Zhang, P., Qin, Z., Zeng, H., Sun, F., 2013. Vapor–Liquid Equilibria for Three Binary Systems of N-Methylethanolamine, N-Methyldiethanolamine, and Ethylene Glycol at P = (40.0, 30.0, and 20.0) kPa. *J. Chem. Eng. Data* 58, 2272–2279. <https://doi.org/10.1021/je400373d>
- Yong, A., Obanijesu, E.O., 2015. Influence of natural gas production chemicals on scale production in MEG regeneration systems. *Chemical Engineering Science* 130, 172–182. <https://doi.org/10.1016/j.ces.2015.03.037>
- Youssef, Z., Barreau, A., Mougin, P., Jose, J., Mokbel, I., 2010. Measurements of Hydrate Dissociation Temperature of Gas Mixtures in the Absence of Any Aqueous Phase and Prediction with the Cubic-Plus-Association Equation of State. *J. Chem. Eng. Data* 55, 2809–2814. <https://doi.org/10.1021/je901001u>
- Zaboon, S., Soames, A., Ghodkay, V., Gubner, R., Barifcani, A., 2017. Recovery of mono-ethylene glycol by distillation and the impact of dissolved salts evaluated through simulation of field data. *Journal of Natural Gas Science and Engineering* 44, 214–232. <https://doi.org/10.1016/j.jngse.2017.04.007>
- Zang, X., Liang, D., 2017. Phase Equilibrium Data for Semiclathrate Hydrate of Synthesized Binary CO₂/CH₄ Gas Mixture in Tetra-n-butylammonium Bromide Aqueous Solution. *J. Chem. Eng. Data* 62, 851–856. <https://doi.org/10.1021/acs.jced.6b00876>
- Zarinabadi, S., Samimi, A., 2011. Problems of hydrate formation in oil and gas pipes deal. *Austr J Basic Appl Sci* 5, 741–745.
- Zelevinsky, S.R., Lee, S.-Y., Holder, G.D., 1999. A Theory of Lattice Distortion in Gas

- Hydrates. *J. Phys. Chem. B* 103, 10250–10257.
<https://doi.org/10.1021/jp9917704>
- Zeng, H., Moudrakovski, I.L., Ripmeester, J.A., Walker, V.K., 2006. Effect of antifreeze protein on nucleation, growth and memory of gas hydrates. *AIChE Journal* 52, 3304–3309. <https://doi.org/10.1002/aic.10929>
- Zoghi, A.T., Feyzi, F., Dehghani, M.R., 2012. Modeling CO₂ Solubility in Aqueous N-methyldiethanolamine Solution by Electrolyte Modified Peng–Robinson Plus Association Equation of State. *Ind. Eng. Chem. Res.* 51, 9875–9885. <https://doi.org/10.1021/ie2026053>

Note: “Every reasonable effort has been made to acknowledge the owners of copyright material. I would be pleased to hear from any copyright owner who has been omitted or incorrectly acknowledged.”

APPENDICES

APPENDIX A. Outline of Algorithm, and MDEA Data

The effect of MDEA on varied MEG mixtures are given in Table A-1.

Table A-1: Effect of MDEA (5 wt%) on MEG (20 wt% and 25 wt%).

Mixture	P (MPa)	T _{exp} (°C)	ΔT _{MEG} (°C)	ΔT _{MDEA} (°C)
MEG-MDEA (20 wt%)	7.34	4.14	-5.77	-0.28
	9.95	6.71	-5.90	-0.25
	15.25	10.22	-6.08	-0.30
	20.21	12.52	-6.20	-0.35
		Average		-0.30
MEG-MDEA (25 wt%)	7.31	2.19	-7.71	-0.29
	10.63	5.26	-7.36	-0.24
	15.22	8.10	-8.20	-0.30
	19.89	10.22	-8.51	-0.34
		Average		-0.29

A simple algorithm is proposed to allow for determining the hydrate equilibrium temperature shift for mixtures containing methyldiethanolamine (MDEA) and monoethylene glycol (MEG). The algorithm relies primarily on two aspects, firstly, the experimental data obtained in this study, and secondly, on the equation of state prediction for the MEG hydrate phase boundary for MEG concentrations outside of the scope of this study. An outline of the algorithm is given in Figure A-1.

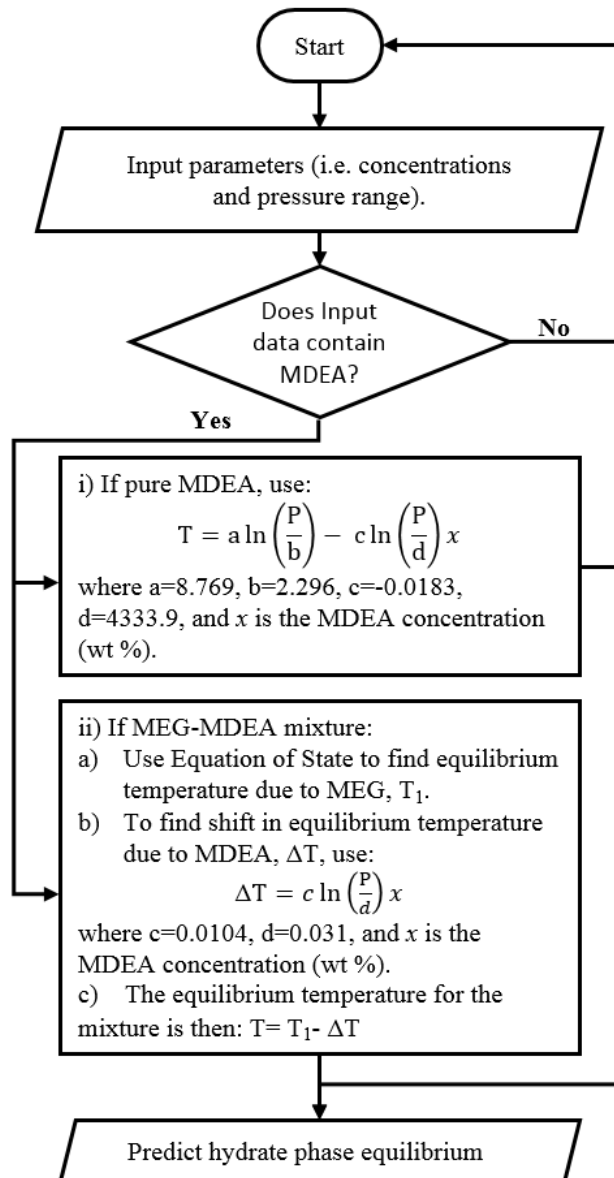


Figure A-1: Outline of the algorithm to predict equilibrium temperature of pure MDEA, and MEG-MDEA solutions at MDEA concentrations of 0 – 7.5 wt%.

APPENDIX B. Computer Script to Process Test Data

The computer script to process raw data and determine the hydrate phase equilibrium conditions was developed using MATLAB. The script is given below.

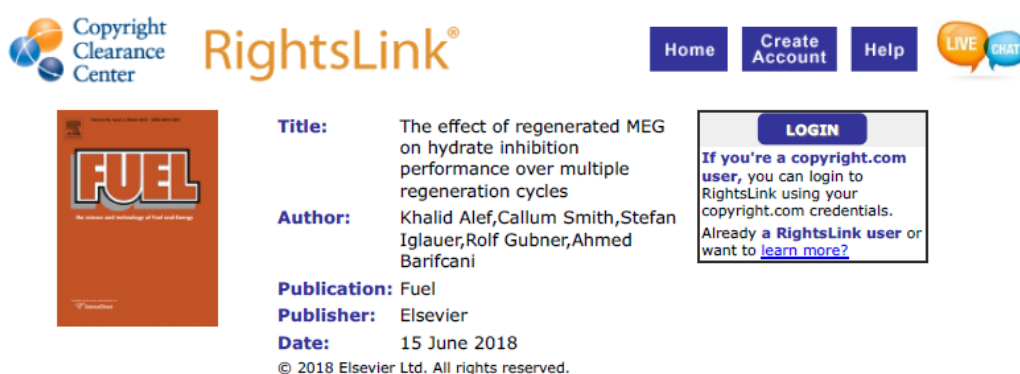
```
function P = HydEqm(HF,filename)
%     Function HydEqm finds and plots the hydrate phase equilibrium point from raw
%     PT data.
%     The function requires the observed hydrate formation point to remove
%     unnecessary data and the source pressure/temperature data from the cooling
%     and heating process using the isochoric test method.
%
%     Author : Khalid Alef
%     Version: 1.0, 31 July. 2018

rawdata = csvread(filename,2,1);           %.read and import raw PT data
data = rawdata(:,1:2);                     %.remove unnecessary data
data(:,1) = data(:,1)./100;                %.convert data to desired units
plot(data(:,2),data(:,1))
idx = data(:,2) < HF;                       %.remove unnecessary data
modiData = data;
modiData(idx,:)=[];
di = modiData(2:end,1)-modiData(1:end-1,1);
cutoff = find(di==max(di));
line1 = modiData(1:cutoff,:);              %.separate cooling and heating
line2 = modiData(cutoff:end,:);
pt1 = polyfit(line1(:,2),line1(:,1),1);     %.fit linear trends
pt2 = polyfit(line2(:,2),line2(:,1),1);
x_intsect = fzero(@(x) polyval(pt1-pt2,x),3); %.intersection
y_intsect = polyval(pt1,x_intsect);
P(1)=x_intsect;
P(2)=y_intsect;
range = HF:0.001:max(modiData(:,2));
val1 = polyval(pt1,range);
val2 = polyval(pt2,range);
figure                                     %.plot the data and trend-lines
plot(line1(:,2),line1(:,1),'co',line2(:,2),line2(:,1),'mo')
hold on
scatter(P(1),P(2), 'filled')
plot(range,val1,'b',range,val2,'r')
output = P;                               %.hydrate equilibrium pressure and temperature
end
```

APPENDIX C. Copyright Permission Statements

This section contains the copyright agreements between the author and Journal for the reuse of the author's own published material within this thesis.

Chapter 2, Article: "The Effect of Regenerated MEG on Hydrate Inhibition Performance Over Multiple Regeneration Cycles" in Journal Fuel.



The screenshot displays the RightsLink interface. At the top left is the Copyright Clearance Center logo. The main header features the RightsLink logo and navigation buttons for Home, Create Account, and Help. A Live Chat button is also present. The article details are as follows:

- Title:** The effect of regenerated MEG on hydrate inhibition performance over multiple regeneration cycles
- Author:** Khalid Alef, Callum Smith, Stefan Iglauer, Rolf Gubner, Ahmed Barifcani
- Publication:** Fuel
- Publisher:** Elsevier
- Date:** 15 June 2018

Below the details is a copyright notice: © 2018 Elsevier Ltd. All rights reserved. To the right of the details is a LOGIN box with the text: "If you're a copyright.com user, you can login to RightsLink using your copyright.com credentials. Already a RightsLink user or want to learn more?"

Please note that, as the author of this Elsevier article, you retain the right to include it in a thesis or dissertation, provided it is not published commercially. Permission is not required, but please ensure that you reference the journal as the original source. For more information on this and on your other retained rights, please visit: <https://www.elsevier.com/about/our-business/policies/copyright#Author-rights>

BACK

CLOSE WINDOW

Copyright © 2019 Copyright Clearance Center, Inc. All Rights Reserved. [Privacy statement](#). [Terms and Conditions](#). Comments? We would like to hear from you. E-mail us at customercare@copyright.com

Chapter 3, Article: “Evaluation of MEG Reclamation and Natural Gas Hydrate Inhibition During Corrosion Control Switchover” in Journal of Petroleum Science and Engineering.



The screenshot shows the RightsLink interface. On the left is the journal cover for 'JOURNAL OF PETROLEUM SCIENCE & ENGINEERING'. The main content area lists the following details:

- Title:** Evaluation of MEG reclamation and natural gas hydrate inhibition during corrosion control switchover
- Author:** Khalid Alef, Rolf Gubner, Stefan Iglauer, Ahmed Barifcani
- Publication:** Journal of Petroleum Science and Engineering
- Publisher:** Elsevier
- Date:** May 2019

At the bottom of the details, it states: © 2018 Elsevier B.V. All rights reserved.

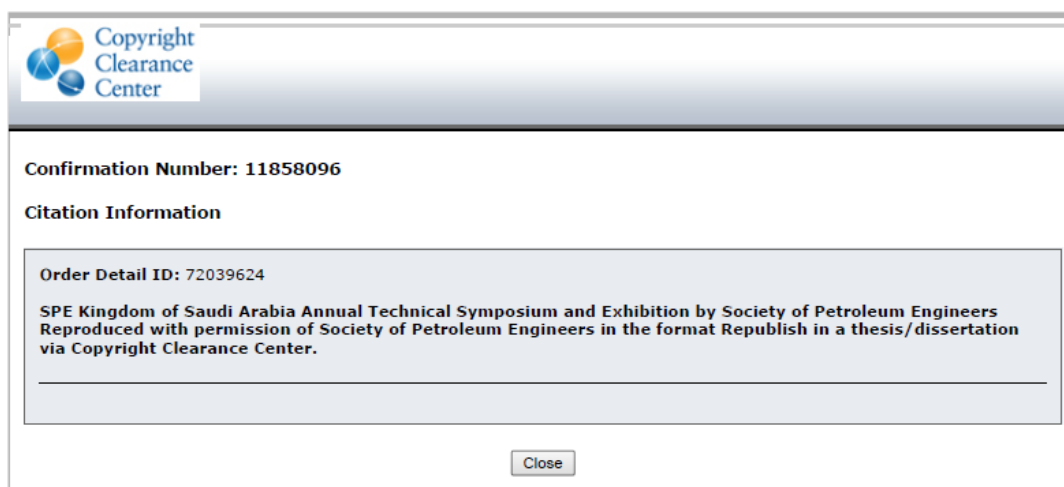
Navigation buttons include Home, Create Account, Help, and a LIVE CHAT icon. A LOGIN box contains the text: 'If you're a copyright.com user, you can login to RightsLink using your copyright.com credentials. Already a RightsLink user or want to learn more?' with a link to learn more.

Please note that, as the author of this Elsevier article, you retain the right to include it in a thesis or dissertation, provided it is not published commercially. Permission is not required, but please ensure that you reference the journal as the original source. For more information on this and on your other retained rights, please visit: <https://www.elsevier.com/about/our-business/policies/copyright#Author-rights>

[BACK](#) [CLOSE WINDOW](#)

Copyright © 2019 Copyright Clearance Center, Inc. All Rights Reserved. [Privacy statement](#). [Terms and Conditions](#).
Comments? We would like to hear from you. E-mail us at customercare@copyright.com

Chapter 4, Article: “The Effect of Salt-Laden Degraded MEG on Gas Hydrate Inhibition” in Society of Petroleum Engineers.



The screenshot shows a confirmation window from the Copyright Clearance Center. It contains the following information:

- Confirmation Number:** 11858096
- Citation Information:**
 - Order Detail ID:** 72039624
 - Text:** SPE Kingdom of Saudi Arabia Annual Technical Symposium and Exhibition by Society of Petroleum Engineers Reproduced with permission of Society of Petroleum Engineers in the format Republish in a thesis/dissertation via Copyright Clearance Center.

A 'Close' button is located at the bottom center of the window.

Chapter 5, Article: "Hydrate Phase Equilibria for Methyldiethanolamine and Empirical Modeling for Prediction" in Journal of Chemical and Engineering Data.



RightsLink®

Home

Create Account

Help



ACS Publications
Most Trusted. Most Cited. Most Read.

Title: Hydrate Phase Equilibria for Methyldiethanolamine and Empirical Modeling for Prediction
Author: Khalid Alef, Stefan Iglauer, Rolf Gubner, et al
Publication: Journal of Chemical and Engineering Data
Publisher: American Chemical Society
Date: Sep 1, 2018
Copyright © 2018, American Chemical Society

LOGIN
If you're a **copyright.com user**, you can login to RightsLink using your copyright.com credentials. Already a **RightsLink user** or want to [learn more?](#)

PERMISSION/LICENSE IS GRANTED FOR YOUR ORDER AT NO CHARGE

This type of permission/license, instead of the standard Terms & Conditions, is sent to you because no fee is being charged for your order. Please note the following:

- Permission is granted for your request in both print and electronic formats, and translations.
- If figures and/or tables were requested, they may be adapted or used in part.
- Please print this page for your records and send a copy of it to your publisher/graduate school.
- Appropriate credit for the requested material should be given as follows: "Reprinted (adapted) with permission from (COMPLETE REFERENCE CITATION). Copyright (YEAR) American Chemical Society." Insert appropriate information in place of the capitalized words.
- One-time permission is granted only for the use specified in your request. No additional uses are granted (such as derivative works or other editions). For any other uses, please submit a new request.

BACK

CLOSE WINDOW

Copyright © 2019 [Copyright Clearance Center, Inc.](#) All Rights Reserved. [Privacy statement.](#) [Terms and Conditions.](#) Comments? We would like to hear from you. E-mail us at customercare@copyright.com

Chapter 6, Article: “Thermodynamic Modeling of Hydrate Phase Equilibria in Methyldiethanolamine Solution in the Presence or Absence of Monoethylene Glycol” in Journal of Chemical and Engineering Data.



RightsLink®

Home

Create Account

Help



Title: Thermodynamic Modeling of Hydrate Phase Equilibria in Methyldiethanolamine Solution in the Presence or Absence of Monoethylene Glycol

Author: Khalid Alef, Stefan Iglauer, Ahmed Barifcani

Publication: Journal of Chemical and Engineering Data

Publisher: American Chemical Society

Date: Sep 1, 2019

Copyright © 2019, American Chemical Society

LOGIN
If you're a **copyright.com** user, you can login to RightsLink using your copyright.com credentials. Already a **RightsLink** user or want to [learn more?](#)

PERMISSION/LICENSE IS GRANTED FOR YOUR ORDER AT NO CHARGE

This type of permission/license, instead of the standard Terms & Conditions, is sent to you because no fee is being charged for your order. Please note the following:

- Permission is granted for your request in both print and electronic formats, and translations.
- If figures and/or tables were requested, they may be adapted or used in part.
- Please print this page for your records and send a copy of it to your publisher/graduate school.
- Appropriate credit for the requested material should be given as follows: "Reprinted (adapted) with permission from (COMPLETE REFERENCE CITATION). Copyright (YEAR) American Chemical Society." Insert appropriate information in place of the capitalized words.
- One-time permission is granted only for the use specified in your request. No additional uses are granted (such as derivative works or other editions). For any other uses, please submit a new request.

BACK

CLOSE WINDOW

Copyright © 2019 [Copyright Clearance Center, Inc.](#) All Rights Reserved. [Privacy statement](#). [Terms and Conditions](#). Comments? We would like to hear from you. E-mail us at customercare@copyright.com

Chapter 7, Article: “Effect of N-Methyl-Diethanolamine and Film Forming Corrosion Inhibitor on Gas Hydrate, and Empirical Modeling for Degradation” in Journal of Petroleum Science and Engineering.

 **Copyright Clearance Center**  **Home** **Create Account** **Help** 

 **Title:** Effect of N-methyl-diethanolamine and film forming corrosion inhibitor on gas hydrate, and empirical modeling for degradation

Author: Khalid Alef,Ahmed Barifcani

Publication: Journal of Petroleum Science and Engineering

Publisher: Elsevier

Date: January 2020

© 2019 Elsevier B.V. All rights reserved.

LOGIN
If you're a **copyright.com user**, you can login to RightsLink using your copyright.com credentials. Already a **RightsLink user** or want to [learn more?](#)

Please note that, as the author of this Elsevier article, you retain the right to include it in a thesis or dissertation, provided it is not published commercially. Permission is not required, but please ensure that you reference the journal as the original source. For more information on this and on your other retained rights, please visit: <https://www.elsevier.com/about/our-business/policies/copyright#Author-rights>

BACK

CLOSE WINDOW

Copyright © 2019 [Copyright Clearance Center, Inc.](#) All Rights Reserved. [Privacy statement](#). [Terms and Conditions](#).
Comments? We would like to hear from you. E-mail us at customercare@copyright.com

Chapter 8, Article: “Effect of Dissolved Oxygen, Sodium Bisulfite, and Oxygen Scavengers on Methane Hydrate Inhibition” in Journal of Chemical and Engineering Data.



RightsLink®

Home

Create Account

Help



Title: Effect of Dissolved Oxygen, Sodium Bisulfite, and Oxygen Scavengers on Methane Hydrate Inhibition
Author: Khalid Alef, Stefan Iglauer, Ahmed Barifcani
Publication: Journal of Chemical and Engineering Data
Publisher: American Chemical Society
Date: May 1, 2018
Copyright © 2018, American Chemical Society

LOGIN
If you're a [copyright.com](#) user, you can login to RightsLink using your [copyright.com](#) credentials. Already a [RightsLink](#) user or want to [learn more?](#)

PERMISSION/LICENSE IS GRANTED FOR YOUR ORDER AT NO CHARGE

This type of permission/license, instead of the standard Terms & Conditions, is sent to you because no fee is being charged for your order. Please note the following:

- Permission is granted for your request in both print and electronic formats, and translations.
- If figures and/or tables were requested, they may be adapted or used in part.
- Please print this page for your records and send a copy of it to your publisher/graduate school.
- Appropriate credit for the requested material should be given as follows: "Reprinted (adapted) with permission from (COMPLETE REFERENCE CITATION). Copyright (YEAR) American Chemical Society." Insert appropriate information in place of the capitalized words.
- One-time permission is granted only for the use specified in your request. No additional uses are granted (such as derivative works or other editions). For any other uses, please submit a new request.

BACK

CLOSE WINDOW

Copyright © 2019 [Copyright Clearance Center, Inc.](#) All Rights Reserved. [Privacy statement](#). [Terms and Conditions](#). Comments? We would like to hear from you. E-mail us at customercare@copyright.com

Chapter 9, Article: "Hydrate Phase Equilibria of Phosphonate Scale Inhibitors, Amines, and Ethylene Glycol" in Journal of Chemical and Engineering Data.



RightsLink®

Home

Create Account

Help



Title: Hydrate Phase Equilibria of Phosphonate Scale Inhibitors, Amines, and Ethylene Glycol
Author: Khalid Alef, Ahmed Barifcani
Publication: Journal of Chemical and Engineering Data
Publisher: American Chemical Society
Date: Jul 1, 2019
Copyright © 2019, American Chemical Society

LOGIN
If you're a **copyright.com** user, you can login to RightsLink using your copyright.com credentials. Already a **RightsLink** user or want to [learn more?](#)

PERMISSION/LICENSE IS GRANTED FOR YOUR ORDER AT NO CHARGE

This type of permission/license, instead of the standard Terms & Conditions, is sent to you because no fee is being charged for your order. Please note the following:

- Permission is granted for your request in both print and electronic formats, and translations.
- If figures and/or tables were requested, they may be adapted or used in part.
- Please print this page for your records and send a copy of it to your publisher/graduate school.
- Appropriate credit for the requested material should be given as follows: "Reprinted (adapted) with permission from (COMPLETE REFERENCE CITATION). Copyright (YEAR) American Chemical Society." Insert appropriate information in place of the capitalized words.
- One-time permission is granted only for the use specified in your request. No additional uses are granted (such as derivative works or other editions). For any other uses, please submit a new request.

BACK

CLOSE WINDOW

Copyright © 2019 [Copyright Clearance Center, Inc.](#) All Rights Reserved. [Privacy statement](#). [Terms and Conditions](#).
Comments? We would like to hear from you. E-mail us at customercare@copyright.com

Chapter 10, Article: “Degradation and Hydrate Phase Equilibria Measurement Methods of Monoethylene Glycol” in Journal MethodsX.



Creative Commons Attribution License (CC BY)

This article is available under the terms of the [Creative Commons Attribution License \(CC BY\)](#). You may copy and distribute the article, create extracts, abstracts and new works from the article, alter and revise the article, text or data mine the article and otherwise reuse the article commercially (including reuse and/or resale of the article) without permission from Elsevier. You must give appropriate credit to the original work, together with a link to the formal publication through the relevant DOI and a link to the Creative Commons user license above. You must indicate if any changes are made but not in any way that suggests the licensor endorses you or your use of the work.

Permission is not required for this type of reuse.

CLOSE WINDOW

Copyright © 2019 [Copyright Clearance Center, Inc.](#) All Rights Reserved.
Comments? We would like to hear from you. E-mail us at customercare@copyright.com

APPENDIX D. Statements of Contribution by Others

Paper: “The effect of regenerated MEG on hydrate inhibition performance over multiple regeneration cycles. Fuel, 2018, 222, 638-647.”

Authors and full affiliations: Khalid Alef¹, Callum Smith¹, Stefan Iglauer², Rolf Gubner¹, Ahmed Barifcani¹.

¹WA School of Mines: Minerals, Energy and Chemical Engineering, Curtin University, Bentley Western Australia 6102, Australia

²School of Engineering, Petroleum Engineering Discipline, Edith Cowan University, Joondalup Western Australia 6027, Australia

	Conception & Design	Acquisition of Data & Method	Data Conditioning & Manipulation	Analysis & Statistical Method	Interpretation & Discussion	Final Approval
Khalid Alef	×	×	×	×	×	×
I acknowledge that these represent my contribution to the above research output. Signature: _____ Date: / / 2018						
Dr. Callum Smith				×		×
I acknowledge that these represent my contribution to the above research output. Signature: _____ Date: / / 2018						
Dr. Stefan Iglauer						×
I acknowledge that these represent my contribution to the above research output. Signature: _____ Date: / / 2018						
Prof. Rolf Gubner						×
I acknowledge that these represent my contribution to the above research output. Signature: _____ Date: / / 2018						
Dr. Ahmed Barifcani						×
I acknowledge that these represent my contribution to the above research output. Signature: _____ Date: / / 2018						

Paper: “Evaluation of MEG Reclamation and Natural Gas Hydrate Inhibition During Corrosion Control Switchover. Journal of Petroleum Science and Engineering, 2019, 176, 1175–1186.”

Authors and full affiliations: Khalid Alef¹, Rolf Gubner¹, Stefan Iglauer², Ahmed Barifcani¹.

¹WA School of Mines: Minerals, Energy and Chemical Engineering, Curtin University, Bentley Western Australia 6102, Australia

²School of Engineering, Petroleum Engineering Discipline, Edith Cowan University, Joondalup Western Australia 6027, Australia

	Conception & Design	Acquisition of Data & Method	Data Conditioning & Manipulation	Analysis & Statistical Method	Interpretation & Discussion	Final Approval
Khalid Alef	×	×	×	×	×	×
I acknowledge that these represent my contribution to the above research output. Signature: _____ Date: / / 2018						
Prof. Rolf Gubner	×				×	×
I acknowledge that these represent my contribution to the above research output. Signature: _____ Date: / / 2018						
Dr. Stefan Iglauer						×
I acknowledge that these represent my contribution to the above research output. Signature: _____ Date: / / 2018						
Dr. Ahmed Barifcani						×
I acknowledge that these represent my contribution to the above research output. Signature: _____ Date: / / 2018						

Paper: “**The Effect of Salt-Laden Degraded MEG on Gas Hydrate Inhibition**. SPE Kingdom of Saudi Arabia Annual Technical Symposium and Exhibition. Society of Petroleum Engineers, 2018.”

Authors and full affiliations: Khalid Alef¹, Ahmed Barifcani¹.

¹WA School of Mines: Minerals, Energy and Chemical Engineering, Curtin University, Bentley Western Australia 6102, Australia

	Conception & Design	Acquisition of Data & Method	Data Conditioning & Manipulation	Analysis & Statistical Method	Interpretation & Discussion	Final Approval
Khalid Alef	×	×	×	×	×	×
I acknowledge that these represent my contribution to the above research output. Signature: _____ Date: / / 2019						
Dr. Ahmed Barifcani						×
I acknowledge that these represent my contribution to the above research output. Signature: _____ Date: / / 2019						

Paper: “Hydrate Phase Equilibria for Methyldiethanolamine and Empirical Modeling for Prediction. Journal of Chemical & Engineering Data, 2018, 63, 3559-65.”

Authors and full affiliations: Khalid Alef¹, Stefan Iglauer², Rolf Gubner¹, Ahmed Barifcani¹.

¹WA School of Mines: Minerals, Energy and Chemical Engineering, Curtin University, Bentley Western Australia 6102, Australia

²School of Engineering, Petroleum Engineering Discipline, Edith Cowan University, Joondalup Western Australia 6027, Australia

	Conception & Design	Acquisition of Data & Method	Data Conditioning & Manipulation	Analysis & Statistical Method	Interpretation & Discussion	Final Approval
Khalid Alef	×	×	×	×	×	×
I acknowledge that these represent my contribution to the above research output. Signature: _____ Date: / / 2018						
Dr. Stefan Iglauer						×
I acknowledge that these represent my contribution to the above research output. Signature: _____ Date: / / 2018						
Prof. Rolf Gubner						×
I acknowledge that these represent my contribution to the above research output. Signature: _____ Date: / / 2018						
Dr. Ahmed Barifcani						×
I acknowledge that these represent my contribution to the above research output. Signature: _____ Date: / / 2018						

Paper: “**Thermodynamic Modeling of Hydrate Phase Equilibria in Methyldiethanolamine Solution in the Presence or Absence of Monoethylene Glycol**. J. Chem. Eng. Data, 2019, 64, 4148-4153.”

Authors and full affiliations: Khalid Alef¹, Stefan Iglauer², Ahmed Barifcani¹.

¹WA School of Mines: Minerals, Energy and Chemical Engineering, Curtin University, Bentley Western Australia 6102, Australia

²School of Engineering, Petroleum Engineering Discipline, Edith Cowan University, Joondalup Western Australia 6027, Australia

	Conception & Design	Acquisition of Data & Method	Data Conditioning & Manipulation	Analysis & Statistical Method	Interpretation & Discussion	Final Approval
Khalid Alef	×	×	×	×	×	×
I acknowledge that these represent my contribution to the above research output. Signature: _____ Date: / / 2019						
Dr. Stefan Iglauer						×
I acknowledge that these represent my contribution to the above research output. Signature: _____ Date: / / 2019						
Dr. Ahmed Barifcani						×
I acknowledge that these represent my contribution to the above research output. Signature: _____ Date: / / 2019						

Paper: “Effect of N-methyl-diethanolamine and film forming corrosion inhibitor on gas hydrate, and empirical modeling for degradation. Journal of Petroleum Science and Engineering, 2020, 184, 106522.”

Authors and full affiliations: Khalid Alef¹, Ahmed Barifcani¹.

¹WA School of Mines: Minerals, Energy and Chemical Engineering, Curtin University, Bentley Western Australia 6102, Australia

	Conception & Design	Acquisition of Data & Method	Data Conditioning & Manipulation	Analysis & Statistical Method	Interpretation & Discussion	Final Approval
Khalid Alef	×	×	×	×	×	×
I acknowledge that these represent my contribution to the above research output. Signature: _____ Date: / / 2019						
Dr. Ahmed Barifcani						×
I acknowledge that these represent my contribution to the above research output. Signature: _____ Date: / / 2019						

Paper: “Effect of Dissolved Oxygen, Sodium Bisulfite, and Oxygen Scavengers on Methane Hydrate Inhibition. J. Chem. Eng. Data, 2018, 63, 1821–1826.”

Authors and full affiliations: Khalid Alef¹, Stefan Iglauer², Ahmed Barifcani¹.

¹WA School of Mines: Minerals, Energy and Chemical Engineering, Curtin University, Bentley Western Australia 6102, Australia

²School of Engineering, Petroleum Engineering Discipline, Edith Cowan University, Joondalup Western Australia 6027, Australia

	Conception & Design	Acquisition of Data & Method	Data Conditioning & Manipulation	Analysis & Statistical Method	Interpretation & Discussion	Final Approval
Khalid Alef	×	×	×	×	×	×
I acknowledge that these represent my contribution to the above research output. Signature: _____ Date: / / 2019						
Dr. Stefan Iglauer						×
I acknowledge that these represent my contribution to the above research output. Signature: _____ Date: / / 2019						
Dr. Ahmed Barifcani						×
I acknowledge that these represent my contribution to the above research output. Signature: _____ Date: / / 2019						

Paper: “**Hydrate Phase Equilibria of Phosphonate Scale Inhibitors, Amines, and Ethylene Glycol**. J. Chem. Eng. Data, 2019, 64, 3205–3210.”

Authors and full affiliations: Khalid Alef¹, Ahmed Barifcani¹.

¹WA School of Mines: Minerals, Energy and Chemical Engineering, Curtin University, Bentley Western Australia 6102, Australia

	Conception & Design	Acquisition of Data & Method	Data Conditioning & Manipulation	Analysis & Statistical Method	Interpretation & Discussion	Final Approval
Khalid Alef	×	×	×	×	×	×
I acknowledge that these represent my contribution to the above research output. Signature: _____ Date: / / 2019						
Dr. Ahmed Barifcani						×
I acknowledge that these represent my contribution to the above research output. Signature: _____ Date: / / 2019						

Paper: “An Innovative Approach to Assessing Gas Hydrate Inhibition and Corrosion Control Strategies. Proceedings of One Curtin International Postgraduate Conference (OCPC), Miri, Sarawak, Malaysia, 2017.”

Authors and full affiliations: Khalid Alef¹, Stefan Iglauer², Ahmed Barifcani¹.

¹WA School of Mines: Minerals, Energy and Chemical Engineering, Curtin University, Bentley Western Australia 6102, Australia

²School of Engineering, Petroleum Engineering Discipline, Edith Cowan University, Joondalup Western Australia 6027, Australia

	Conception & Design	Acquisition of Data & Method	Data Conditioning & Manipulation	Analysis & Statistical Method	Interpretation & Discussion	Final Approval
Khalid Alef	×	×	×	×	×	×
I acknowledge that these represent my contribution to the above research output. Signature: _____ Date: / / 2019						
Dr. Stefan Iglauer						×
I acknowledge that these represent my contribution to the above research output. Signature: _____ Date: / / 2019						
Dr. Ahmed Barifcani						×
I acknowledge that these represent my contribution to the above research output. Signature: _____ Date: / / 2019						

Paper: “**Degradation and hydrate phase equilibria measurement methods of monoethylene glycol.** MethodsX, 2019, 6, 6–14.”

Authors and full affiliations: Khalid Alef¹, Stefan Iglauer², Ahmed Barifcani¹.

¹WA School of Mines: Minerals, Energy and Chemical Engineering, Curtin University, Bentley Western Australia 6102, Australia

²School of Engineering, Petroleum Engineering Discipline, Edith Cowan University, Joondalup Western Australia 6027, Australia

	Conception & Design	Acquisition of Data & Method	Data Conditioning & Manipulation	Analysis & Statistical Method	Interpretation & Discussion	Final Approval
Khalid Alef	×	×	×	×	×	×
I acknowledge that these represent my contribution to the above research output. Signature: _____ Date: / / 2019						
Dr. Stefan Iglauer						×
I acknowledge that these represent my contribution to the above research output. Signature: _____ Date: / / 2019						
Dr. Ahmed Barifcani						×
I acknowledge that these represent my contribution to the above research output. Signature: _____ Date: / / 2019						